An Investigation into the Surface-Based Host-Guest Chemistry of an Octanuclear Coordination Cage

Michael David Ludden

A thesis submitted to the University of Warwick in partial fulfilment of the requirements for the degree of Doctor of Philosophy in Chemistry

University of Warwick, Department of Chemistry

September 2021

Table of Contents

Acknowledgements

"You can do a PhD in six months. The reason they're three years or more is because it takes that long to get to a level where you can do everything in those six months." – Mike Ward

The above quote is one that has stuck with me throughout my PhD and is a fantastic example of not only his experience as a supervisor but also the wonderful sense of humour that Mike has. It has been an absolute pleasure to work under his tutelage for the past four years and I am indebted to him for all the support he's provided me.

There are, of course, several members of the group besides Mike who have contributed greatly to my time at Warwick, all of whom deserve a mention in this section. First and foremost, the people who were part of the group when we were just starting up in our new surroundings – Chris and Stephen. Without them, the first 18 months or so of my PhD would have been a huge struggle, and the knowledge I gained from working alongside them both has served me well ever since.

Jerry re-joining during my second year was a very welcome addition to the group, mainly because he didn't complain when I took control of the lab's music. His seemingly endless list of potential ideas was always entertaining to talk about as well. A shout-out also goes to Max, Callum and Garrett for the many pub trips and out-of-lab adventures that usually involved drinking, just not in the pub. Thanks also to Cristina, Burin, Xuejian, Atena, and Ahmed for sharing time with me as part of the group, and for making the lab and office such a pleasant place to be. And finally, thanks to the MChem/URSS students who were part of the group, mainly the ones I supervised (Karen, Raoul, and Natasha) but also those I didn't.

There have been countless staff and fellow students within the department without whom I could not have done half the work I've done, so they are also more than deserving of a mention here.

To everyone I've met through UWBC, especially the Senior Men's squad, thank you. I've made some very dependable friends during my time here and the training and races provided a much-needed respite from the lab at times. I'm looking forward to seeing you all again sometime in the near future.

Thanks also to my friends from Sheffield (who I've seen far too infrequently over the past four years). If you're reading this, you definitely qualify as being a good friend of mine because who has time to read this bit, in all honesty?

The final mention must go to my family, who have backed me from the very start, even from accepting the offer of a PhD. Their unwavering support got me through several of the tougher periods of this journey and I'd like to acknowledge that here.

Author's Declaration

This thesis is submitted to the University of Warwick in support of my application for the degree of Doctor of Philosophy. It has been composed by myself and has not been submitted in any previous application for any degree.

The work presented (including data generated and data analysis) was carried out by the author except in the cases outlined below:

Synthesis of nitrobenzisoxazole – carried out by Max Tipping (Chapter 2).

Crystal structure analysis of nitrobenzisoxazole by Dr Chris Taylor (Chapter 2)

Synthesis of the cage $H^{Cr/Zn}$ and $H^{Cr/Co}$ and mass spectrometry of the cage $H^{Cr/Zn}$ – carried out by Dr Jerico Piper (Chapter 5).

Parts of this thesis have been published by the author. The list of publications can be seen below:

Christopher G. P. Taylor, Stephen P. Argent, Michael D. Ludden, Jerico R. Piper, Cristina Mozaceanu, Sarah A. Barnett, and Michael D. Ward,
"One Guest or Two? A Crystallographic and Solution Study of Guest Binding in a Cubic Coordination Cage" *Chem. Eur. J.*, 2020, **26**, 3054 –3064.

Michael D. Ludden and Michael D. Ward,
"Outside the box: quantifying interactions of anions with the exterior surface of a cationic coordination cage" *Dalton Trans.*, 2021, **50**, 2782–2791.

Michael D. Ludden, Christopher G. P. Taylor, and Michael D. Ward,
"Orthogonal binding and displacement of different guest types using a coordination cage host with cavity-based and surface-based binding sites" *Chem. Sci.*, 2021, **12**, 12640-12650.

Michael D. Ludden, Kellie Tuck, Jack C. Dorrat, Nicholas Williams, Jennifer S. Train, Max B. Tipping, Christopher G. P. Taylor, and Michael D. Ward,
"Interaction of anions with the surface of a coordination cage in aqueous solution probed by their effect on a cage-catalysed Kemp elimination" *Chem. Sci.,* 2021, **12**, 14781–14791.

Abstract

Chapter 1 – The first chapter of this work provides an overview of the subject area, including the history of supramolecular chemistry from its inception to the present day. The design and synthesis of coordination cages is also described, including the forces behind self-assembly and examples of applications that cages have been used for. The chapter concludes with a timeline of the work conducted by the Ward group, contextualising the work undertaken within this thesis.

Chapter 2 – This chapter covers the factors behind the water solubility of Ward group cages, specifically the octanuclear cubic cage $[M_8L_{12}]^{16+}$. Anion exchange studies have been carried out to determine the conversion from BF_4^- anions to other anions such as Cl^-, NO_3^- and HCO_3^-. The effect of altering the anionic composition of the cage on the catalysis of nitrobenzisoxazole to 2-cyano-4-nitrophenolate was also investigated, which revealed distinct differences in reaction rate depending on the nature of the anion.

Chapter 3 – Having determined that different anions will bind to the cage with varying affinities, a fluorescence displacement assay was developed to allow association constants to be calculated for a wide range of anions binding to the cage's exterior surface, ranging from simple inorganic anions such as fluoride to larger organic anions *e.g.,* gluconate. The stoichiometry of binding for anionic fluorophores such as fluorescein and hydroxypyrene tris-sulfonate to the cage's exterior was also investigated.

Chapter 4 – With the knowledge that surface-bound fluorophores could be displaced, a colourimetric sensor for guest binding was designed using both cavity- and surface-bound fluorophores. This sensor is able to produce a different colour response depending on whether the analyte molecule binds on the inside or outside of the cage (or both) and can distinguish between these three different modes of binding.

Chapter 5 – A novel mixed-metal cage $[Cr_4Co_4L_{12}](Cl)_{20}$ was synthesised and subsequent guest-binding studies were carried out to investigate whether the higher charge of this complex would affect the binding constants of previously used fluorophore guest molecules *e.g.* fluorescein.

Memorial plaque to Franz Hofmeister, located at the Medical Faculty of Charles University in Prague, Czech Republic and presented by yours truly. The Hofmeister series is a key component for several facets of this thesis.

Abbreviations

Asc	sodium ascorbate
anth	anthracene
B	Jones-Dole coefficient
BCP	bromocresol purple
bk	background
bpy/bipy	bipyridine
calc	calculated
cat	catalytic
CIE	International Commission on Illumination
C_{11}	cycloundecanone
DAN	dansyl acid
DMF	dimethylformamide
DMF·DMA	*N,N*-dimethylformamide dimethyl acetal
DMSO	dimethyl sulfoxide
DNA	Deoxyribonucleic acid
dppp	1,3-(diphenylphosphino)propane
DVB	divinylbenzene
en	ethylenediamine
eq	equivalents
ESI	Electrospray Ionisation
EY	Eosin Y
fac	facial
FI	Fluorescence Intensity
FLU	fluorescein
G	Guest
GOLD	Genetic Optimisation of Ligand Docking
H	Host
h	hours
H-bond	hydrogen bond

HPTS	8-hydroxypyrene-1,3,6-trisulfonic acid
ICT	Intramolecular Charge Transfer
IDA	Indicator Displacement Assay
ISR	Indicator-Spacer-Receptor
K	equilibrium constant
k	rate constant
L	Ligand
LED	Light-Emitting Diode
M	Metal
m-	meta-
MAC	4-methyl-7-amino coumarin
MeCN	acetonitrile
mer	meridional
MLCT	Metal-Ligand Charge Transfer
MS	Mass Spectrometry
naph	naphthalene
NBF	N-methyl-7-nitrobenzofurazan
NBzI	5-nitrobenzisoxazole
NMR	Nuclear Magnetic Resonance
NOESY	Nuclear Overhauser Effect Spectroscopy
o-	ortho-
p-	para-
PAH	Polycyclic Aromatic Hydrocarbon
pD	potential of deuterium
pH	potential of hydrogen
phph	phenolphthalein
PyPz	pyridyl pyrazole
Q_{zz}	quadrupole moment
RGB	red-green-blue
RNA	Ribonucleic acid
SDS	sodium dodecyl sulfate

SE	Standard Error
t	time
TBAF	tetrabutylammonium fluoride
THF	tetrahydrofuran
TLC	Thin Layer Chromatography
TMV	Tobacco Mosaic Virus
TON	turnover number
Tp	tris(pyrazolyl)borate
TSC	trisodium citrate
T1D	*trans*-1-decalone
UV	Ultraviolet
vdW	van der Waals
vis	visible
2CNP	2-cyano-4-nitrophenolate
2D	2-dimensional
3D	3-dimensional
6C-FLU	6-carboxyfluorescein
β	H-bond acceptor strength
ΔG	Change in Gibbs' free energy
ΔH	Change in enthalpy
ΔS	Change in entropy

Chapter 1

Introduction

1.1. “Supramolecular chemistry”

The term “Supramolecular chemistry” is synonymous with the term “chemistry beyond the molecule” and was coined by Jean-Marie Lehn in 1969 during his work on inclusion complexes and cryptands.[1] The word ‘supramolecular’ could be dated to even earlier than this, with Wolf and co-workers using the term “Übermolekül” in their 1937 paper on carboxylic acid dimers.[2] Since its inception, supramolecular chemistry has developed into the field of chemistry encompassing structures assembled through non-covalent interactions.

Chemists working during the emergence of this field reported discoveries and developed concepts that are now indispensable for any work done in supramolecular chemistry such as self-assembly, preorganisation or molecular recognition. Landmark work such as that done by Crick and Watson on the helical structure of DNA complete with complementary base pairs, or the Nobel Prize-worthy discoveries of crown ethers and structurally similar cryptands and spherands by Pedersen, Cram and Lehn, laid the foundations for the field to expand rapidly as academia realised its potential.[3–6] More recently, the 2016 Nobel Prize was also awarded to researchers in the field of supramolecular chemistry: Stoddart, Sauvage and Feringa were awarded the prize for their work on “molecular machines”.[7]

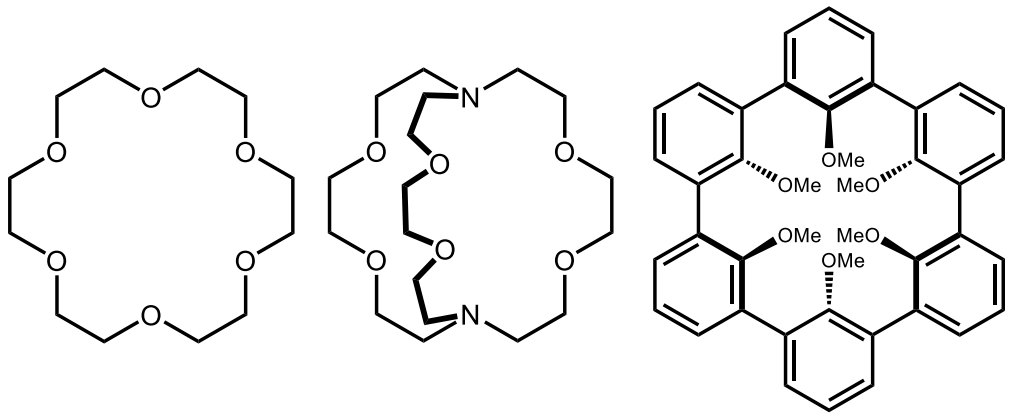

Figure 1.1 – Some of the first examples of supramolecular hosts: a crown ether, cryptand and spherand.[3-6]

Since its inception, the field has expanded rapidly with artificial supramolecular systems becoming increasingly complex in design. From its serendipitous origins to the careful and measured designs of more recent assemblies, supramolecular chemistry has caught the attention of academics of varying disciplines.

1.2. Self-Assembly

One of the most important principles in supramolecular chemistry is self-assembly.[8] This concerns the formation of supramolecular structures in solution and involves the bringing together of several components in a reversible manner spontaneously, *i.e.* without an external stimulus. The competition between enthalpic contributions from the formation of bonds and the entropic effects of bringing together multiple small components to form one larger component is a delicate balance. For a supramolecular structure to form, the contributions from ΔH must outweigh an unfavourable ΔS. This allows the formation of a more complex structure in solution; the reversibility of non-covalent interactions means that incorrect formations can disassemble and allow error-correction on the path to the final supramolecule which is the thermodynamic minimum-energy assembly.[9] Self-assembly can be seen in nature, forming functional systems using the same chemical principles that are now routinely used in a lab. An example commonly quoted is the Tobacco Mosaic Virus (TMV); the protein units must first, individually, adopt their ternary folded structure before many of these assemble about the central templating RNA strand.[10] In total, 2131 subunits come together to form the complete TMV through this self-assembly method. This assembly process is sensitive to conditions: changes to the pH or temperature result in disassembly back to component parts, which can then reform the final structure upon a return to the original conditions.[11]

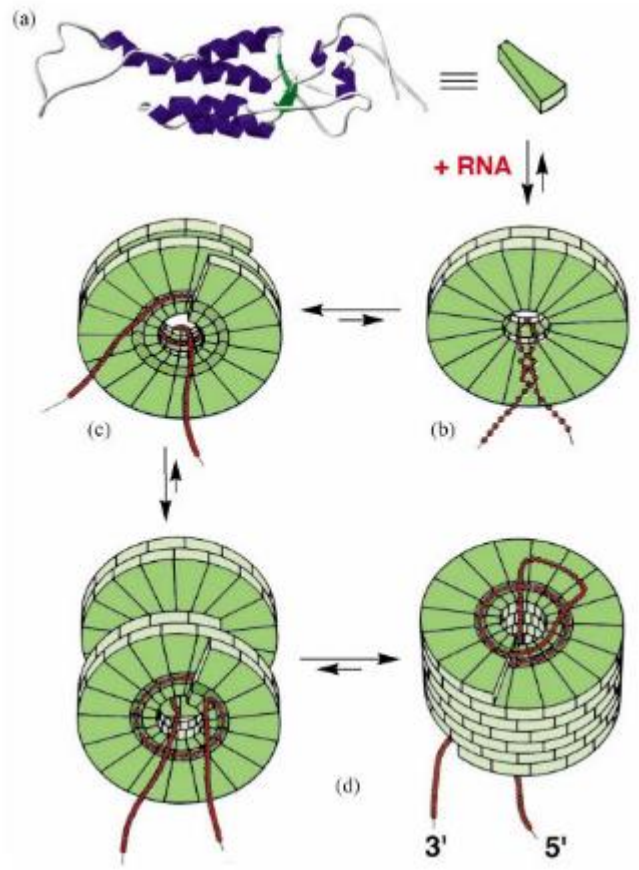

Figure 1.2 – Self-assembly of the Tobacco Mosaic Virus (TMV) from its constituent parts.[11]

The concept of self-assembly is fascinating in itself – imagine shaking a disassembled jigsaw in a box and opening the box to find the puzzle complete. The number of possible combinations the components can order themselves in is factorial, so for the correct outcome to occur spontaneously seems statistically unlikely, yet in biological systems this happens regularly. Templation and preorganisation, along with favourable enthalpies from the formation of multiple bonds, contribute heavily to the formation of such assemblies. Many chemists have turned their attention to biological systems to mimic the process of forming large, complex systems to carry out specific roles. Synthetically creating a molecule as complex as a protein or lipid is highly time and resource consuming, therefore the prospect of cutting down the demands for such a synthesis through better understanding and application of self-assembly is an attractive one.[12]

The interactions holding these structures together are individually weak, allowing reversibility, but when acting collectively are enough to form the end product. Non-covalent interactions can include hydrogen bonding, π-π stacking, van der Waals / dispersion forces and electrostatic interactions, the strength of which range from in the order of ≈1 kJ mol^{-1} for a weak van der Waals interaction to 160 kJ mol^{-1} for a F^{-}···H-F single hydrogen bond.[13] Whilst individual interactions may only be considered weak relative to a typical covalent bond, the cumulative effect of several interactions working cooperatively is sufficient to hold together vast assemblies in solution. Of these interactions, both hydrogen bonds and metal-ligand coordinate bonds are popular features of supramolecular assemblies due to their well-defined geometries. Knowledge of the directionality of interactions such as these allows the predictable design of structures.[14]

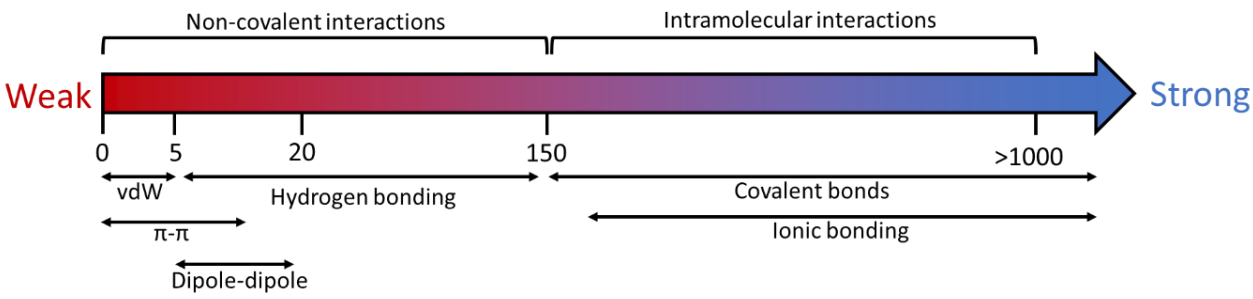

Figure 1.3 – A representation of the relative strengths of both intramolecular and intermolecular interactions.

1.3. Self-recognition within self-assembly

Self-recognition (sometimes termed self-organisation) is a phenomenon often seen during the formation of supramolecular complexes in solution. In short, it is the process by which multiple individual components of the same type spontaneously assemble in a highly selective fashion into a well-defined, discrete supramolecular architecture.[15] An important contributory effect behind self-recognition is positive cooperativity, whereby the first binding event reduces the free energy change (ΔG) for subsequent binding events.[16] Positive cooperativity exists in several forms, such as aggregation involving favourable π-stacking or intramolecular chelation. The chelate effect is itself an example of positive cooperativity.[17] Examples of self-

recognition exist in systems such as metal helicates, which are discussed later in this introduction. In this example, including more than one length of a helicating ligand strand in a mixture and adding metal ions results in all threads of the same length combining to form helicates, to maximise the site occupancy of the metal ions.[18] This was reported by Lehn from his studies on the metal helicates seen in Figure 1.4. Following this, Nitschke and Lehn described the formation of 2x2 grid-type structures selectively from a combinatorial library of starting components.[19] The starting components would undergo a condensation reaction in the presence of a zinc (II) salt, driven by metal coordination. The result was formation of the desired product with selectivity of >99% through self-recognition between components.

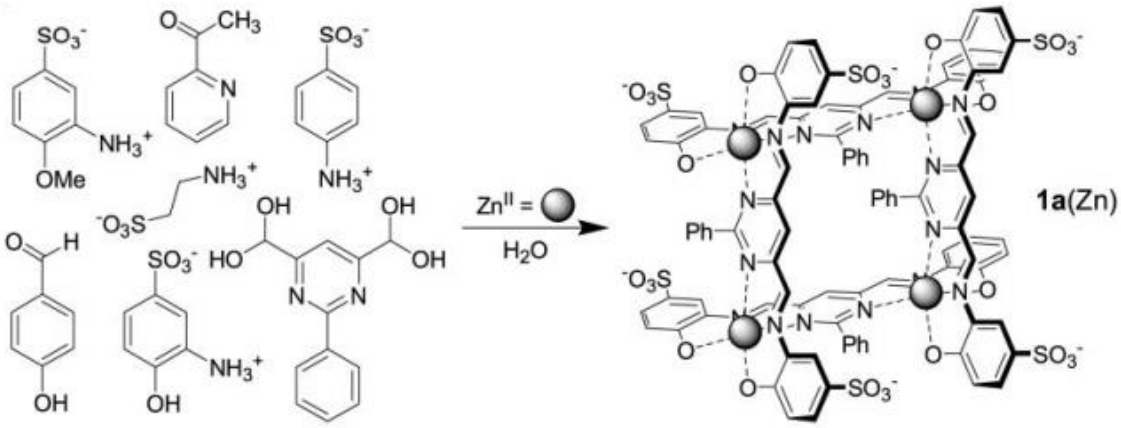

Figure 1.4 – Self-organisation of 2x2 grid architectures from a library of possible starting components.[19]

1.4. Self-assembly in chemistry

One of the first examples of a self-assembled complex reported was in 1987 by Lehn and co-workers.[18] By combining poly-bipyridine functionalities and metal ions, a short metal helicate was formed. The final structure could be varied by changing the metal ion – Cu(I) has a preference for a tetrahedral conformation and so will bind two ligand strands around it, whereas Ni(II) prefers an octahedral geometry and therefore will form a triply-stranded helicate preferentially. By positioning methyl groups on the oligo-bipyridine chains, a mixture of metal ions and differing helicate chains can selectively form trinuclear double and triple helicates spontaneously in solution. Positive co-operativity plays a large part in forming these helicates – the

binding of the first metal ion to two ligand strands in the Cu(I) complex, for example, improves the binding affinity for a following interaction by preorganising the two ligands into a conformation where an additional Cu(I) ion can easily bind, allowing formation to occur more readily.

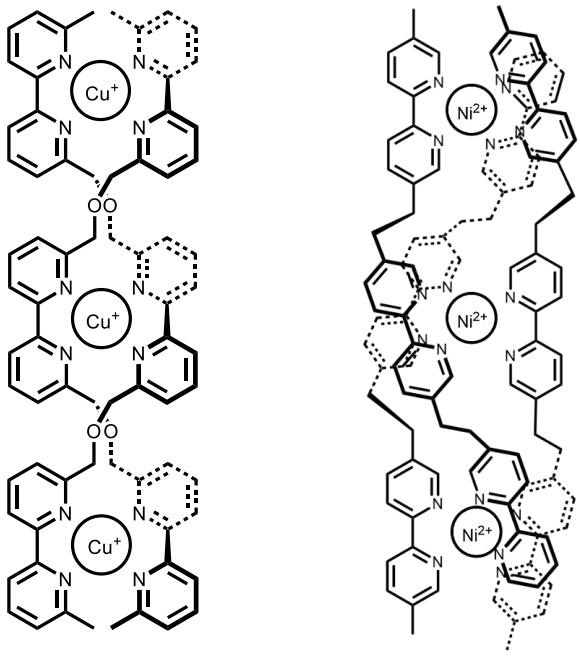

Figure 1.5 – A 2-stranded Cu(I) helicate and a 3-stranded Ni(II) helicate. The valence preferences of the metal ion dictate the chemistry of the helicate formed.

Raymond and co-workers also reported formation of metal helices using a similar system.[20] Rather than the bipyridyl donors and Cu(I) ions used by Lehn, Raymond's group used catecholamide donors paired with Ga(III) ions and made the same observation – all chains of the same length formed helicates with the other chains of that length, resulting in no mixed-ligand species being formed.

Incorporation of metal ions into supramolecular architectures opened a realm of possibilities involving metal coordinative bonds from suitable donors such as nitrogen or oxygen atoms with available lone pairs, with the interactions having predictable directionality. One of the first examples of this was published by Fujita and co-workers in 1990 and involved 4,4'-bipyridyl units bridging four Pd(II) units at the vertices of a square with ethylene-diamine groups capping the corners of the structure.[21] One of the most striking things about the 'molecular square' was how

straightforward the synthesis was – simple mixing of the metal salt with the bridging ligand at room temperature. This type of structure was also reported using a different metal by Hupp and co-workers, who used $Re(CO)_3Cl$ vertices bridged by 4,4'-bipyridyl units in a similar manner to Fujita.[22] The formation of these squares affords the square as the only final product, driven by the strong preference of the Pd(II) ions for specific coordination geometries in which the ligands are 90°, proving that this is thermodynamically the most stable species that can be formed.

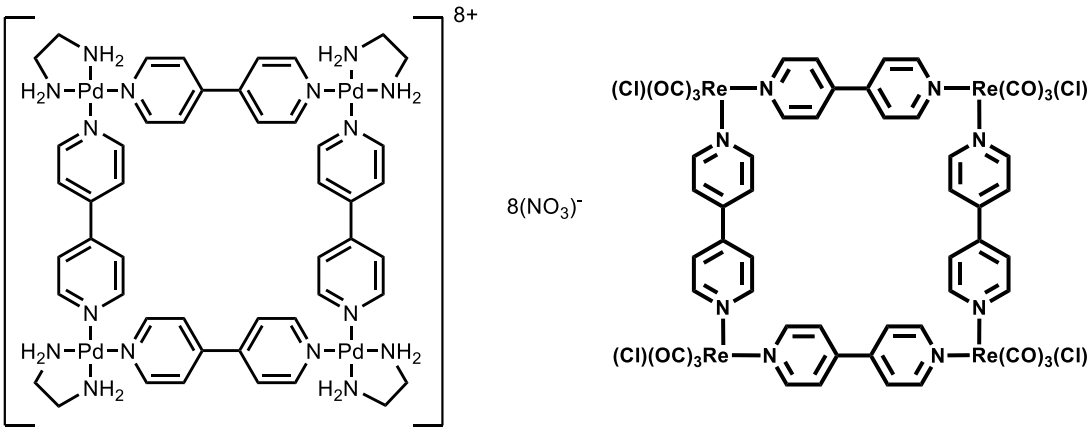

Figure 1.6 – Molecular squares formed from 4,4'-bipyridine ligands and metal ion vertices.[21,22]

The synthesis of these molecular squares highlighted the ease with which a supramolecule could theoretically be designed – to make this square, four square planar or octahedral metal ions were used at the vertices with each ion having two vacant binding sites predetermined to be *cis*. This allowed the bridging ligands to form the four edges and assemble, predictably, the square. Stang *et al.* decided to develop this idea and built a library of possible corners (angular units) and linear edge units to connect them.[23] By choosing appropriate combinations of corners and edges a range of 2D shapes could be predictably formed, ranging from 2 components for a square to 12 components for a hexagon (Figure 1.7). In this work, vertices were typically constructed from Pt(II) moieties either free as the *cis*-capped square planar complex or affixed to either anthracene or phenanthrene backbones. This gave a choice of vertex angles: 90°, 180° or 60° respectively.

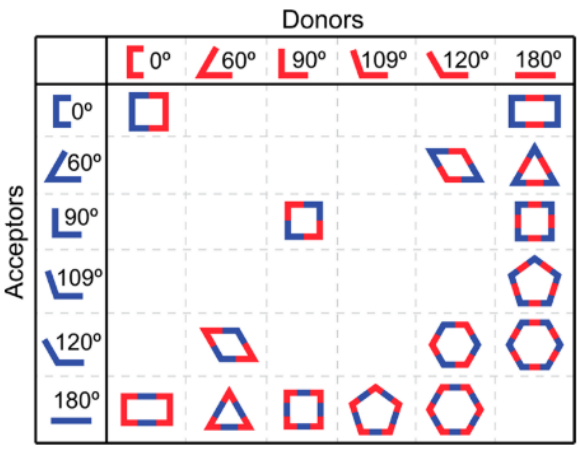

Figure 1.7 – Possible combinations of donors and acceptors with varying angles between termini can produce a wide range of final products.[23]

Following this work on 2D supramolecular structures, several groups prepared metal/ligand assemblies that were constructed in three dimensions. The first example was that of Saalfrank *et al.* who reported the synthesis of an adamantoid-style tetrahedral complex comprising of either Mg(II) or Zn(II) ions and ligands with two bidentate oxygen-donor termini that could connect two metal ions, giving a M_4L_6 structure with a metal ion at each vertex and a bridging ligand spanning each edge.[24] This type of tetrahedral scaffold is common in coordination chemistry, with many groups reporting tetrahedral architectures for varying combinations of donor groups and metal ions.

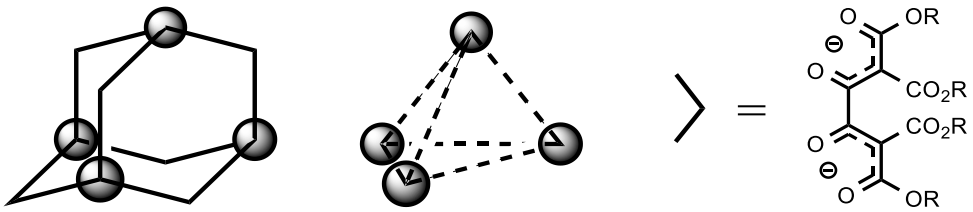

Figure 1.8 – Saalfrank's tetrahedral adamantoid-style complex and the ligand used.

The Raymond group designed a catecholamide-based ligand to disfavour helicate formation that resulted in a tetrahedral M_4L_6 species containing Ga(III) vertices when mixed stoichiometrically with $Ga(acac)_3$ (with KOH and Et_4NCl present).[25] Stang was able to apply the design principles for 2D structures in creating 3D structures in a similar manner.[26] Addition of a third point of connection to components allowed for

edges to reach out in three dimensions giving rise to new possibilities for supramolecular design. This work could predict the final 3D structure based on the angles between donor 'arms' in the starting components, an aspect of supramolecular chemistry that is much sought after but often difficult to achieve. Figure 1.9 shows how these connections could be made and the structures that are formed, giving rise to elaborate cage assemblies based on the geometries of relatively simple component parts.

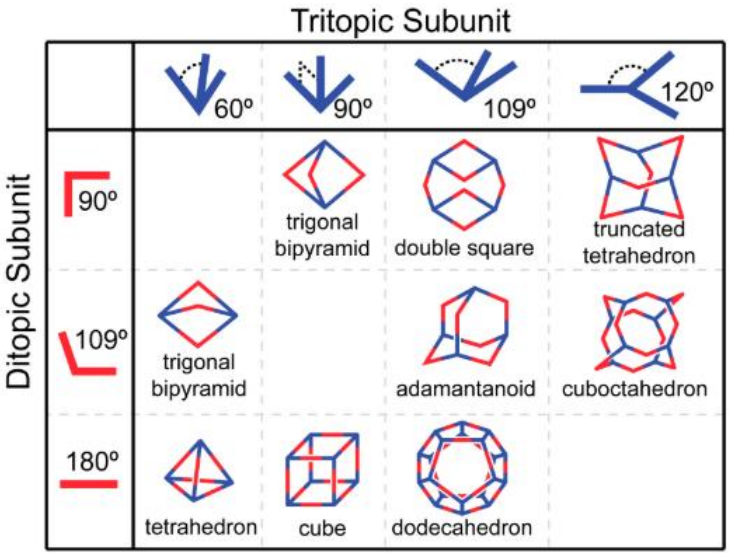

Figure 1.9 – Constructing 3D architectures from combinations of subunits using similar principles as seen in Figure 1.7.[26]

1.5. Design Principles

As seen earlier, constructing supramolecular metal/ligand assemblies of a specific shape can be done through rational design. There are two common methods of design: (i) create edges then let the metal ion dictate the geometry at the corners; or (ii) create the face of the assembled supramolecule and then join the faces using metal ions. The latter method as a route to supramolecular structures was pioneered by Fujita and co-workers, producing several novel structures through connecting face-capping ligands using Pd(II) vertices. Examples include a M_3L_2 “cage-like” complex and a M_6L_4 “adamantane-like” complex.[27] Raymond and co-workers also utilised face-directed assembly in the formation of a M_4L_4 tetrahedron using a tritopic, face-capping analogue of the edge-bridging ligand seen in previous publications.[28]

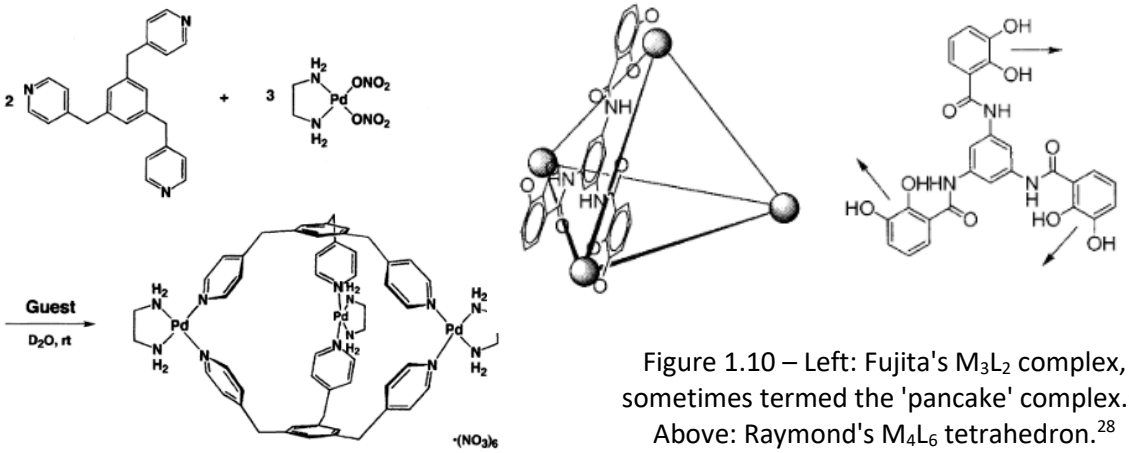

Figure 1.10 – Left: Fujita's M_3L_2 complex, sometimes termed the 'pancake' complex.[27] Above: Raymond's M_4L_6 tetrahedron.[28]

Using the same combination of pyridyl donors and Pd(II) vertices, Fujita *et al.* also constructed supramolecular scaffolds through edge-directed methods. A 2006 publication by the group describes the preparation of a pair of interconverting structures: either an M_3L_6 double-walled triangle or an M_4L_8 tetrahedron.[29]

Figure 1.11 – Two interconverting structures comprising of the same components reported by Fujita.[29]

Interconversion between species in solution is dependent on several environmental factors such as concentration of components or temperature. This had been demonstrated previously in the formation of the molecular square – a minor product was also found to have formed under certain conditions, which transpired to be a triangle consisting of the same components.[30] Raising the temperature resulted in more conversion to the triangle in solution whilst a higher concentration of components favoured the square. Entropic and enthalpic effects are the cause of this interconversion; entropically the triangle is favoured as it forms a larger number of structures which each contain fewer components but enthalpically the square is favoured due to the strain that is present within the bonds of the triangle.

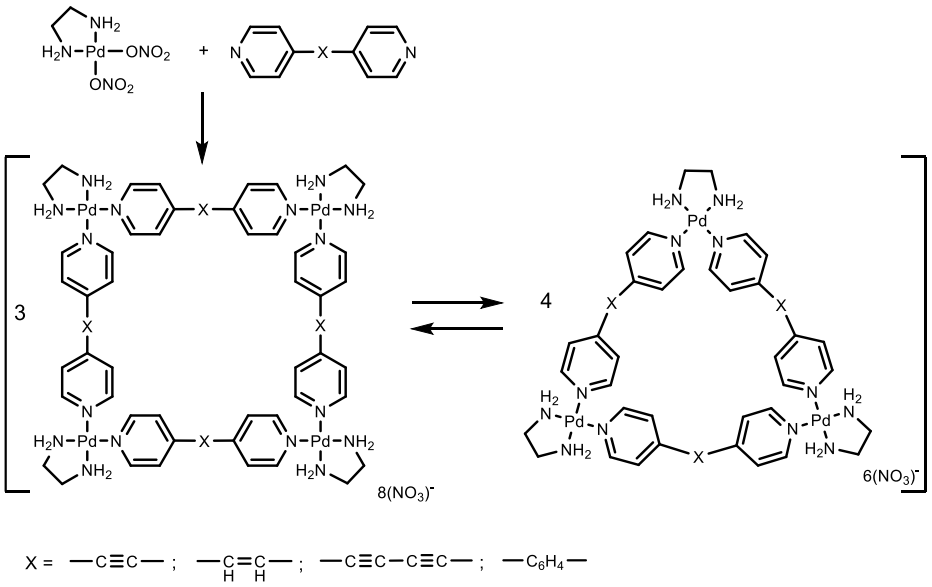

Figure 1.12 – Interconversion between molecular square and triangle. The preferred structure depends on temperature and concentration of components in solution.[30]

Design of supramolecules is not limited to the use of metal-ligand coordination to bring components together. As mentioned previously, complementary hydrogen bonding between components can result in several moderately strong bonds forming together which can hold together complexes in solution. DNA is an obvious example of this, with hydrogen bonding between base pairs holding two strands together in the famous double helix formation. Biology is often a source of inspiration for chemical systems, and academic groups were able to transpose the motifs seen in DNA into other supramolecular systems.[31] Whitesides *et al.* reported synthesis of a "rosette", a template based on dimers of cyanuric acid and melamine with three H-bonds formed between each dimer (Fig. 1.13).[32] J. Rebek, Jr. reported assembly of a self-complementary "softball" structure, with glycoluril carbonyl groups being acceptors for the N-H donors found at either end of the molecule, seen in Figure 1.14.[33]

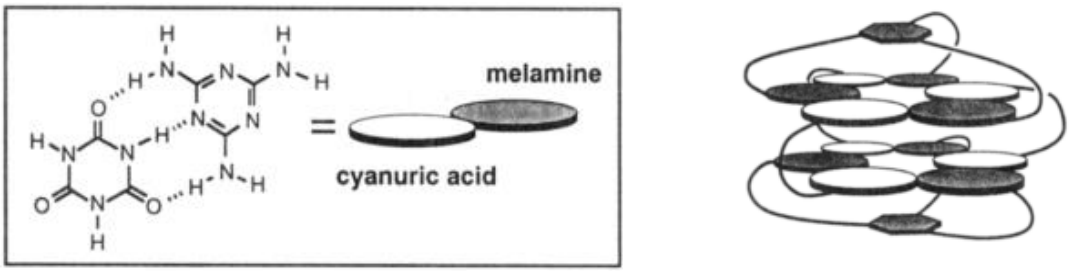

Figure 1.13 – Whitesides' rosette, formed through complimentary hydrogen bond donor/acceptor groups.[32]

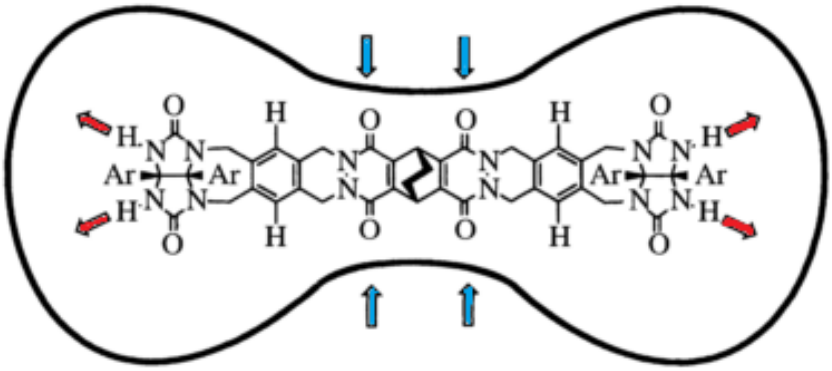

Figure 1.14 – Rebek's softball ligand. This self-assembles to form a cage through hydrogen bond formation between the N-H donors at each end (red arrows) and the carbonyl acceptors in the centre (blue arrows).[33]

π-Stacking has also been utilised as a weak interaction in several supramolecular structures. One such example is Stoddart's [2]-catenane, which forms through a templation pathway – the bis(paraphenylene)-34-crown-10 is held in place through favourable charge-assisted π-stacking interactions with the tetracationic cyclobis(paraquat-*p*-phenylene), which forms the second ring of the catenane through reaction with bis(bromomethyl)benzene.[34]

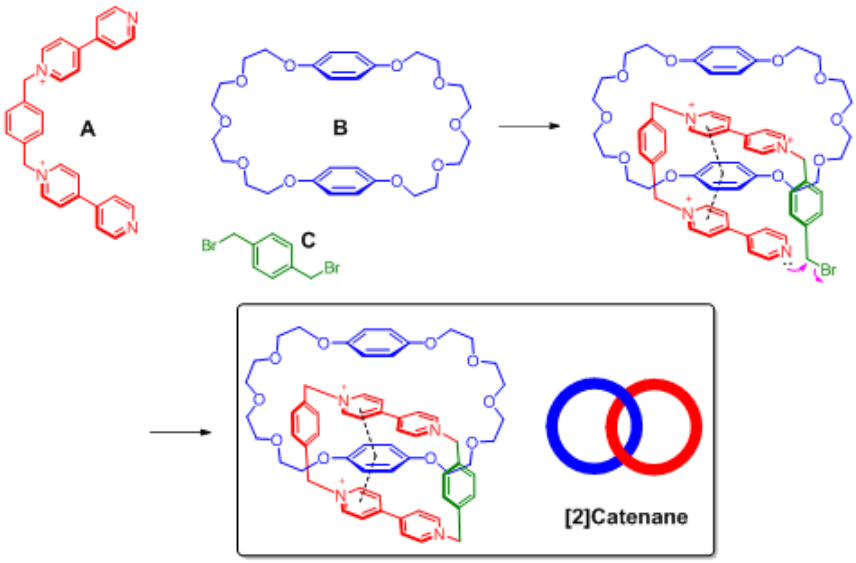

Figure 1.15 – Formation of a [2]-catenane from three components. Component A is held in the necessary conformation by B to undergo a reaction with component C and close the second ring.[34]

Templation involves holding the components of the supramolecule in a certain position or orientation through non-covalent interactions whilst the structure assembles relative to that component. The formation of the second ring in the catenane is completed through covalent modification, a process used to fix a self-assembled structure in place with non-reversible covalent bond formation. The hormone insulin is a biological example of this; insulin consists of two polypeptide chains, A and B, and is formed from a much larger molecule, preproinsulin. This precursor peptide can self-assemble into a conformation that allows all A and B groups into the correct relative orientations to create disulfide links bridging the two chains; this is the covalent modification step. Once these bonds have irreversibly formed, the excess polypeptide is removed, and active insulin remains.[8]

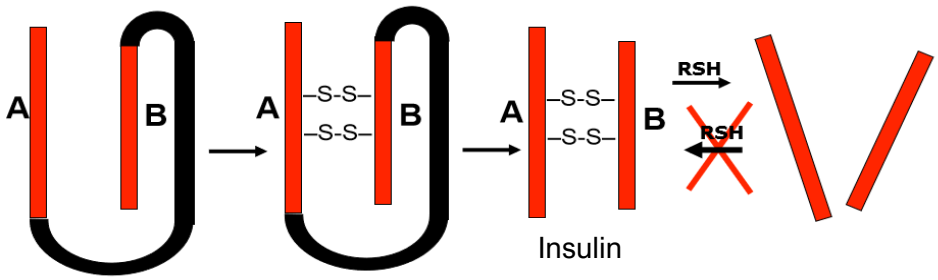

Figure 1.16 – Formation of insulin from preproinsulin using disulfide bond formation.

The rigidity that comes with aromatic backbones makes them a popular choice for ligand synthesis. By limiting the number of rotatable bonds within a ligand, the direction of assembly is easier to predict and angles between points of connection can be more readily calculated. Fujita demonstrated this by combining rigid ditopic ligands with a fixed curvature between two pyridyl donors with Pd(II) ions to form large spherical polyhedra of increasing complexity. These polyhedra have formula M_nL_{2n} and have been reported to form the structures where n = 6, 12, 24, 30 and 48.[35–37] Subtle differences in the ligand result in a completely different product, demonstrating that microscopic changes in component geometries can give rise to macroscopic differences in the final assembled structures. The largest reported structure contains 144 individual components that assemble to form a pseudo-spherical cage with an interior cavity volume of *ca.* 270,000 Å^3, occupied by solvents.[37]

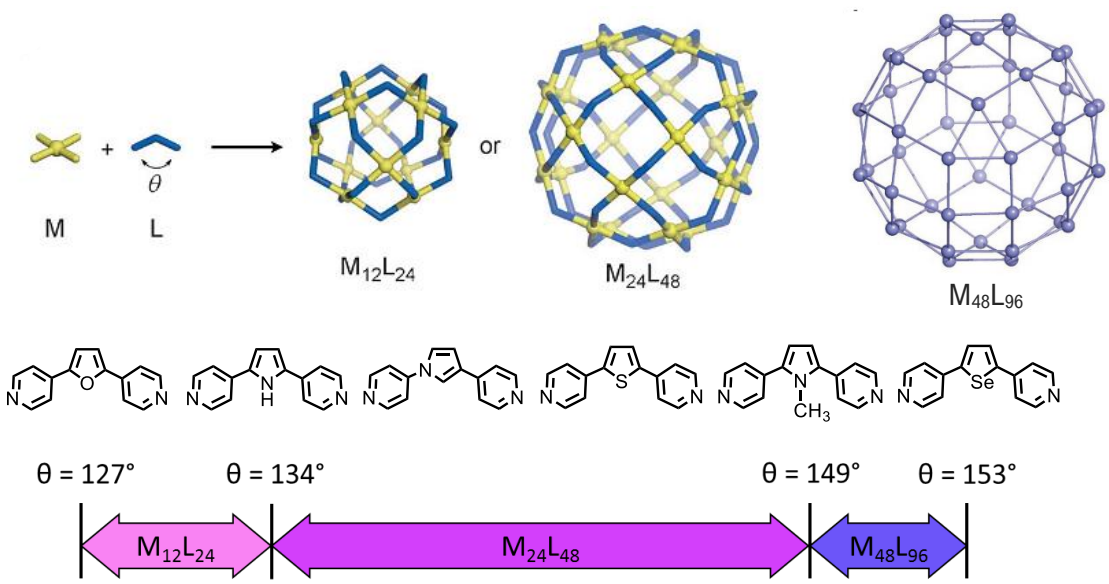

Figure 1.17 – Synthesis of high nuclearity structures from two components. Increasing the angle of the ligand towards 180° favours larger complexes.[35-37]

1.6. Host-Guest Chemistry

An integral part of supramolecular chemistry is host-guest chemistry. Large molecules can interact with and encapsulate smaller molecules through non-covalent means, forming a host-guest complex. Both association strength and host-guest stoichiometry can vary, and the phenomenon is often represented as seen in Figure 1.18.

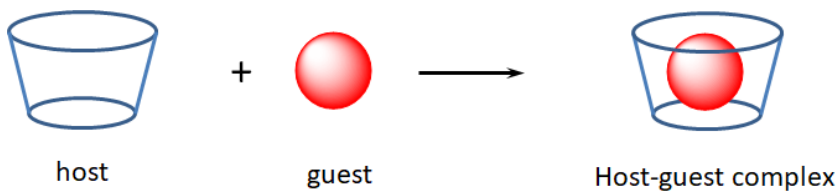

Figure 1.18 – A pictorial depiction of host-guest complexes.

Creation of a predesigned cavity for a specific size or shape of guest is a narrative that runs from the inception of supramolecular chemistry with Pedersen's work on crown ethers. With varying ring size of crown ethers came a preference for certain metal ions based on their diameter – smaller rings such as 15-crown-5 preferentially associates with Na^+, whilst 18-crown-6 associates more strongly with K^+. For even larger cations a sandwich complex could form, with a crown ether above and below

the cation.[38] Cryptands show much more strict selectivity for cations due to their binding site, or cavity, being more well defined in three dimensions in contrast to the crown ethers.

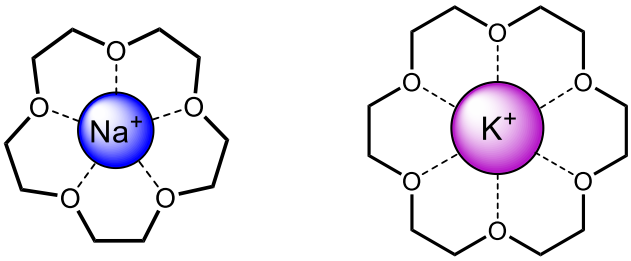

Figure 1.19 – Crown ethers display a preference for different metal cations depending on the size of the ring.

Natural examples of predesigned cavities for host-guest interactions are provided by enzymes. The active site of an enzyme usually has a cleft, the shape of which is complementary to the desired guest, creating selectivity. The model for such selectivity was termed the “lock and key” model, a metaphor drawn between a key fitting in a lock and the specific guest binding within an enzyme’s active site. Over time the binding method of substrate and enzyme has been refined from Fischer’s “lock and key” model to a more sophisticated “induced fit” model which better explains known behaviour.[39] This newer model suggests that the active site of an enzyme can adapt its shape in some cases to provide a better fit for the incoming guest, rather than the site being fixed in one conformation.

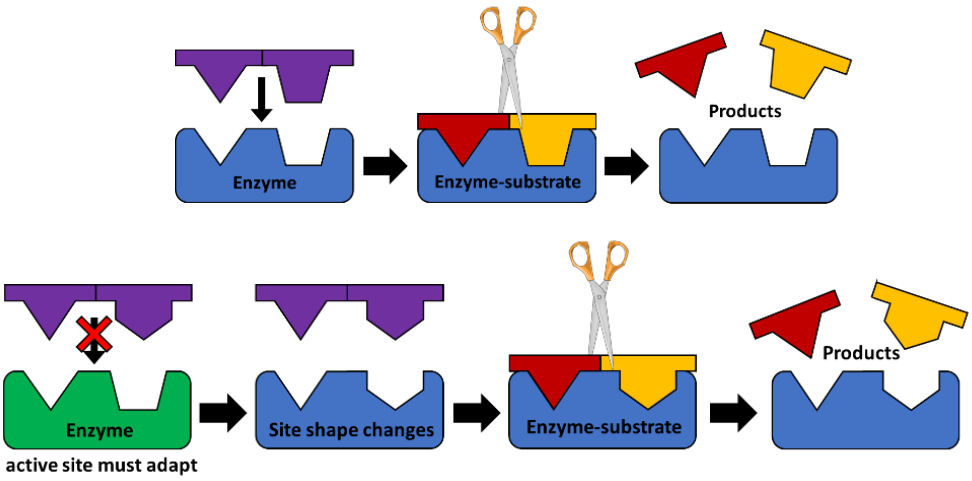

Figure 1.20 – A comparison of the 'lock and key' model (top) vs 'induced fit' (bottom).

The process of association between a host's binding pocket or cavity and a guest molecule is reliant on the same processes that bring together supramolecular complexes in solution. Non-covalent interactions such as electrostatics, van der Waals, π-stacking and hydrogen bonding can all drive guest binding either individually or cumulatively. Solvent effects can also influence guest binding dramatically.

Electrostatic interactions are interactions between either induced or permanent dipoles within neighbouring molecules. A molecule containing an electronegative atom such as oxygen, nitrogen, sulphur, or fluorine will possess a permanent dipole moment owing to the distribution of charge imparted by the aforementioned atom(s). Molecules can also contain electronegative atoms but no net dipole moment due to symmetry within the molecule *e.g.,* tetrachloromethane.[40]

Dipole-induced dipole interactions involve the generation of a temporary dipole in a normally non-polar molecule through an interaction with a neighbouring polar molecule whose vibration or rotation generates a local oscillating electric field which perturbs the electron density of the non-polar molecule, generating a short-lived electrostatic interaction between the permanent and temporary dipoles. This requires the molecules to be within close proximity of each other.[40]

London dispersion forces describe the instantaneous formation of a dipole in a non-polar molecule by random vibrations. The partial dipole on one molecule then will cause the neighbouring molecules to adjust their electric distributions accordingly and become attracted to each other. These are more loosely termed as *van der Waals* forces.[40]

π-π interactions are seen between aromatic molecules that have a quadrupole moment. This is usually characterised by the negative cloud of electron density above and below the ring of the molecule. In some instances, such as hexafluorobenzene, this is reversed, and the negative charge is centred in the ring itself with regions of positive electrostatic potential above and below. The π-electron clouds are attracted to the delta-positive protons of these systems and will attract or repel each other depending on their relative orientation. The two attractive orientations are a

staggered conformation and edge-to-face interaction, whilst directly stacked rings will repel each other (Fig. 1.21).[41]

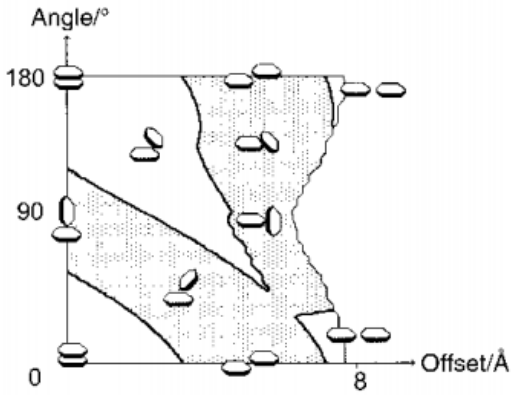

Figure 1.21 – Favourable and unfavourable interactions between two π systems based on their angle relative to each other. Areas where the interaction would be favourable are shaded light grey.[41]

π-stacking is seen in many supramolecular assemblies. Attractive forces between electron rich and electron poor aromatic systems have been well documented by the groups of Hunter and Siegel.[42,43] One case of π-stacking being exploited in supramolecular design is the Buckycatcher, essentially a pair of molecular tweezers. Two corannulene 'sockets' can interact strongly with one C_{60} fullerene molecule through π-stacking to give an inclusion complex.[44]

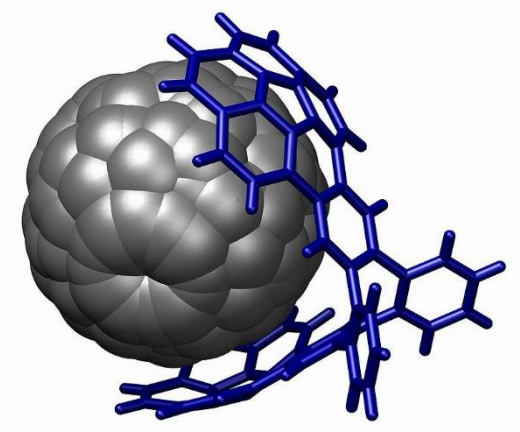

Figure 1.22 – A Buckycatcher host molecule interacting with a C_{60} fullerene guest through intermolecular π-stacking.[44]

The solvent can play a large role in the interaction between a host and a guest molecule. Interactions between solvent and molecules in solution depend largely on their polarity – as shown by the classic "like dissolves like" principle. The molecules

present in the solvent will have an affinity for both the solvent and each other. If the attraction between solvent and solute outweighs solute-solute attraction, then the molecules will be solvated and dispersed within the solution. If the solvent does not interact favourably with the molecules within it then the solute molecules will remain aggregated and not dissolve. In the case of host-guest interactions in solvent, if the host-guest interaction is preferred to either species being solvated then formation of the **H·G** complex will dominate over individually solvated components. Having both a host and guest that do not interact well with the solvent results in *solvophobic effects* which increases the association between host and guest.

The hydrophobic effect is the above phenomenon occurring in aqueous media. The hydrophobic effect has been studied rigorously but its origins are disputed. There are two main definitions – the 'classical' and 'nonclassical' hydrophobic effect.[45,46] The classical definition is sometimes known as the "Iceberg model" and is entropy based. This describes the formation of 'cages' of water molecules around the surface of a hydrophobic solute in aqueous solution. As the water molecules in the bulk solution will hydrogen bond to each other, addition of a hydrophobic species that cannot hydrogen bond will disrupt this network between molecules and cause the water molecules to form a 'cage' around the hydrophobic species. These water molecules have restricted mobility, and therefore the free energy of the system decreases. Hydrophobic species will aggregate in water, minimising the exposed surface area and hence minimising the number of restricted water molecules. Aggregation of hydrophobic molecules releases some of the restricted water molecules and increases the overall entropy.[47,48]

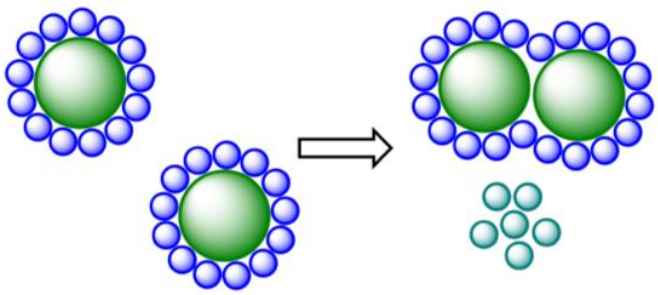

Figure 1.23 – Aggregation of solvated hydrophobic species releases some solvent molecules back into solution. This increases the entropy of the system and is favourable.[48]

The second definition of hydrophobicity is enthalpy based and often involves the release of water from inside a supramolecular cavity. Water that occupies the cavity of structures such as cucurbiturils or even coordination cages is considered 'frustrated' due to a deficiency of intermolecular hydrogen bonds. This deficiency is caused by the restrictive nature of the cavity – any water molecules found inside the cavity will struggle to find sufficient hydrogen-bonding partners in the limited space surrounding them, as the cavity walls are likely organic and poor at hydrogen-bonding. Reintroduction of this 'high-energy' water into the bulk solution through displacement using a hydrophobic guest allows formation of new hydrogen bonds up to the ideal maximum of nearly 4 per water molecule, leading to a negative enthalpy change. This effect underpins very high association constants between host and guest in some synthetic cucurbituril host systems with aromatic guests, which have been calculated up to 10^{17} M^{-1}, exceeding anything observed in natural systems. This effect depends strongly on the cavity size as it is optimal when a significant number of water molecule guests are 'frustrated' by being unable to form enough hydrogen-bonds with each other compared to bulk solution putting them into a high-energy state.[49]

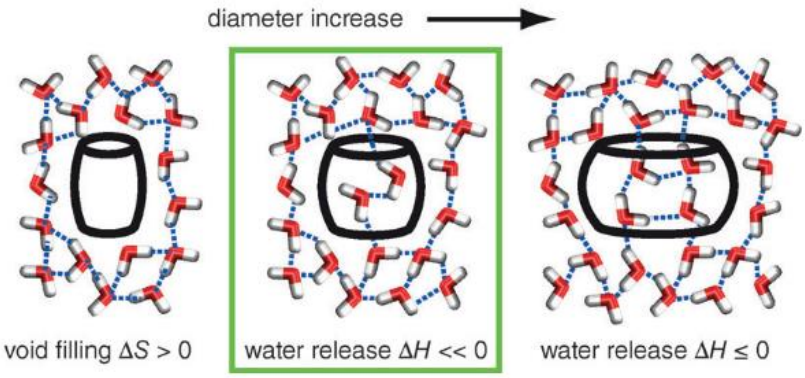

Figure 1.24 – The size of the cavity affects water molecules trapped inside. These molecules are deficient of H-bonds compared to those in the bulk solvent.[49]

It is likely that different contributions to the hydrophobic effect will dominate in different supramolecular systems, depending on the cavity present and the nature of the guest. Regardless, the hydrophobic effect plays a large part in many host-guest systems and is a key driving force for host and guest association whether through entropic or enthalpic means.[50,51]

1.7. Applications of coordination cages

The field of supramolecular chemistry focuses not only on creating novel molecular architectures but also finding solutions to problems such as catalysis, sensing, or molecular transport. Many reactions have been found to be catalysed within the cavity of coordination cages. The confined space of a molecular cavity or presence of particular functional groups within the cavity can often result in unorthodox reaction pathways compared to bulk solution.

The Diels-Alder reaction is one such example that has been studied by academic groups for catalysis using a coordination cage. Rebek and co-workers reported catalysis of the Diels-Alder reaction between *para*-benzoquinone and a thiophene dioxide derivative, in the cavity of a hollow molecular softball.[52,53] In this case, the *p*-benzoquinone starting material has a much higher affinity for the cavity than the product, facilitating turnover by allowing more starting material to bind and eject the product.

Fujita and co-workers also studied the Diels-Alder reaction with one of their octahedral palladium-based cages. [2+4] thermal addition reactions were found to be catalysed with high regioselectivity, sometimes giving regioisomers that do not normally arise. In the cavity of the host cage, molecules which would be considered to otherwise be poorly reactive such as triphenylene or perylene are able to undergo the Diels-Alder reaction in yields upwards of 90%.[54]

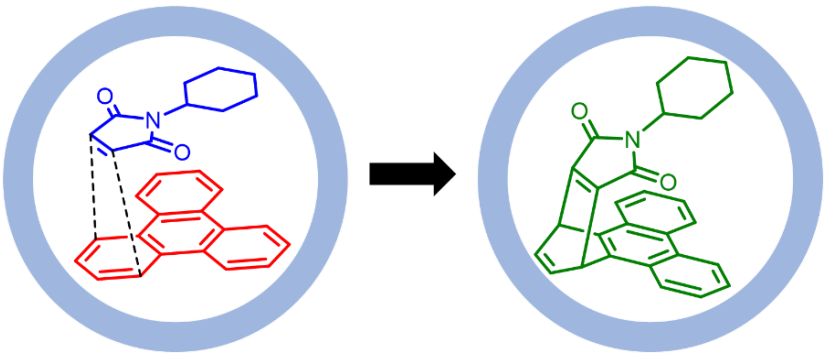

Figure 1.25 – The cavity of a coordination cage enhances the reactivity of otherwise poorly reactive materials such as triphenylene for the Diels-Alder reaction.[54]

Fujita's group have also reported catalysis of similar reactions using their Pd_6L_4 octahedron as the host. [2+2] photodimerization and pairwise selective [2+2] cross-photodimerization reactions were found to occur with substantial rate acceleration and stereocontrol.[55] The control over product formation derives from the orientation that the cage's cavity imposes on the substrates when bound in the confined space.

Another reaction that is orientation dependent is the aza-Cope rearrangement. Raymond and co-workers reported rate enhancements for several iterations of enammonium cations which were favourably uptaken by their negatively charged Ga_4L_6 cage. 2D NOESY studies pointed to a preorganised reactive conformation being adopted by the guest inside the cavity, which allowed for much quicker rates of rearrangement than was observed with no cage present – when the molecule was therefore not preorganised into a conformation resembling the reaction transition state.[56]

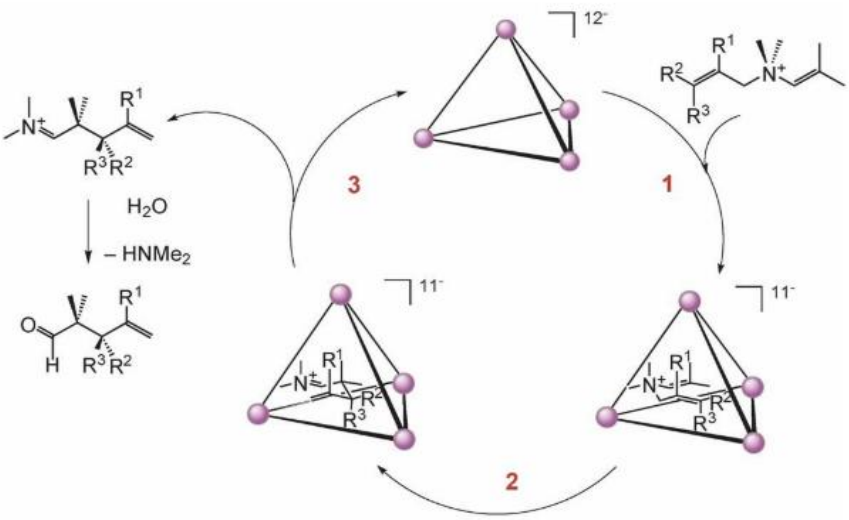

Figure 1.26 – The proposed catalytic cycle for the aza-Cope rearrangement of ammonium cations.[56]

In some instances, careful and specific cavity design can allow mimics of natural systems to be created. Hupp and co-workers developed a synthetic mimic for cytochrome P450 that involved a manganese porphyrin centre encapsulated within a supramolecular assembly, similar to the iron analogue found in the catalytic centre of P450.[57] In nature, cytochrome P450 is responsible for the oxidation of many biological compounds and this synthetic mimic can catalyse the epoxidation of olefins. The catalytic centre by itself will degrade after roughly 50 catalytic cycles but

coupled with a large preorganized, porphyrin-derived cavity structure and bound through directed coordination, the now-encapsulated Mn(II) centre can reach TON's of over 20,000.

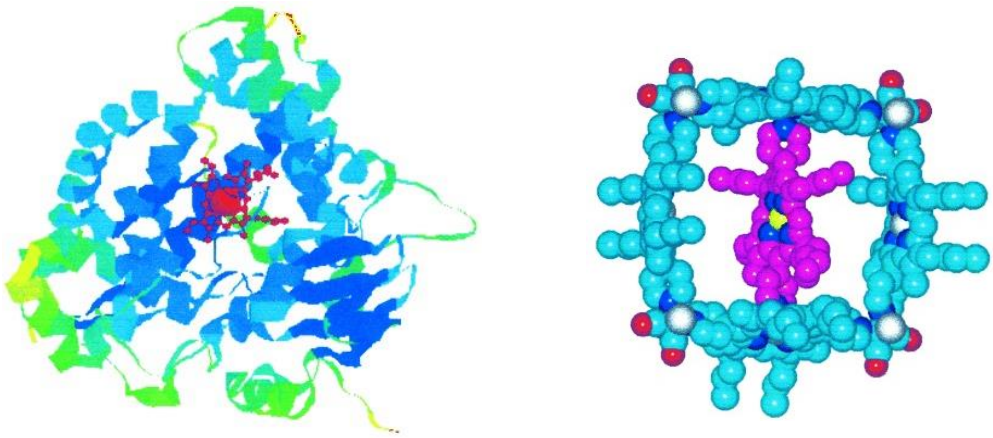

Figure 1.27 – Left: cytochrome P450 with active centre outlined.
Right: Hupp's porphyrin based P450 mimic capable of epoxidation of olefins.[57]

Phase transfer agents are compounds that are capable of moving molecular cargo from one solvent phase to another, *e.g.* aqueous to organic.[58] They are of particular interest for new, green approaches to synthesis and catalysis owing to their compatibility with water. Another use that has become apparent is for selective transport. The cavities of coordination cages are often suited to a certain size or shape of guest molecule and can selectively shuttle this molecule across a biphasic interface if the surrounding cage has the requisite solubility properties.

Fujita *et al.* published work on phase transfer catalysis using their Pd_6L_4 octahedron, the same cage as mentioned earlier for Diels-Alder catalysis.[59] The water-soluble cage was able to uptake styrene from a suspension in the aqueous phase and enable the Wacker oxidation process to occur in the presence of $(en)Pd(NO_3)_2$. In the absence of cage, no conversion to acetophenone was observed. Yields of up to 84% conversion were achieved for electron-rich guests.

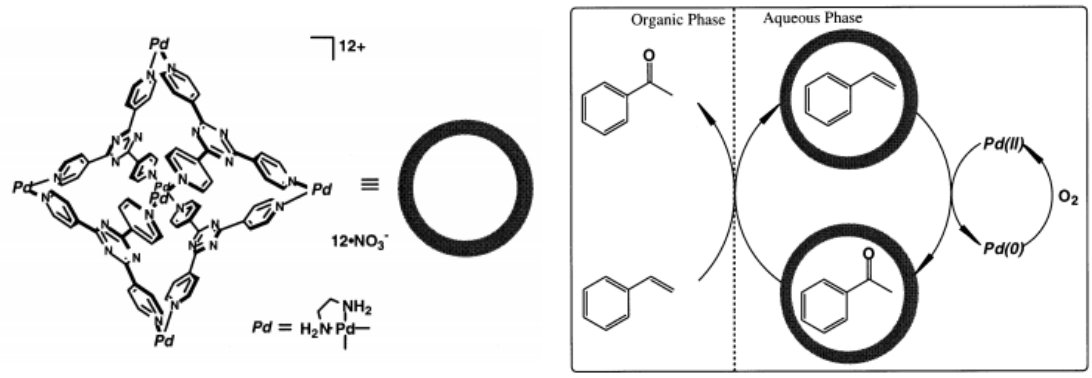

Figure 1.28 – Left: Fujita's Pd(II) M_6L_4 coordination cage capable of acting as a phase transfer catalyst. Right: The catalytic cycle for the Wacker oxidation of styrene.[59]

Another group who more recently have made considerable strides in this area is the Nitschke group. A series of papers have been published since 2017 describing the transport of molecular guests across a phase interface with use of a coordination cage. Guests are uptaken in aqueous media, driven by the hydrophobic effect, and transported to a non-aqueous phase such as ethyl acetate or an ionic liquid.[60] The change of phase is mediated by anion exchange of the cage complex from a hydrophilic anion such as sulfate to something hydrophobic, *e.g.* BF_4^- or $(BArF)^-$. This has been demonstrated to work with three cages of increasing volume.[61]

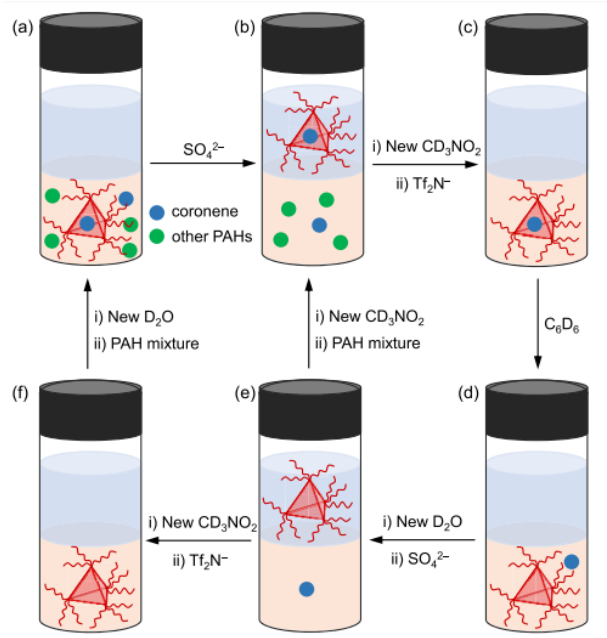

Figure 1.29 – An outline of Nitschke's demonstrated selective recycling of coronene from a mixture of PAH's. Phase transfer is a key part of the cycle and allows the cage to be recycled.[60]

Guest selectivity imparted by the cavity has also been demonstrated with polycyclic aromatic hydrocarbons (PAH's), showing a preference for the strongly binding coronene over other smaller PAH's.[62]

Coordination cages also have found use in sensing of analytes. Sensors can be categorised based on their response upon interaction with the desired analyte. Common response mechanisms are changes in absorption, fluorescence emission, or redox potential. Components capable of displaying such changes in signal can be incorporated into supramolecular frameworks, allowing cages to act as sensors.

The typical representation of a sensor consists of a recognition moiety and a signalling moiety, usually connected by a spacer, in an 'ISR' (indicator-spacer-receptor) system. In many cases the spacer is conjugated to allow electronic communication between the receptor and indicator.[63]

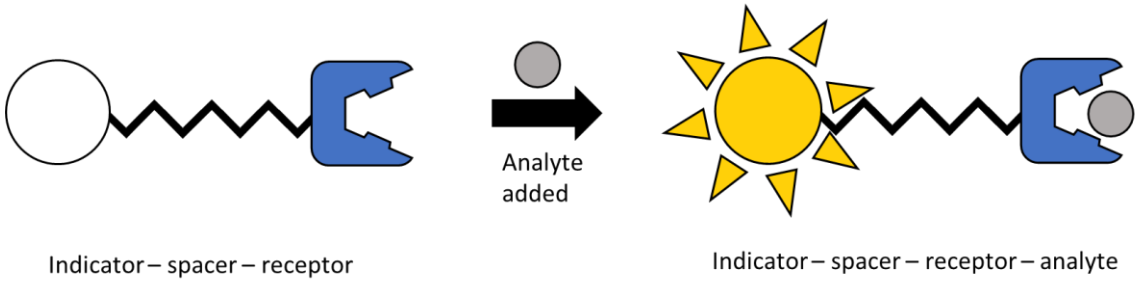

Figure 1.30 – Pictorial representation of an ISR sensing system. Binding of the desired analyte causes the indicator to be 'switched on', giving a measurable response.

There are also displacement assays, sometimes called indicator displacement assays (IDAs). IDAs involve the receptor binding the indicator first: upon addition of a competing analyte the indicator is released to produce a signal, often restoration of fluorescence from the free indicator which was quenched when it was bound to the cage. IDAs offer many advantages over covalently bound sensors such as less

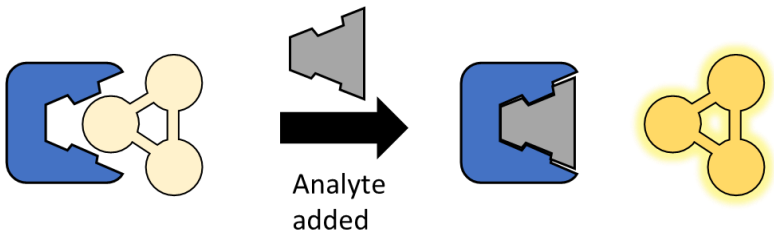

Figure 1.31 – Pictorial representation of an IDA sensing system. The analyte in this case competes for a binding site with the indicator, which shows a response upon displacement.

complicated synthetic routes and suitability for more than one indicator per receptor.[64]

Coordination cages show ability to behave as sensors due to the presence of a cavity which can uptake guest molecules, or analytes. This action of guest binding may cause a change in the properties of the cage surrounding it or displace an associated indicator. In short, cages can be designed to work as either ISR or IDA sensors. Metal-organic complexes such as coordination cages can display interesting optical properties arising from the choice of metal ions used in the assembly or incorporation of chromophores into the ligands.

One of the first examples of a coordination complex acting as a sensor for guest binding was Hupp's molecular square, mentioned earlier in this introduction. Consisting of *fac*-$Re(CO)_3Cl(4,4'\text{-bpy})_2$ units combined with $Pd(dppp)(OTf)_2$ corners ((4,4'-bpy) = 4,4'-bipyridine, (dppp) = 1,3-(diphenylphosphino)propane), the complex possessed a MLCT state, which when excited produced luminescent emission from the supramolecule. This emission intensity of the sensor in acetone was seen to increase upon addition of the ClO_4^- anion binding inside the 4+ cavity.[65]

Another complex capable of sensing guest binding is a Ru/Re macrocycle published by the Thomas group. In water this macrocycle displays luminescence through a relatively intense emission band from a Ru(II)-(2,2'-bipy) ^{3}MLCT excited state centred around 650–670 nm. Titration of mono- and bicyclic molecules such as 1,4-dimethoxybenzene and 1-naphthol into aqueous solutions of the Ru/Re macrocycle resulted in large changes in the absorption spectra but no change in emission intensity.[66] A further study using anions as potential guest molecules yielded a different result – this time the emission of the macrocycle was seen to change upon anion binding. Titrations with BF_4^-, BPh_4^- and SO_4^{2-} performed in acetonitrile all led to a progressive enhancement in luminescence intensity of the host as the anions bound in the cavity.[67]

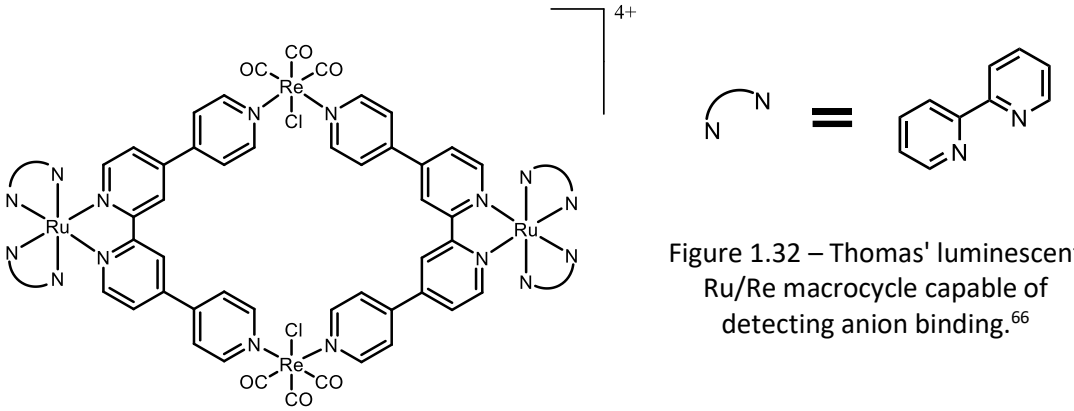

Figure 1.32 – Thomas' luminescent Ru/Re macrocycle capable of detecting anion binding.[66]

Nitschke and co-workers reported a series of tetrahedral cages that displayed striking fluorescence characteristics, owing to the inclusion of both BODIPY and pyrene moieties in the cage's subcomponents.[68] These cages can interact with anions resulting in changes to the fluorescence spectrum, with a regular increase seen upon sequential additions of the anions Cl^-, F^-, N_3^- and OAc^-. The changes were seen at concentrations as low as nanomolar for acetate. The interaction between the cage and anions was determined through changes in the ^{19}F NMR spectrum of the BODIPY molecule. The interactions attributed to these changes in observed properties are both electrostatic and anion-π interactions.

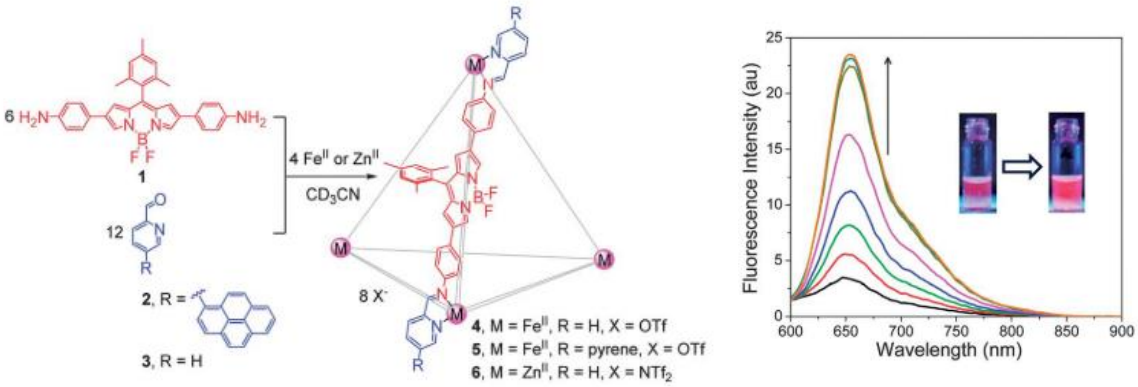

Figure 1.33 – Incorporation of fluorescent groups such as pyrene and BODIPY produce an assembly that can act as a sensor for guest molecules, in this case anions. A fluorescent response is seen upon the addition of various anions as their tetrabutylammonium salts in acetonitrile.[68]

1.8. The Ward Group

The Ward group have research aims rooted in supramolecular chemistry, and the design and synthesis of novel coordination cages is one of them since the first example published in 1995. Early work centred around the design of bis- and tris-polydentate ligands applicable in coordination chemistry and the binding which occurs upon addition of metal ions. A mainstay feature of chemistry in the Ward group is the chelating pyridyl-pyrazole unit (PyPz) – a bidentate nitrogen-donor with a reactive pyrazole N(1) position that can be used for further functionalisation.[69]

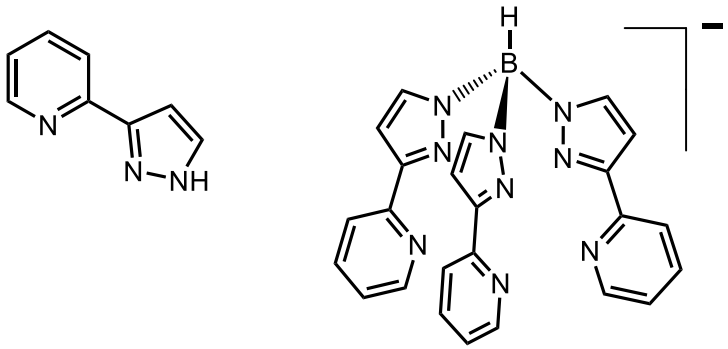

Figure 1.34 – The PyPz subunit characteristic of work within the Ward group and the ligand $[Tp^{Py}]^-$.

The ligand $[Tp^{Py}]^-$ was the first to incorporate PyPz arms to coordinate to a transition metal ion. As shown in Figure 1.34, the assembly orientates the three bidentate arms facing inwards, able to coordinate to an appropriate metal ion in a roughly trigonal prismatic conformation. This was demonstrated to be the case for Co(II), giving the mononuclear complex $[Co(TpPy)]^+$. With zinc or manganese, however, a higher order complex was detected by mass spectrometry. These were subsequently found to be M_4L_4 tetrahedra with each $[Tp^{Py}]^-$ ligand binding to three metal centres, capping a triangular face of the M_4 tetrahedron, rather than forming mononuclear complexes.[70]

Encouraged by the initial results using PyPz subunits, attention was turned to producing a variety of ligands incorporating this functionality. Boron linkers were dropped in favour of aromatic spacers with methylene arms, primarily for stability but also for ease of synthesis and to give scope for exploring various possible

aromatic spacers. The first ligand synthesised in this manner was $L^{o\text{-}Ph}$ where *o*-Ph is short for *ortho*-phenyl.

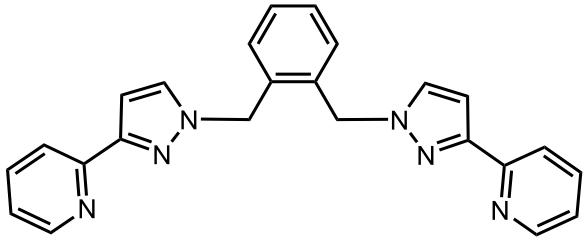

Figure 1.35 – Ligand $L^{o\text{-}Ph}$

Much like the $[Tp^{Py}]^-$ ligand, $L^{o\text{-}Ph}$ can form mononuclear complexes with Cu(II) ions.[71] This is attributed to the short distance between the chelating arms, allowing one ligand to coordinate both bidentate arms to one Cu(II) ion. As was the case with $[Tp^{Py}]^-$, other metal ions give rise to different structures. Addition of metals with a preference for an octahedral donor geometry such as Co(II) or Zn(II) gave rise to a tetrahedral M_4L_6 species, with each edge of the M_4 tetrahedral metal ion array being spanned by $L^{o\text{-}Ph}$. Interestingly, the tetrahedron was found by crystallography to contain one BF_4^- or ClO_4^- anion within the central cavity. Studies by NMR spectroscopy showed no exchange between the cavity-bound anion and those accumulated around the cage's exterior. Further investigation revealed that the cavity-bound anion acted as a template for complex formation, a feature not observed with other anions such as acetate.[72]

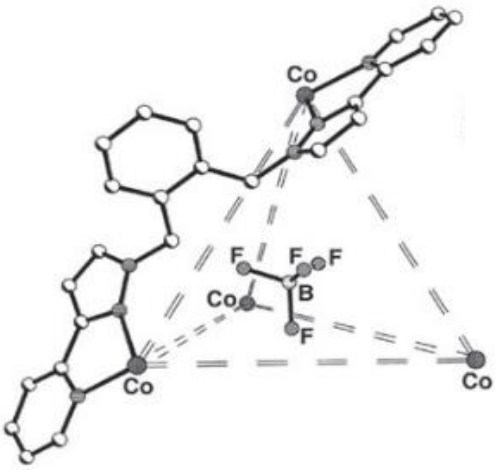

Figure 1.36 – The outline of the M_4L_6 structure complete with trapped BF_4^- anion within the cavity.[72]

Expanding the reach of this ligand by using a biphenyl spacer group rather than the *ortho*-phenyl group also produces an M_4L_6 tetrahedral assembly. The complex is larger owing to the added length of the biphenyl group and contains a larger cavity as a result. A BF_4^- anion can still reside within the cavity but is a much poorer fit for the cage than for the $L^{o\text{-Ph}}$ equivalent. In this case, exchange between the cavity-bound anion and the surrounding solution does occur and was tracked by low temperature ^{11}B NMR spectroscopy.[73]

Following this work, other aromatic spacer groups were investigated to expand the library of ligands to trial in complex formation. The *meta*- and *para*- isomers of the phenylene spacer were also successful, with the *meta*-phenylene ligand $L^{m\text{-Ph}}$ giving rise to interconverting M_6L_9 'open book' / M_8L_{12} cube structures.[74] Whilst the increase in size between the product of $L^{o\text{-Ph}}$ and $L^{m\text{-Ph}}$ was noteworthy, the product formed using $L^{p\text{-Ph}}$ was somewhat unpredictable. The structure characterised was an $M_{16}L_{24}$ tetra-capped truncated tetrahedron, which however rearranged to smaller cages such as an M_6L_9 trigonal prism in solution.

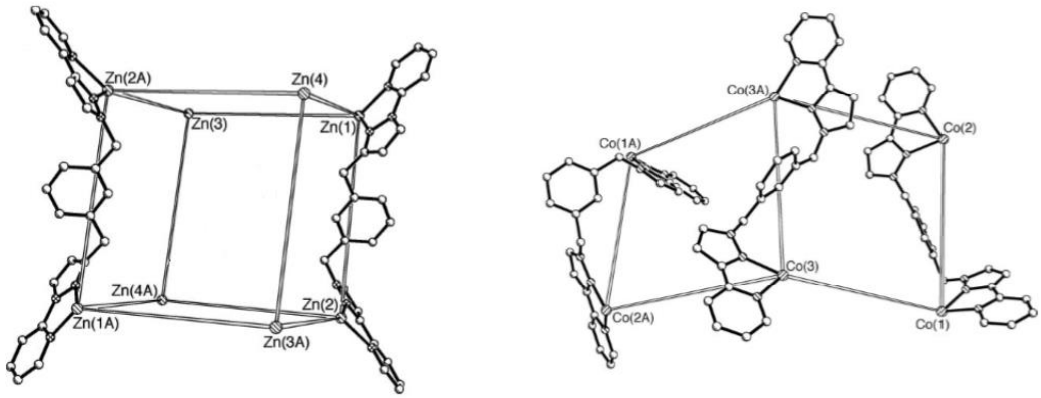

Figure 1.37 – The two interconverting structures formed through combining M(II) and $L^{m\text{-Ph}}$: a M_8L_{12} cube and a M_6L_9 open book structure.[74]

Larger aromatic spacers such as naphthyl and anthracenyl groups were next to be used in ligand synthesis. The ligands $L^{1,8\text{-naph}}$, $L^{1,5\text{-naph}}$ and $L^{9,10\text{-anth}}$ were synthesised and complexes prepared using either M(I) (M = Cu, Ag) for $L^{1,8\text{-naph}}$ exclusively, or M(II) ions (M = Co, Ni, Cu, Zn, Cd). $L^{1,8\text{-naph}}$ behaves similarly to $L^{o\text{-Ph}}$ in that both arms of the ligand are close enough to interact with the same metal ion, allowing for mononuclear complexes to form with metals with lower coordination tendencies

such as Cu(I) or Ag(I). With octahedral M(II) ions, $L^{1,8\text{-naph}}$ forms a $M_{12}L_{18}$ truncated tetrahedral cage. The larger structure possesses a cavity of ≈200 $Å^3$ which is occupied by counter-anions such as BF_4^-, as seen in previous structures. Another interesting feature is the stacking between neighbouring ligands present in the framework – alternating naphthyl (electron rich) and PyPz (electron poor) groups from adjacent, overlapping ligand fragments form favourable charge-assisted π-π interactions around the exterior surface, which aid the stability of the complex in solution.[75]

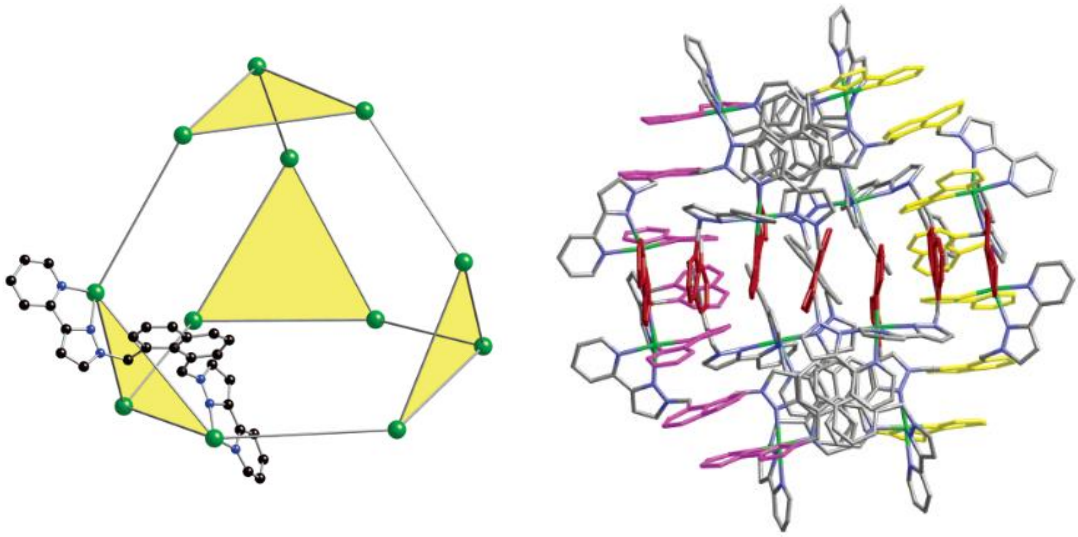

Figure 1.38 – Ligand $L^{1,8\text{-naph}}$ forms a $M_{12}L_{18}$ truncated tetrahedron that displays π-stacking between electron-rich and electron-poor groups (highlighted in red, right-hand diagram).[75]

Later work using the ligand $L^{1,8\text{-naph}}$ uncovered more complicated behaviour of the complexes formed. What was initially characterised crystallographically to be a $M_{12}L_{16}$ truncated tetrahedron was found to also interconvert slowly in solution to both a M_2L_3 dinuclear meso-helicate and a M_4L_6 tetrahedral cage. ^1H NMR studies found that increasing temperature and increasing dilution favours fragmentation to give a larger proportion of the smaller assemblies for entropic reasons.[76] This draws parallels with the interconverting molecular squares and triangles example reported by Fujita earlier in the introduction.[29]

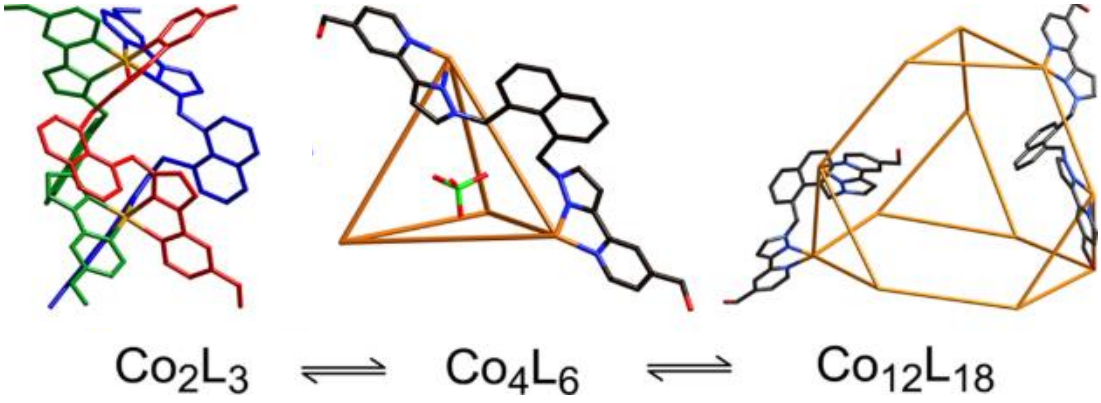

Figure 1.39 – The possible structures formed using $L^{1,8\text{-naph}}$. These interconvert slowly in solution.[76]

$L^{1,5\text{-naph}}$ and $L^{9,10\text{-anth}}$ both formed cubic molecular cage structures with a M_8L_{12} stoichiometry. The anthracene-based structure was found to dissociate in polar solvents and could not be characterised by NMR or mass spectrometry studies. This was attributed to a lack of π-stacking between the ligands, a feature that was observable when other aromatic spacers such as naphthalene were used in the ligands. The stability brought by the inter-ligand stacking is a key part in the formation of these cages in solution. The M_8L_{12} cube formed using $L^{1,5\text{-naph}}$ showed a different ligand arrangement, and will be discussed in detail in the next subsection.[77]

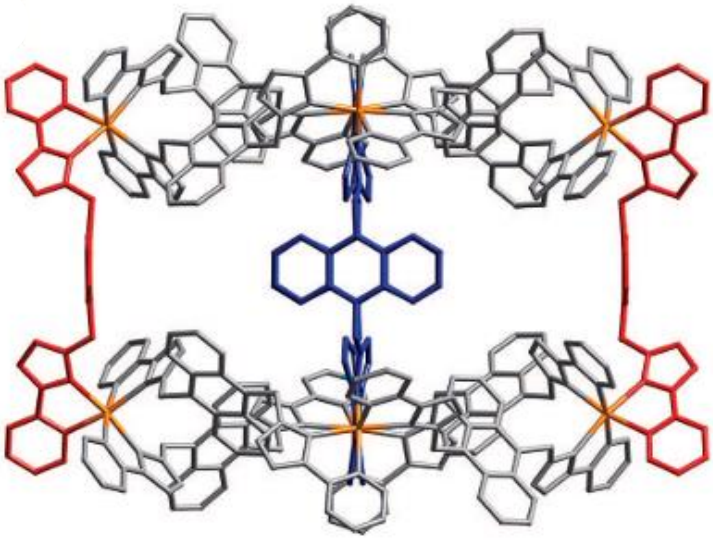

Figure 1.40 – The $L^{9,10\text{-anth}}$ ligand forms a M_8L_{12} cube crystal structure but dissociates in solution into its constituent parts.[77]

1.9. The M_8L_{12} Cube

The cage formed upon complexation of the ligand $L^{1,5\text{-naph}}$ to transition metal dications such as Co(II) or Cd(II) is an M_8L_{12} cube with S_6 symmetry, differing from the cube structures formed by previous ligands. There is extensive π-stacking between electron-poor PyPz units and electron-rich naphthalene units that alternate around the cage's periphery. This structural feature imparts stability and as a result this complex retains its structural integrity in solution.[77]

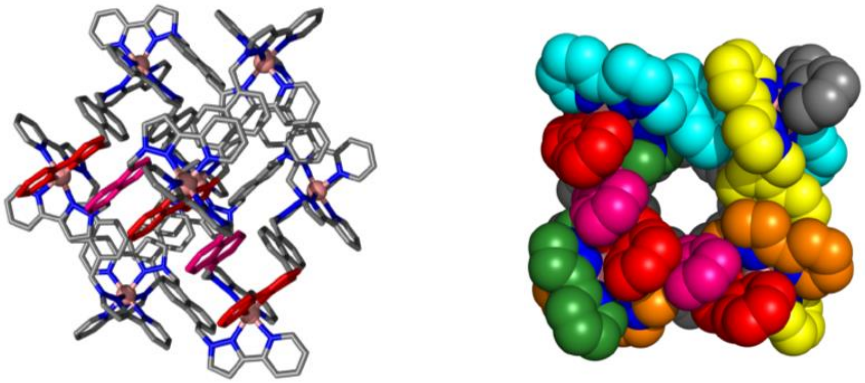

Figure 1.41 – Crystal structure of the $L^{1,5\text{-naph}}$ M_8L_{12} cube. The inter-ligand π-stacking is highlighted on the left diagram.[77]

As mentioned, the symmetry of the cage is S_6; a diagonally opposite pair of metal ions have a facial tris-chelate arrangement, with the other six being meridional. The symmetry within the structure simplifies the ^{1}H NMR spectrum greatly, with two independent ligand environments (one sixth of the cage structure is unique) leading to a total of 44 individual proton signals. The two ligand environments are those that connect one of the two *fac*- vertices to a *mer*- vertex and those that bridge two *mer*-vertices. ^{1}H NMR spectroscopy studies of the isostructural Cd cage confirm the 2:6 *fac:mer* metal ratio through a 1:3 peak integral ratio in the ^{113}Cd NMR spectrum (Figure 1.42).

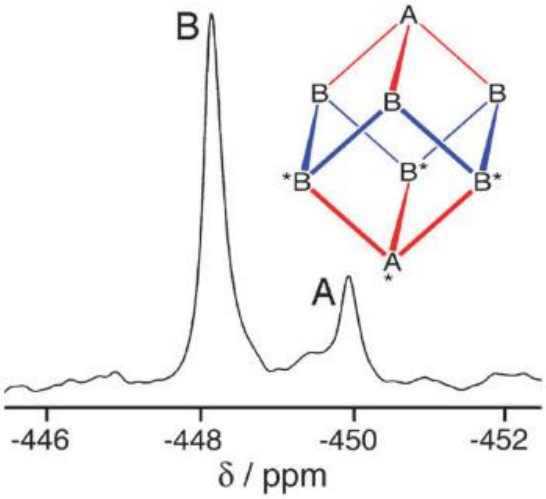

Figure 1.42 – ^{113}Cd NMR region of the $L^{1,5\text{-naph}}$ cube. The 1:3 ratio denotes the 2:6 ratio of *fac*:*mer* geometries present at the metal vertices.[77]

The *fac*-tris-chelate metal vertices are an important feature of this cube. At these two points, the ligands are arranged in such a way that protons from the ligands are convergent in the cage's cavity, forming an H-bond donor site which is where guests with electron-rich atoms can bind. Combined with the large cavity (volume 407 Å^3), potential was seen for guest binding to be investigated.

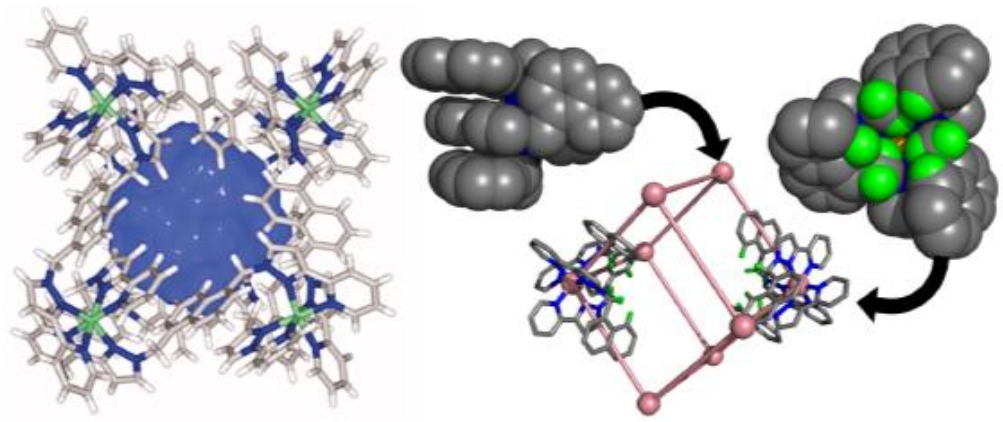

Figure 1.43 – Left: crystal structure of the $L^{1,5\text{-naph}}$ cube with the cavity illustrated by the blue sphere. Right: the converging C-H protons that form a 'binding pocket' at the two *fac*- sites.

To probe the cage's guest binding ability, a library of 23 potential guests was evaluated for binding by ^{1}H NMR titrations. Most of this set were planar aromatic guests with molecular volumes ranging from 88 to 261 Å^3 and with a variety of functional groups present. The accessible volume of the cavity was calculated to be

407 Å^3, which when applying Rebek's rule of 55% gives an ideal guest molecular volume of 224 Å^3.[78] Surprisingly, the only guest out of the initial set of 23 which caused a change in the cage's NMR spectrum indicating guest binding, was coumarin, calculated to bind with K = 78 M^{-1}. The interaction between host and guest was attributed to be the formation of H bonds between the *fac*- site H-bond donor array and the carbonyl group of coumarin.[79]

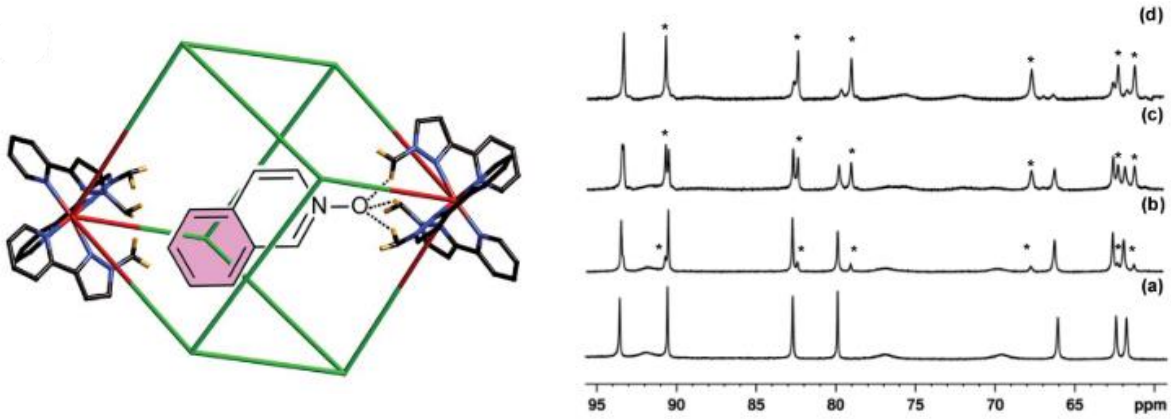

Figure 1.44 – Left: a guest molecule (isoquinoline N-oxide) binding within the cavity through H-bond interactions with the *fac*- site. Right: the changes observed by NMR as the guest binds (studies conducted in deuterated acetonitrile).[77]

The factors underpinning guest binding in acetonitrile were looked into further through binding studies of guests isostructural with coumarin but with differing hydrogen bond accepting groups. Guest binding was again followed by ^{1}H NMR spectroscopy, with signals for the host and free guest gradually replaced with bound guest peaks as the titration progressed. Integration of the **H·G** peaks allowed for binding constants to be calculated for each guest, the results of which showed a clear correlation between H-bond acceptor strength of the guest (β value) and association constant K. Comparison of bicyclic and monocyclic guests also revealed higher K values for bicyclic guests, suggesting that aromatic interactions were contributing to the binding process as well. The highest binding constant calculated in this study was 2100 M^{-1} for isoquinoline N-oxide, which had the highest β value at 9.8 and is consequently the best H-bond acceptor of the group.[80]

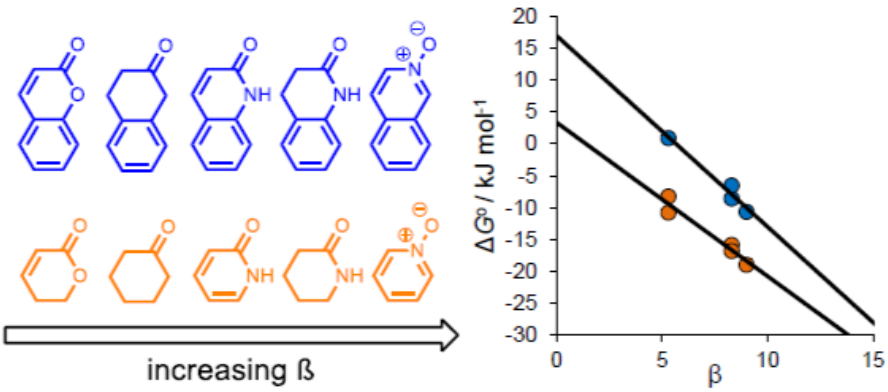

Figure 1.45 – Increasing β value (H-bond acceptor strength) relates directly to the strength of guest binding in acetonitrile (ΔG).[78]

As all binding studies to this point had been conducted in d_3-MeCN, a water-soluble cage system was sought after to exploit the hydrophobic effect as a driving force in guest binding. The resulting cage, $\mathbf{H^W}$, is isostructural with the previous complex but features two CH_2OH pendent groups per ligand. These groups face outwards into the surrounding solvent and help to solubilise the assembly in water. Repeating the binding experiments that were conducted with the previous unsubstituted host $\mathbf{H^A}$ in d_3-MeCN with the new analogue in D_2O produced higher binding constants for most of the guests, as expected given that the hydrophobic effect is now also operating. The trend of higher *K* values for higher β values was seen to reverse, however, presumably because the guests now form stronger H-bonds with the bulk water than with the interior of the cage.[81]

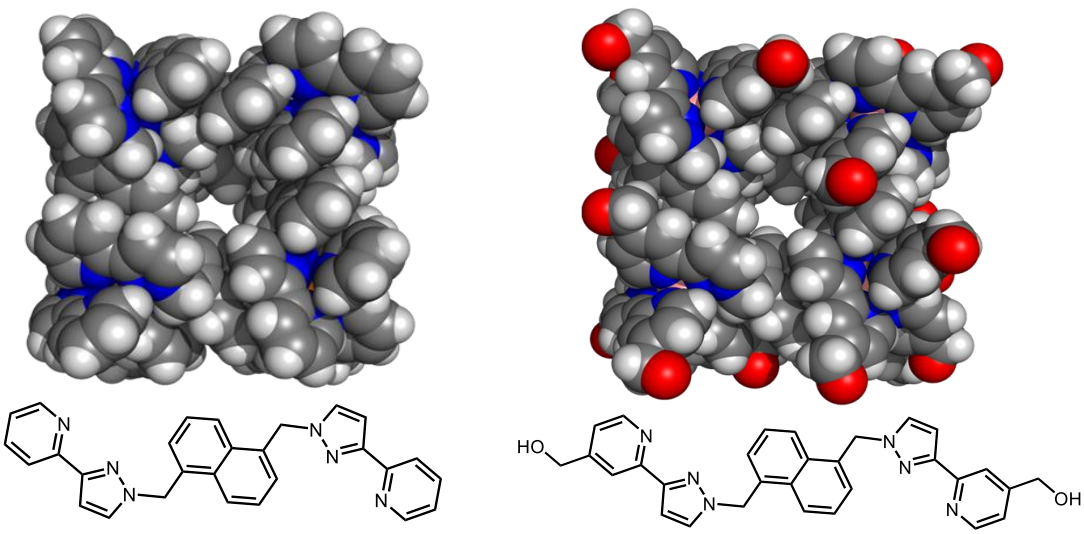

Figure 1.46 – The isostructural cages H^A and H^W and the ligands used in their assembly. 'A' denotes acetonitrile soluble and 'W' denotes water soluble.[76]

Whilst the procedure of finding guests that bind in the cage cavity was proving reasonably successful, there was a lot of time-consuming and expensive trial and error involved. Looking to improve the chances of success for identifying potential guests, the software GOLD was employed (GOLD = Genetic Optimisation of Ligand Docking) to calculate cage/guest binding strengths in water and thereby help to identify new guests. The use of this *in silico* method allowed for greatly increased guest screening whilst not using any chemicals and could be run from the comfort of a desk in the office.

By calculating the binding constants for a library of known guests, to calibrate the software, the scoring function for log *K* values could be adjusted as needed until predicted binding values matched known ones as well as possible. The final equation to predict binding based on a set of known guest parameters can be seen below:

$$\log K_{calc} = -4.48f(\text{ligand\_clash}) + 0.20f(\text{part\_buried}) - 0.10f(\text{non-polar}) + 0.90f(\text{ligand\_torsion}) - 0.93f(\text{ligand\_flexibility})$$

Equation 1.1 – Updated scoring function for guest binding using the software package GOLD.

Using the above scoring function, 3000 potential new guests were screened using GOLD. Of the best results, 15 guests were chosen that had high predicted log *K* values. These guests had their *K* values determined experimentally to compare to those calculated by GOLD. The set were all found to bind with free energy values close to the predicted values, confirming the predictive value of the GOLD screening process. Encouragingly the root mean square deviation was equal for the new guests to the training set of guests (0.79 for both).[82]

Guest binding could now be tested preliminarily before being experimentally confirmed – a big step forward for discovering new host-guest systems. The final piece of the puzzle was the method of binding. It was already known that the hydrophobic effect was at work for host-guest interactions for this cage in water, but as mentioned earlier in this introduction there is more than one model for the hydrophobic effect.[49]

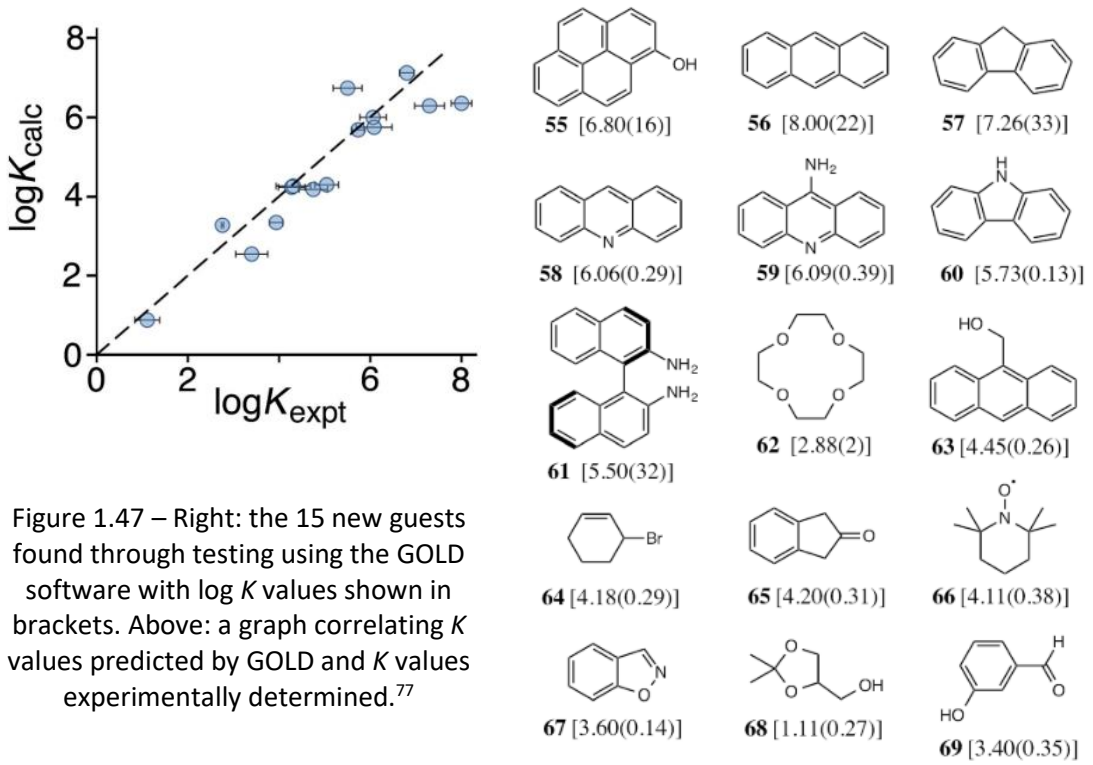

Figure 1.47 – Right: the 15 new guests found through testing using the GOLD software with log *K* values shown in brackets. Above: a graph correlating *K* values predicted by GOLD and *K* values experimentally determined.[77]

Crystals of the water-soluble cage grown in the absence of a guest molecule show a cluster of water molecules residing within the cage's cavity. Ten individual water molecules occupy the cavity, forming a network of intermolecular hydrogen bonds between both themselves and the tetrafluoroborate anions that can be found in the portals on the cage's faces. Calculating the number of H-bonds per water molecule gave a value of *ca.* 3.2, notably lower than the average of 3.7 H-bonds per water molecule in bulk solution. This shortage of H-bonding is the source of the high-energy or 'frustrated' water molecules inside supramolecular cavities. Upon guest binding, the release of these water molecules into the bulk solution allows them to form additional H-bonds with water molecules which is enthalpically favourable. NMR studies on guest binding at varying temperatures allowed analysis of the binding action through a Van't Hoff plot. For all guests examined, ΔG for binding was dominated by the negative ΔH term – consistent with the release of high-energy water and a principally enthalpy-based hydrophobic effect.[51]

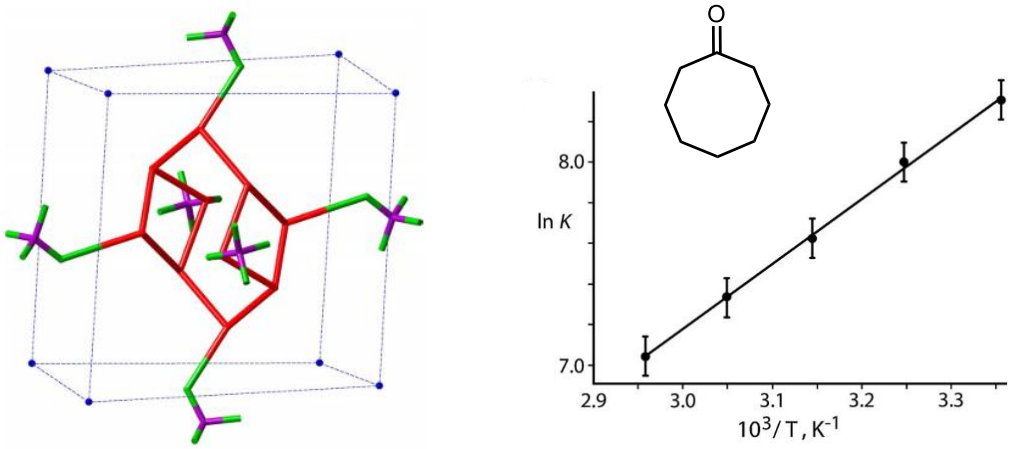

Figure 1.48 – Left: a network of hydrogen bonds between BF_4^- anions in the 'windows' of the cage's faces and the 10 water molecules residing inside the cavity. Right: a Van't Hoff plot for a cyclooctanone guest molecule binding at varying temperatures.[46]

The image seen on the left in Figure 1.48 provides a nice segue into the interactions of species with the cage's surface. In this instance, the BF_4^- anions surrounding the cage and counterbalancing the positive charge of the Co(II) ions also network with water molecules situated inside the cavity of the cage. In crystal structures, anions such as BF_4^- or Cl^- can be seen residing in the 'windows' on the faces of the cage, as they are often a complimentary size for the diameter of the portal. Larger anions such as phenolates have also been demonstrated to interact with the cage's exterior through the formation of H-bonds between protons on the ligands of the cage and the anionic oxygen of the phenolate; this interaction of anions with the cage's surface is a recurring theme of the work presented in the following chapters of this thesis.

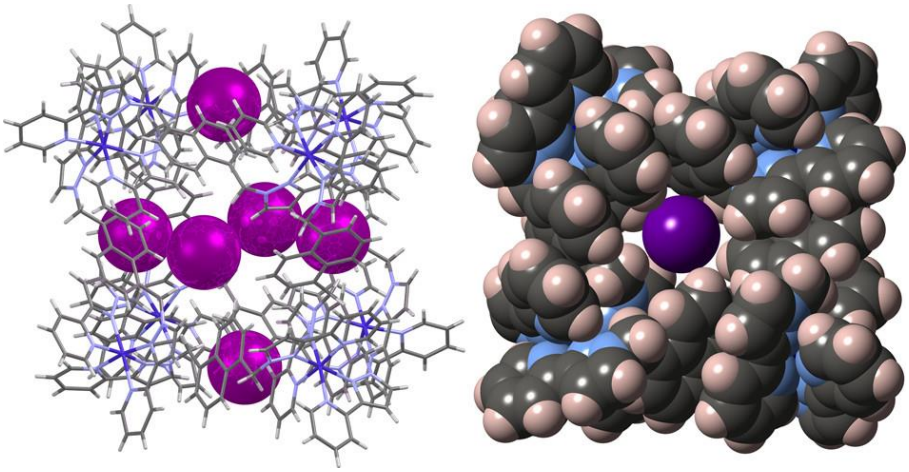

Figure 1.49 – A crystal structure of the M_8L_{12} cube featuring iodide anions in each of the 'windows' on the faces of the cage.

1.10. Project Aims

The introduction to this thesis contains multiple examples of the interesting and unconventional chemistry that occurs inside cavities of coordination cages. The focus has been primarily on guest binding within the hollow containers, and resulting examples of catalysis, transport and sensing all based on guest binding in the cage cavity. In contrast to this, reports of guest interactions with the *exterior* of coordination cages are scarcer, as the relative amount of content for cavity- and surface-based interactions discussed within this introduction exemplifies. Previous work within the Ward group has detailed the interactions of anions associated with the exterior of cages – in the regions proximal to highly positive metal ions several C–H···X^- interactions can form.[83] Anions also reside in the 'windows' found on the faces of the cubic cage as many are a good fit for the diameter of the portal. More recent crystallography studies have revealed that small organic guests will interact with the cage's exterior as well as binding inside the cavity. This has been echoed by work undertaken by Nitschke and Raymond.[84,85]

This project sets out to explore the potential of coordination cage surfaces for applications that have been previously demonstrated using the cavity of a supramolecule, namely sensing of guest molecules/anions and catalysis. Chapter 2 details an investigation into the solubilising effects of changing the counter-anion of the cubic $[M_8L_{12}]^{16+}$ coordination cage followed by investigating the effect of different anions' presence on a Kemp elimination reaction catalysed by the same cage. Chapter 3 describes the design and results of a fluorescence displacement assay for anions that can interact with the cage's exterior, along with binding of several fluorescent species and the differences in properties such as stoichiometry between surface and cavity binding. Chapter 4 reports development of a colourimetric RGB sensor which produces differing fluorescence responses depending on the 'mode' of analyte binding, and can distinguish between species that cavity bind, surface bind or can occupy both the interior and exterior of the cage. Chapter 5 introduces a new mixed-metal cubic cage along with a comparative study of binding both cavity-bound and surface-bound fluorophores.

1.11. References

1 G. R. Desiraju, *Nature*, 2001, **412**, 397–400.

2 K. L. Wolf, H. Frahm and H. Harms, *Zeitschrift für Phys. Chemie*, 1937, **36**, 237–287.

3 J. D. Watson and F. H. C. Crick, *Nature*, 1953, 171, 737–738.

4 C. J. Pedersen, *J. Am. Chem. Soc.*, 1967, **89**, 2495–2496.

5 D. J. Cram and J. M. Cram, *Science*, 1974, **183**, 803–809.

6 B. Dietrich, J. P. Sauvage and J. M. Lehn, *Tetrahedron Lett.*, 1969, **10**, 2889–2892.

7 Nobel Media AB 2020., The Nobel Prize in Chemistry 2016.

8 J. S. Lindsey, *New J. Chem.*, 1991, **15**, 153–180.

9 J. W. Steed and J. L. Atwood, *Supramolecular Chemistry*, Wiley, 2nd edn., 2009.

10 A. Klug, *Philos. Trans. R. Soc. Lond. B. Biol. Sci.*, 1999, **354**, 531–5.

11 L. M. Greig and D. Philp, *Chem. Soc. Rev.*, 2001, **30**, 287–300.

12 D. A. Uhlenheuer, K. Petkau and L. Brunsveld, *Chem. Soc. Rev.*, 2010, **39**, 2817–2826.

13 C. Schalley, *Analytical Methods in Supramolecular Chemistry*, 2007.

14 J. P. Glusker, Springer, Berlin, Heidelberg, 1998, pp. 1–56.

15 A. Pfeil and J. M. Lehn, *J. Chem. Soc. Chem. Commun.*, 1992, 838–840.

16 L. K. S. Von Krbek, C. A. Schalley and P. Thordarson, *Chem. Soc. Rev.*, 2017, 46, 2622–2637.

17 C. A. Hunter and H. L. Anderson, *Angew. Chemie - Int. Ed.*, 2009, **48**, 7488–7499.

18 J. M. Lehn, A. Rigault, J. Siegel, J. Harrowfield, B. Chevrier and D. Moras, *Proc.*

Natl. Acad. Sci. USA, 1987, **84**, 2565–2569.

19 J. R. Nitschke and J. M. Lehn, *Proc. Natl. Acad. Sci. U. S. A.*, 2003, **100**, 11970–11974.

20 D. L. Caulder and K. N. Raymond, *Angew. Chemie Int. Ed. English*, 1997, **36**, 1440–1442.

21 M. Fujita, J. Yazaki and K. Ogura, *J. Am. Chem. Soc.,* 1990, **112**, 5646–5648.

22 R. V Slone, J. T. Hupp, C. L. Stern and T. E. Albrecht-Schmitt, *Inorg. Chem.*, 1996, **35**, 4096–4097.

23 P. J. Stang, *Chem. - A Eur. J.*, 1998, **4**, 19–27.

24 R. W. Saalfrank, A. Stark, K. Peters and H. G. von Schnering, *Angew. Chemie Int. Ed. English*, 1988, **27**, 851–853.

25 D. L. Caulder, R. E. Powers, T. N. Parac and K. N. Raymond, *Angew. Chemie Int. Ed.*, 1998, **37**, 1840–1843.

26 S. Leininger, B. Olenyuk and P. J. Stang, *Chem. Rev.*, 2000, **100**, 853–908.

27 M. Fujita and K. Ogura, *Bull. Chem. Soc. Jpn.*, 1996, **69**, 1471–1482.

28 D. L. Caulder and K. N. Raymond, *Acc. Chem. Res.*, 1999, **32**, 975–982.

29 D. K. Chand, K. Biradha, M. Kawano, S. Sakamoto, K. Yamaguchi and M. Fujita, *Chem. - An Asian J.*, 2006, **1**, 82–90.

30 M. Fujita, O. Sasaki, T. Mitsuhashi, T. Fujita, J. Yazaki, K. Yamaguchi and K. Ogura, *Chem. Commun.*, 1996, 1535–1536.

31 N. C. Seeman, *Nature*, 2003, 421, 427–431.

32 J. P. Mathias, C. T. Seto, E. E. Simanek and G. M. Whitesides, *J. Am. Chem. Soc.*, 1994, **116**, 1725–1736.

33 J. Kang and J. Rebek J., *Nature*, 1996, **382**, 239–241.

34 P. R. Ashton, T. T. Goodnow, A. E. Kaifer, M. V. Reddington, A. M. Z. Slawin, N. Spencer, J. F. Stoddart, C. Vicent and D. J. Williams, *Angew. Chemie Int. Ed.*

English, 1989, **28**, 1396–1399.

35 Q. F. Sun, J. Iwasa, D. Ogawa, Y. Ishido, S. Sato, T. Ozeki, Y. Sei, K. Yamaguchi and M. Fujita, *Science*, 2010, **328**, 1144–1147.

36 J. Bunzen, J. Iwasa, P. Bonakdarzadeh, E. Numata, K. Rissanen, S. Sato and M. Fujita, *Angew. Chemie - Int. Ed.*, 2012, **51**, 3161–3163.

37 D. Fujita, Y. Ueda, S. Sato, N. Mizuno, T. Kumasaka and M. Fujita, *Nature*, 2016, **540**, 563–566.

38 C. J. Pedersen, *Science*, 1988, **241**, 536–540.

39 A. Tripathi and V. A. Bankaitis, *J. Mol. Med. Clin. Appl.*, 2017, **2(1)**, DOI:10.16966/2575-0305.106.

40 C. A. Hunter, *Angew. Chemie - Int. Ed.*, 2004, **43**, 5310–5324.

41 C. A. Hunter and J. K. M. Sanders, *J. Am. Chem. Soc.*, 1990, **112**, 5525–5534.

42 F. Cozzi, M. Cinquini, R. Annuziata and J. S. Siegel, *J. Am. Chem. Soc.*, 1993, **115**, 5330–5331.

43 S. L. Cockroft, C. A. Hunter, K. R. Lawson, J. Perkins and C. J. Urch, *J. Am. Chem. Soc.*, 2005, **127**, 8594–8595.

44 A. Sygula, F. R. Fronczek, R. Sygula, P. W. Rabideau and M. M. Olmstead, *J. Am. Chem. Soc.*, 2007, **129**, 3842–3843.

45 H. J. Schneider, *Angew. Chemie - Int. Ed.*, 2009, **48**, 3924–3977.

46 N. Muller, *Acc. Chem. Res.*, 1990, **23**, 23–28.

47 C. Tanford, *Proc. Natl. Acad. Sci.*, 1979, **76**, 4175–4176.

48 F. Biedermann, V. D. Uzunova, O. A. Scherman, W. M. Nau and A. De Simone, *J. Am. Chem. Soc.*, 2012, **134**, 15318–15323.

49 F. Biedermann, W. M. Nau and H. J. Schneider, *Angew. Chemie - Int. Ed.*, 2014, **53**, 11158–11171.

50 S. M. Biros, R. G. Bergman and K. N. Raymond, *J. Am. Chem. Soc.*, 2007, **129**,

12094–12095.

51 A. J. Metherell, W. Cullen, N. H. Williams and M. D. Ward, *Chem. - A Eur. J.*, 2018, **24**, 1554–1560.

52 J. Kang and J. Rebek, *Nature*, 1997, **385**, 50–52.

53 J. Kang, J. Santamaria, G. Hilmersson and J. Rebek J., *J. Am. Chem. Soc.*, 1998, **120**, 7389–7390.

54 Y. Nishioka, T. Yamaguchi, M. Yoshizawa and M. Fujita, *J. Am. Chem. Soc.*, 2007, **129**, 7000–7001.

55 M. Yoshizawa and M. Fujita, *Pure Appl. Chem.*, 2005, **77**, 1107–1112.

56 D. Fiedler, R. G. Bergman and K. N. Raymond, *Angew. Chemie - Int. Ed.*, 2004, **43**, 6748–6751.

57 M. L. Merlau, M. D. P. Mejia, S. T. Nguyen and J. T. Hupp, *Angew. Chemie - Int. Ed.*, 2001, **40**, 4239–4242.

58 C. M. Starks, C. L. Liotta, M. E. Halpern, C. M. Starks, C. L. Liotta and M. E. Halpern, in *Phase-Transfer Catalysis*, Springer Netherlands, 1994, pp. 1–22.

59 H. Ito, T. Kusukawa and M. Fujita, *Chem. Lett.*, 2000, 598–599.

60 A. B. Grommet and J. R. Nitschke, *J. Am. Chem. Soc.*, 2017, **139**, 2176–2179.

61 A. B. Grommet, J. B. Hoffman, E. G. Percástegui, J. Mosquera, D. J. Howe, J. L. Bolliger and J. R. Nitschke, *J. Am. Chem. Soc.*, 2018, **140**, 14770–14776.

62 D. Zhang, T. K. Ronson, R. Lavendomme and J. R. Nitschke, *J. Am. Chem. Soc.*, 2019, **141**, 18949–18953.

63 S. L. Wiskur, H. Ait-Haddou, J. J. Lavigne and E. V. Anslyn, *Acc. Chem. Res.*, 2001, **34**, 963–972.

64 B. T. Nguyen and E. V. Anslyn, *Coord. Chem. Rev.*, 2006, **250**, 3118–3127.

65 R. V. Slone, D. I. Yoon, R. M. Calhoun and J. T. Hupp, *J. Am. Chem. Soc.*, 1995, **117**, 11813–11814.

66 P. De Wolf, S. L. Heath and J. A. Thomas, *Chem. Commun.*, 2002, **8**, 2540–2541.

67 P. De Wolf, P. Waywell, M. Hanson, S. L. Heath, A. J. H. M. Meijer, S. J. Teat and J. A. Thomas, *Chem. - A Eur. J.*, 2006, **12**, 2188–2195.

68 P. P. Neelakandan, A. Jiménez and J. R. Nitschke, *Chem. Sci.*, 2014, **5**, 908–915.

69 M. D. Ward, *Chem. Commun.*, 2009, 4487–4499.

70 R. L. Paul, A. J. Amoroso, P. L. Jones, S. M. Couchman, Z. R. Reeves, L. H. Rees, J. C. Jeffery, J. A. McCleverty and M. D. Ward, *J. Chem. Soc. Dalt. Trans.*, 1999, 1563–1568.

71 J. S. Fleming, K. L. V Mann, C. A. Carraz, E. Psillakis, J. C. Jeffery, J. A. McCleverty and M. D. Ward, *Angew. Chemie - Int. Ed.*, 1998, **37**, 1279–1281.

72 R. L. Paul, Z. R. Bell, J. C. Jeffery, J. A. McCleverty and M. D. Ward, *Proc. Natl. Acad. Sci.*, 2002, **99**, 4883–4888.

73 R. L. Paul, Z. R. Bell, J. S. Fleming, J. C. Jeffery, J. A. McCleverty and M. D. Ward, *Heteroat. Chem.*, 2002, **13**, 567–573.

74 S. P. Argent, H. Adams, L. P. Harding and M. D. Ward, *Dalt. Trans.*, 2006, 542–544.

75 S. P. Argent, H. Adams, T. Riis-Johannessen, J. C. Jeffery, L. P. Harding, O. Mamula and M. D. Ward, *Inorg. Chem.*, 2006, **45**, 3905–3919.

76 W. Cullen, C. A. Hunter and M. D. Ward, *Inorg. Chem.*, 2015, **54**, 2626–2637.

77 I. S. Tidmarsh, T. B. Faust, H. Adams, L. P. Harding, L. Russo, W. Clegg and M. D. Ward, *J. Am. Chem. Soc.*, 2008, **130**, 15167–15175.

78 S. Mecozzi and J. Rebek, *Chem. - A Eur. J.*, 1998, **4**, 1016–1022.

79 S. Turega, M. Whitehead, B. R. Hall, M. F. Haddow, C. A. Hunter and M. D. Ward, *Chem. Commun.*, 2012, **48**, 2752–2754.

80 S. Turega, M. Whitehead, B. R. Hall, A. J. H. M. Meijer, C. A. Hunter and M. D. Ward, *Inorg. Chem.*, 2013, **52**, 1122–1132.

81 M. Whitehead, S. Turega, A. Stephenson, C. A. Hunter and M. D. Ward, *Chem. Sci.*, 2013, **4**, 2744.

82 W. Cullen, S. Turega, C. A. Hunter and M. D. Ward, *Chem. Sci.*, 2015, **6**, 2790–2794.

83 M. D. Ward, C. A. Hunter and N. H. Williams, *Acc. Chem. Res.*, 2018, **51**, 2073–2082.

84 F. J. Rizzuto, W.-Y. Wu, T. K. Ronson and J. R. Nitschke, *Angew. Chemie*, 2016, **128**, 8090–8094.

85 C. Sgarlata, J. S. Mugridge, M. D. Pluth, B. E. F. Tiedemann, V. Zito, G. Arena and K. N. Raymond, *J. Am. Chem. Soc.*, 2010, **132**, 1005–1009.

Chapter 2

Anion interactions with the host cage H^W and their effect on catalysis

2.1. Introduction

Within the field of supramolecular chemistry, a multitude of intermolecular interactions are observable, which contribute to the formation of supramolecular complexes *via* self-assembly. Interactions such as hydrogen bonding, π-π stacking, van der Waals forces and electrostatic interactions were mentioned and described in the previous chapter.[1–3] One area that has not yet been covered, however, is the interaction of anions with supramolecular architectures. Using metal ions as a component in coordination complexes usually also introduces anions to the system as a means of reaching a neutral net charge for the complex, unless the ligand used is itself anionic such as the catecholates reported by Saalfrank and Raymond.[4,5,6]

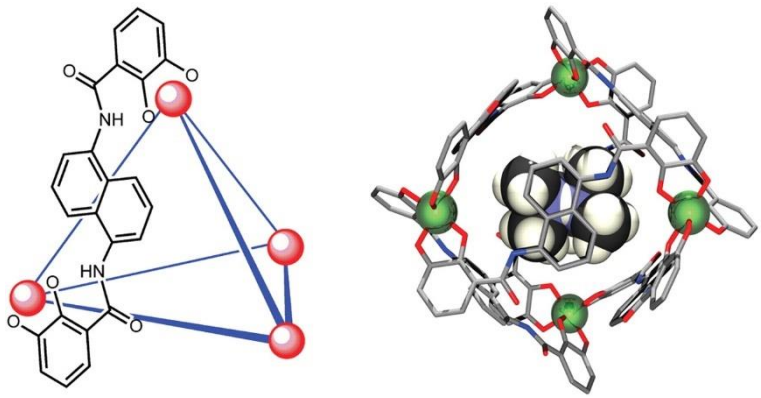

Figure 2.1 – Raymond's M_4L_6 tetrahedron uses catechol donor oxygens to coordinate to the metal, giving an overall charge of 12- for the assembly.[6]

In many cases, anions will interact with the (cationic) supramolecular assembly. Attractive electrostatic interactions between the positively charged cage and negative anions will be present, but other interactions may also be at play. Anions and π-systems can interact ('anion-π' interactions) due to the unique charge distribution seen in for electron-deficient aromatic systems.[7] A positive quadrupole moment as seen for neutral molecules such as C_6F_6, denoted as Q_{zz}, allows interaction with negatively charged anions. Larger quadrupole moments produce a greater contribution to electrostatic interactions.[8]

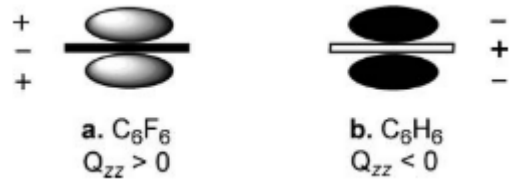

Figure 2.2 – Electron density diagrams for electron-deficient and electron-rich systems.[8]

Anions can also interact with H-bond donors. The positive partial charge on the H-atom of a hydrogen bond donor will interact favourably with a negatively charged anion through an electrostatic effect. These H-bond/anion interactions are prevalent in natural systems such as proteins of *E. Coli* and *S. typhimurium,* which bind dihydrogen phosphate and sulfate anions, respectively. The array of H-bond donors in these systems is orientated such that they complement the tetrahedral shape of phosphate or sulfate perfectly; this produces selective binding of these anions only.[9] The preorganisation seen in natural systems such as these is designed to overcome the high strength of anion solvation by surrounding water molecules – a common problem with anion recognition in aqueous environments.

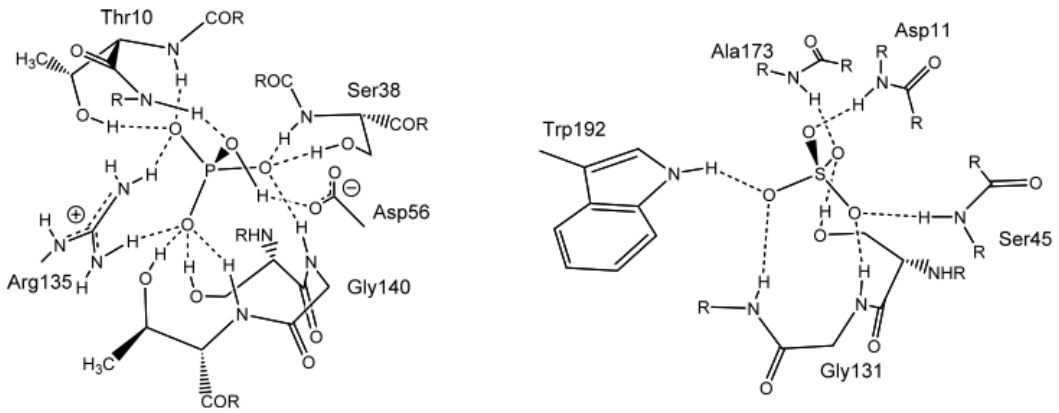

Figure 2.3 – Anion receptors found in natural systems form multiple H-bonds through proximal donor groups.[9]

This principle has been transcribed into design of synthetic receptors for anions, for example using amide groups. The macrocyclic anion receptors such as those reported separately by Beer and Anslyn utilise cavity-directed amide H-bonds to bind anionic species.[10,11]

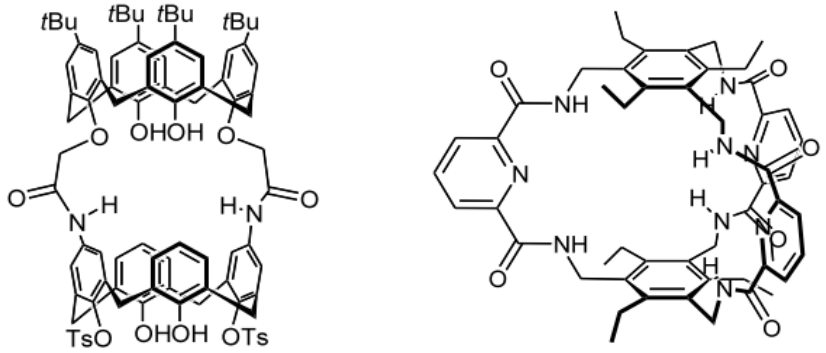

Figure 2.4 – Left: A calix[4]arene based macrocycle capable of binding F^- and Cl^- anions reported by Beer.[10] Right: Anslyn's bicyclic cyclophane featuring an ensemble of inwards facing N-H bonds that will interact with anions.[11]

Metal-incorporating supramolecular structures have also been designed for anion-specific binding. Work from as early as 2004 by Gale, Loeb and co-workers reported platinum-based square planar complexes that could change conformation depending on the anion present.[12] The structure itself was loosely based on that of a calix[4]arene, with the square-planar Pt(II) ion acting as the point around which the H-bonding arms were assembled. For anions such as the halide series, Cl^-, Br^- and I^-, a 2:1 anion:complex stoichiometry was seen, as two separate receptors could interact with the anions independently. With sulfate and phosphate, the conformation of the host changes to a 'cone' shape, with all four arms pointing upwards and lying on the same face as the Pt(II) complex, providing a H-bond donor array which converged on a single anion.

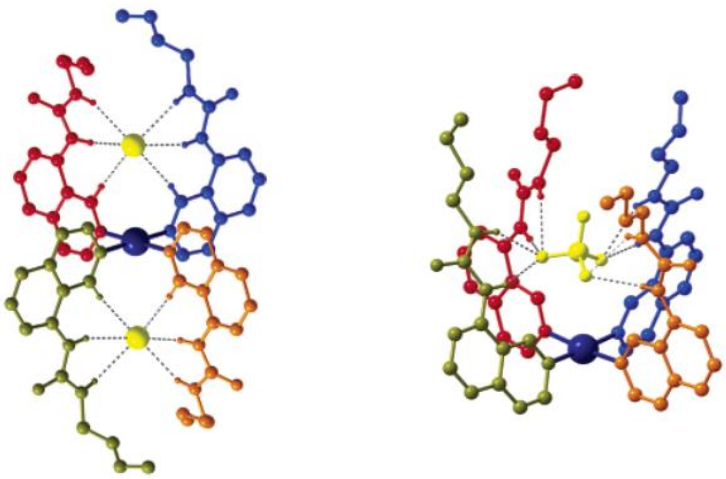

Figure 2.5 – The two conformations adopted by the Pt(II) complex: a two-up, two-down configuration capable of binding two separate anions or a cone shape which surrounds a SO_4^{2-} anion.[12]

An example that does not rely on amide N–H donors to complex an anion is the tripodal metallocryptand reported by Fabbrizzi and coworkers.[13] Combination of a predesigned ligand featuring bipyridyl units with Fe(II) gives a cage with a cavity large enough to bind anions. The electron density on the imidazolium C-H protons is reduced further by the positive charge on the neighbouring nitrogen atom, enhancing their ability as H-bond donors. Both spherical ions such as Cl^- or Br^- and linear ions such as N_3^-, NCO^- or NCS^- were found to bind.

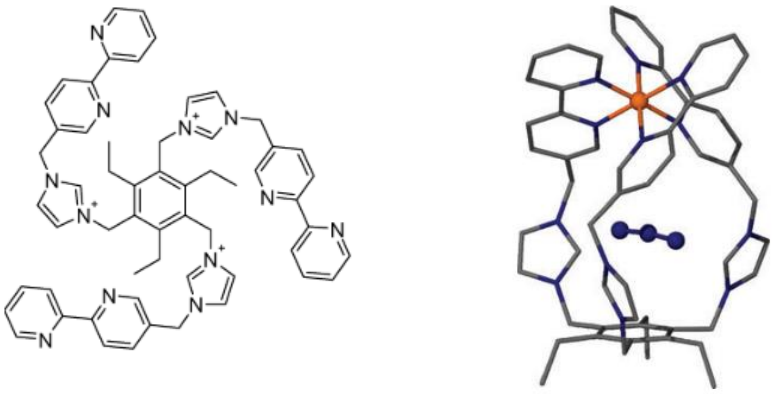

Figure 2.6 – Fabbrizzi's tripodal metallocryptand and the complex formed upon addition of Fe(II) which can uptake anions such as N_3^-, pictured.[13]

Several examples of metal-ligand complexes incorporating electron-deficient aromatic systems have also been demonstrated to interact with anions. Work undertaken by the Dunbar group focuses heavily on the formation of supramolecular assemblies templated by the anion present. Using inherently electron-deficient ligands such as those shown in Figure 2.7 combined with metal ions, metallacycles of varying stoichiometries are formed.[14]

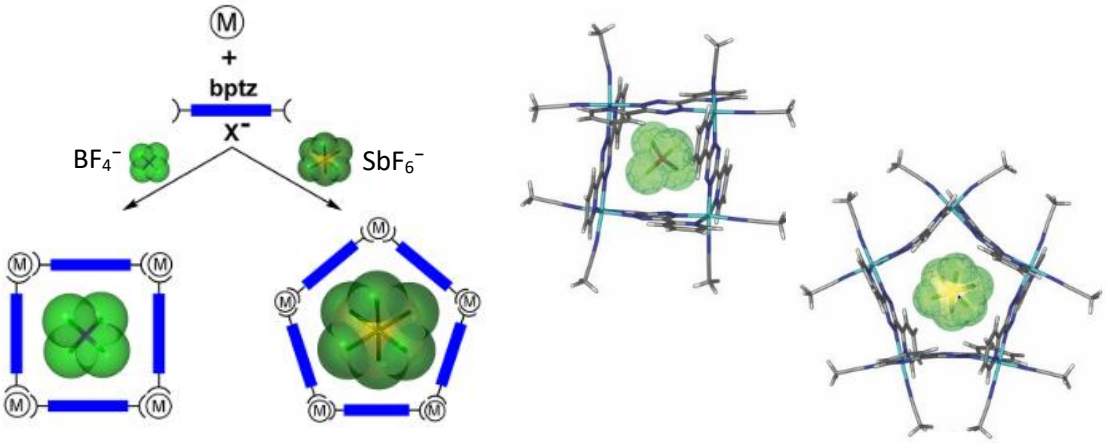

Figure 2.7 – Templation of metallacycles through a central anion produces different structures depending on the anion's size and shape.[14]

The nature of the counter-anion has a significant impact on the structure of the surrounding metal/ligand assembly. Smaller anions such as BF_4^- and ClO_4^- will preferentially template a molecular square, but larger anions such as SbF_6^- or PF_6^- form a pentagonal metal/ligand array. This difference in final product structure is attributed to the contacts formed between the electron-deficient (π-acidic) tetrazine core of the ligand and the anion.[15]

Templation plays a key role in the formation of these metallacycles, as has been seen in examples reported by other groups. One of the most famous examples of anion-based templation is Lehn's circular double helicate – containing a single Cl^- anion in its centre. The Cl^- anion is an integral part of this structure; mass spectrometry studies showed the chloride bound in all fragments found, hinting at a high association strength between the two.[16]

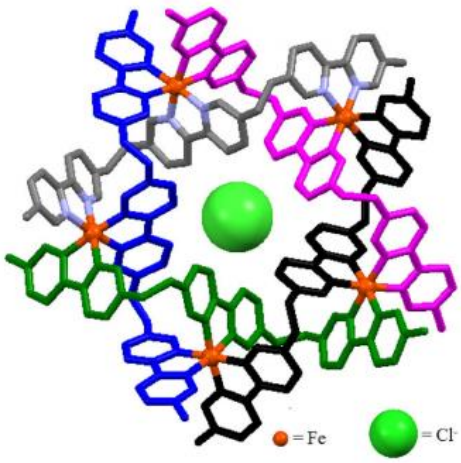

Figure 2.8 – Lehn's circular helicate with bound chloride ion in its centre.[17]

Templation of supramolecular assemblies by encapsulated anions has been shown to occur in structures reported by the Ward group. The M_4L_6 tetrahedron formed with $L^{o\text{-}Ph}$ contains a BF_4^- anion within its central cavity which remains tightly bound and does not leave the cavity in MeCN solution. Close inspection of the interactions between anion and surrounding cage shows the BF_4^- anion being complementary in both charge and shape to the cavity. With respect to the M_4L_6 tetrahedron, the BF_4^- anion is inverted such that each F atom is directed to the space at the centre of a

triangular face. This allows formation of multiple C-H•••F^- hydrogen bonds and assists the formation of the tetrahedron.[18]

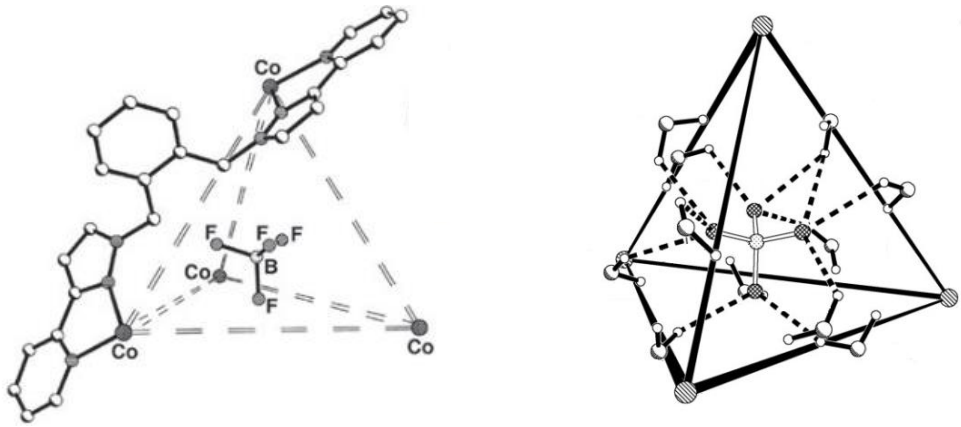

Figure 2.9 – Ward's tetrahedral M_4L_6 cage formed through templation using a BF_4^- anion within the cavity. Dashed lines on the right-hand figure indicate ligand-BF_4^- H-bonds.[18]

The nature of the anions present in a supramolecular system can often impart effects on the chemistry of the system. Water-soluble analogues of the cubic M_8L_{12} cage $\mathbf{H^A}$ (A = acetonitrile soluble) have been prepared through use of anion exchange resins. The first example given by the Ward group involves exchange of BF_4^- for Cl^-, as attempts to form the water-soluble chloride cage from ligand and $CoCl_2$ were unsuccessful. Forming the organic soluble cage with BF_4^- anions first then performing anion exchange with chloride renders the complex water-soluble whilst retaining structural integrity. Concentrations of up to 1 mM of cage in aqueous solution were reported.[19]

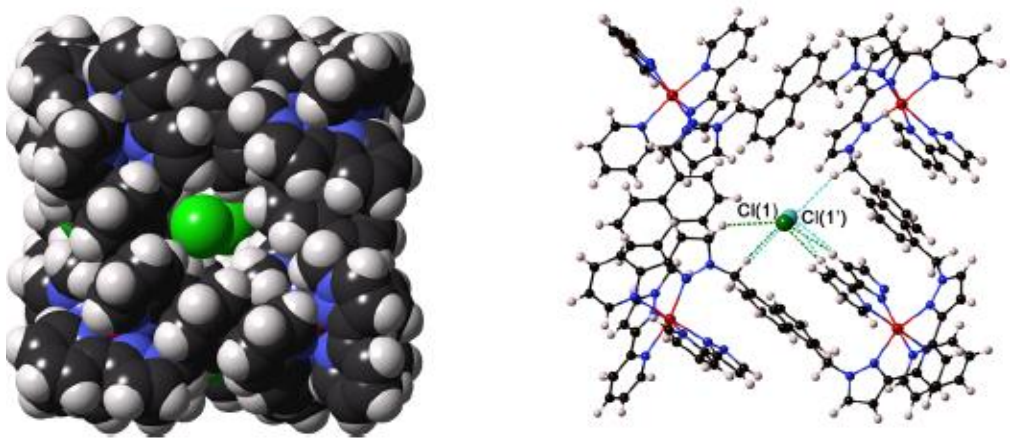

Figure 2.10 – A crystal structure of the anion exchanged cage H^A·Cl with chloride anion visible in the window on the near-side face of the cube.[19]

The first focus of this work was to convert the cage **H^A** to a water-soluble analogue using anions other than chloride in the search for a cage that behaved the same as **H^W** but without the more complicated ligand synthesis that is required to add the pendent hydroxymethyl groups. Chloride salts of unsubstituted **H^A**, whilst more water-soluble, tend to give reduced association constants for guests in aqueous solution compared to **H^W**, which has since been attributed to competition for the cage's cavity from the chloride ions.[20] Finding an anion that imparts water solubility on the cage **H^A** without also affecting the host-guest chemistry will quicken the synthetic route without the anion hindering guest binding.

2.2. Results and Discussion

2.2.1. Anion Exchange of cages

Nitschke and co-workers reported in 2017 that anion exchange of a porphyrin-faced cubic cage allowed a water-insoluble cage to become soluble in water. This was the first report of its kind and demonstrated how the properties of cages could vary by simply exchanging the anions associated with the structure. By substituting triflate anions with sulfate anions, the cage displays water solubility which can be reversed by changing the anions back to triflate.[21] This method has been used to utilise cages as phase-transport agents, carrying guests such as coronene between phases, triggered by exchange of anions.[22]

This work provided the initial impetus for the new results reported within this chapter. The water-solubility of the cage **H^W** is due not only to the peripheral hydroxymethyl groups but also the hydrolysis of the BF_4^- anions to fluoride and borate species. Whilst this method is straightforward, the exact composition of the mixture of anions generated by hydrolysis is unclear. Having an alternative that involves direct anion exchange using an agent such as a tetrabutylammonium or potassium salt should give more predictable and repeatable results and one clear product with a known anion composition. Borate was a logical choice of starting point as the cage **H^W** is stable with borate anions, the borate anion is highly hydrophilic, and its chemistry is already well documented.

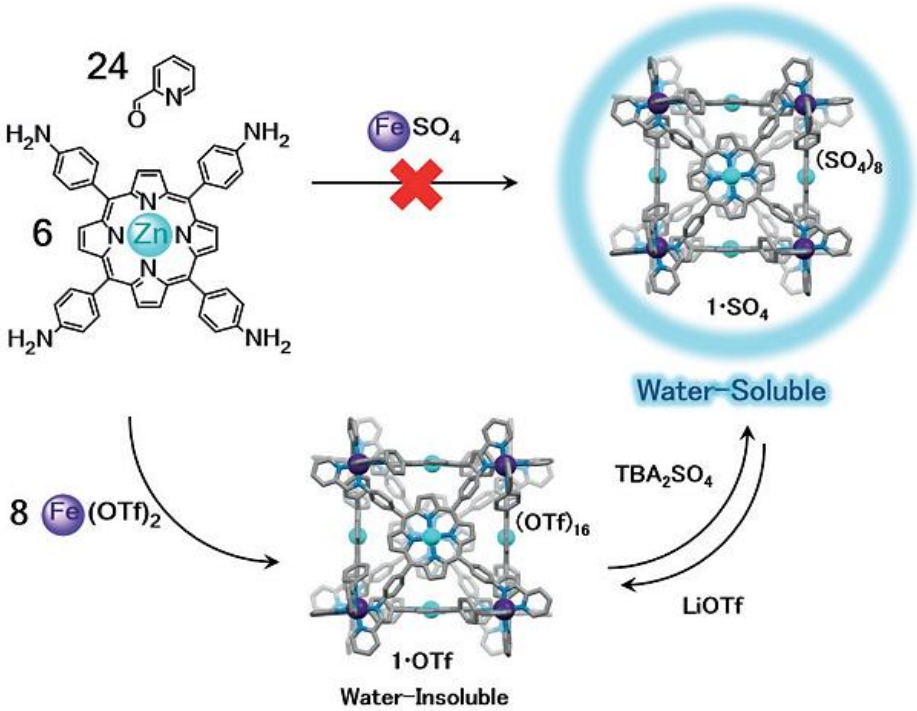

Figure 2.11 – The formation of a water-soluble cage from non-water-soluble components as reported by Nitschke.[21]

The tendency of cages to decompose when presented directly with a large excess of (possibly coordinating) anions prompted a search for a suitable method for the anion exchange, which lead to investigation into the possibility of modifying Dowex resin to mediate anion exchange. This 'resin' is based on a microporous copolymer of styrene and divinylbenzene which is then functionalised with quaternary ammonium cations. The surface of these polystyrene/DVB beads hosts mobile Cl^- anions that can exchange with anions in solution, or in this case the BF_4^- anions surrounding the cage. Consultation of the literature for reported uses of anion exchange resins such as Dowex provided the inspiration for the following work. Anion exchange resins are utilised as part of the process of water purification, whether it be to soften water through substitution of anions or to remove impurities such as dissolved organic matter.[23,24] A 2011 publication in the journal *Water Research* detailed how the mobile anion on anion exchange resins – in this case chloride – can be substituted through 'regeneration' using a salt solution of a different desired anion. The paper used the hydrogencarbonate (bicarbonate) anion, HCO_3^-. This seemed like a sensible starting point to test this anion-exchange method on the $[M_8L_{12}]^{16+}$ cages, and so a

bicarbonate-loaded Dowex resin was prepared as per the literature (see experimental section).[25]

To test the resin, 8 mg of cage **H^A** as its tetrafluoroborate salt, along with a generous amount of converted resin, was stirred in D_2O for 16 hours. The cage **H^A** is not soluble in water as its tetrafluoroborate salt, giving a cloudy suspension. With the resin present, the solution was disappointingly still cloudy, but rather than prematurely conclude that the resin had failed, the solution was filtered with use of a Millipore filter. This resulted in a clear, faintly orange solution which was analysed by ^{1}H NMR spectroscopy. Surprisingly, the spectrum clearly showed the presence of cage, with its characteristic set of peaks spread over a range of around 200 ppm.

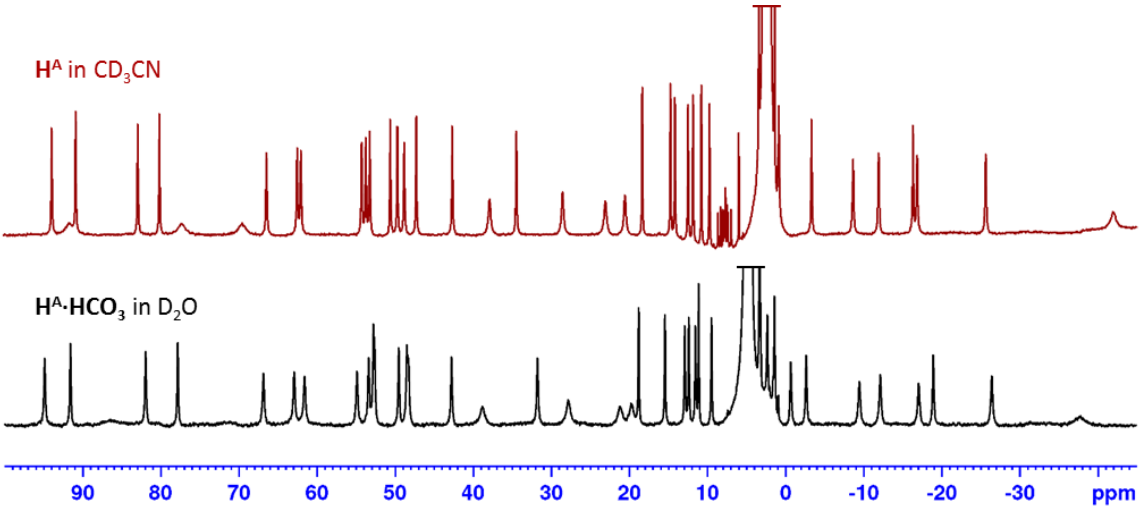

Figure 2.12 – The resulting NMR spectrum of the H^A/HCO_3^- stirred in D_2O.
The red spectrum is the original H^A/BF_4^- sample in CD_3CN.

Following this experiment, attempts were made to load a selection of other anions that were available as their sodium salts onto the same Dowex resin. The anions $B(OH)_4^-$, NO_3^-, $H_2PO_4^-$ and $S_2O_3^{2-}$ were all substituted for chloride on 5 mL portions of wetted Dowex resin. These converted resins were then used in attempts to water-solubilise samples of **H^A** in D_2O, as done with HCO_3^- previously. Suspensions of **H^A** powder and the substituted resins were stirred overnight in D_2O.

The samples containing **H^A·NO_3** and **H^A·S_2O_3** had cleared during the overnight stir, indicating solubilisation of **H^A** following successful exchange from tetrafluoroborate to a more hydrophilic anion, whereas the samples **H^A·H_2PO_4**, **H^A·$B(OH)_4$** and **H^A·Cl**

remained cloudy. After centrifuging the samples to separate out the solid resin from the sample, the resulting solutions were analysed by ^{1}H NMR spectroscopy. The spectra obtained are shown in Figure 2.13.

Despite three of the samples being cloudy after stirring with the anion-substituted Dowex for upwards of 16 hours (implying possible incomplete anion-exchange of the water-solubilising anions), after centrifugation there was a good amount of now water-solubilised cage detectable by ^{1}H NMR spectroscopy for all the samples tested apart from **H^A·B(OH)$_4$**. This was encouraging considering the broad range of anions used and how unrefined the method was at this stage. Another point worth making here is that each **H^A·X** (where X = Cl^-, NO_3^-, $H_2PO_4^-$ and $S_2O_3^{2-}$) sample has a distinct pattern to its ^{1}H peaks, with each being slightly different, confirming that the conversion of **H^A** to a water-soluble salt was not just due to residual chloride arising from incomplete substitution of the resin before use. The distinct spectra also suggest that the anions are binding to the cage's exterior and not dissociating into the surrounding solution. The reason for anion exchange with borate being unsuccessful was not determined, but the other samples were examined further.

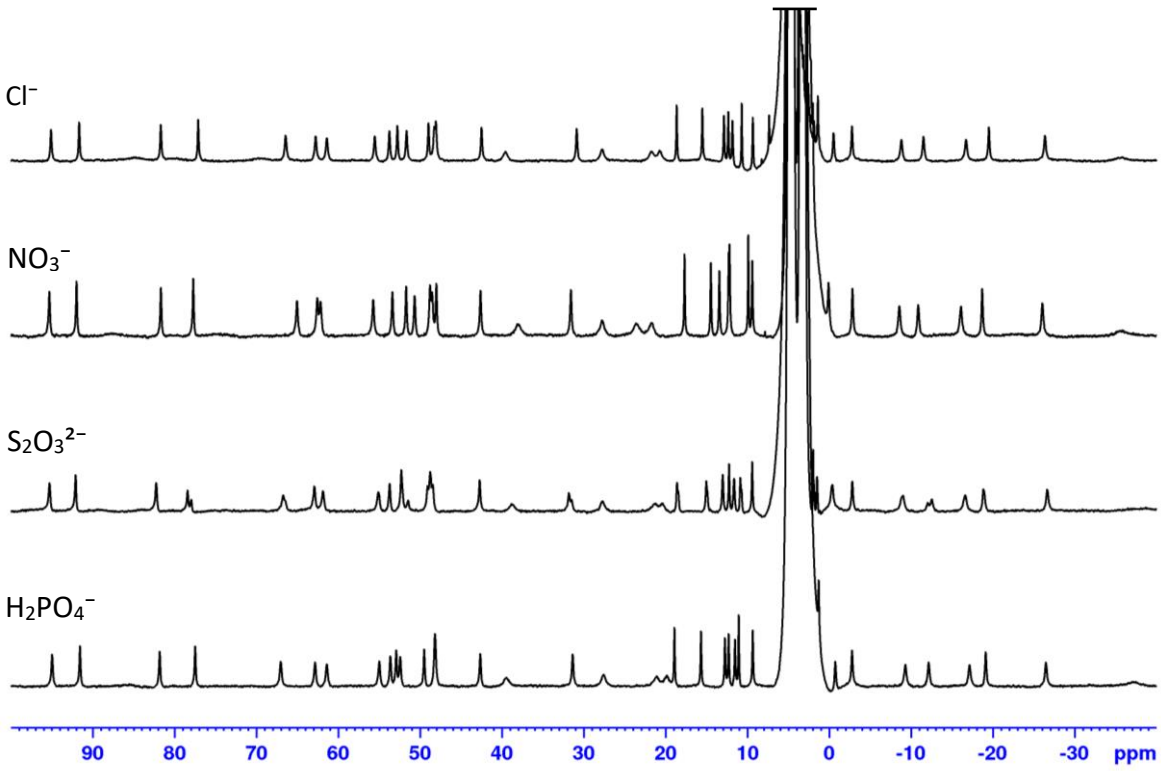

Figure 2.13 – ^{1}H NMR spectra of anion-exchanged **H^A** samples. All spectra recorded in D_2O.

Another analytical method available to investigate anion-exchange of the cage is UV/vis spectroscopy. UV/vis would allow a concentration for the sample to be determined and from this the degree of conversion determined also. For this, the previous procedure of stirring the cage $\mathbf{H^A}$ in D_2O with various anion-exchanged resins was repeated. Samples of $\mathbf{H^A{\cdot}X}$ were prepared, centrifuged, and filtered through a 0.2 µm filter (X = HCO_3^-, NO_3^-, SO_4^{2-}, $H_2PO_4^-$ and IO_3^-). For comparison, $\mathbf{H^A{\cdot}BF_4}$ was also prepared in acetonitrile.

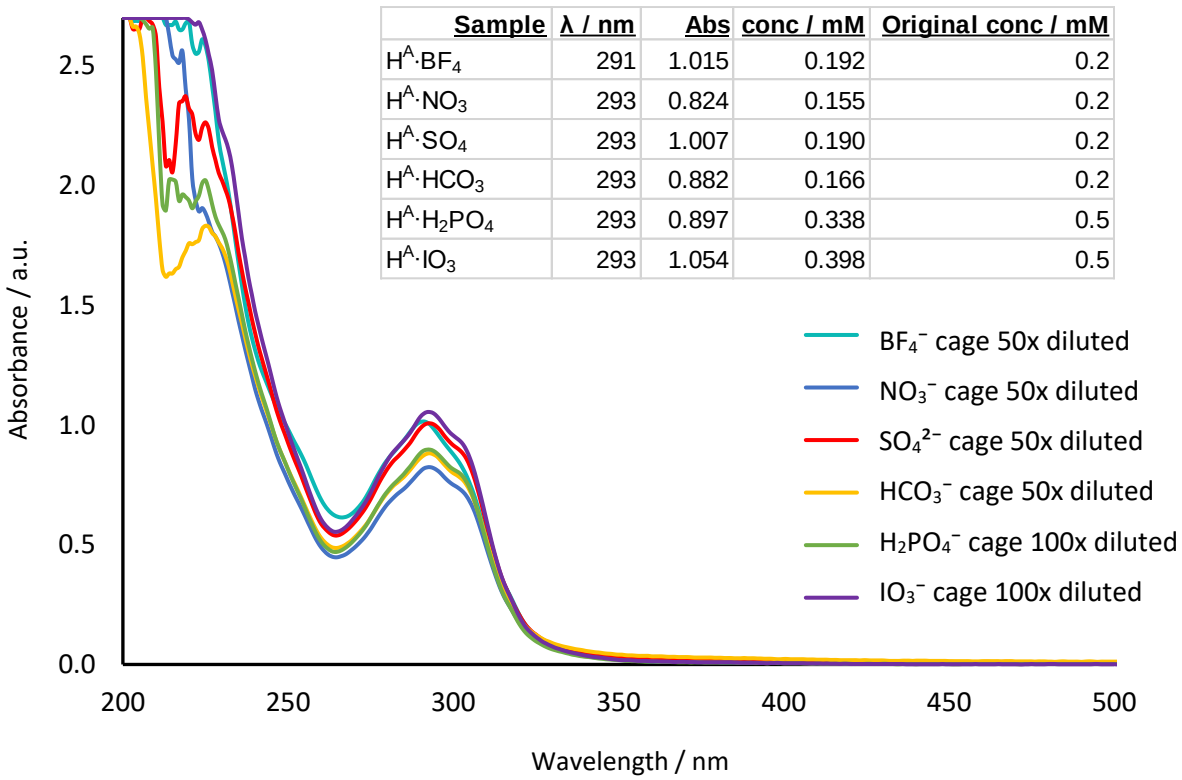

Sample	λ / nm	Abs	conc / mM	Original conc / mM
$H^A{\cdot}BF_4$	291	1.015	0.192	0.2
$H^A{\cdot}NO_3$	293	0.824	0.155	0.2
$H^A{\cdot}SO_4$	293	1.007	0.190	0.2
$H^A{\cdot}HCO_3$	293	0.882	0.166	0.2
$H^A{\cdot}H_2PO_4$	293	0.897	0.338	0.5
$H^A{\cdot}IO_3$	293	1.054	0.398	0.5

Figure 2.14 – stacked UV/vis spectra of the anion exchanged cages $\mathbf{H^A{\cdot}X}$ (X = NO_3^-, SO_4^{2-}, HCO_3^-, $H_2PO_4^-$, IO_3^-) and calculated concentrations.

The conversion of $\mathbf{H^A{\cdot}BF_4}$ to water-soluble analogues with different anions proceeded with varying success, as shown by UV/vis spectra of anion-exchanged aqueous solutions which did not have the same intensity. There were some losses in all cases upon conversion (typically 20-25%), which is expected when filtering through Millipore filters to remove any unconverted solid from the solution. The inset table in Figure 2.14 shows the resulting concentrations of each cage after stirring with the corresponding anion-exchange resin and what the starting

concentration should be, if the anion-exchange process were 100% efficient, based on the mass of the cage used for that sample.

From these samples, sulfate seemed to offer the best conversion: with an expected final concentration of 0.2 mM (for 100% conversion), the sulfate resin gave an anion-exchanged cage concentration in water of 0.19 mM. Conversely, use of nitrate afforded a final concentration of $\mathbf{H^A{\cdot}NO_3}$ in water of 0.155 mM (a 77.5% conversion). This trend followed that shown by the Hofmeister series of anions, which describes how anions interact with bulk water in solution. Anions that increase the order of water molecules around them and are therefore strongly hydrated are typically those with high negative charge, such as CO_3^{2-} or SO_4^{2-}. It therefore follows that these anions should aid water solubility most and therefore conversion, which seems to agree with the data on anion-exchange yields obtained from UV/vis spectroscopy.

Some samples were recorded at a higher starting concentration as a straightforward test to see if higher sample concentrations in water were possible after anion-exchange, with up to 1 mM of water-soluble $\mathbf{H^A{\cdot}Cl}$ being reported using the chloride-loaded Dowex. A ^{1}H NMR spectrum could be recorded of a sample of $\mathbf{H^A{\cdot}HCO_3}$ at a concentration of 1 mM, which suggests that the anion exchange method remains viable using pre-prepared resins. (See appendix 2.6.1 for full spectrum).

To better understand the process of conversion from BF_4^- to a different anion, a method that could detect any residual BF_4^- anions was needed. ^{19}F NMR spectroscopy was a suitable candidate for these experiments as none of the hydrophilic anions used to replace tetrafluoroborate contained fluorine atoms. 2 mM sodium triflate was used as an internal standard for both a chemical shift reference and for integration of any peaks found. If any residual BF_4^- was detected, integration of this signal compared to the triflate standard would allow the concentration of BF_4^- to be calculated. From this the degree of conversion could be determined.

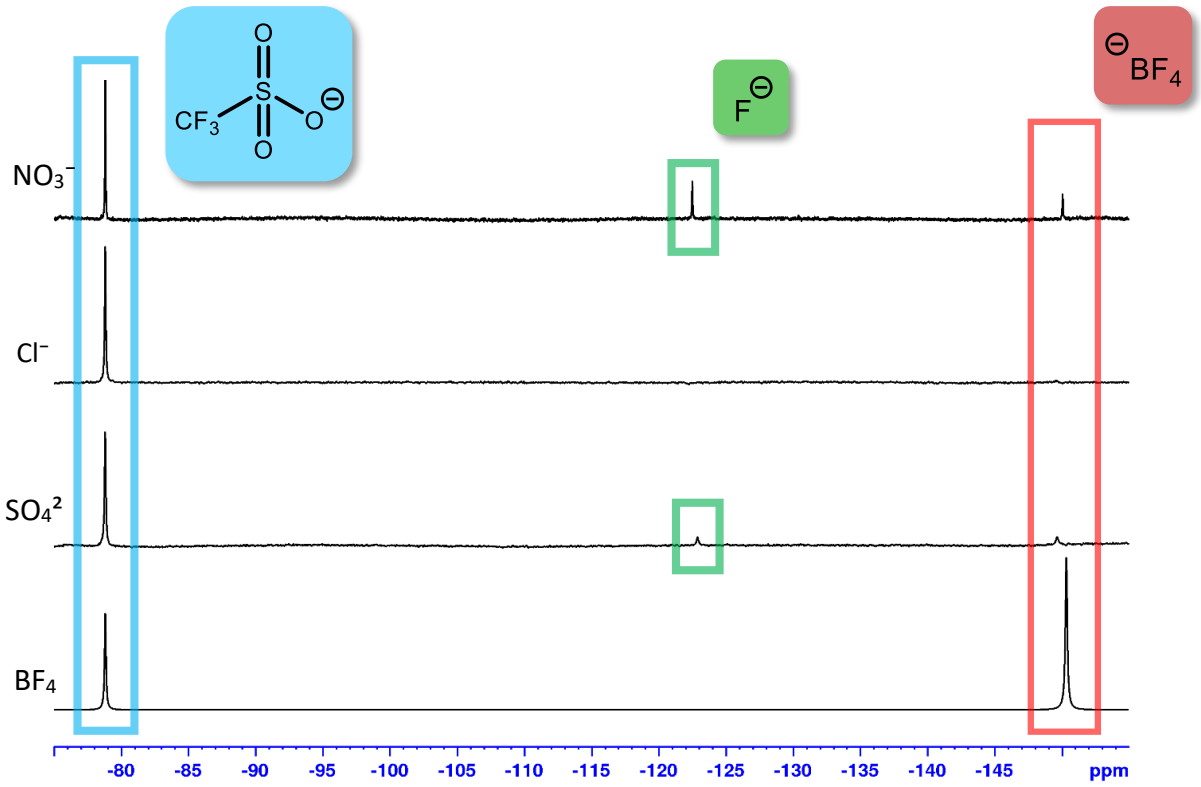

Figure 2.15 – Stacked ^{19}F NMR spectra of anion substituted cages $\mathbf{H^A{\cdot}X}$ where X = BF_4^-, SO_4^{2-}, Cl^- and NO_3^-. Samples recorded in D_2O.

After recording ^{19}F spectra of samples of exchanged cages, it became apparent that some samples contained not only BF_4^- peaks from incomplete anion exchange but also contained free fluoride peaks as well. Figure 2.15 shows the resulting ^{19}F spectra of three different anion-exchanged cages. Chloride exchange proceeds with total conversion with no production of fluoride ions. Nitrate and sulfate on the other hand both show residual BF_4^- peaks along with signals for fluoride at -122 ppm.

To refine this ^{19}F NMR analysis method before conducting further experiments, the addition of sodium triflate was altered. In the first iteration of the experiment, sodium triflate was weighed out in individual weighing boats and added to samples separately; this meant there was not a completely constant concentration between samples. For subsequent experiments, this method was changed to using a pre-made stock solution of sodium triflate in D_2O at 20 mM which would be mixed with the cage samples in a 9:1 ratio in the NMR tube. This ensures complete consistency of the sodium triflate concentration for calibration of integrals.

One other change made was the resin itself. After working with the Dowex 1x2 form for several experiments, the resin was changed to Amberlite IRA-400 mesh. The reasoning behind this was that it bypassed the centrifugation step for filtering the solutions post-exchange: Amberlite beads are of a much larger diameter and therefore can be separated from the solution through using a needle and syringe rather than transferral to a centrifuge tube. The downside to increasing the bead diameter is a drop in surface area, but this can be countered by using more resin per exchange experiment. Amberlite resins for all previously mentioned anions were prepared in the same manner as the Dowex 1x2 resins used before.

The ^{19}F NMR experiments after anion-exchange were then repeated and integrals calculated for the peaks found. This was done for cages **H^A·BF_4, H^A·SO_4, H^A·NO_3** and **H^A·HCO_3.**

a) $$n_{BF4} = \frac{3}{4} n_{NaOTf} \times \left(\frac{\int BF4}{\int NaOTf} \right)$$

b) $$n_{F-} = 3 n_{NaOTf} \times \left(\frac{\int F-}{\int NaOTf} \right)$$

Equation 2.1 – a) calculating the number of BF_4^- anions remaining on the cage H^A after conversion. b) calculating the number of F^- anions remaining on the cage after conversion.

Anion exchanged	AE Run2	BF_4's	F's	AE Run3	BF_4's	F's	Avg BF_4's	Avg F^-
BF_4^-	#2	16	0	#3	16	0	16	0
NO_3^-	#2	1	9	#3	1	6	1	7.5
SO_4^{2-}	#2	1	4	#3	1	4	1	4
HCO_3^-	#2	1	4	#3	/	/	1	4

Table 2.1 – Collated data from two repeats of anion exchange experiments involving peak integration of ^{19}F NMR spectra.

The data shown in Table 2.1 brings together the results from two repeats of anion exchange followed by ^{19}F NMR spectroscopy. Each of these samples of **H^A·BF_4** plus the relevant anion-exchanged resin was stirred overnight and filtered using a Millipore filter if necessary. Looking at the average final compositions of the anions associated with the cages we can draw two observations: firstly, the cages do not fully exchange their BF_4^- anions to the anions tested. All of the samples retain at least one BF_4^- anion and varying numbers of fluoride anions are also present. The retention of BF_4^- is consistent with findings from crystal soaking data using anions

such as Cl^- and I^- from previous publications by the Ward group.[19] The residual fluoride, as seen in the NMR spectra depicted in Figure 2.15, actually amounts to several anions per cage, ranging between 9 and 4 depending on the resin. Following anion exchange with nitrate, this means most of the anions are not NO_3^- but F^-, and for sulfate and bicarbonate there are typically 5 SO_4^{2-} or 11 HCO_3^- anions around the cage. Whilst this extent of conversion is sufficient to water-solubilise the cages, the inconsistencies seen with extents of conversion render this method unsuitable for cage preparation in any context where precise knowledge of the anion composition is required.

To investigate whether the stir duration with the anion-exchange resin influenced the overall conversion, some simple tests were performed, the first of which was whether any of the mixtures containing **H^A·BF_4** plus the relevant anion-exchanged resin became clear (indicating complete water-solubilisation) early in the stir. Monitoring the Amberlite resin stirs by eye brought an interesting observation. For a bicarbonate-loaded resin, the initially cloudy suspension was seen to clear in approximately 20 minutes. The stir was stopped at this point and filtered as per previous procedures and an NMR spectrum taken. The resulting NMR spectrum was of good quality and correlated with other spectra recorded for **H^A·HCO_3** previously.

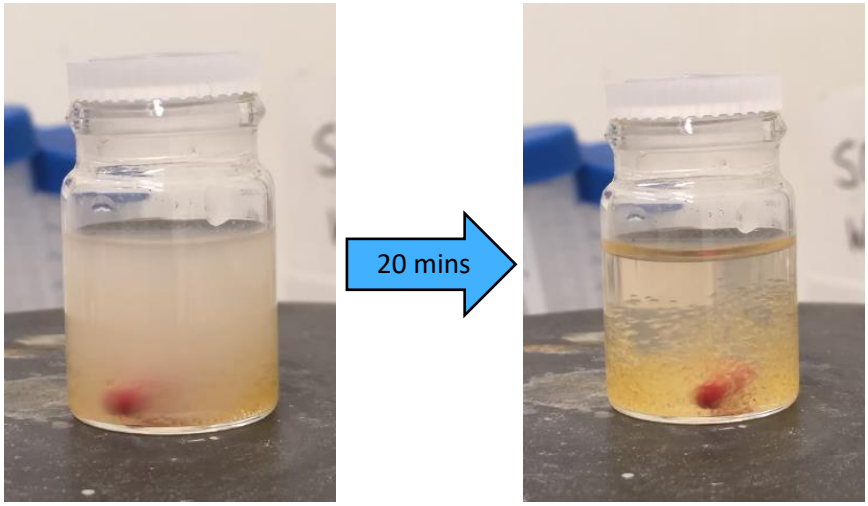

Figure 2.16 – photographs of the cage H^A in D_2O with HCO_3^- converted resin present. The sample can be seen to clear after only 20 minutes of stirring.

A follow-up experiment was conducted using a dihydrogen phosphate-loaded resin and **H^A·BF_4**, involving two samples run in tandem. One was stopped as soon as the sample had cleared – again this occurred after approximately 20 minutes. The other sample was left for a total of 5 days and was found to be cloudy after this duration. Both samples were filtered, and UV/vis and ^{19}F NMR spectra recorded for both.

The ^{19}F NMR spectra in Figure 2.17 shows a clear difference between the anion composition associated with **H^A** after the two stirring experiments. The size of the BF_4^- peak relative to triflate for the 20-minute stir is considerable, whereas after 5 days this peak was barely visible. Clearly, longer stirring times leads to higher conversions even if the sample is rendered water-soluble at a fairly early stage in the anion-exchange process. This is not the whole story, however, as the sample that was left stirring for 5 days had become cloudy by the end, indicative of partial decomposition of the cage having occurred.

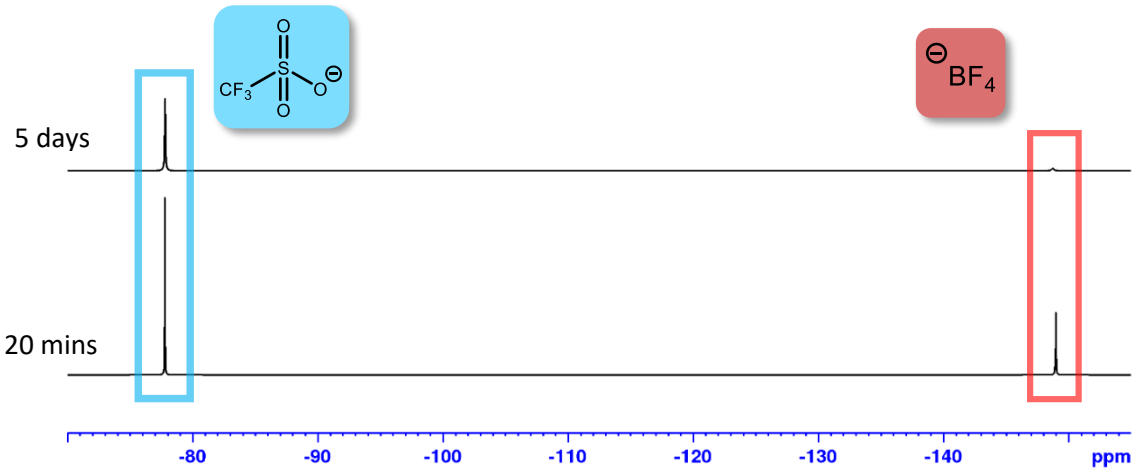

Figure 2.17 – comparison of stir lengths by ^{19}F NMR. Both samples were the cage H^A stirred with $H_2PO_4^-$ resin in D_2O.

A look at the UV/vis spectrum of both samples also shows a clear disparity between the two solutions. The naphthyl peak seen around 293 nm is present for both samples but at a much lower intensity for the sample left for 5 days. Calculating concentrations from these values shows that there is about half the concentration of cage in the sample left for 5 days as there is in the anion-exchanged experiment that was conducted for only 20 minutes.

This suggests that for $H_2PO_4^-$, the anion in this example, the optimum point for water solubility is not full conversion from BF_4^- to 16 $H_2PO_4^-$ anions but somewhere in between. The number of BF_4^- anions present after 20 minutes of stirring is calculated to be 3 (using Equation 2.1), but this drops to only 1 BF_4^- remaining after leaving the exchange for longer. The disadvantage to a higher degree of conversion is a significant drop in cage concentration in water due to decomposition. Given this, any further anion-exchange experiments following this experiment were monitored closely and were stopped and filtered as soon as the sample was seen to clear, as opposed to being left overnight. This avoids any decomposition of the type that was seen with dihydrogen phosphate as the anion being exchanged.

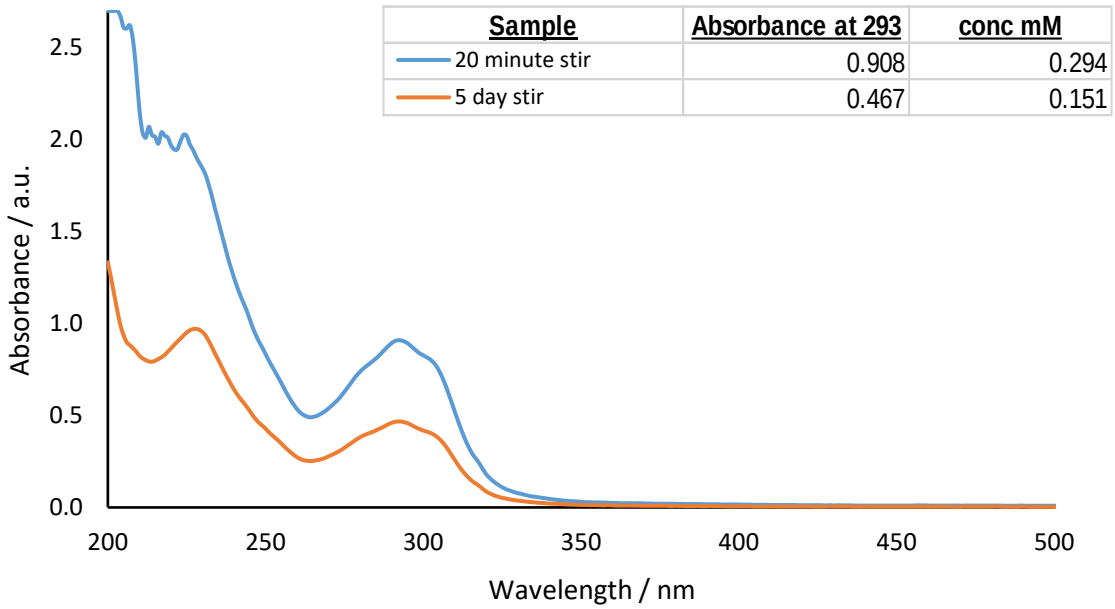

Sample	Absorbance at 293	conc mM
20 minute stir	0.908	0.294
5 day stir	0.467	0.151

Figure 2.18 – comparison of UV/vis spectra for two identical samples stirred for a different amount of time. The peak at 293 nm is clearly lesser for the sample stirred for 5 days compared to 20 minutes. Calculated concentrations are given in the inset table.

The main reasoning for finding a consistent method of making $\mathbf{H^A}$ water-soluble by anion exchange was to avoid the need to covalently attach water-solubilising groups to the ligands, thereby reducing the time and cost of cage synthesis. Another issue was the unclear anionic make-up of the hydrolysed $\mathbf{H^W}$ cage arising from partial hydrolysis of the tetrafluoroborate anions. The ^{19}F NMR spectrum of $\mathbf{H^W}$ once dissolved in water showed the presence of several fluorine-containing species, including free fluoride alongside what were likely partially-hydrolysed borates

$BF_x(OH)_y$. Even in a dissolved sample of **H^W** there is a signal due to BF_4^- at -148.5 ppm, corroborating the earlier findings that full conversion from BF_4^- is not always necessary to achieve water solubility.

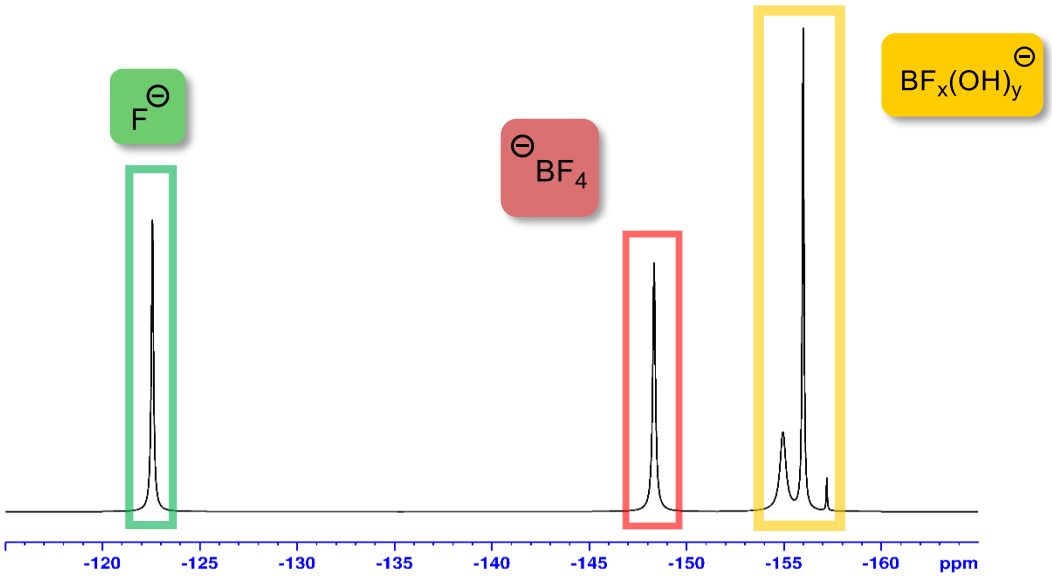

Figure 2.19 – Partial ^{19}F NMR spectrum of **H^W** in D_2O showing the resulting mixture of borate products after dissolution (hydrolysis).

After numerous conversions and analysis through ^{19}F NMR spectroscopy, it was clear that the outcome of anion exchange is not as straightforward as initially thought, with varying degrees of conversion and evidence of decomposition in some cases. Whilst this project had intended to find a consistent alternative to water-solubilising the supramolecular assemblies commonly used within the group, these findings proved that the anion exchange method for water solubilisation has its own limitations. Some conclusions could made as a result of this work, however. Working with the anion exchange resins to create water-soluble cages had shown that changing the anion had a dramatic effect on the cage's solubility characteristics. Some caused the cages to become water soluble, others induced precipitation out of solution. The variance in outcome upon changing the counter-anion for the cage **H^A·BF_4** prompted an investigation into other effects of the anion-cage interactions beyond water solubility. The next section of this chapter introduces and discusses the effect of various anions on the catalysis of the Kemp elimination.

2.2.2. Anion effects on the Kemp Elimination of nitrobenzisoxazole

A 2016 paper published by Ward and co-workers reported acceleration of the Kemp elimination of benzisoxazole facilitated by the cubic cage $\mathbf{H^W}$.[26] This ring-opening reaction, generating 2-cyanophenolate as the product, was aided by the accumulation of hydroxide anions around the 16+ cage surface due to electrostatic factors, meaning that the local pH of the cavity-bound substrate (surrounded by hydroxide ions in the cage windows) could be much higher than the pH of the solution. The localised accumulation of OH^- around the cavity-bound guest causes the pH to be close to 14 when the bulk solution may only be at a pH of around 8. This high local concentration of OH^- anions leads to a substantial rate increase for the conversion of benzisoxazole to 2-cyanophenolate in the presence of the cage.

A further publication concerning the Kemp elimination reaction of benzisoxazole followed.[19] This experiment had used a chloride-substituted analogue of $\mathbf{H^A}$ ($\mathbf{H^A{\cdot}Cl}$) for the same experiment as the previous paper – catalysis of the Kemp elimination using the cage. The first, and potentially most important finding, was that the rate of catalysis using the chloride substituted cage was around two orders of magnitude slower than with $\mathbf{H^W}$ (tetrafluoroborate salt). The competition for the anion-binding sites on the surface of the cage between chloride and OH^- anions from the bulk solution results in a reduction in the rate of catalysis owing to the reduction in local concentration of hydroxide. Increasing the amount of chloride in the solution by adding subsequent sodium chloride slowed the catalysis further still, confirming the previous finding. Secondly, adding fluoride to the solution as sodium fluoride showed inhibition of catalysis but not to the same extent as for chloride. This implied different strengths of association between the cage's surface and different anions.

To examine the properties of anion exchanged cages in more detail, an experiment focusing on the catalysis of nitrobenzisoxazole was designed. 5-nitrobenzisoxazole (**NBzI**) has the benefit of displaying a visible colour change upon ring-opening as the cyano-nitrophenolate product is a yellow colour arising from strong absorption at *ca.* 400 nm from a phenolate-to-nitro charge-transfer π-π* transition. Using UV/vis absorption as the method of monitoring reaction progress rather than ^{1}H NMR

methods, which had been used previously, allowed multiple repeats for the same reaction to be run together using a plate reader.

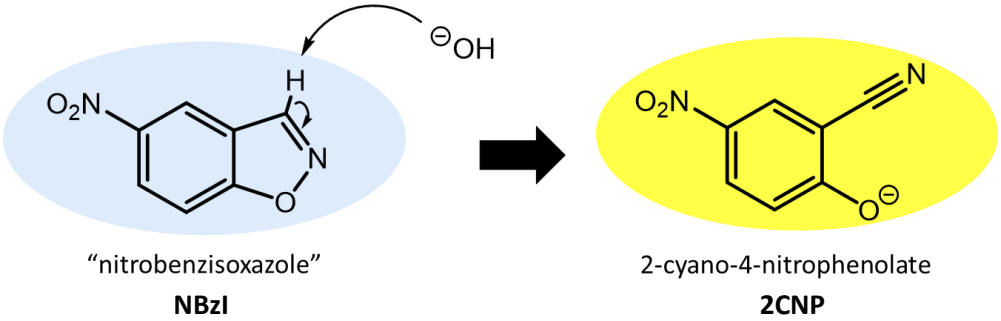

Figure 2.20 – schematic of the Kemp elimination of 5-nitrobenzisoxazole by hydroxide. Formation of the product can be tracked by UV/vis spectroscopy.

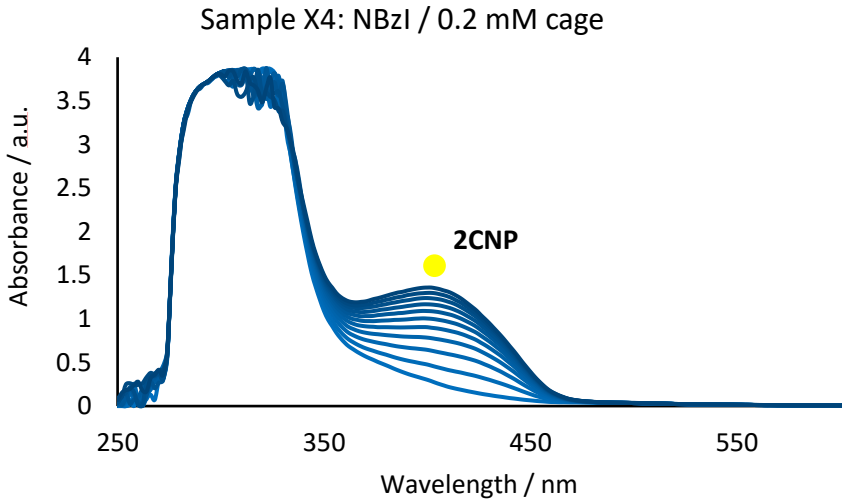

Figure 2.21 – Increase in absorption for the product 2CNP over time in the presence of 0.2 mM H^W acting as the catalyst. [NBzI] = 0.25 mM, pH 8.5.

Initial experiments sought to find suitable conditions to observe the catalysis provided by the cage $\mathbf{H^W}$. Borate buffer at a pD between 7.5 and 9.0 has been used successfully in the hydrolysis of phosphotriesters by the cage $\mathbf{H^W}$ in previous experiments.[27] To slow the reaction for studies involving anion inhibition, the buffer system used for these experiments was phosphate buffer, at a pH of 7.0. The lower concentration of base present in the solution result in slower rates of reaction for the conversion of **NBzI**, which is preferable for experiments taking place over the course of several hours.

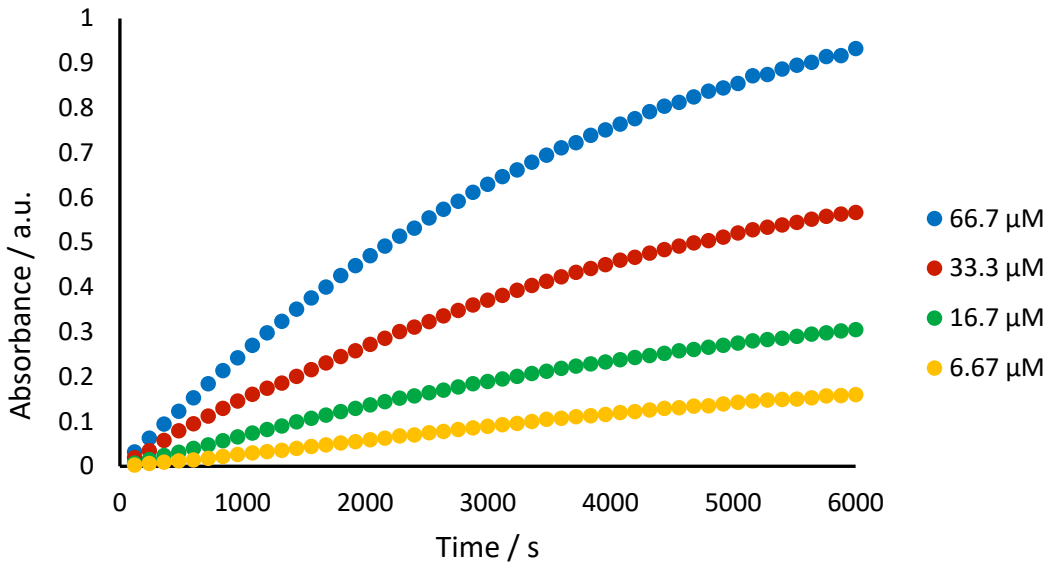

Figure 2.22 – Conversion of NBzI to 2CNP in the presence of varying amounts of H^W. [NBzI] = 0.2 mM, 16.7 mM phosphate buffer pH 7.

Recording the absorption at the peak for **NBzI** as it grows over time by UV/vis spectroscopy shows the effect of increasing the concentration of catalyst present. With more cage added, the rate of conversion from nitrobenzisoxazole to 2-cyano-4-nitrophenolate increased with a first-order relationship to [$\mathbf{H^W}$], determined by plotting k_{cat} against the concentration of catalyst added. Figure 2.23 shows the correlation between the two values at four different concentrations of cage.

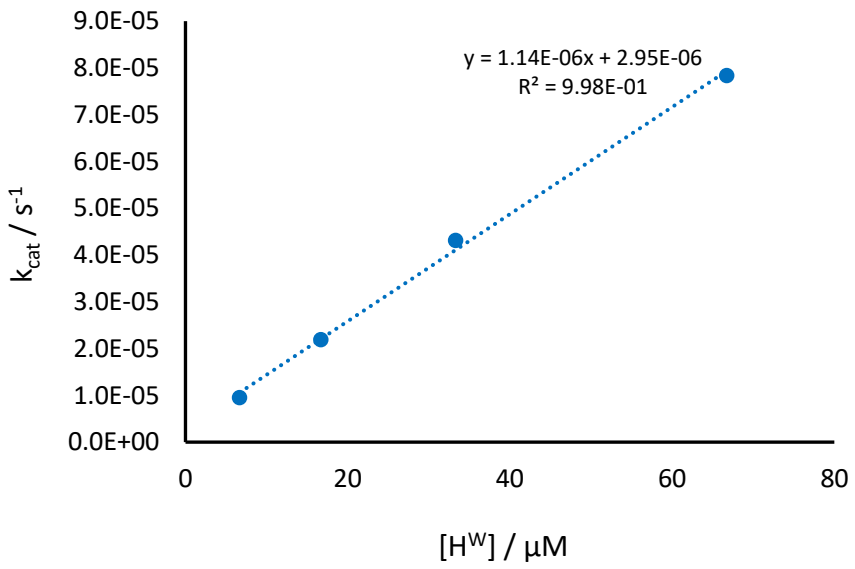

Figure 2.23 – values calculated for k_{cat} vs the concentration of H^W used. [NBzI] = 0.2 mM, 16.7 mM phosphate buffer pH 7.

Sample	λ / nm	$[H^W]$ / μM	k_{cat} / s^{-1}	SE of k_{cat}	% error	k_2 / M^{-1} s^{-1}
X1	380	0	1.47E-05*	2.34E-07	1.59	
X2	404	66.7	7.84E-05	6.28E-07	0.80	1.18
X3	396	33.3	4.32E-05	5.77E-07	1.34	1.30
X4	388	16.67	2.19E-05	9.89E-08	0.45	1.31
X5	382	6.67	9.53E-06	1.2E-07	1.26	1.43

Table 2.2 – Tabulated data for the initial rate experiments using NBzI and varying concentrations of H^W. [NBzI] = 0.2 mM, 16.7 mM phosphate buffer pH 7. *background reaction, not catalysed.

These experiments produce k_{cat} values between 9.53 x 10^{-6} s^{-1} for 6.67 μM of cage to 7.84 x 10^{-5} s^{-1} for 66.7 μM, with k_2 values between 1.18-1.43 M^{-1} s^{-1}. These values are taken using the first 20 points of the data shown above where the graphs are linear. Different wavelengths were used for the calculations of initial rates as the maximum absorption shifts depending on the concentration of cage. This is hypothesised to be a result of the product phenolate binding to the exterior surface of the cage, red-shifting the absorbance of **2CNP**. The higher the concentration of cage present, the higher the wavelength of maximum absorption observed, as seen in the second column of Table 2.2. This observation will be touched upon again later in this section.

Having determined that the conversion of **NBzI** to **2CNP** is first order with respect to cage, we can return to examining the rate laws relating to this system in more detail. The rate of the background reaction depends upon both the concentration of starting material (**NBzI**) and base (OH^-) and can be fit to the kinetic scheme as shown in Equation 2.2, below:

$$rate = k[NBzI][OH^-]$$

Equation 2.2 – The rate law for conversion of NBzI to 2CNP in the absence of cage.

A rate constant for the background reaction can be determined by rearranging Equation 2.2 into a pseudo first order expression as the concentration of base remains constant throughout the reaction due to the presence of phosphate buffer. Taking $[OH^-]$ as constant, we get Equation 2.3.

$$[NBzI] = [NBzI]_0\, e^{-k_{bk}t} \qquad where\ k_{bk} = k[OH^-]$$

Equation 2.3 – The pseudo first order rate law for the background reaction of NBzI to 2CNP.

As we cannot directly monitor the consumption of **NBzI** during the reaction, we instead observe the production of **2CNP** by UV/vis spectroscopy and calculate a value for [**NBzI**] from the calculated concentration of **2CNP**. Equation 2.4 was used to determine a value for k_{bk} by plotting the data as a straight-line graph. This produced both a value for k_{bk} and the standard error for the curve fitting, the values of which are shown in Table 2.2.

$$\ln\frac{[NBzI]}{[NBzI]_0} = -k_{bk}t \qquad where\ k_{bk} = k[OH^-]$$

Equation 2.4 – The rearranged pseudo first order rate law for the background reaction of NBzI to 2CNP.

For the reaction involving the cage acting as a catalyst, a term for the concentration of $\mathbf{H^W}$ must also be added. This produces a third order rate law, seen in Equation 2.5:

$$rate = k'[NBzI][OH^-][H^W]$$

Equation 2.5 – The rate equation for the cage-catalysed conversion of NBzI to 2CNP.

This equation can also be simplified by considering that the concentration of base and cage are both constant throughout the reaction. Using a new rate constant, k_{cat}, we get Equation 2.6:

$$rate = k_{cat}[NBzI] \qquad where\ k_{cat} = k'[H^W][OH^-]$$

Equation 2.6 – The simplified, pseudo first order rate equation for the cage-catalysed conversion of NBzI to 2CNP.

The overall rate observed during these experiments is actually a sum of the two reactions described above, with both the catalysed and background reactions occurring at the same time. The equation encompassing both of these reactions as simplified pseudo first order rate laws is given in Equation 2.7, overleaf.

$$rate = k_{bk}[NBzI] + k_{cat}[NBzI]$$

$$where\ k_{bk} = k[OH^-]\ and\ k_{cat} = k'[H^W][OH^-]$$

Equation 2.7 – Overall rate law for the observed reaction of NBzI to 2CNP.

To obtain the second-order rate constant for the catalysed reactions, we divide the value of k_{cat} by $[H^W]$ to give a value for k_2. The value for $[OH^-]$ was treated as a constant as conditions were kept the same for all experiments and this term appeared in all rate laws.

Before moving onto testing the effects of adding various anions to the catalytic system, control experiments had to be conducted. The first of these involved addition of the guest molecule cycloundecanone (C_{11}), a known cavity-binding guest with a high binding constant (> 10^6 M^{-1}). The addition of cycloundecanone in this experiment was intended to 'block' the cavity and therefore stop catalysis occurring within the cavity of the cage. As the graph in Figure 2.24 shows, there is no such inhibition seen in the presence of C_{11}. This observation coupled with the modest rates of catalysis seen for nitrobenzisoxazole compared to its unsubstituted benzisoxazole predecessor both suggest that catalysis in this instance is occurring not within the cavity of the cage but on its surface, as we have observed with catalysed hydrolysis of some phosphate esters.[27] In theory this is logically sound – the surfaces of the cage are hydrophobic in nature and so due to the hydrophobic effect, molecules such as nitrobenzisoxazole can associate with the cage's exterior surface as well as binding to the interior cavity. As previously mentioned, the surface is also home to hydroxide anions which are attracted to the positive cage through electrostatic interactions. The cage in this case can be considered as an agent that brings both species needed to react together through orthogonal interactions, either inside the cavity or on the exterior surface.

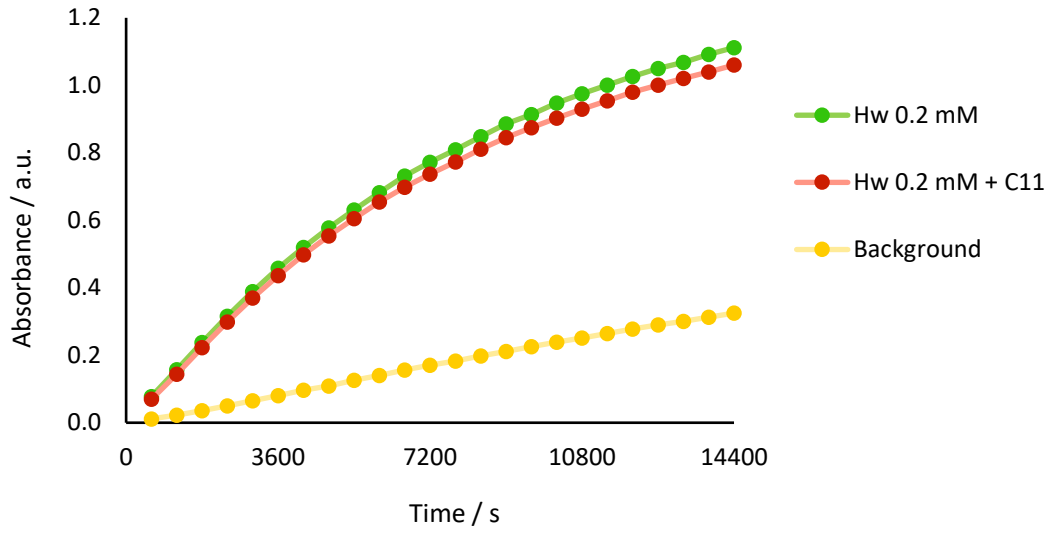

Figure 2.24 – Effect of adding an inhibitor to the reaction. C_{11} does not appear to hinder the progress of the reaction despite binding strongly within the cage's cavity, indicating catalysis occurs on the cage's surface. [H^W] = 0.1 mM, [NBzI] = 0.15 mM, [C_{11}] = 5 mM, 16.7 mM pH 7 phosphate buffer.

Crystal structure analysis of both unsubstituted benzisoxazole and 5-nitrobenzisoxazole performed by Dr Chris Taylor has revealed that both species can be found situated inside the cavity of **H^W**, with interactions between the polar regions of the guest molecule and the protons situated at one of the *fac*-tris-chelate sites of the cube's interior surface. Benzisoxazole binds through the oxygen atom within the 5-membered ring, forming hydrogen bonds with the proximal C-H protons on the naphthyl groups of the ligands, which act as weak H-bond donors. Nitrobenzisoxazole, however, binds in a different orientation, with the oxygen atoms of the nitro group acting as the H-bond acceptors and forming multiple interactions with the hydrogens of the ligand.

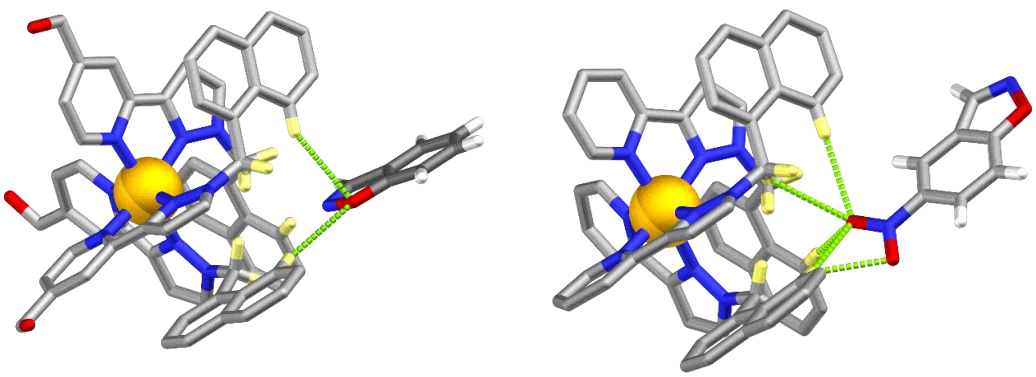

Figure 2.25 – Comparison of binding modes for benzisoxazole (left) and 5-nitrobenzisoxazole (right) at the *fac*- site found within the cavity of H^W.

It is important to note that the conditions for crystal soaking (as used in the 'crystalline sponge' method popularised by Fujita)[28] are vastly different from the conditions used for the catalysis experiments in dilute solution, so the observations made from the crystal structure do not necessarily match solution behaviour. For example, the 'crystalline sponge' method has produced examples of two molecules binding within the cavity of **H^W**, occupying up to 87% of the cavity's volume – a feat that would not be possible under dilute solution conditions.[29]

Having found that the catalysis of nitrobenzisoxazole to 2-cyano-4-nitrophenolate occurs in the presence of the cage **H^W** even when the cavity is occupied by C_{11}, we set out to investigate the effect of anions on the catalysis. In order to avoid any inconsistences in the extent of anion replacement associated with use of ion-exchange resins, known amounts of different salt solutions were added to the reaction mixtures containing **H^W** and **NBzI** so a known concentration of added anion was present for each experiment. The first experiment in this series involved the addition of chloride to a solution of **NBzI**, both in the presence and absence of the catalyst **H^W**. This experiment aimed to confirm that it was the contribution of **H^W** responsible for the acceleration in rate seen and not an effect possible by the addition of chloride alone.

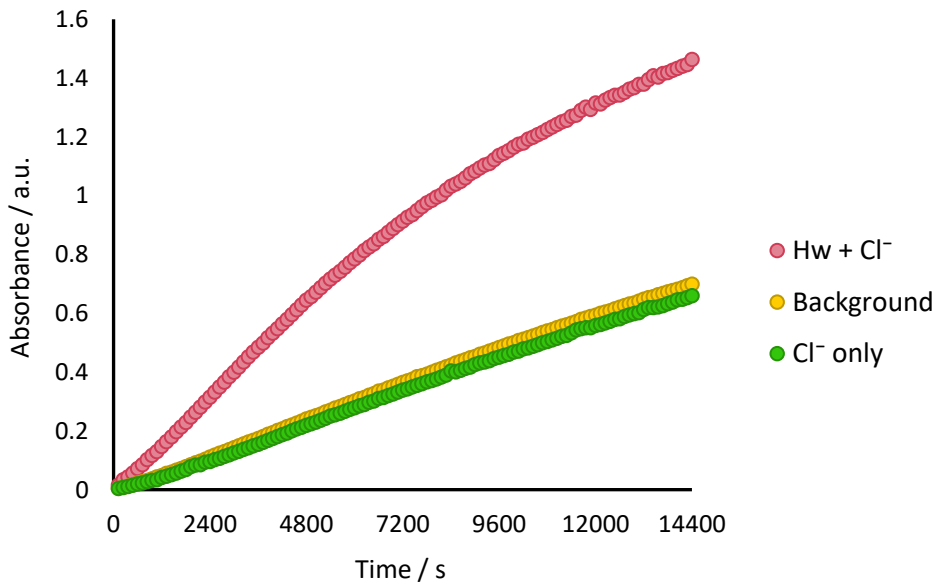

Figure 2.26 – Chloride alone does not catalyse the reaction, proving that H^W is responsible for catalysis. [H^W] = 50 µM, [NBzI] = 0.2 mM, 16.7 mM pH 7 phosphate buffer.

As shown in Figure 2.26, the sample containing only chloride alongside **NBzI** proceeds at a rate comparable to the background reaction. When $\mathbf{H^W}$ is introduced, the reaction profile changes dramatically and the rate increases. Table 2.3 provides a comparison of the calculated rates for each of the three samples, calculated using early-stage data from plots of the background-subtracted linear ln(NBzI) vs time (details provided in the experimental section).

Sample	$[H^W]$ / µM	k_{bk} / s^{-1}	k_{cat} / s^{-1}	SE of k_{cat}	% error	k_2 / M^{-1} s^{-1}
Background	0	1.47E-05		2.34E-07	1.6	
H^W only	66.7		7.24E-05	4.88E-07	0.7	1.09
H^W + Cl^-	50		1.88E-05	2.45E-07	1.3	0.38
Cl^- only	0	1.00E-05		3.10E-07	3.1	

Table 2.3 – Tabulated data for the control experiment confirming that H^W and not the added anion is accelerating the reaction. [NBzI] = 0.2 mM, $[Cl^-]$ = 10 mM, 16.7 mM pH 7 phosphate buffer.

As the numbers show, both the background and chloride-only samples show rates in the order of 1 x 10^{-5} s^{-1}, compared to 7.24 x 10^{-5} s^{-1} upon addition of $\mathbf{H^W}$. This increase in rate can be attributed solely to the cage acting as the catalyst for the reaction. As expected, the sample containing both $\mathbf{H^W}$ and chloride returned a lower value for k_{cat} than $\mathbf{H^W}$ alone, as seen with benzisoxazole in previous work.

Following this control experiment, the range of anions tested for their effect on the rate of catalysis in a system containing both **NBzI** and $\mathbf{H^W}$ was expanded to include species spanning the Hofmeister series from one extreme to the other. The anions F^-, Cl^-, Br^-, NO_3^-, SO_4^{2-}, IO_3^-, HCO_3^- and I^- were added as their sodium salts in two separate experiments run in tandem – one using an anion concentration of 1.67 mM and the second using a concentration of 16.7 mM.

$$SO_4^{2-} > IO_3^- > F^- > HCO_3^- > Cl^- > Br^- > NO_3^-$$

Kosmotropes **Chaotropes**

Figure 2.27 – A shortened version of the Hofmeister series containing only the anions tested in the NBzI/H^W system.

Typically, a higher concentration of anion will decrease the rate of phenolate production, but not all anions affect the reaction to the same degree. Referring to the Hofmeister series, the anions at one extreme are kosmotropes and therefore expected to 'order' the bulk water in solution around them, making them better solvated and less likely to associate with the cage's surface – so have a less inhibiting effect on the catalysed reaction. At the other end of the series are chaotropes, species that will disrupt the H-bond network present in bulk water. These will likely have a higher affinity for the cage's surface and compete more readily with hydroxide ions for surface binding.

The iodide anion caused rapid decomposition of the cage, owing to its suitability as a ligand for Co(II) ions. As a result, no data was retrieved for these samples. The other anions all had different effects on the rate of the cage-catalysed Kemp elimination when added at the same concentration. The data collected for F^-, Cl^-, Br^-, NO_3^-, SO_4^{2-}, IO_3^-, HCO_3^- and no salt added are shown in Figure 2.28.

The data obtained from the experiments using the added anion at a concentration of 1.67 mM returned some interesting results. The first thing of note is how the most chaotropic (effectively, hydrophobic) anions tested, namely bromide and nitrate, both produced the greatest degree of inhibition. Compared to the calculated second order rate constant (k_2) for $\mathbf{H^W}$ alone, bromide reduces this value to just a third of its initial value, whilst nitrate reduces it to around a quarter. The anions found away from the chaotropic end of the Hofmeister series show one of two effects on the rate of reaction. Chloride, iodate and sulfate all reduce the rate of reaction to a similar degree, with a reduction in k_2 of between 17-23% for the three anions. The calculated values can be seen in Table 2.4, shown below. Bicarbonate and fluoride, however, show a different result despite being situated towards the centre of the Hofmeister series.

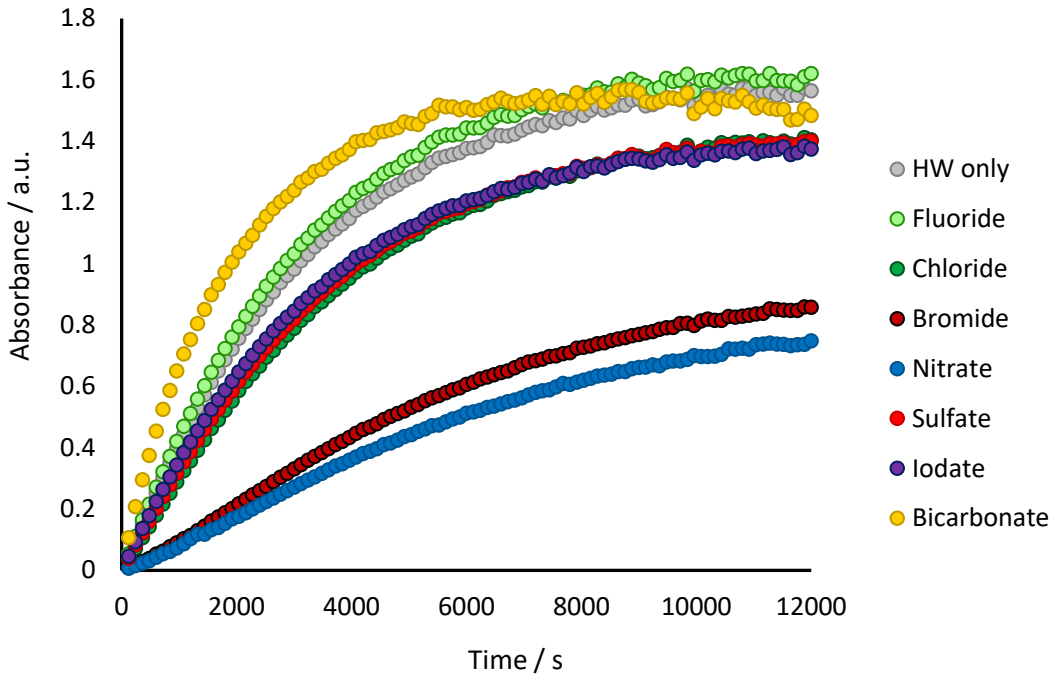

Figure 2.28 – Reaction profiles for NBzI/H^W with each sample containing 1.67 mM of one of the listed anions. The order seen broadly matches the Hofmeister series, with well-solvated kosmotropes inhibiting the reaction less than hydrophobic chaotropes. [H^W] = 0.125 mM, [NBzI] = 0.2 mM, 16.7 mM pH 7 phosphate buffer.

Sample	Anion	[H^W] / mM	k_{cat} / s^{-1}	SE in k_{cat}	% error	k_2 / M^{-1} s^{-1}
X1	None	0	1.80E-05*	2.76E-07	1.5	
X2	None	0.125	1.35E-04	9.97E-07	0.7	1.08
X3	F^-	0.125	1.42E-04	1.08E-06	0.8	1.14
X4	Cl^-	0.125	1.01E-04	2.80E-07	0.3	0.81
X5	Br^-	0.125	3.58E-05	6.37E-07	1.8	0.29
X6	NO_3^-	0.125	2.92E-05	4.96E-07	1.7	0.23
X7	SO_4^{2-}	0.125	1.07E-04	5.52E-07	0.5	0.85
X8	IO_3^-	0.125	1.12E-04	1.10E-06	1.0	0.89
X9	HCO_3^-	0.125	1.88E-04	5.62E-06	3.0	1.51

Table 2.4 – Tabulated data listing calculated first-order catalysed rate constants, k_{cat}, for each of the various anions, along with the second-order rate constant, k_2. [H^W] = 0.125 mM, [NBzI] = 0.2 mM, 16.7 mM pH 7 phosphate buffer. *background rate (not catalysed).

The second observation arising from the data presented above is the acceleration in rate caused by addition of the anions bicarbonate and fluoride. Both anions increase the second order rate constant compared to **H^W** with no anions added. In the case of bicarbonate, it was hypothesised before the experiment was performed that the rate

may increase in the presence of HCO_3^- anions, owing to its basicity as an anion. The increase in rate upon addition of fluoride, however, was unexpected. Further experiments designed to investigate this result are discussed shortly.

The data gathered using anions added at 16.7 mM, a tenfold increase on the first group of experiments, produced the same relative effects but to a greater degree. The increase in rate of reaction caused by fluoride was more obvious, whilst the inhibition caused by bromide and nitrate reduced the rate by nearly a whole order of magnitude. This set of experiments helps distinguish the effect of chloride compared to both iodate and sulfate. With the higher concentration of anions in solution, the relative positions of Cl^- and IO_3^- on the Hofmeister series align with the calculated rate constants. Sulfate, on the other hand, is the only dianion tested in this set of samples and does not affect the rate as predicted by the ordering of the Hofmeister series. We hypothesise that the additional charge per sulfate molecule results in fewer anions binding to the cage's exterior and therefore the observed inhibition is less than a species such as chloride where the number of anions required to balance the charge of the cage is twice that of sulfate's. More surface sites being occupied by the added anion will result in less hydroxide available to deprotonate the starting

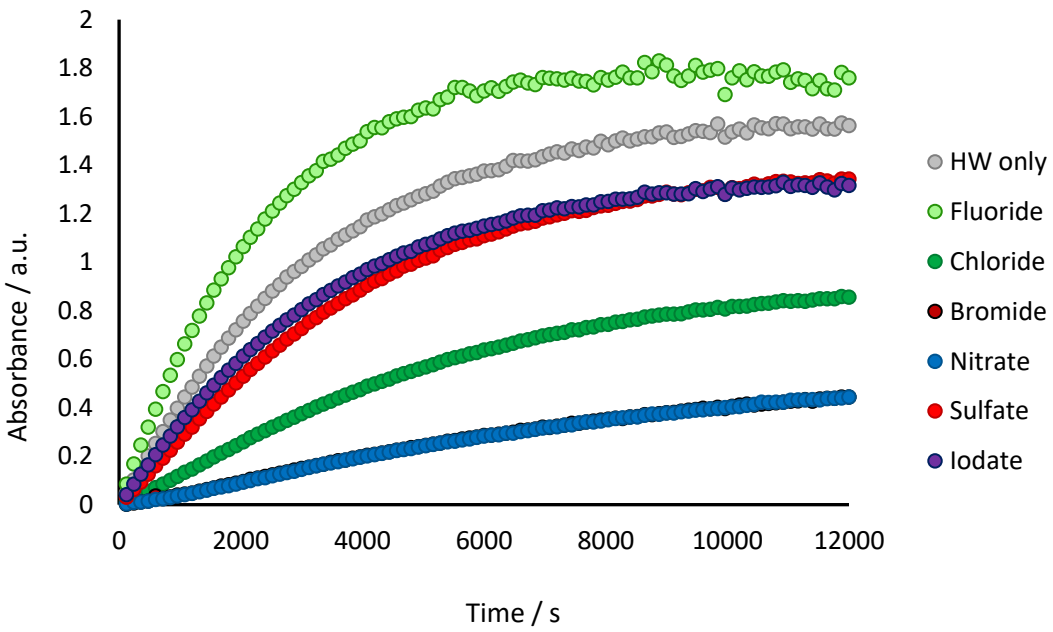

Figure 2.29 – Reaction profiles for NBzI/H^W with each sample containing 16.7 mM of one of the listed anions. The effects seen at the lower concentration of anions are magnified at this higher concentration. [H^W] = 0.125 mM, [NBzI] = 0.2 mM, 16.7 mM pH 7 phosphate buffer. (Bromide is covered by the curve for nitrate).

material, and a lower rate of reaction as a result. Absent from this set of results is bicarbonate – at a concentration of 16.7 mM it was evident that the pH of the solution had risen above 7, and this caused the data to be unsuitable for comparison to the other anions.

Sample	Anion	$[H^W]$ / mM	k_{cat} / s^{-1}	SE in k_{cat}	% error	k_2 / M^{-1} s^{-1}
X1	None	0	1.80E-05*	2.76E-07	1.5	
X2	None	0.125	1.35E-04	9.97E-07	0.7	1.08
X11	F^-	0.125	2.00E-04	2.48E-06	1.2	1.60
X12	Cl^-	0.125	4.28E-05	3.55E-07	0.8	0.34
X13	Br^-	0.125	1.55E-05	4.87E-07	3.1	0.12
X14	NO_3^-	0.125	1.50E-05	3.60E-07	2.4	0.12
X15	SO_4^{2-}	0.125	9.10E-05	2.77E-07	0.3	0.73
X16	IO_3^-	0.125	1.05E-04	9.07E-07	0.9	0.84

Table 2.5 – Tabulated data listing calculated first-order catalysed rate constants, k_{cat}, for each of the various anions, along with the second-order rate constant, k_2. $[H^W]$ = 0.125 mM, [NBzI] = 0.2 mM, 16.7 mM pH 7 phosphate buffer. *background rate (not catalysed).

Returning to the observation made earlier regarding the acceleration of rate by both HCO_3^- and F^-, an experiment was devised to confirm that these molecules were acting in some capacity as a base within the system, causing the increased rate of reaction seen for both samples. The anions formate and acetate were also used in

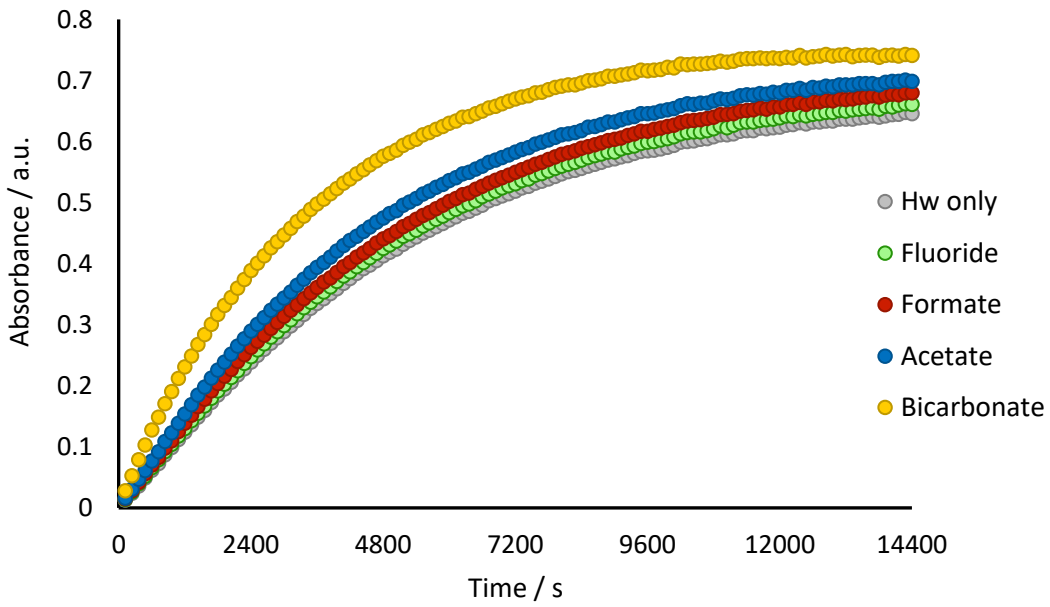

Figure 2.30 – Reaction profiles for conversion of NBzI to 2CNP by H^W in the presence of anions of increasing basicity at 1mM. $[H^W]$ = 0.05 mM, [NBzI] = 0.1 mM, 16.7 mM pH 7 phosphate buffer.

this experiment, as the conjugate acids of these anions have a pK_a between that of fluoride and bicarbonate (3.2 and 6.8, respectively). It was hoped that the addition of both OFm^- and OAc^- to the **NBzI/H^W** system would cause an increase in rate in both samples. The resulting data from this experiment is shown below in Figure 2.30.

Sample	Anion	calc k_{cat} / s^{-1}	SE k_{cat} / s^{-1}	% error	k_2 / M^{-1} s^{-1}	pK_a
X1	None	2.11E-05*	2.98E-07	1.4		
X2	None	6.19E-05	2.41E-07	0.4	1.24	
X3	F^-	6.42E-05	1.48E-07	0.2	1.28	3.20
X4	OFm^-	6.92E-05	2.35E-07	0.3	1.38	3.86
X5	OAc^-	7.71E-05	2.85E-07	0.4	1.54	4.87
X6	HCO_3^-	1.08E-04	1.45E-06	1.3	2.15	6.80

Table 2.6 – Tabulated data comparing the catalysed rate constants in the presence of basic anions @ 1mM. [H^W] = 0.05 mM, [NBzI] = 0.1 mM, 50 mM pH 7 phosphate buffer. *background rate, not catalysed.

The data presented in Figure 2.30 and Table 2.6 show a clear picture of the effect these anions have on the catalysis of nitrobenzisoxazole. Each anion of increasing basicity resulted in a faster rate of reaction for **NBzI**, confirming the result seen for fluoride and bicarbonate in previous experiments. A relationship can be drawn between the calculated values of k_{cat} and the pK_a of the conjugate acid in question which shows a clear correlation between basicity of added anion and rate of reaction even at the same (buffered) overall pH for the bulk solution.

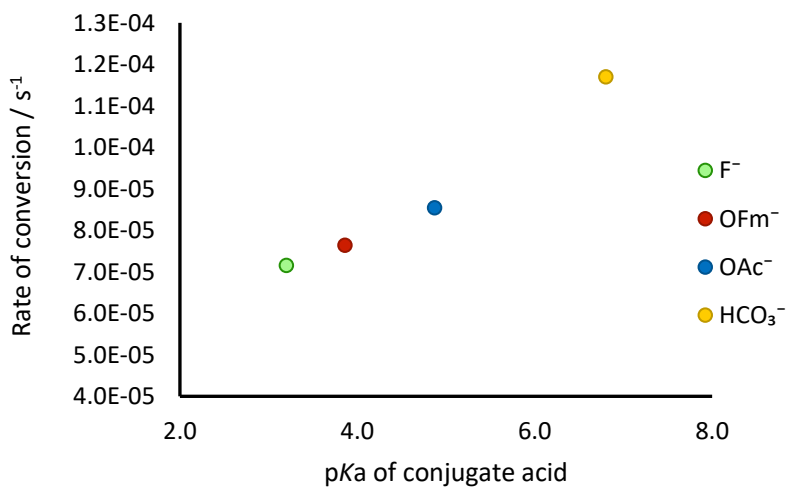

Figure 2.31 – A graph to visualise the results in the previous two figures: using k_{cat} and conjugate acid pK_a as the axes, this shows that the basicity of the added anion does influence the rate of reaction.

This experiment confirmed the hypothesis that addition of basic anions to **H^W/NBzI** would increase the rate of catalysis. **H^W** acts as the mediator for this process, bringing together the basic anions with the nitrobenzisoxazole starting material through a combination of electrostatic attraction and hydrophobic effects. This ability is provided by the pairing of high positive charge due to the Co(II) ions situated at the cage's vertices and the hydrophobic exterior surface of the cage. To confirm that the addition of these anions was not altering the pH of the solution, a comparison between two samples, one with cage present and one without cage was set up, similar to the control experiments performed before previous experiments.

As Figure 2.32 shows, the presence of bicarbonate at a low concentration (1.67 mM) has little effect on the reaction in the absence of the catalyst **H^W**, with the rate constant being close to that of background reaction (1.38×10^{-5} s^{-1} for the sample containing bicarbonate compared to 1.80×10^{-5} s^{-1} for the background rate). Add **H^W** to the reaction, however, and the rate constant k_{cat} increases to 1.74×10^{-4} s^{-1}, almost a tenfold increase. This confirms that the bicarbonate anion will only act as a base in this reaction when brought into close proximity of the **NBzI** substrate by the cage, allowing deprotonation and conversion to the phenolate product to occur.

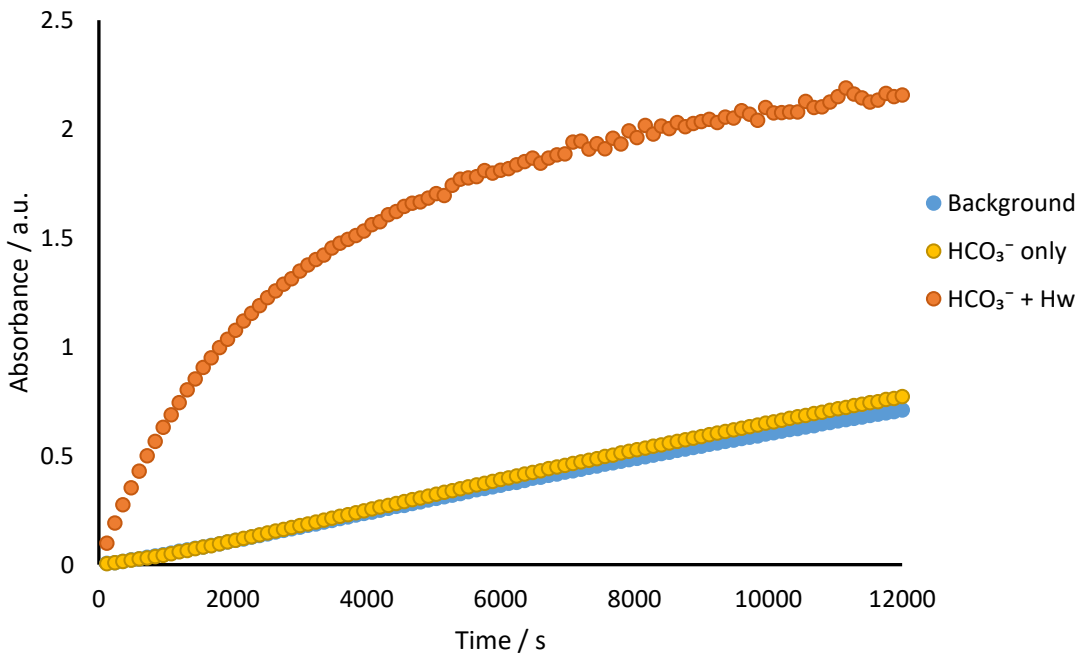

Figure 2.32 – A control experiment to ensure that bicarbonate alone was not influencing the reaction, through a change in pH or otherwise. [H^W] = 0.125 mM, [NBzI] = 0.2 mM, [HCO_3^-] = 1.67 mM, 16.7 mM pH 7 phosphate buffer.

Previous studies on catalysis of the Kemp elimination of benzisoxazole using **H^W** performed using NMR spectroscopy involved additions of increasing concentrations of anions to evaluate their effects as inhibitors. These studies included an experiment that added chloride to the system in varying amounts, starting with 16 equivalents, and increasing to 32 and 48 equivalents. Each addition showed a reduction in rate and caused the profile to become more sigmoidal in shape due to the onset of autocatalysis.[19] Since the work conducted in this chapter had focused heavily on the role of anions in the catalysis of **NBzI**, an experiment to mimic this was devised. The experiment involved the anions chloride, bromide, and nitrate – added in varying equivalents doubling from 1 equivalent up to 128 equivalents and one final iteration with 200 equivalents of anion. Using a concentration of **H^W** of 50 µM and **NBzI** at 100 µM, these reactions were carried out and the rates compared.

The graphs portraying the data for the conversion of **NBzI** to **2CNP** with **H^W** as the catalyst in the presence of increasing equivalents of Cl^-, Br^- and NO_3^- can be seen in Figure 2.34. Increasing concentrations of each anion provides the same overall effect on first inspection – with increasing concentration of the added anion comes greater inhibition of the cage's ability to catalyse the reaction. For some of the datasets, the profile of the signal curve appears to become more sigmoidal with increasing equivalents of added anion; the sigmoidal profile is characteristic of autocatalysis occurring.[19,30] This effect is more pronounced for chloride than bromide and nitrate. As the concentration of **2CNP** increases, the phenolate product accumulates around the cage's exterior, acting as the base for the reaction. As the concentration of surface-bound **2CNP** increases, the rate subsequently also increases.

For this to occur, the **2CNP** product must be able to bind to the surface, where it can interact with unreacted starting material. This process requires **2CNP**'s affinity for the cage's surface to be greater than the anion added, otherwise the product will be free in solution and cannot be involved in the reaction.

To deduce the position of **2CNP** within the series of anions that have been used to inhibit catalysis, a makeshift displacement experiment was designed. This experiment took advantage of the observation that the absorption maximum for the product **2CNP** red-shifts by *ca.* 25 nm when in the presence of the cage – this is an

indicator of association between the phenolate and the cage. If this absorption maximum shifts back to a shorter wavelength (characteristic of free **2CNP**) after addition of a particular anion, that anion has a higher affinity for the cage's surface than **2CNP** and has displaced any bound **2CNP** from the cage's surface.

The anions F^-, IO_3^-, Cl^-, Br^- and NO_3^- were added as their sodium salts to a solution containing **2CNP** and $\mathbf{H^W}$ in a 2:1 stoichiometry. 10 equivalents of each anion were used. The results of this experiment are presented in Figure 2.33.

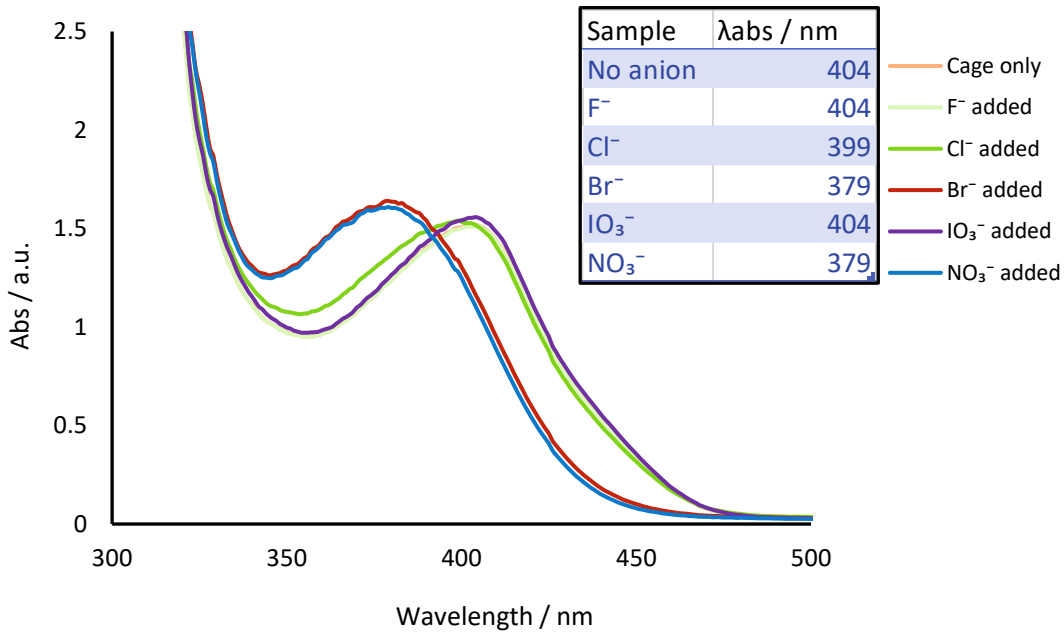

Figure 2.33 – UV/vis absorption spectra of 2CNP/H^W + additional anions at 10 equivalents. [H^W] = 0.05 mM, [2CNP] = 0.1 mM, [anion] = 0.5 mM, 16.7 mM pH 7 phosphate buffer.

As the graph in Figure 2.33 shows, there is a blue-shift observable for the **2CNP** absorption maximum in the presence of an excess of the chaotropic anions bromide and nitrate, due to their high affinity for the cage's surface. These anions displace the **2CNP** that was bound to the cage, resulting in the peak absorbance being seen at 379 nm (free **2CNP** in water) rather than 404 nm (cage-bound **2CNP**). Chloride produces a similar result but to a far lesser extent – blue-shifting the absorbance by only 5 nm. Fluoride and iodate do not appear to affect the absorbance of **2CNP** and can therefore be deduced to bind to the surface of $\mathbf{H^W}$ more weakly than **2CNP**.

Relating this experiment to the previous one, it is now clearer why the sigmoidal profile (indicative of autocatalysis occurring) is only seen for some samples but not all samples. Many of the measurements using lower amounts of chloride (< 64 equivalents) possess a sigmoidal profile, whilst this feature is far less obvious for bromide and particularly difficult to detect for nitrate. Hypothetically, this may be due to the relative affinities of the anions for the cage compared to **2CNP**. As bromide and nitrate (at 10 equivalents) both seem to displace any bound phenolate, it seems that the autocatalytic pathway is less prevalent for these anions as the **2CNP** cannot bind to the cage in the presence of these strongly competing anions; the sigmoidal shape can only be seen for the datasets using very small amounts of these anions. With chloride's affinity being lower and more comparable to **2CNP**, autocatalytic behaviour appears more easily in the presence of chloride.

A separate study of the data highlighted another possible reason for the apparent sigmoidal character to some of the curves. In some cases, as the reaction proceeds there is a gradual change in λ_{max} of the **2CNP** absorption maximum as the proportion of free/bound product changes. A change in balance between free and surface-bound **2CNP** as the reaction proceeds could potentially lead to the extinction coefficient at the monitoring wavelength increasing slightly as the reaction proceeds which would give this effect. It is important to note at this point that this effect occurs over a long period of time, and so the k_{cat} values calculated using initial rates earlier in this chapter for various experiments are still valid.

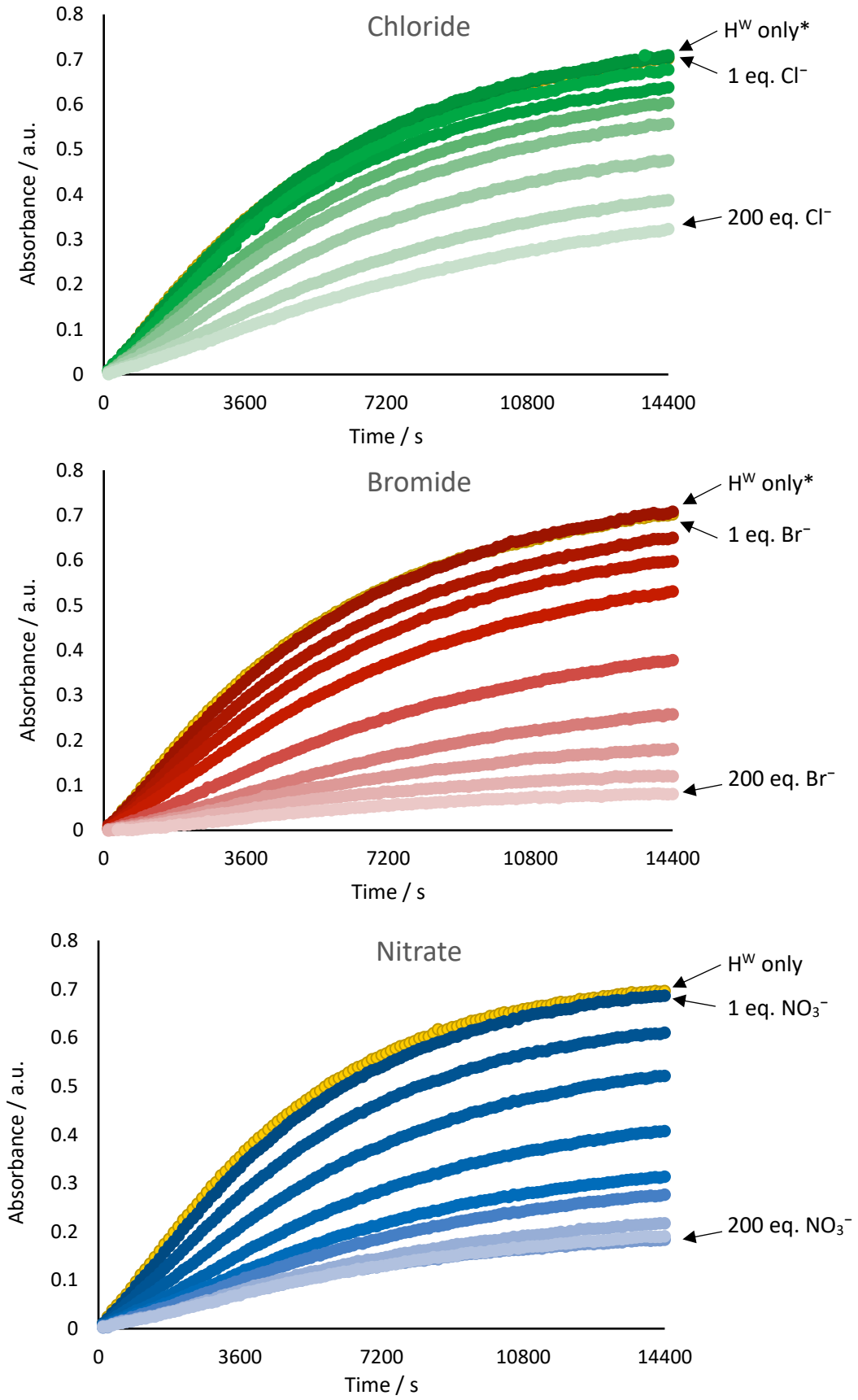

Figure 2.34 – Reaction profiles for the conversion of NBzI to 2CNP by H^W in the presence of increasing equivalents of Cl^-, Br^- and NO_3^-. [NBzI] = 0.1 mM, [H^W] = 0.05 mM, 16.7 mM pH 7 phosphate buffer. *"H^W only" covered by another dataset.

The experiment involving increasing equivalents of added anion was also conducted using fluoride as the anion. As previously shown in this chapter, fluoride increases the rate of reaction due to its basic nature, so it was expected that a steady increase in reaction rate would be seen as more fluoride was added.

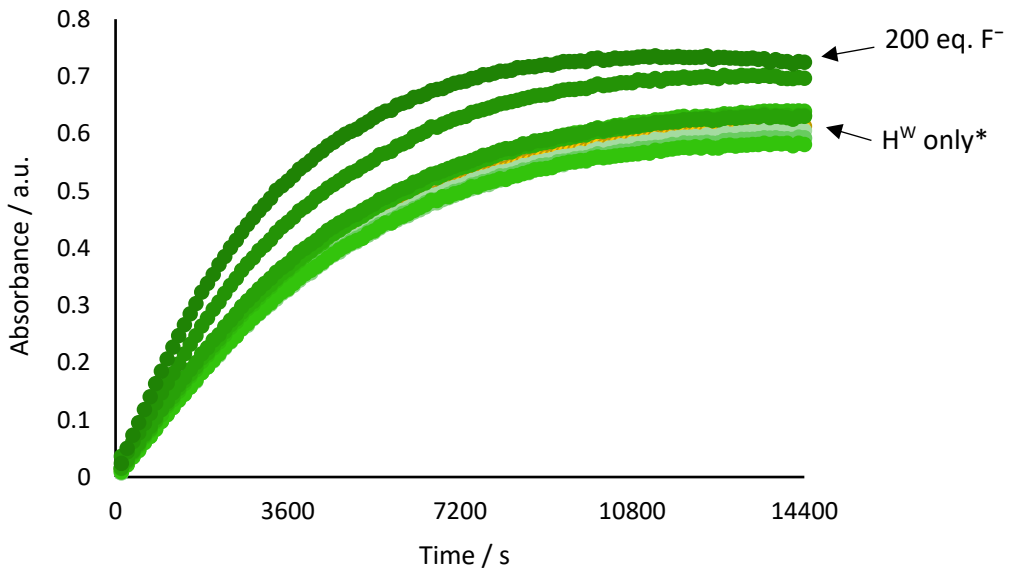

Figure 2.35 – Reaction profiles for the conversion of NBzI to 2CNP by H^W in the presence of increasing equivalents of F^-. [NBzI] = 0.1 mM, [H^W] = 0.05 mM, 16.7 mM pH 7 phosphate buffer. *"H^W only" covered by another dataset.

As shown in Figure 2.35, there is a clear increase in rate of reaction for the samples with more equivalents of fluoride present. This observation aligns with experimental data obtained previously, showing that fluoride's basic nature assists the deprotonation step of the reaction. Interestingly, the fewer equivalents (between 1 and 8) of added fluoride appear to inhibit the reaction slightly, with the rate only increasing beyond that using only **H^W** alone after 16 equivalents of fluoride was added. This observation is likely caused by a minimum concentration of fluoride being needed to accumulate around the cage's exterior before the anion can act as part of the reaction pathway. Importantly, this is distinct from the behaviour observed with the anions chloride, bromide, and nitrate, which all produce a decrease in rate with increasing number of equivalents added.

A final experiment was devised to observe the effect of increasing concentration of **2CNP** product on the rate of reaction. The conditions of the previous experiment were retained but this time using **2CNP** as the added anion, at concentrations of 10, 20, 50 and 100 µM. Concentrations higher than this were unusable owing to the high absorbance of the **2CNP** product, making measurements unreliable.

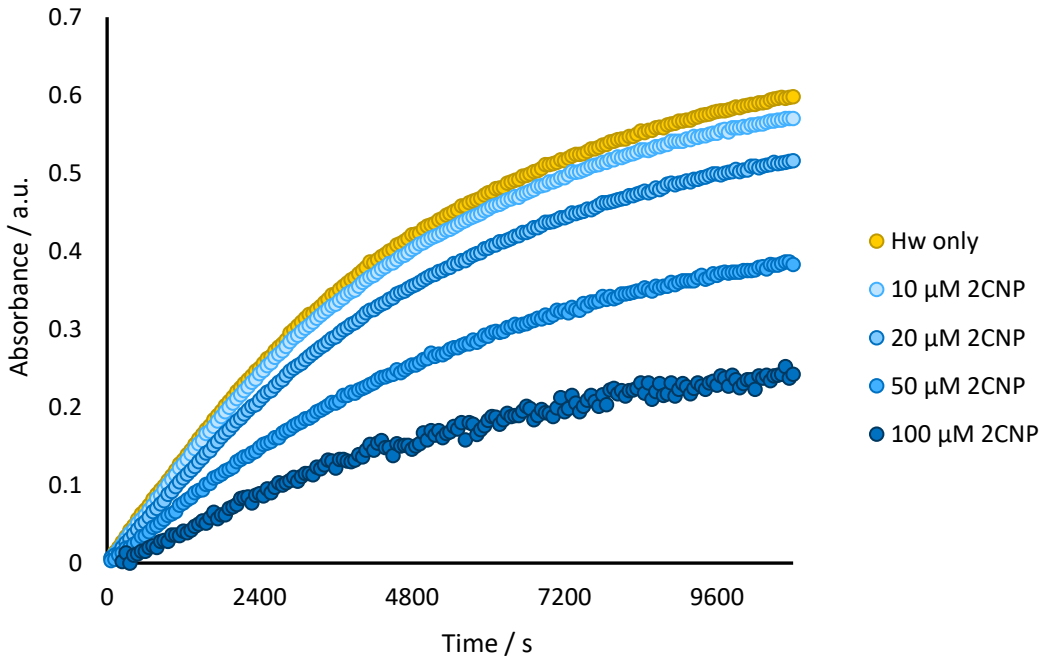

Figure 2.36 – Reaction profiles for the conversion of NBzI to 2CNP by H^W in the presence of increasing equivalents of 2CNP. [NBzI] = 0.1 mM, [H^W] = 0.05 mM, 16.7 mM pH 7 phosphate buffer.

Interestingly, the presence of **2CNP** from the start of this reaction appears to hinder the reaction rather than catalyse it. Using the unsubstituted version of benzisoxazole, autocatalysis was prominently seen as the concentration of product increased over time, whereas with nitrobenzisoxazole this effect is not present. This is likely due to the binding method of the **NBzI** starting material – as the molecule binds to the cage's surface and not within the cavity, any bound **2CNP** will be occupying potential binding sites for **NBzI**, slowing the reaction. The potential for **2CNP** to act as the base in the reaction is also reduced, as the binding mode will involve the phenolate moiety pointing towards the cage's surface and will therefore not be involved in the ring-opening reaction. This is in contrast to the basic anions seen earlier (formate, acetate etc).

2.3. Conclusions

This chapter opened with an investigation into the scope of anion exchange on the organic-soluble cage **H^A**. Known to be water-soluble after exchange of BF_4^- to Cl^-, this technique was extended to enable other anions to be exchanged as counter-anions for **H^A** such as HCO_3^-, NO_3^- and SO_4^{2-}. Successful anion exchange using pre-loaded Dowex or Amberlite resins was confirmed by both ^{1}H NMR and UV/vis spectroscopy for the now water-soluble cages. Subsequent experiments focused on the degree of conversion – that is, the number of new anions that are associated with the cage in its water-soluble state. This was studied by ^{19}F NMR spectroscopy, monitoring both the depletion of BF_4^- as the resin exchanges it for the desired anion and the appearance of fluoride from the decomposition of BF_4^- in water. These experiments found that the anion exchange was almost always incomplete, and the resulting cage complex would usually retain at least one BF_4^- anion along with free fluoride anions in several cases. The nitrate-exchanged cage **H^A·NO_3**, for example, only contained 6 NO_3^- anions compared to 9 F^- anions; this is likely the cause of water-solubility in this particular example. Several water-soluble variants of **H^A** were produced through this modified resin anion-exchange method, but due to inconsistencies with the degree of conversion and end concentration, this method was not used moving forward for experiments where knowledge of the anion composition was important because of its effect on catalytic behaviour. For the experiments involving catalysis, the water-solubilised cage **H^W** had an undetermined anionic composition after dissolution in water through hydrolysis. However, with the sample used remaining consistent throughout the duration of the catalytic studies, there was no variation in the anions associated with the cage which reduces the likelihood of experimental variation due to the sample of **H^W** used.

The variation in solubility properties of the cage when anion exchanged with different anions prompted a different route of investigation, namely the inhibition of a catalytic reaction through the presence of various anions. The Kemp elimination of 5-nitrobenzisoxazole was found to be catalysed by **H^W** but, unlike the reaction using the unsubstituted precursor benzisoxazole, catalysis did not appear to occur within the cage's cavity as demonstrated by the fact that cycloundecanone, a strongly

binding cavity-bound guest, did not slow the reaction – suggesting that catalysis was occurring on the cage's exterior surface. A range of anions from across the Hofmeister series were added to the reaction to observe their effects on the catalysed reaction rate. Broadly, the trend seen was that reaction inhibition increased with increasing hydrophobicity of anion; the slowest rate (greatest degree of inhibition of catalysis) observed was for nitrate, the most chaotropic of the anions tested. There was a definite correlation seen between k_{cat} and the position of the added anion on the Hofmeister series.

Not all the anions studied hindered the catalytic reaction, however. Both HCO_3^- and F^- were seen to increase the rate of reaction, presumably due to their inherent basicity and desolvation when they bind to the cage surface, as seen with phenolates in previous work.[19] To confirm this was the case, the anions formate and acetate were also tested. Addition of either of these anions to **H^W/NBzI** mixtures increased the catalysis rate compared to just **H^W**, with the order for k_{cat} being $F^- < OFm^- < OAc^- < HCO_3^-$. This aligns with the p$K_a$ values of the conjugate acids of the anions. As a control experiment, HCO_3^- was tested with and without **H^W** to check that the rate increase seen was due to the cage and not an increase in solution pH. As the rate barely increased beyond the background rate in the absence of **H^W**, the catalytic effect seen could be attributed to the combination of cage and surface-bound HCO_3^- together, and not the solution pH changing.

Incrementally increasing the concentration of an anion that hinders the reaction such as chloride or bromide leads to a steady reduction in catalysed reaction rate. For chloride, an increasingly sigmoidal profile is seen as the number of equivalents of added anion is increased, which suggests an autocatalytic reaction pathway forming involving the 2-cyanonitrophenolate product. This effect is more pronounced for chloride than bromide or nitrate, as bromide and nitrate prevent **2CNP** from being involved in the ring-opening reaction, which is the origin of the autocatalytic pathway. Autocatalysis, however, can be discounted as addition of **2CNP** to the reaction slows the rate of reaction, likely through occupying potential binding sites for **NBzI**, and **2CNP** binding stronger due to its anionic nature.

2.4. Experimental details

2.4.1. General experimental details

Anion exchange resins were purchased from Sigma Aldrich. All salts used within this chapter were obtained from commercial sources and used as supplied. 5-nitrobenzisoxazole (NBzI) was synthesised by Max Tipping. Instruments used in data collection were as follows: UV/vis spectra were obtained using a BMG ClarioStar plate reader and 96-well plates. NMR spectra were obtained using either a Bruker Avance 300 MHz or a Bruker Avance III HD 400 MHz machine. Mass spectrometry was conducted using an Agilent 6130B ESI-MS machine. pH adjustments were made using a Hanna Instruments HI2210 pH meter fitted with a Hamilton SpinTrode probe. Specific experimental details are provided in the following sections.

2.4.2. Synthesis of the organic-soluble cage H^A

2.4.2.1. Synthesis of 1,5-di(bromomethyl)naphthalene

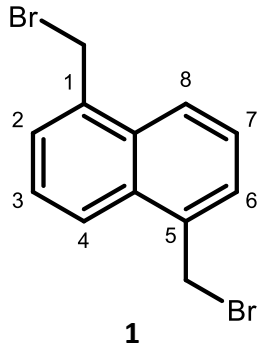

1,5-dimethylnaphthalene (5 g, 32 mmol) was dissolved in 200 mL of $CHCl_3$. To this, 11.75 g of N-bromo-succinimide was added (66 mmol, 2.1 equivalents) followed by 10 mg of azobisisobutyronitrile to act as the free radical initiator. This solution was refluxed at 60 °C whilst under irradiation from a halogen lamp in a cycle of 15 minutes on, 15 minutes off. This process was maintained for 2 h, after which the solvent was removed under reduced pressure. The off-white solid was washed with deionised water and allowed to dry, returning 7.13 g of product (71 % yield).

^{1}H NMR ($CDCl_3$, 300 MHz) δ: 8.19 (d, 2H, J = 8.8 Hz, $H^{4,8}$), 7.57 (m, 4H, $H^{2,3,6,7}$), 4.96 (s, 4H, naph-CH_2)

EI-MS *m/z*: 314.0 $[M]^+$, 233.1 $[M – Br]^+$, 154.2 $[M – 2Br]^+$

This experimental procedure is taken from and in agreement with reference 31.

2.4.2.2. Synthesis of ligand L^A

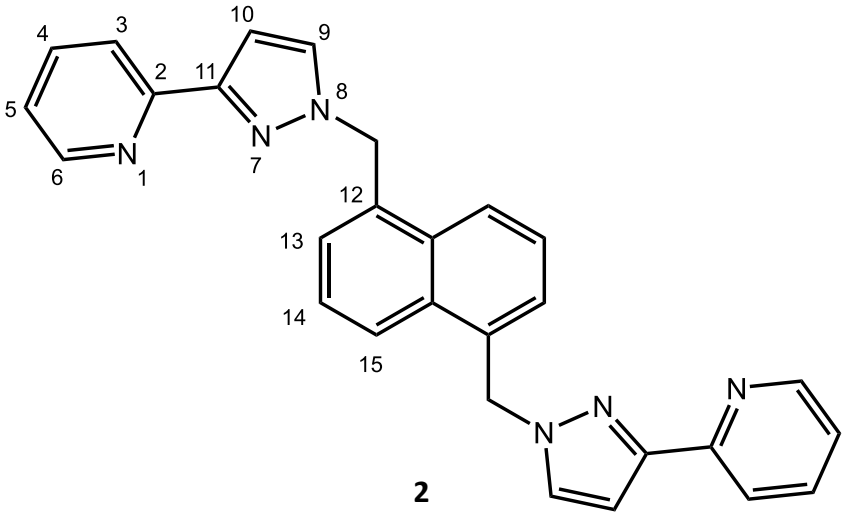

1.86 g (12.81 mmol) of 3-(2-pyridyl)pyrazole (PyPzH) was mixed with 2 g (6.37 mmol) of 1,5-di(bromomethyl)naphthalene in 100 mL of THF and stirred until full dissolution had occurred. In a separate vessel, 1 g of NaOH was dissolved in 25 mL of deionised H_2O and subsequently added to the reaction mixture. Teflon tape was fitted to any glass joints in the reaction apparatus and the solution brought to reflux at 70 °C for 18 h. After this time, the aqueous NaOH layer was removed from the reaction vessel by pipette and the organic solvent removed under reduced pressure. A brown solid was produced which was purified through recrystallisation ($CHCl_3$/hexane). This afforded a white powder (1.69 g, 60% yield).

^{1}H NMR: (400 MHz, CDCl3): δ 8.67 (d, 2H, *J* = 4.5 Hz, pyridyl H^6), 8.09 (d, 2H, *J* = 8.5 Hz, naphthyl H^{15}), 8.00 (d, 2H, *J* = 8.5 Hz, pyridyl H^3), 7.75 (2H, t, *J* = 7.5 Hz, naphthyl H^{14}), 7.52 (2H, t, *J* = 7.5 Hz, naphthyl H^{13}), 7.37 (2H, d, *J* = 7 Hz, pyridyl H^5), 7.23 (2H, t, *J* = 6 Hz, pyrazolyl H^9), 6.89 (2H, s, pyrazolyl H^{10}), 5.90 (4H, s, naphthyl-CH_2-PyPz).

2.4.2.3. Synthesis of coordination cage H^A

Ligand L^A (200 mg, 0.452 mmol) and $Co(BF_4)_2.6H_2O$ (80 mg, 0.344 mmol) were combined in 50 mL of MeOH and refluxed at 70 °C for 18 h. The precipitate that formed was filtered off and washed with 2 x 20 mL portions of the following in the order given: ice cold MeOH, CH_2Cl_2, Et_2O. This produced an orange-coloured solid which could be characterised by NMR spectroscopy.

The experimental procedures for Sections 2.4.2.2 and 2.4.2.3 are taken from and are in agreement with reference 32.

2.4.3. Synthesis of the water-soluble cage H^W

2.4.3.1. Protecting the OH group of 4-hydroxymethyl pyridine

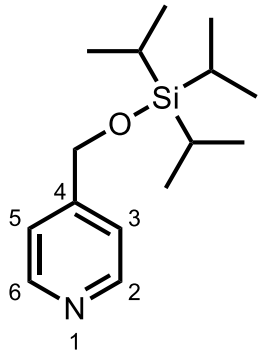

3

Under a N_2 atmosphere, 16.06 g of imidazole (0.236 mol) was dissolved in 100 mL of CH_2Cl_2:DMF (9:1 v:v ratio). Once the imidazole had dissolved, triisopropylsilyl chloride (35 mL, 0.165 mol) was slowly added. After complete addition, the mixture was stirred for a further 10 minutes. 4-hydroxymethyl pyridine (15.05 g, 0.138 mol) was then added and the mixture left stirring at room temperature for 18 h. Following this, the solvent was removed under reduced pressure and 100 mL of deionised H_2O added to the residue. The product was extracted using 2 x 100 mL portions of EtOAc:hexane (1:1 v:v), the organic layers combined and dried using $MgSO_4$. Removal of the solvent under reduced pressure afforded the product as a yellow oil (35.6 g, 98 % yield).

^{1}H NMR (300 MHz, $CDCl_3$): δ 8.57 (dd, 2H, $J_{1,2}$ = 1.5 Hz, $J_{1,3}$ = 6 Hz, pyridyl $H^{2,6}$), 7.31 (d, 2H, J = 6 Hz, pyridyl $H^{3,5}$), 4.86 (s, 2H, pyridyl-CH_2-OTIPS), 1.13 (s, 12H, Si-^{i}*Pr*), 1.11 (s, 6H, Si-^{i}*Pr*), 1.09 (s, 3H, Si-^{i}*Pr*).

ES-MS *m/z* (%): 266.2 $[M + H]^+$

2.4.3.2. Acylation of the protected pyridine

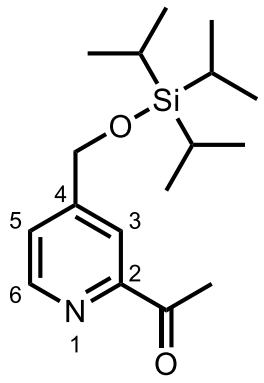

4

25 g of the protected pyridine **3** (94.2 mmol) was dissolved in 200 mL of CH_2Cl_2. To this, 150 mL of deionised H_2O was added, followed by 20 mL of pyruvic acid (282.6 mmol) and 43 g of $(NH_4)_2S_2O_8$ (188.4 mmol) which were washed into the reaction vessel with a further 50 mL of deionised H_2O. After stirring for 10 minutes, $AgNO_3$ (1.6 g, 9.42 mmol) was added, and the reaction brought to reflux at 40 °C for 1 h. After this time, the reaction was allowed to cool and subsequently basified to pH 10 using 25% w:w NaOH solution. The layers were separated, and the aqueous layer extracted using 4 x 100 mL portions of CH_2Cl_2. The organic layers were combined and dried using $MgSO_4$, then the solvent removed under reduced pressure. The residue was further purified by column chromatography (SiO_2, 30:70 v:v EtOAc:hexane) to afford a yellow oil (15.35 g, 53 % yield).

^{1}H NMR (300 MHz, $CDCl_3$) δ: 8.62 (d, 1H, $J_{1,3}$ = 5 Hz, pyridyl H^6), 7.95 (s, 1H, pyridyl H^3), 7.53 (d, 1H, $J_{1,3}$ = 5 Hz, pyridyl H^5), 4.87 (2H, s, pyridyl-CH_2-OTIPS), 2.70 (3H, s, pyridyl 2-acyl CH_3), 1.02 (s, 21H, Si-^{i}*Pr*)

ES-MS *m/z* (%): 330.2 $[M + Na]^+$ (100), 308.2 $[M + H]^+$ (67).

2.4.3.3. Conversion to keto-enamine

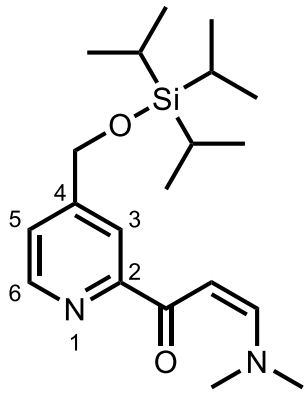

5

16.8 g of the now acylated pyridine **4** (54.6 mmol) was combined with 9.76 g of DMF·DMA (11 mL, 81.9 mmol) and 20 mL of DMF. The reaction was refluxed at 110 °C for 16 h, after which time the solvent was removed with the assistance of 2 x 50 mL portions of xylene. The residue was a dark orange oil which was taken forward without further purification (18.5 g, 93 % yield).

^{1}H NMR (300 MHz, $CDCl_3$) δ: 8.57 (d, 1H, *J* = 5 Hz, pyridyl H^6), 8.03 (s, 1H, pyridyl H^3), 7.88 (d, 1H, *J* = 12.7 Hz, C*H*-NMe_2), 7.44 (d, 1H, *J* = 5 Hz, pyridyl H^5) 6.43 (d, 1H, *J* = 12.7 Hz, C*H*-C=O), 4.86 (s, 2H, pyridyl-CH_2-OTIPS), 3.13 (s, 3H, N-CH_3), 2.96 (s, 3H, N-CH_3), 1.08 (s, 18H, Si-^{i}Pr).

ES-MS *m/z* (%) 363.4 $[M + H]^+$

2.4.3.4. Formation of OTIPS-PyPzH

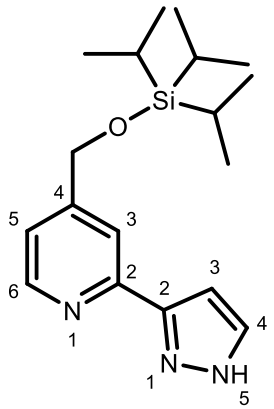

6

6.42 g of keto-enamine product **5** (17.7 mmol) was dissolved in 40 mL of EtOH. Under constant stirring, 3.5 mL of hydrazine monohydrate (72 mmol, 4 eq.) was added, and the reaction brought to reflux at 60 °C for 1 h. The solvent was then removed under reduced pressure and the residue purified by column chromatography (SiO_2, 5:95 v:v MeOH:CH_2Cl_2). This afforded a dark brown oil which slowly solidified over time (4.05 g, 69 % yield).

^{1}H NMR (300 MHz, $CDCl_3$) δ: 8.62 (d, 1H, *J* = 5.2 Hz, pyridyl H^6), 7.74 (s, 1H, pyridyl H^3), 7.63 (d, 1H, *J* = 2 Hz, pyrazolyl H^4), 7.23 (d, 1H, *J* = 5.2 Hz, pyridyl H^5), 6.76 (d, 1H, *J* = 2 Hz, pyrazolyl H^3), 4.85 (s, 2H, pyridyl-CH_2-OTIPS), 1.08 (s, 10H, Si-^{i}Pr), 1.07 (s, 11H, Si-^{i}Pr).

ES-MS *m/z* (%): 332.3 $[M + H]^+$

2.4.3.5. Formation of protected ligand L^{OTIPS}

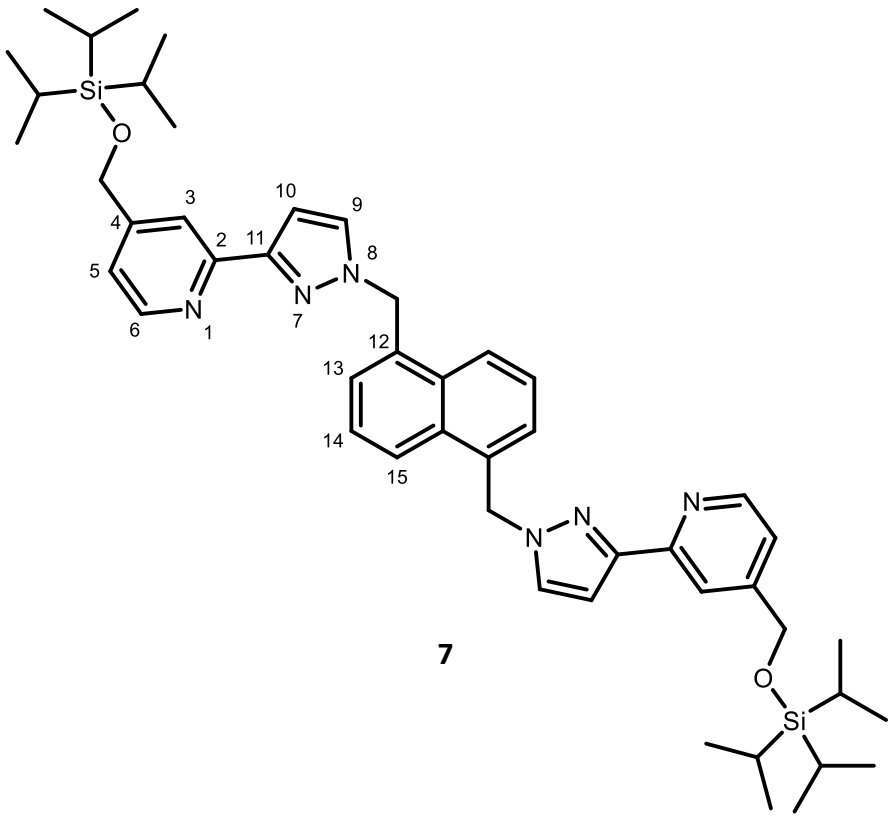

7

6.21 g of the protected PyPzH **6** (18.7 mmol, 2 eq.) was dissolved in 100 mL of dry THF under a N_2 atmosphere. NaH (1.50 g, 75 mmol, 4 eq.) was added as a 60%

suspension in mineral oil and the reaction mixture stirred for 5 minutes. Di(bromomethyl)naphthalene was then added (2.80 g, 8.9 mmol) and the reaction brought to reflux at 70 °C for 16 h. Thin layer chromatography (TLC) was used to monitor the reaction's progress (4:96 v:v MeOH:CH_2Cl_2). After the reaction was complete, MeOH was added to the solution until effervescence stopped to quench any unreacted NaH. The solvent was removed under reduced pressure and the residue filtered through a Celite plug using the same solvent system as for the TLC. The solvent was again removed, and the crude product purified by column chromatography (SiO_2, 4:96 v:v MeOH:CH_2Cl_2). This afforded a yellow oil (6.53 g, 90 % yield).

^{1}H NMR ($CDCl_3$, 300 MHz) δ: 8.60 (d, 2H, *J* = 5.1 Hz, pyridyl H^6), 8.05 (d, 2H, *J* = 8.6 Hz, naphthyl H^{15}), 7.89 (s, 2H, pyridyl H^3), 7.48 (t, 2H, *J* = 7.8 Hz, naphthyl H^{14}), 7.34 (d, 2H, *J* = 7 Hz, naphthyl H^{13}), 7.29 (d, 2H, *J* = 5.1 Hz, pyridyl H^5), 7.25 (d, 2H, *J* = 2.4 Hz, pyrazolyl H^9), 6.83 (d, 2H, *J* = 2.4 Hz, pyrazolyl H^{10}), 5.86 (s, 4H, naphthyl-CH_2-PyPz), 4.89 (s, 4H, PyPz-CH_2-OTIPS) 1.11 (s, 14H, Si-^{i}*Pr*), 1.09 (s, 10H, Si-^{i}*Pr*).

2.4.3.6. Deprotection of L^{OTIPS} to form L^W

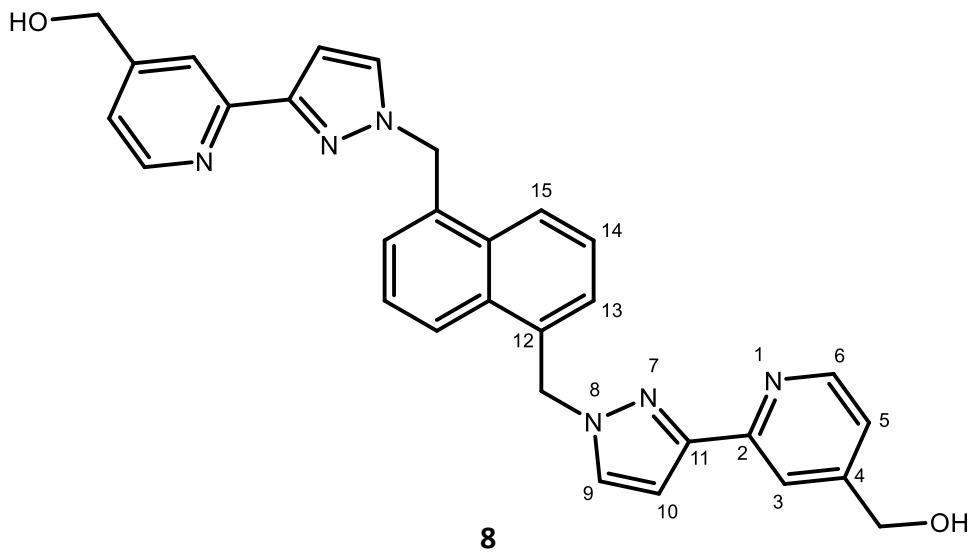

8

2.91 g of the ligand **7** (3.57 mmol) was dissolved in 20 mL of THF. Under constant stirring, 7.5 mL of TBAF (1.0M in THF) (7.5 mmol, 2.1 eq.) was added and the reaction monitored by TLC (5:95 v:v MeOH:CH_2Cl_2) until full deprotection was seen. At this

point, the solvent was removed under reduced pressure to near dryness. 50 mL of both CH_2Cl_2 and deionised H_2O were added, causing the product to precipitate out of solution. The solid was filtered off and washed with cold CH_2Cl_2. A cream-coloured powder was obtained (1.48 g, 83 % yield).

^{1}H NMR (400 MHz, d^6-DMSO): δ 8.47 (2H, d, *J* = 4.8 Hz, H_6), 8.22 (2H, d, *J* = 8.8 Hz, H_3), 7.88 (4H, s, H_5/H_{15}), 7.58 (2H, t, *J* = 8 Hz, H_{14}), 7.28 (2H, d, *J* = 6.8 Hz, H_9), 7.20 (2H, d, *J* = 4.8 Hz, H_{13}), 6.84 (2H, s, H_{10}), 5.94 (4H, s, pz-N-CH_2), 4.56 (4H, s, py-CH_2OH).

The synthetic procedures described in Sections 2.4.3 are taken from and in agreement with reference 33.

2.4.3.7. Formation of H^W

A 7 mL squat glass vial was charged with the ligand **8** (45 mg, 0.09 mmol), $Co(BF_4)_2{\cdot}6H_2O$ (25 mg, 0.073 mmol, slight excess) and 7 mL of methanol. This was placed inside a Teflon inner for a metal autoclave and heated using an oven at 120 °C for 12 h followed by a gradual decrease in temperature for a further 12 h until the system had reached room temperature.

This process resulted in X-ray quality crystals of the cage $[Co_8L^W{}_{12}][BF_4]_{16}$. These were collected still solvated by the mother liquor, separated with use of a centrifuge, and washed with ice cold methanol (20 mL), dichloromethane (20 mL) and diethyl ether (20 mL). This produced a pale orange powder which was dried *in vacuo* and analysed

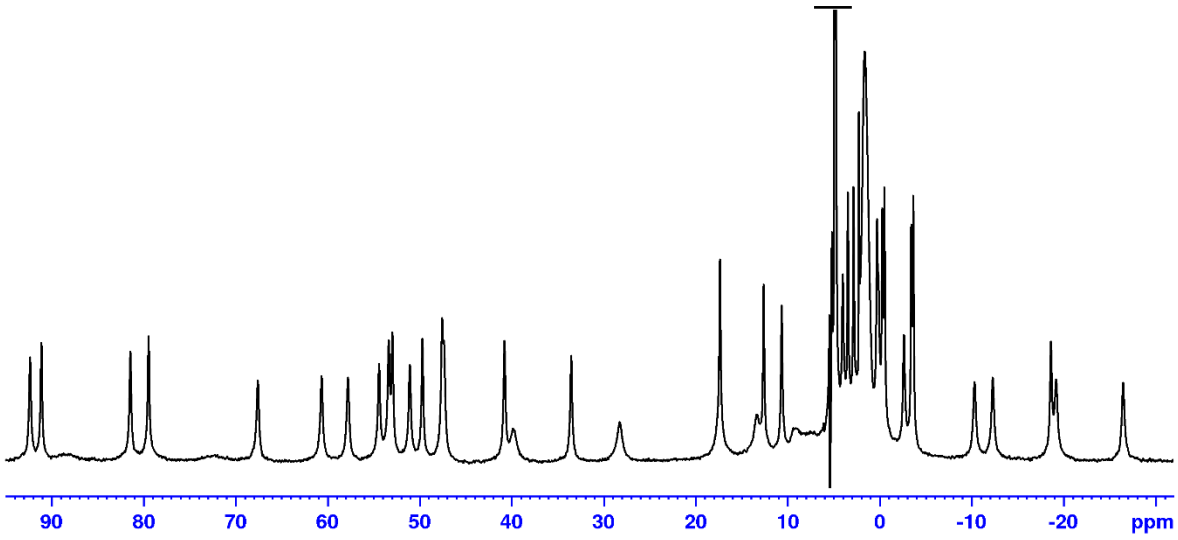

by ^{1}H NMR, the spectrum of which can be seen below. ESI-MS was also performed on the final product, the results of which are shown in Appendix 2.6.2. The synthetic route followed was taken from reference 34, and the resulting characterisation was in agreement with the published data.

2.4.4. Preparation of anion-exchanged resins from Amberlite IRA-400 mesh

Conversion of chloride-type resins was undertaken using typically 20 cm^3 of wetted resin in a 250 mL screw-top jar. The exchange capacity of the resin was found in the Dow company data booklet online to be 1.6 milli-equivalents per cm^3 of wetted resin, allowing a total mobile concentration of chloride to be calculated. A solution of the anion to be exchanged was prepared at 10x the concentration of chloride, eg. A 0.32 M solution of $NaNO_3$ for 20 mL of chloride resin. The resin was stirred for 30 minutes in the salt solution and then rinsed with 250 mL deionised water to remove any residual salt. The prepared resins were stored in a small amount of deionised water and rinsed with D_2O before use for NMR spectroscopy experiments.

2.4.5. Preparation of anion-exchanged resins from Dowex Marathon OH form

Converting Marathon OH^- form resin was undertaken in the same manner as with the Amberlite form used previously, but with new concentrations of salt solutions owing to the different exchange capacity: Marathon OH^- form has a capacity of 1.0 milli-equivalents per cm^3 of wetted resin.

2.4.6. Conversion of H^A to water-soluble analogues eg. $H^A{\cdot}HCO_3$

7.2 mg of H^A was suspended in 5 mL of D_2O. To this, approximately 1 mL of wetted resin (prewashed in D_2O) was added, and the sample stirred for between 20 minutes to 18 hours depending on the experiment. After exchange was complete, the solution was separated by the resin through one of two methods: a) centrifugation, typically used for the smaller diameter resin Dowex 1x2 Cl^- form, or b) drawing the solution through a syringe needle, which is too narrow for the Amberlite and Marathon resins.

If the solution were cloudy at this point it would be passed through a Millipore filter (0.2 µM) before the concentration was checked by UV/vis spectroscopy.

2.4.7. ^{19}F NMR experiments for H^A·X samples

0.9 mL of the converted H^A·X sample was combined with 0.1 mL of a sodium triflate solution used as a calibrant for both the ppm and integrals of the resulting spectrum. The NaOTf solution was prepared by dissolving 34.4 mg in 10 mL of D_2O, giving a 20 mM solution that was 2 mM in the NMR tube. Knowing this concentration allowed accurate determination of concentrations for BF_4^- and F^- and subsequently the number of each anion in each cage sample. ^{19}F NMR spectroscopy experiments were run on a Bruker Avance iii HD400 spectrometer calibrated to 300 K.

2.4.8. ^{1}H NMR experiments for H^A·X samples

After following the procedure for converting H^A to a water-soluble analogue as described in 2.4.4, a ^{1}H spectrum of the cage being studied was obtained using a Bruker Avance 300 MHz spectrometer calibrated to 300 K. The acquisition parameters used were as follows: 3072 scans, a receiver gain of 256 and a scan region of -100 to +120 ppm.

2.4.9. Determining the rate of reaction for NBzI in the presence of H^W

For any reactions monitored over time by UV/vis, the rate was determined through monitoring the absorbance of the product 2-cyano-4-nitrophenolate at 400 nm if in the presence of **H^W** and 380 nm if only **NBzI** was used (unless stated otherwise). The extinction coefficient quoted in the literature is 15800 M^{-1} cm^{-1} (reference 35) and using this a concentration of product could be calculated from the absorbance. Each dataset was corrected by first setting the absorbance at t = 0 s to equal zero, followed by subtracting the background absorbance at each data point to give the catalysed reaction profile. Taking the natural log of the concentration of starting material and using the LINEST function in Excel, a rate constant could be determined for each

dataset along with the standard error for the data. This analysis function was typically used over the first 20 datapoints, giving an initial rate.

Experiments performed to observe the reaction of nitrobenzisoxazole to 2-cyano-4-nitrophenolate were prepared using a 96-well plate with an individual well volume of 300 µL per sample. Sample preparation involved mixing of the cage, buffer, and any added solutions of anions as their sodium salts and finally adding a solution of nitrobenzisoxazole before immediately transferring the plate to the instrument and beginning monitoring the reaction. For reported data, 4 repeats were typically run in parallel, and the data averaged.

2.5. References

1 J. P. Mathias, C. T. Seto, E. E. Simanek and G. M. Whitesides, *J. Am. Chem. Soc.*, 1994, **116**, 1725–1736.

2 C. A. Hunter, K. R. Lawson, J. Perkins and C. J. Urch, *J. Chem. Soc. Perkin Trans. 2*, 2001, 651–669.

3 C. A. Hunter, *Angew. Chemie - Int. Ed.*, 2004, **43**, 5310–5324.

4 R. W. Saalfrank, A. Stark, K. Peters and H. G. von Schnering, *Angew. Chemie Int. Ed. English*, 1988, **27**, 851–853.

5 D. L. Caulder, R. E. Powers, T. N. Parac and K. N. Raymond, *Angew. Chemie Int. Ed.*, 1998, **37**, 1840–1843.

6 M. D. Pluth, R. G. Bergman and K. H. Raymond, *Science (80-.).*, 2007, **316**, 85–88.

7 A. Clements and M. Lewis, *J. Phys. Chem. A*, 2006, **110**, 12705–12710.

8 B. L. Schottel, H. T. Chifotides and K. R. Dunbar, *Chem. Soc. Rev.*, 2008, **37**, 68–83.

9 K. Choi and A. D. Hamilton, *Coord. Chem. Rev.*, 2003, **240**, 101–110.

10 P. D. Beer, P. A. Gale and D. Hesek, *Tetrahedron Lett.*, 1995, **36**, 767–770.

11 A. P. Bisson, V. M. Lynch, M. K. C. Monahan and E. V. Anslyn, *Angew. Chemie (International Ed. English)*, 1997, **36**, 2340–2342.

12 C. R. Bondy, P. A. Gale and S. J. Loeb, *J. Am. Chem. Soc.*, 2004, **126**, 5030–5031.

13 V. Amendola, M. Boiocchi, B. Colasson, L. Fabbrizzi, M. J. Rodriguez Douton and F. Ugozzoli, *Angew. Chemie - Int. Ed.*, 2006, **45**, 6920–6924.

14 H. T. Chifotides and K. R. Dunbar, *Acc. Chem. Res.*, 2013, **46**, 894–906.

15 A. Frontera, *Coord. Chem. Rev.*, 2013, **257**, 1716–1727.

16 B. Hasenknopf, J. M. Lehn, B. O. Kneisel, G. Baum and D. Fenske, *Angew.*

Chemie (International Ed. English), 1996, **35**, 1838–1840.

17 A. P. Paneerselvam, S. S. Mishra and D. K. Chand, *J. Chem. Sci.*, 2018, **130**, 96.

18 J. S. Fleming, K. L. V Mann, C. A. Carraz, E. Psillakis, J. C. Jeffery, J. A. McCleverty and M. D. Ward, *Angew. Chemie - Int. Ed.*, 1998, **37**, 1279–1281.

19 W. Cullen, A. J. Metherell, A. B. Wragg, C. G. P. Taylor, N. H. Williams and M. D. Ward, *J. Am. Chem. Soc.*, 2018, **140**, 2821–2828.

20 M. D. Ludden, *Unpublished Results*, 2017.

21 E. G. Percástegui, J. Mosquera and J. R. Nitschke, *Angew. Chemie - Int. Ed.*, 2017, **56**, 9136–9140.

22 A. B. Grommet, J. B. Hoffman, E. G. Percástegui, J. Mosquera, D. J. Howe, J. L. Bolliger and J. R. Nitschke, *J. Am. Chem. Soc.*, 2018, **140**, 14770–14776.

23 H. Humbert, H. Gallard, H. Suty and J. P. Croué, *Water Res.*, 2005, **39**, 1699–1708.

24 J. N. Apell and T. H. Boyer, *Water Res.*, 2010, **44**, 2419–2430.

25 C. A. Rokicki and T. H. Boyer, *Water Res.*, 2011, **45**, 1329–1337.

26 W. Cullen, M. C. Misuraca, C. A. Hunter, N. H. Williams and M. D. Ward, *Nat Chem.*, 2016, **8**, 1–6.

27 C. G. P. Taylor, A. J. Metherell, S. P. Argent, F. M. Ashour, N. H. Williams and M. D. Ward, *Chem. - A Eur. J.*, 2020, **26**, 3065–3073.

28 Y. Inokuma, S. Yoshioka, J. Ariyoshi, T. Arai, Y. Hitora, K. Takada, S. Matsunaga, K. Rissanen and M. Fujita, *Nature*, 2013, **495**, 461–466.

29 C. G. P. Taylor, S. P. Argent, M. D. Ludden, J. R. Piper, C. Mozaceanu, S. A. Barnett and M. D. Ward, *Chem. - A Eur. J.*, 2020, **26**, 3054–3064.

30 A. K. Horváth, *Phys. Chem. Chem. Phys.*, 2021, **23**, 7178–7189.

31 R. H. Fleming, F. H. Quina and G. S. Hammond, *J. Am. Chem. Soc.*, 1974, **96**, 7738–7741.

32 I. S. Tidmarsh, T. B. Faust, H. Adams, L. P. Harding, L. Russo, W. Clegg and M. D. Ward, *J. Am. Chem. Soc.*, 2008, **130**, 15167–15175.

33 G. D. Jackson, M. B. Tipping, C. G. P. Taylor, J. R. Piper, C. Pritchard, C. Mozaceanu and M. D. Ward, *Chemistry (Easton).*, 2021, **3**, 1203–1214.

34 M. Whitehead, S. Turega, A. Stephenson, C. A. Hunter and M. D. Ward, *Chem. Sci.*, 2013, **4**, 2744.

35 I. V. Korendovych, D. W. Kulp, Y. Wu, H. Cheng, H. Roder and W. F. DeGrado, *Proc. Natl. Acad. Sci. U. S. A.*, 2011, **108**, 6823–6827.

2.6. Appendices

2.6.1. NMR spectrum of 1 mM $H^A \cdot HCO_3$

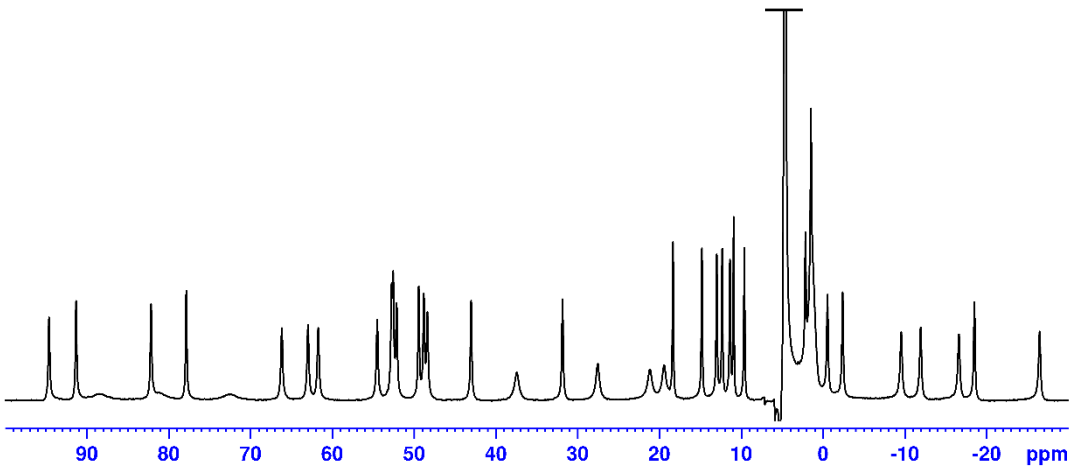

2.6.2. Mass Spectrometry results for H^W

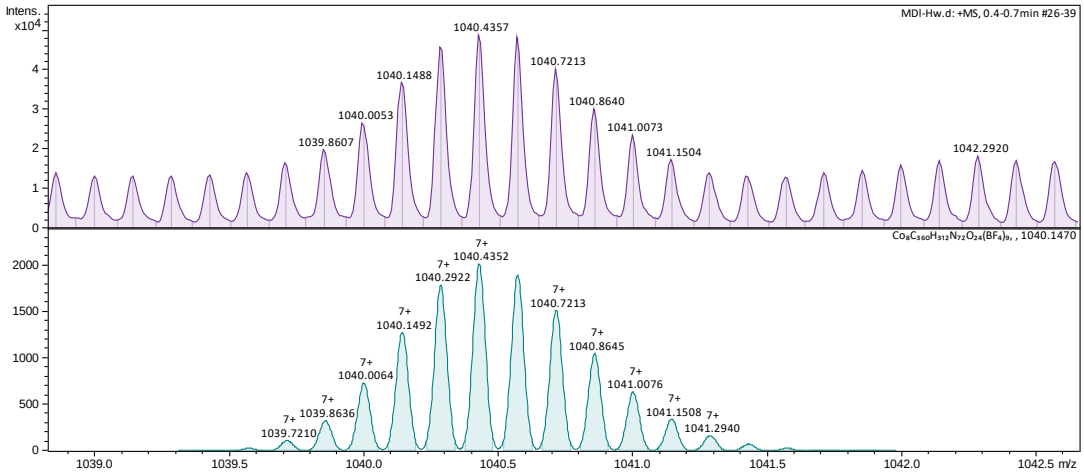

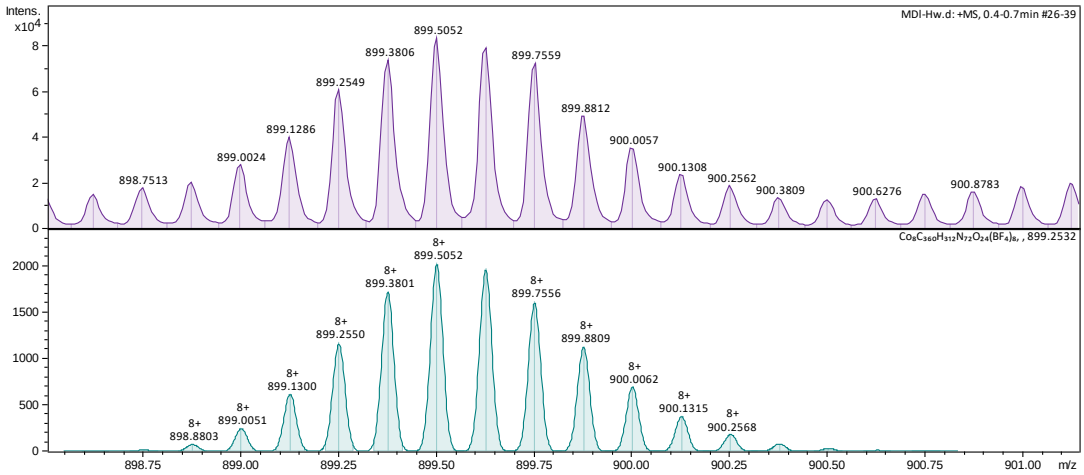

Anion exchanged	[NaOTf] / mM	NaOTf integral	ppm	BF4 integral	ppm	BF4* integral	ppm*	F- integral	ppm
BF4	2.00	570.65	-78.874	1178.761	-150.411	/	/	/	/
NO3	2.00	54.01	-78.518	3.705	-149.739	0.957	-149.687	13.964	-122.203
SO4	2.00	109.43	-78.056	9.714	-149.37	3.964	-149.316	13.983	-122.324
HCO3	2.00	77.12	-78.052	8.686	-149.344	1.062	-149.29	9.609	-122.133

Anion exchanged	Integral per F atom NaOTf	Integral per F atom BF4	Ratio of BF4:NaOTf	mMol of BF4	#BF4's per cage	Nearest whole number	Cage formula
BF4	190.22	294.69	1.55	3.10	16.138	16	$[H^A](BF_4)_{16}$
NO3	18.00	1.17	0.06	0.13	0.669	1	$[H^A](BF_4)(F)_9(NO_3)_6$
SO4	36.48	3.42	0.09	0.19	0.968	1	$[H^A](BF_4)(F)_4(SO_4)_{5.5}$
HCO3	25.71	2.44	0.09	0.19	0.979	1	$[H^A](BF_4)(F)_4(HCO_3)_{11}$

Anion exchanged	Integral per F atom NaOTf	Integral per F atom F-	Ratio of F-:NaOTf	mMol of F-	Free F- ions per cage	Nearest whole number	Cage formula
BF4	190.22	0	0.00	0.00	0.000	0	$[H^A](BF_4)_{16}$
NO3	18.00	13.964	0.78	1.55	8.834	9	$[H^A](BF_4)(F)_9(NO_3)_6$
SO4	36.48	13.983	0.38	0.77	4.366	4	$[H^A](BF_4)(F)_4(SO_4)_{5.5}$
HCO3	25.71	9.609	0.37	0.75	4.257	4	$[H^A](BF_4)(F)_4(HCO_3)_{11}$

2.6.3. Anion Exchange data from the second set of experiments using the cage **H^A** and prepared anion exchange resins for NO_3^-, SO_4^{2-} and HCO_3^-. BF_4^- in the table denotes no exchange resin used.

Anion exchanged	[NaOTf] / mM	NaOTf integral	ppm	BF4 integral	ppm	BF4* integral	ppm*	F- integral	ppm
BF4	2.00	509.89	-78.805	1096.589	-150.339	/	/	/	/
SO4	2.00	729.52	-78.798	99.79	-149.659	/	/	83.741	-122.895
Cl	2.00	610.59	-78.803	18.795	-149.603	/	/	8.527	-122.273
NO3	2.00	219.18	-78.808	24.221	-150.067	/	/	35.892	-122.501
H2PO4 (20 min)	2.00	181.03	-77.789	79.951	-149.001	27.745	-148.95	/	/
H2PO4 (5 day)	2.00	460.32	-78.038	43.782	-148.992	/	/	/	/
S2O3 (15 min)	2.00	176.44	-77.654	29.709	-149.137	5.012	-149.082	22.343	-122.088
IO3 (25 min)	2.00	272.73	-77.444	52.401	-148.972	/	/	10.93	-122.042
OAc (30 min)	2.00	389.08	-77.352	112.68	-148.856	/	/	46.823	-122.297

Anion exchanged	Integral per F atom NaOTf	Integral per F atom BF4	Ratio of BF4:NaOTf	mMol of BF4	#BF4's per cage	Nearest whole number
BF4	169.96	274.15	1.61	3.23	16.130	16
SO4	243.17	24.95	0.10	0.21	1.080	1
Cl	203.53	4.70	0.02	0.05	0.231	0
NO3	73.06	6.06	0.08	0.17	1.069	1
H2PO4 (20 min)	60.34	26.92	0.45	0.89	3.035	3
H2PO4 (5 day)	153.44	10.95	0.07	0.14	0.945	1
S2O3 (15 min)	58.81	8.68	0.15	0.30	0.656	1
IO3 (25 min)	90.91	13.10	0.14	0.29	0.805	1
OAc (30 min)	129.69	28.17	0.22	0.43	0.957	1

Anion exchanged	Integral per F atom NaOTf	Integral per F atom F-	Ratio of F-:NaOTf	mMol of F-	Free F- ions per cage	Nearest whole number
BF4	169.96	0.00	0.00	0.00	0.000	0
SO4	243.17	83.74	0.34	0.69	3.625	4
Cl	203.53	8.53	0.04	0.08	0.466	0
NO3	73.06	35.89	0.49	0.98	6.339	6
S2O3 (15 min)	60.34	22.34	0.37	0.74	1.646	2
IO3 (25 min)	153.44	10.93	0.07	0.14	0.358	0
OAc (30 min)	58.81	46.82	0.80	1.59	3.507	4

2.6.4. Anion Exchange data from the third set of experiments using the cage $\mathbf{H^A}$ and prepared anion exchange resins for NO_3^-, SO_4^{2-}, HCO_3^-, $H_2PO_4^-$, $S_2O_3^{2-}$, IO_3^- and OAc^-. BF_4^- in the table denotes no exchange resin used.

Chapter 3

A fluorescence displacement assay for detecting anion interactions with H^W

3.1. Introduction

The sensing of analyte molecules is a common goal for many supramolecular chemists.[1] Through considered design, host molecules that can bind specific guest molecules can be synthesised. However, synthesising a suitable receptor is only part of the task in hand: binding a substrate within the receptor must also modulate the output signal of an indicator component, usually connected to the receptor site through some form of aromatic spacer. These indicator-spacer-receptor (ISR) assays often involve complicated synthetic routes. Indicator displacement assays (IDAs) however, are viewed as viable alternatives to traditional ISR assays as the indicator is noncovalently attached to the receptor. Anslyn in particular has driven this field forward, showing that many synthetic receptors can become IDAs if the right indicator species is used.[2,3]

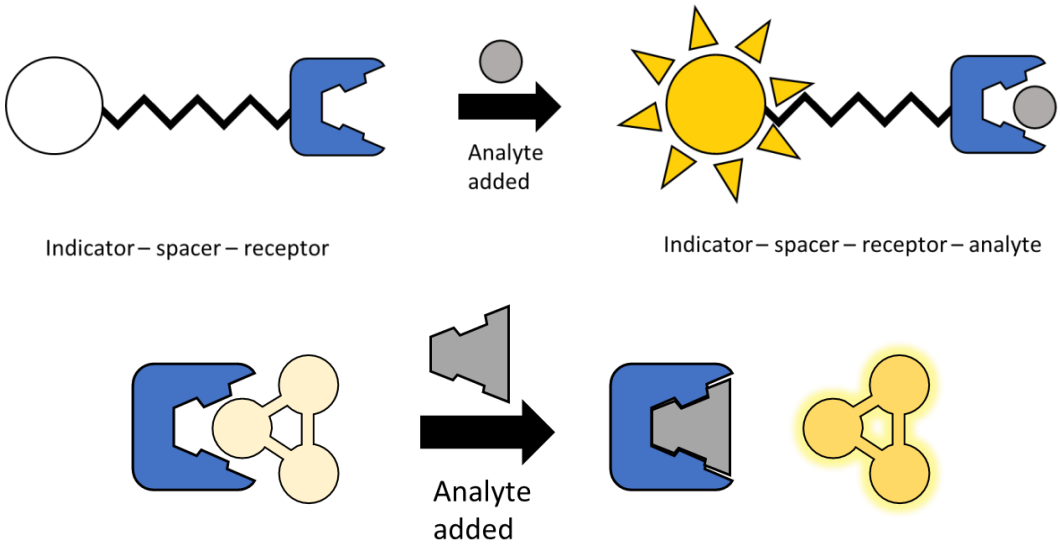

Figure 3.1 – Sketches of the two indicator systems discussed within the main text and their function. Top: an ISR-type sensor. Bottom: an IDA-type sensor.

Examples of synthetic IDAs in the literature are numerous. The observable change in output property varies, with changes in optical properties being the most common. Fluorescence displacement assays involve a restoration of fluorescence upon displacement of the bound fluorophore from within the supramolecular host. Fabbrizzi and co-workers reported one such assay that involved a cryptand-style host molecule capable of binding 6-carboxy-tetramethyl-rhodamine within the cavity. Upon inclusion, the fluorescence was progressively quenched, allowing an increase

of fluorescence to be seen when the correct analyte (L-glutamate) was added, displacing the bound rhodamine. From this, a binding constant for glutamate within the cage could be calculated.[4]

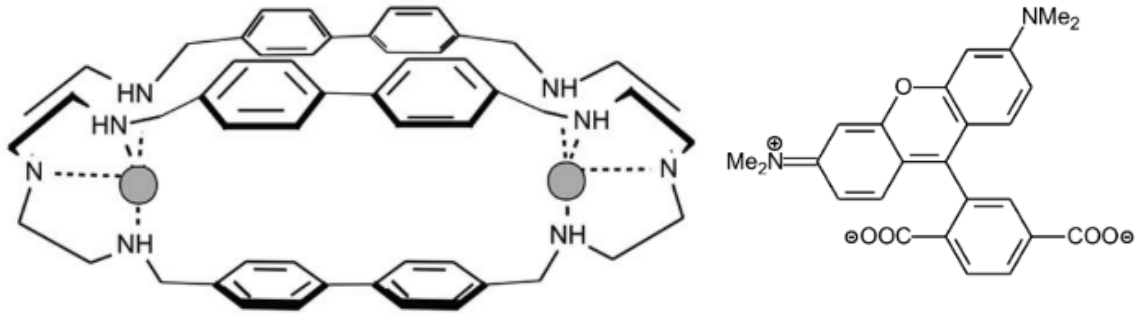

Figure 3.2 - Fabbrizzi's glutamate-sensing Cu(II)-based cage. The two Cu(II) cations (grey circles) interact with the carboxylate groups of 6-carboxy-tetramethyl-rhodamine (right) and also the competing guest, glutamate.[4]

Ghosh and co-workers published work in 2012 incorporating fluorescein as the fluorescent reporter component of the sensor, bound within the cleft of a cationic pyridinium-based receptor. This combination showed restoration of fluorescence from displaced fluorescein upon addition of hydrogen pyrophosphate selectively. The fluorescence response was detectable by the naked eye.[5]

A fluorescence displacement assay has also been designed by the Ward group in previous work to measure the strength of guest binding within a cage cavity. Using the host cage **H^W** and the organic fluorophore 4-methyl-7-amino coumarin (**MAC**) as a cavity-binding guest, progressive quenching of fluorescence was seen, as **MAC** bound inside the cage in water. Displacement of bound **MAC** occurred upon addition of a guest capable of also binding inside the cavity. By monitoring the increase in emission as **MAC** was displaced, binding constants were calculated for many different analyte guests and in some cases was corroborated by NMR spectroscopy measurements.[6]

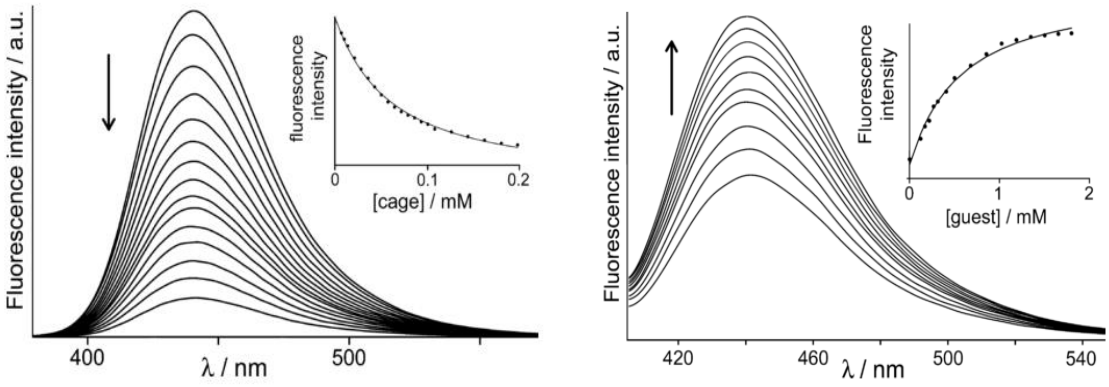

Figure 3.3 – Left: progressive quenching of fluorescence of the small organic fluorophore MAC upon addition of a $M_8L_{12}^{16+}$ cobalt cage in H_2O. Right: subsequent restoration of MAC fluorescence upon addition of a competing guest (isoquinoline N-oxide).[6]

Whilst the uptake of guests into the cavity can be monitored using **MAC** as the indicator, there is no current method of quantifying the strength of association of anionic guests to the cage's surface. As the previous chapter detailed, anions have varying affinities for the binding sites situated around the exterior of the cage, as shown by the degree to which they slow the Kemp elimination reaction. A system which could extract binding constants for this association with anions would be of particular benefit to confirm the findings seen in the previous chapter. The work that follows in this chapter will discuss the design and use of a new fluorescence displacement assay to evaluate surface anion binding, again utilising the cage $\mathbf{H^W}$ but this time with a surface-bound fluorophore. This investigation contrasts with work conducted previously using $\mathbf{H^W}$, as the focus is not on guest binding within the cavity of the cage but instead looks at interactions that occur on the cage's exterior – an area of supramolecular chemistry that has received far less attention until recently.

3.2. Results and Discussion

3.2.1. Fluorescein / H^W displacement assay

i) Development of the assay

As was discussed in the previous chapter, we have an expanding knowledge of supramolecular structures involving the cage $\mathbf{H^W}$ and surface-binding species such as anions. Whilst the inhibiting effect on catalysis upon addition of various anions

showed the effects clearly enough, we sought a method of quantifying the association constants for binding of anions to the cage surface. The displacement assay for cavity-bound guests within **H^W** involved displacement of the fluorophore **MAC**, so extension of this principle to analysis of surface-bound guests was next investigated. The planned design of the system requires a surface bound fluorophore that would be quenched upon association with the cage and would show a restoration of fluorescence upon displacement using anions.

Recent work has demonstrated the interaction of anionic species such as phenolates with the exterior of the cage **H^W**.[7] For example, the absorption maximum of 2-cyanophenolate, discussed in the previous chapter, undergoes a red-shift upon association with the exterior of the cage **H^W**. This interaction shows that larger anionic species, as well as small inorganic ions such as chloride or nitrate, can also bind to the cage's exterior. The fluorophore fluorescein was considered for testing as it possesses both phenolate and carboxylate functional groups above pH 6.5, and so at pH 8.5 in a buffered solution would be dianionic. The UV/vis spectrum of fluorescein (**FLU**) in mildly basic aqueous solution shows peak absorption at 490 nm and emission at 515 nm which makes it beneficial to use in combination with **H^W**, as its absorption maxima is far away from the cage's absorption. The water solubility of fluorescein is also considerable, especially when deprotonated.

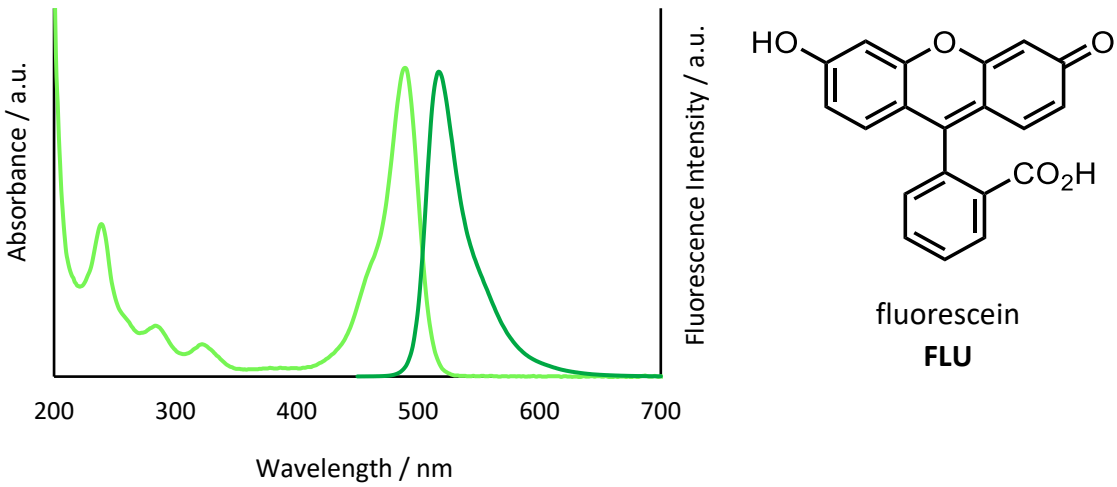

Figure 3.4 – Left: the UV/vis absorption spectrum and fluorescence emission spectrum of fluorescein at pH 8.5. Right: the structure of fluorescein (FLU).

To observe whether any quenching of **FLU** occurred during this association between cage and fluorescein, a titration was performed, monitoring emission of **FLU** upon sequential additions of cage. Figure 3.5 shows the progressive quenching of fluorescein emission upon addition of cage, which could be fitted to a 1:1 binding isotherm. From this, the binding constant for the interaction of **FLU** with the surface of $\mathbf{H^W}$ can be determined as 1.0 x 10^5 M^{-1}.

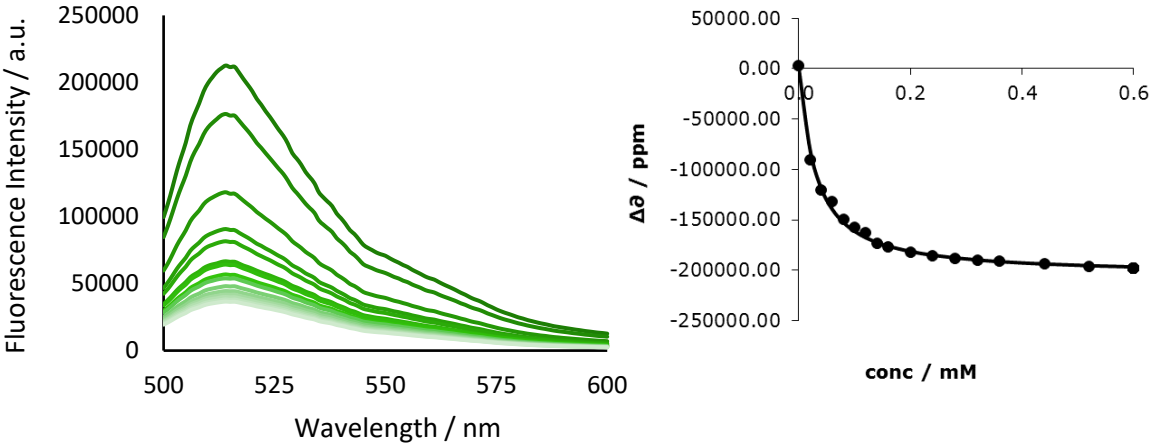

Figure 3.5 – quenching of FLU through sequential addition of H^W. Left: resulting spectra throughout the titration. Right: signal curve of peak fluorescence at 515 nm. [FLU] = 20 µM, [H^W] = 0-200 µM, 50 mM borate buffer pH 8.5.

The calculation of the binding constant was undertaken using an Excel-based macro which fits the data from quenching titrations such as the one shown above to binding isotherms and returns a value for *K*, the binding constant with $\mathbf{H^W}$. In the case of fluorescein, all the points were deliberately taken using a > 1:1 ratio of $\mathbf{H^W}$:**FLU** to avoid having multiple fluorophores binding to one cage, which would complicate the analysis. The returned *K* value was calculated using the concentration of available faces, to account for the six individual binding sites that are accessible on the cage's surface; the result is a *K* value for association between **FLU** and one cage face and assumes that all cage faces act as independent binding sites.

To confirm that binding did occur on the surface of the cage and not within the cavity, a competition experiment was set up. Using the strong cavity binding guest cycloundecanone, displacement of the bound fluorescein was attempted to see if there was any indication that the cavity was involved in this quenching. As the graph in Figure 3.6 shows, even at concentrations of 1 mM of cycloundecanone there is no significant restoration of fluorescence emission of **FLU**. This concentration is sufficient to fully displace a similar concentration of bound **MAC** from the cavity so we can assume from this that fluorescein is not cavity bound, confirming our hypothesis that the interaction of cage with **FLU** is surface based.

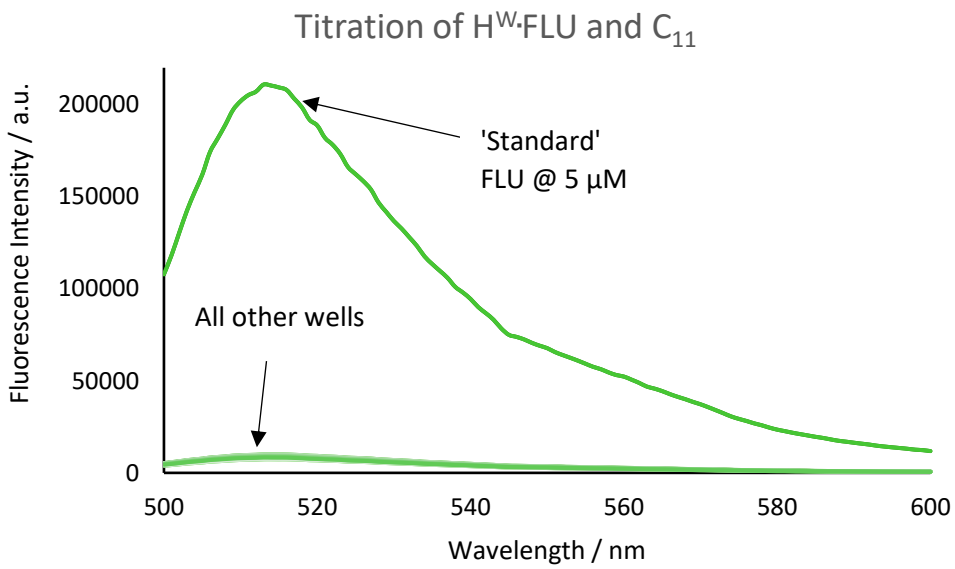

Figure 3.6 – attempted displacement of bound FLU using the guest cycloundecanone. A standard of free FLU at 5 µM was also recorded. No change was observable for FLU emission.

To see if the binding is reversible, as seen for the cavity-based quenching of **MAC**, the combination of **FLU** and **H^W** was evaluated as the basis of a displacement assay. Initially the anions chloride, sulfate and nitrate were used as analytes as they represent much of the range of the Hofmeister series. Sulfate is kosmotropic and orders water molecules surrounding it whilst nitrate is chaotropic and will disrupt the H-bond network between water molecules. Chloride sits in the middle of these two, displaying neither effect prominently.

Pleasingly, all three anions returned a promising result. In each case, titration of the anion as its sodium salt into a **FLU/H^W** mixture showed a gradual increase in fluorescence intensity, indicating that displacement of **FLU** from the surface of the cage was occurring, bringing with it a restoration of emission. Binding constants for these three anions could be calculated from the displacement data through the same method used with cavity-binding guests published in the literature.[6] This returned values of 7.5 x 10^2 M^{-1} for chloride, 3.1 x 10^3 M^{-1} for nitrate and 3.6 x 10^3 M^{-1} for sulfate. As expected, nitrate returned a higher *K* value than chloride, on the basis that it binds more strongly to the cage surface as it is more hydrophobic (see Chapter 2). Sulfate was the strongest binding of the three anions measured, despite its hydrophilicity. It appears that the higher negative charge present on sulfate (making it hydrophilic and strongly solvated, and therefore expected to bind weakly) provides an electrostatic interaction with the 16+ cage surface that is stronger than with monoanions and strengthens the interaction between cage and anion.

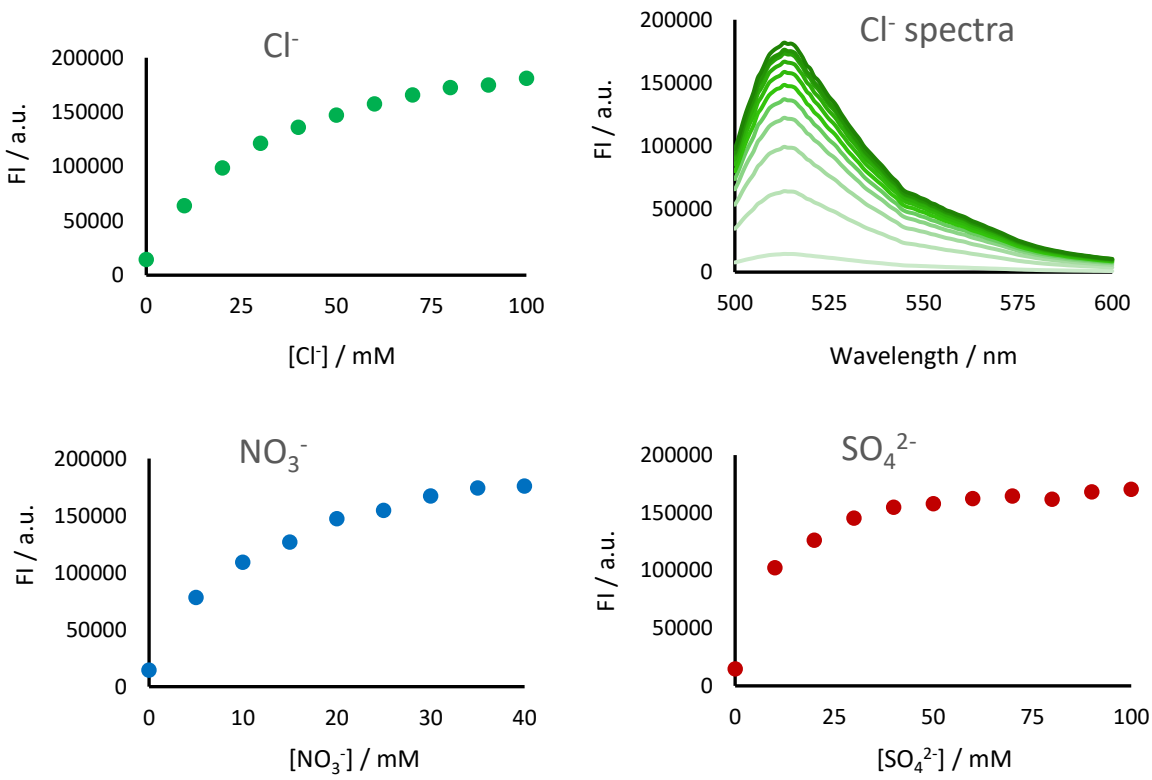

Figure 3.7 – restoration of FLU emission upon addition of NaCl, $NaNO_3$ and Na_2SO_4. The signal curves are recorded at 515 nm. An example set of spectra are given top right for chloride. [FLU] = 5 µM, [H^W] = 50 µM, 50 mM borate buffer pH 8.5.

ii) Testing a range of anions

To confirm the above and to develop an understanding of the influences behind surface binding, a range of other anions were tested using this displacement assay. Anions spanning the range of the Hofmeister series were used to evaluate the correlation between the strength of association of any anion to the cage, and its position in the series.

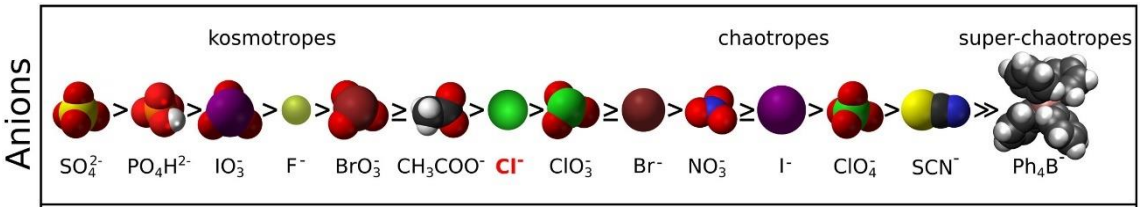

Figure 3.8 – the Hofmeister series. Many of the anions tested in this assay can be found on this diagram, with $S_2O_3^{2-}$ the only exception.[8]

The full range of anions tested is as follows: SO_4^{2-}, $S_2O_3^{2-}$, HPO_4^{2-}, IO_3^-, F^-, OAc^-, Cl^-, Br^-, NO_3^-, I^-. These can be compared at the same concentration, showing from the titration curves a relative order of binding strength. *K* values were calculated for all the above anions using the methodology described above.

The data from the experiment involving halide salts is shown below. The anions were titrated into a **FLU**/**H^W** mixture up to a concentration of 30 mM. The graphs showing restoration of **FLU** emission show the order for strength of binding to **H^W**, from

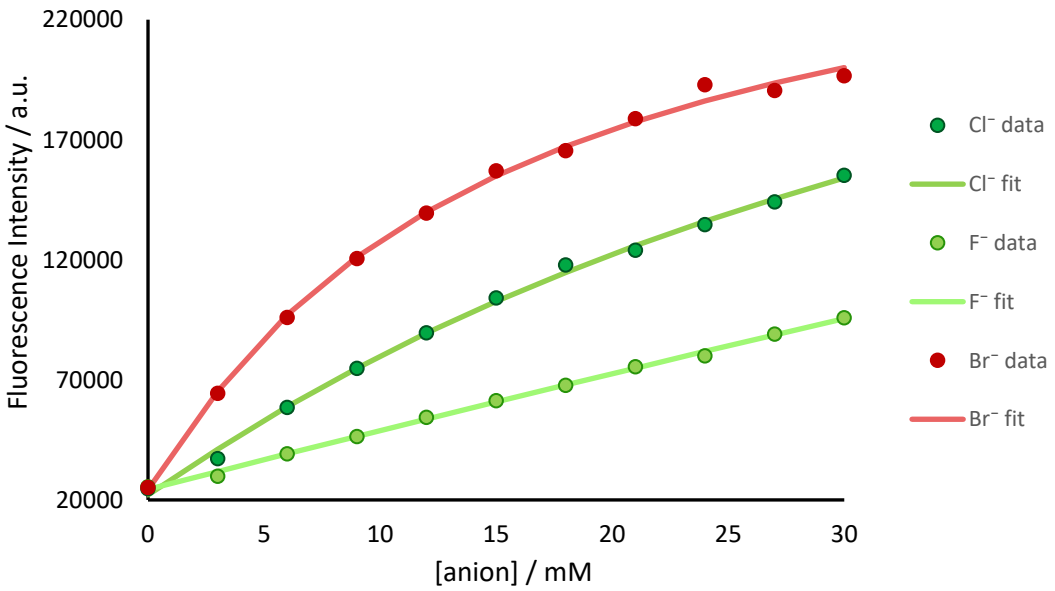

Figure 3.9 – direct comparison of the resulting signal curves after displacement with F^-, Cl^- and Br^-. [FLU] = 5 µM, [H^W] = 50 µM, 50 mM borate buffer pH 8.5.

weakest to strongest, to be $F^- < Cl^- < Br^-$. Relating this to the Hofmeister series we see that more kosmotropic anions (*i.e.,* more hydrophilic) bind more weakly to the cage's exterior surface than do chaotropic anions. Iodide is not shown in this data set as the cage samples precipitated instantly after addition of sodium iodide solution.

Extending this to include the other anions tested – IO_3^- and OAc^- – we can order the singly charged anions based on the calculated binding constants. Table 3.1 shows the anions tested and the calculated *K* values for 1:1 binding to $\mathbf{H^W}$. Looking at this data we can see that, for the most part, this affinity generally follows the order seen in the Hofmeister series, with occasional exceptions (*e.g.* iodate is misplaced).[8]

Anion	*K* value / M^{-1}	*B* coefficient
$\mathbf{F^-}$	2.5×10^2	0.107
$\mathbf{OAc^-}$	4.6×10^2	0.246
$\mathbf{IO_3^-}$	4.7×10^2	0.157
$\mathbf{Cl^-}$	7.5×10^2	-0.005
$\mathbf{Br^-}$	2.9×10^3	-0.033
$\mathbf{NO_3^-}$	3.1×10^3	-0.043

Weakest binding

↓

Strongest binding

Table 3.1 – calculated *K* values for mono-anionic species using the FLU/H^W assay along with relative ***B*** coefficient.

The relationship between bulk water and solutes such as salts dissolved within it is a complex one, with several interactions needing to be considered to conclude the driving forces behind the varying strengths of association seen here. Water as a solvent can form a network of intermolecular hydrogen bonds – two donated from the hydrogen atoms on each molecule and two accepted by the oxygen's lone pairs. This network is responsible for many of the unique properties of water such as its high liquid density. Addition of new species into a solution of water will in some way disrupt the natural network of H-bonds, whether it be through the solute's hydrophobic surface area, as seen with many of the organic guest molecules found to bind within the cavity of $\mathbf{H^W}$, or by rearrangement of the molecules to solvate an ionic species such as sodium chloride. The surrounding of ions by water molecules is known as hydration. Ions with higher charge density such as fluoride are more strongly hydrated (with a higher negative enthalpy of hydration) than larger, more diffuse ions such as iodide.

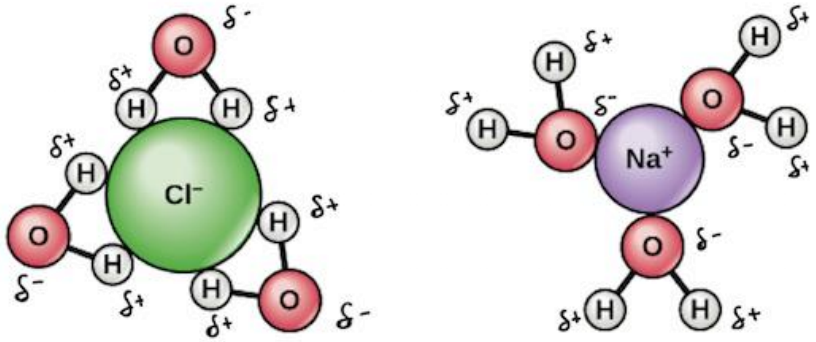

Figure 3.10 – hydration of ions in solution by water molecules. H_2O will orient itself to favour the electrostatic interactions between the positive/negative parts of the molecule and the relevant ion.[9]

The Hofmeister series itself is based on any given ion's ability to interact with proteins in aqueous solution. This in itself is a balance between how the ion interacts with the surrounding water, and with large supramolecular structures (such as proteins) in solution. The mechanism by which water interacts with ions is still a thoroughly researched topic, with no single concise explanation. The terms 'kosmotrope' and 'chaotrope' used to assign ions on either end of the Hofmeister series are descriptive of the resulting hydration of an ion after dissolution in water. Anionic *kosmotropes* order the water around them through interactions between the anion and the water molecules whereas anionic *chaotropes* interact with water more weakly than water interacts with itself and therefore disrupt the H-bond network.

The hydration of a dissolved anion is quantified by the Jones-Dole coefficient ***B***, which has basis in the viscosity of salt solutions in water. A positive ***B*** value indicates a kosmotrope whilst a negative ***B*** value indicates a chaotrope. As the data in Table 3.1 showed, there is a correlation between the ***B*** value for the anions tested and their binding constant to the cage's exterior. The correlation is not exact, for the kosmotropes especially. This suggests there is also another factor involved for anion/$\mathbf{H^W}$ binding strength. Comparison of anions at both the kosmotropic and chaotropic ends of the series can shed light on the factors behind association. Fluoride and iodate are both kosmotropic, with iodate possessing a slightly higher ***B*** value at 0.157 compared to 0.107. Out of the two, however, iodate has a higher binding constant to $\mathbf{H^W}$. The reason behind this could be attributed to the negative

charge of the iodate anion being spread over three oxygen atoms, lowering the overall negative charge density. Studies on the iodate anion in solution have revealed that the iodine atom (formally I^+) can be treated as a strongly-hydrated cation whilst the negative charge spread across the oxygen atoms results in a low charge density per oxygen, affecting its behaviour in solution.[10] A similar picture can be painted for the comparison of bromide and nitrate with both species acting as chaotropes, having similarly negative ***B*** values of -0.033 and -0.043 respectively. The negative charge for nitrate is also spread across the three oxygen atoms, giving a higher binding constant than bromide. It appears from these results that charge density plays a role in association strength of anions to the cage's surface. There may also be a preference for H-bond donor type, with C-H protons on the cage's exterior able to interact with surface-bound anions. Iodate and nitrate may possess an inherent preference for C-H bond donors over the O-H donors found in bulk water, relating to relative hardness/softness of the donor/acceptor pair themselves.[11,12] Another factor may be the multiple oxygens possessed by iodate and nitrate, with each partially negative oxygen able to form a H-bond to the cage surface. The potential array of H-bonds these anions could form may be a stronger overall interaction than for a single-point anion such as fluoride.

The series of anions that are 2- in charge can also be evaluated. Sulfate, thiosulfate and hydrogen phosphate were all tested as their sodium salts in the same manner as the mono-anions discussed above. The association constant for thiosulfate is the highest recorded at 4.0×10^3 M^{-1} but according to the Hofmeister series, $S_2O_3^{2-}$ is one of the most kosmotropic of the anions tested, implying that – being highly solvated – it should bind weakly to the cage's surface. The higher negative charge could be the source of the larger association constants for the dianions, with the anion/$\mathbf{H^W}$ interaction containing an electrostatic component: the mutual attraction between the 16+ cage and 2- thiosulfate anion compensates the high cost of desolvating the anion. This is also the case for sulfate and hydrogen phosphate, which are both also 2- anions and have binding constants higher than expected solely based on their position in the Hofmeister series. The relative order of the 2- anions for binding to $\mathbf{H^W}$ also raises another observation about binding; the *K* values increase as the anion

itself becomes 'softer'. The radius of the anion increases in the order HPO_4^{2-} < SO_4^{2-} < $S_2O_3^{2-}$, which when the charge remains the same leads to a lower charge density.[13]

Anion	*K* value / M^{-1}	Radius / pm
HPO_4^{2-}	2.1 x 10^3	200
SO_4^{2-}	3.6 x 10^3	230
$S_2O_3^{2-}$	4.0 x 10^3	250

Table 3.2 – calculated *K* values for dianionic species along with ionic radius. The trend appears to be increasing ionic radius leads to a higher binding constant at constant charge. Radii taken from reference 13.

The lower charge density (and reduced solvation in water) apparently also leads to a higher binding constant in this scenario. This aligns with the observations made for the mono-anions, with the softer anions nitrate and iodate binding more strongly than the relatively harder anions fluoride and bromide.

iii) Investigating the effect of carbon chain length of anions

The next set of anions tested using this displacement assay were structurally related, with variation of the carbon chain length of the anion. The anions formate, acetate, propionate and butyrate were used to displace **FLU** from the surface of $\mathbf{H^W}$ through binding of the anions to the $\mathbf{H^W}$ surface *via* the carboxylate terminus. With neutral guests that bind *within* the cavity, such as cyclic aliphatic ketones, increasing the carbon chain length brought with it an increase in hydrophobicity leading to higher binding constants. This increase was found to be a contribution of roughly 5 kJ mol^{-1} per CH_2 group, an amount expected on the basis of the hydrophobic effect.[6] Using these carboxylate anions it was hoped that any hydrophobic contribution to *surface* binding would be highlighted.

The experiment comparing linear carboxylates gave a surprising result, even after multiple repeats. Out of the four molecules, formate produced a clearly higher binding constant than the other carboxylates. Acetate, propionate, and butyrate all gave similar values. The result of the experiment is shown in Figure 3.11.

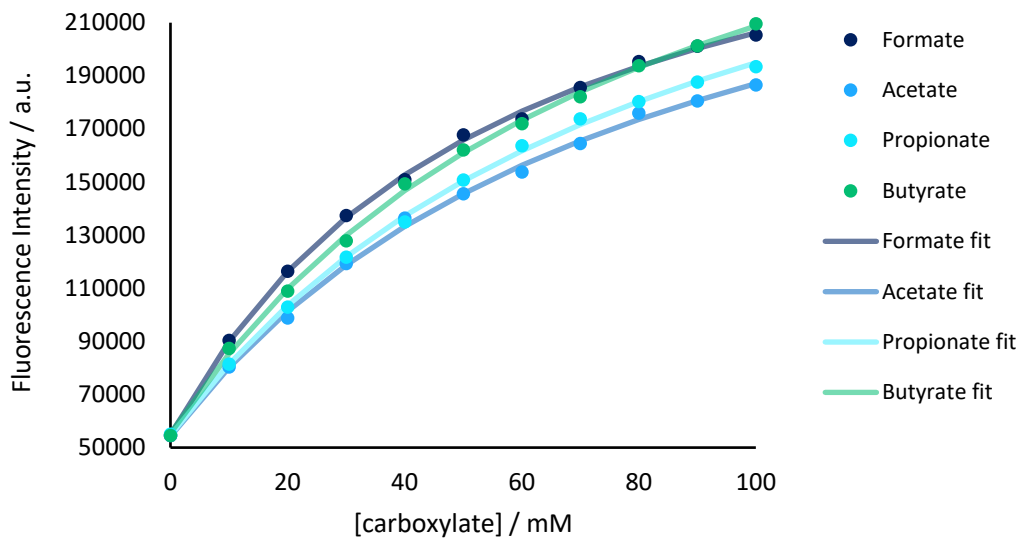

Figure 3.11 – direct comparison of carboxylate anions of increasing carbon chain length starting with formate up to butyrate. [FLU] = 5 µM, [H^W] = 50 µM, 50 mM borate buffer pH 8.5.

The reasoning behind formate being the strongest binder out of these carboxylates lies in its weak interactions with the surrounding water. Formate is by definition a chaotrope and more weakly hydrated than alkyl carboxylates, with a ***B*** coefficient of -0.052. It is this reluctance to interact with water (easy desolvation) that induces a higher binding constant of 8.4 x 10^2 M^{-1} for formate. Comparing this to the kosmotropic longer chained carboxylates which display *K* values between 3.9 x 10^2 M^{-1} and 4.7 x 10^2 M^{-1}, we see that the predominant effect here is hydration. Table 3.3 shows the *K* values along with the corresponding ***B*** coefficients for these carboxylates.

Anion	*K* value / M^{-1}	*B* coefficient
OFm^-	8.4 x 10^2	-0.052
OAc^-	4.7 x 10^2	0.246
OPr^-	4.4 x 10^2	0.339
OBu^-	3.9 x 10^2	0.419

Table 3.3 – calculated *K* values for the carboxylate series tested along with their relative ***B*** coefficients.

As the length of the carbon chain increases, the general trend for both *K* values and ***B*** coefficient is clear. What appears counterintuitive is that addition of carbon chains to the carboxylate ends up slightly increasing the hydration of the anion as a whole.

The CH_2/CH_3 groups of the anion are hydrated by a number of water molecules, resulting in the molecules acting as structure makers despite the intrinsic hydrophobicity of hydrocarbon chains such as these.[14,15] This leads to lower *K* values for the carboxylates larger than formate, the H atom of which is not hydrated. Note that this is a contrasting effect to what happens when a larger hydrophobic species binds inside the cage cavity and liberates more water molecules into the bulk aqueous phase where they can be more strongly hydrated. With the surface binding of carboxylate anions, the alkyl chains likely remain projecting into the aqueous phase and so do not change their environment (or hydration state) when the carboxylate terminus interacts with the surface of $\mathbf{H^W}$. Hence, we see no significant effect of alkyl chain length on the binding strength of carboxylates to $\mathbf{H^W}$.

iv) Investigating the effect of head group of anions

Having investigated whether increasing the hydrophobic component of carboxylate anions affects the anion's binding constant as a whole, the next experiment involved changing the head group of an anion to compare binding strength for the same carbon chain length. To test this, two pairs of carboxylate and sulfonate anions with the same alkyl chains were compared using the same $\mathbf{H^W}$**/FLU** displacement assay. Propionate and butyrate were again employed, and for comparison propyl and butyl sulfonate were used.

Figure 3.12 shows the results of this comparison. The graph indicates two sets of data which are similar in *K* value. The two carboxylates (shown in blue) increase the fluorescence intensity less as the concentration is increased compared to the two sulfonate anions (red). The weaker binding seen for carboxylates compared to sulfonates again correlates with the Hofmeister series – for example, CO_3^{2-} is considered more kosmotropic than SO_4^{2-}. Work done by Kunz and co-workers ordered the common head groups of colloidal groups based on their preference for either sodium or potassium ions. This order is in agreement with the corresponding water affinities, and orders carboxylate as being more kosmotropic than sulfonate.[16]

This aligns with the data obtained in this experiment, showing that the two carboxylates bind weaker to the cage's surface than the two sulfonates.

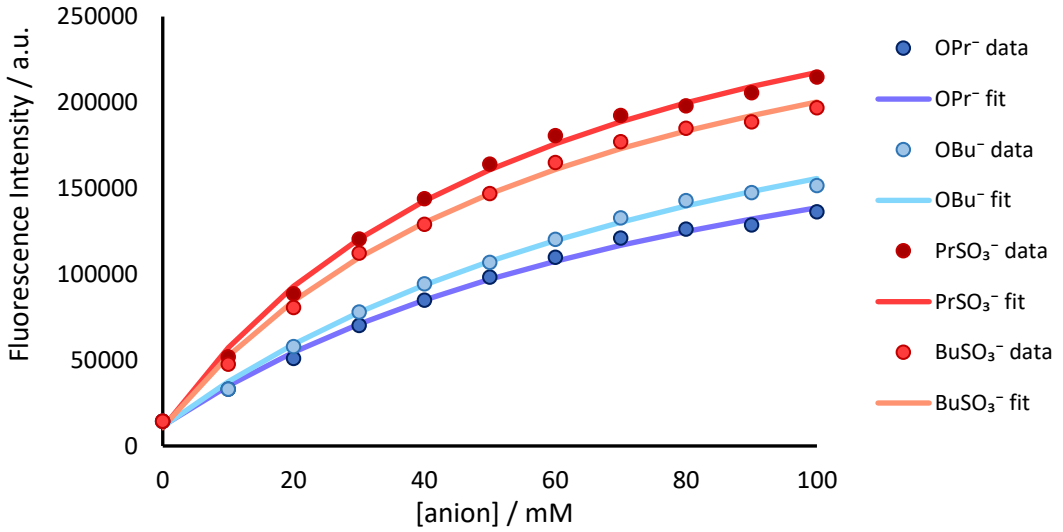

Figure 3.12 – comparison of displacement using carboxylate and sulfonate molecules of the same chain length. [FLU] = 5 µm, [H^W] = 50 µM, 50 mM borate buffer pH 8.5.

In terms of binding constants, both the carboxylates and sulfonates give *K* values over a narrow range, all sitting between 390 and 530 M^{-1}. This small variation compared to the larger changes seen between anions such as fluoride to nitrate shows that both carboxylate and sulfonate head groups remain kosmotropic in nature regardless of the hydrophobic side chain present. The ***B*** values of propionate and propyl sulfonate show a subtle difference which is reflected in their relative binding constants: OPr^- has a ***B*** value of 0.339 compared to the value for $PrSO_3^-$ of 0.305. The lower ***B*** value suggests weaker interactions with water, which in turn leads to better

Anion	*K* value / M^{-1}
OPr^-	4.4×10^2
OBu^-	3.9×10^2
$PrSO_3^-$	5.3×10^2
$BuSO_3^-$	5.0×10^2

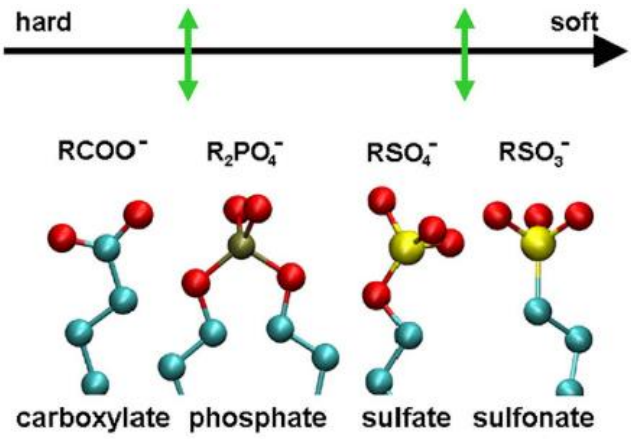

Figure 3.13 – Table 3.4, inset: comparison of calculated *K* values for propyl and butyl carboxylates/sulfonates. Main figure: relative hardness of end group as reported by Kunz *et al.*[16]

interactions with hydrophobic species such as **H^W**. The same will also be true for both butyl species as the length of the carbon chain increases.

v) Binding of larger organic anions

To broaden the scope of this assay method, the following tests moved away from smaller, mostly inorganic anions to larger organic anions such as the sodium salts of common poly-carboxylates. The molecules chosen were gluconate, malate, tartrate and succinate.

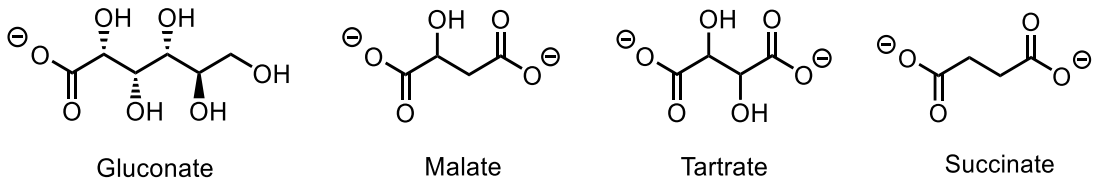

Figure 3.14 – the organic carboxylate anions tested.

These molecules are generally structurally similar, consisting of either one or two carboxylate end groups connected by carbon chains, some appended with hydroxy groups. To ensure that solubility was not an issue, the same limiting concentration of 20 mM was chosen for all four analytes. The results of this experiment are shown in Figure 3.15.

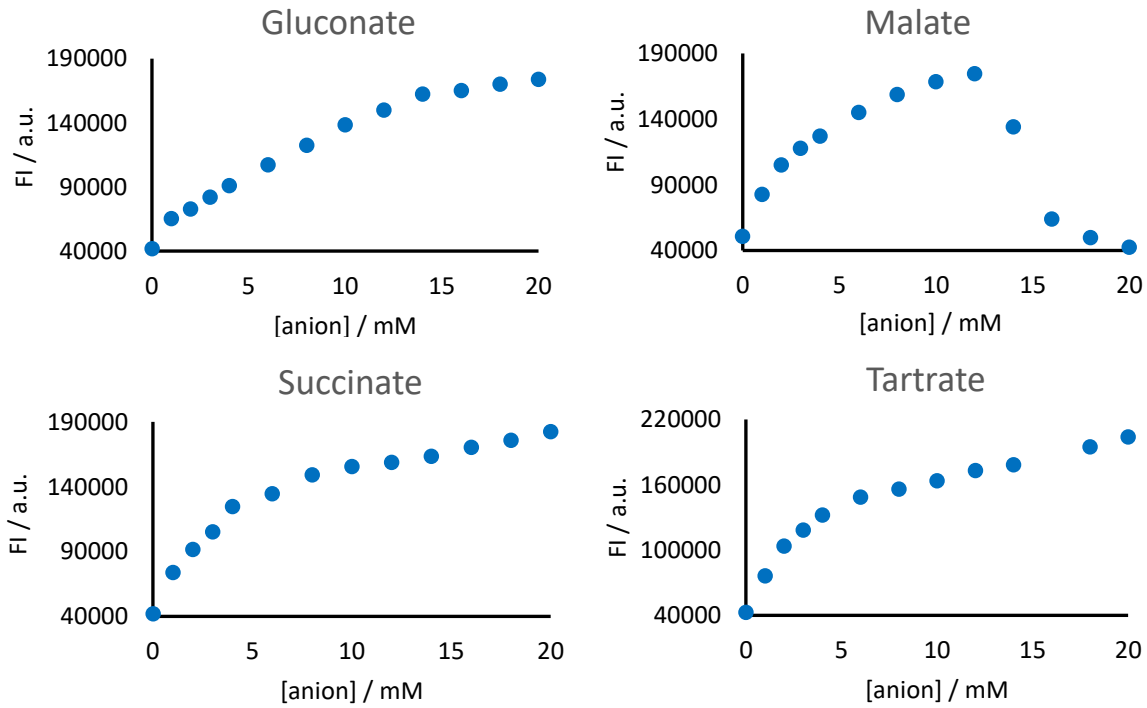

Figure 3.15 – resulting signal curves taken at 515 nm of displacement of bound FLU using the organic anions listed in Figure 3.14. [FLU] = 5 µM, [H^W] = 50 µM, 50 mM borate buffer pH 8.5.

During this titration, each anion generated a progressive increase in fluorescence intensity as the bound fluorescein was displaced. Solubility issues were encountered for malate, as seen by the sharp decrease in emission beyond 12 mM of analyte, indicating precipitation of the cage/anion combination. Fortunately, the earlier part of the curve contained enough data points for fitting to a 1:1 isotherm and calculating a binding constant. *K* values were calculated for all species tested in this experiment and are presented in Table 3.5.

Anion	*K* value / M^{-1}
Gluconate	2.9×10^3
Succinate	6.5×10^3
Tartrate	7.2×10^3
Malate	7.6×10^3

Table 3.5 – calculated *K* values for the organic anions discussed above.

As the values show, all four molecules bind to the cage's surface with association constants of the same order of magnitude. The difference between a 1- and the 2- species arising from electrostatic factors is highlighted with gluconate (1-) having a *K* value roughly half that of the next weakest binding species, succinate. Succinate, malate, and tartrate (all being 2-) bind with similar affinity: the different structures of these anions, in particular the varying numbers of hydroxy groups, appears to make little difference. This is possibly as these are not involved in the interaction with the cage surface, which will involve only the carboxylate termini, but remain hydrated before and after binding to $\mathbf{H^W}$.

3.2.2. Investigating the stoichiometry of H^W·FLU complexes

The results presented in parts **i-v** of section 3.2.1 detail the association and subsequent displacement of the molecule fluorescein to the exterior of the cage $\mathbf{H^W}$. To gain insight into the stoichiometry of binding, Job plot experiments were conducted using the two components of the system – $\mathbf{H^W}$ and **FLU**. This was done by mixing equimolar solutions of both cage and fluorophore in varying ratios to give a series of solutions containing different mole fractions of the two components but the same overall concentration. The y-axis shows the extent of quenching of **FLU**, *i.e.*, the

drop in fluorescence compared to the expected fluorescence intensity value for the concentration of **FLU** present at any given point. Thus, this serves as an indicator of how much **FLU** is bound to the cage surface and thereby quenched at any composition.

Figure 3.16 shows the resulting Job plot for this experiment. The peak difference in fluorescence intensity sits far over to the right, at a high mole fraction of **FLU**. The peak is at 0.83, indicative of formation of a 5:1 **FLU**:$\mathbf{H^W}$ stoichiometry at this overall concentration. This strongly suggests that a molecule of fluorescein can bind to each face of the cube, which would give a stoichiometry of 6:1 (and a maximum at a mole fraction of 0.86). This is dependent on the binding being of sufficient strength at this concentration: statistical factors normally result in decreases in successive binding constant, and in addition the binding of the final molecule to make a 6:1 **FLU**:$\mathbf{H^W}$ assembly may be sterically hindered, or be electrostatically limited by the build-up of negative charge as other fluorescein molecules aggregate about the cage's exterior. As the Job plot experiment shows, at this concentration and this pH (8.5) the 5:1 species dominates the speciation. The overall charge of the complex in this state is 6+, with the 16+ charge of the cage being countered by 10- contributed by the 5 bound fluorescein molecules. The fact that five **FLU** guests can bind does suggest that in principle binding of a sixth one could be possible under sufficiently forcing conditions.

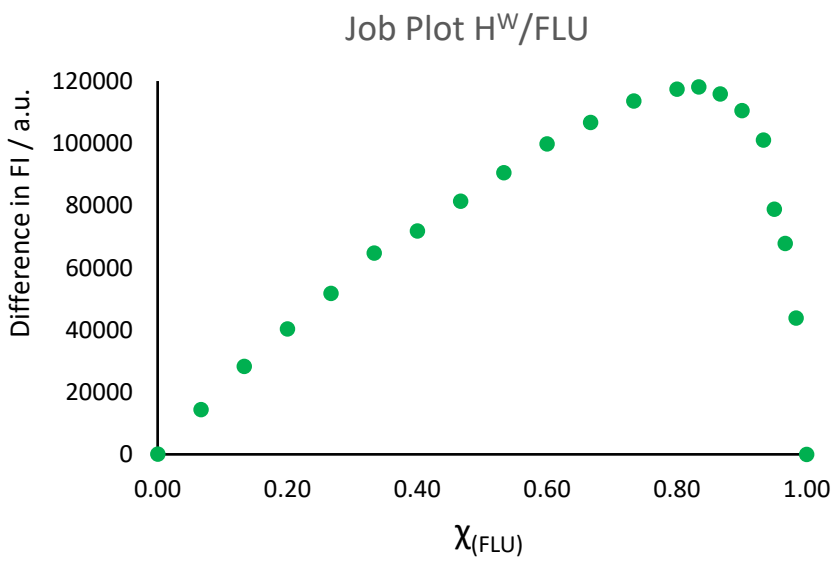

Figure 3.16 – Job plot investigating FLU/H^W speciation. [FLU] = 0.1 mM, [H^W] = 0.1 mM, 50 mM borate buffer pH 8.5.

The experiment was also attempted by means of a different method. NMR spectroscopy was used as an alternative, but sample preparation proved a stumbling block to constructing a Job plot using this analytical method. To collect ^{1}H NMR spectra of suitable signal to noise ratio, a concentration of 0.1 mM **H^W** is needed at the minimum. The issue with this in a Job plot is that the sample with a high mole fraction of fluorescein would require a very low concentration of cage and therefore the spectra collected will be unusable. The experimental method was modified to use samples of varying ratio of host to fluorophore, starting at purely cage and ending at an 8:1 ratio of **FLU**:**H^W**. In this instance, sample solubility was the issue and the samples beyond a 1:1 ratio precipitated out before sample collection could be completed. The combination of solubility limitations arising from the generally higher concentration range required for NMR spectroscopy, and the inherently lower sensitivity of NMR compared to fluorescence which works perfectly well at µM concentrations, makes this method impractical.

3.2.3. Binding of fluorescein derivatives to H^W

To further investigate the contributions towards the binding constants of surface bound fluorophores, two additional fluorescein derivatives were also selected for quenching experiments. The two molecules were 6-carboxyfluorescein (**6C-FLU**), appended with an extra carboxylate group compared to **FLU**, and tetrabromofluorescein, or Eosin Y (**EY**). It was thought that both species would bind more strongly than unsubstituted fluorescein owing to both electrostatic and hydrophobic contributions being covered by these molecules, with **6C-FLU** having a 3- charge rather than 2- at pH 8.5, and **EY** possessing higher hydrophobicity due to the bromine substituents.[17] We were interested to see how binding of these molecules to **H^W** was different (if at all) to binding of **FLU**.

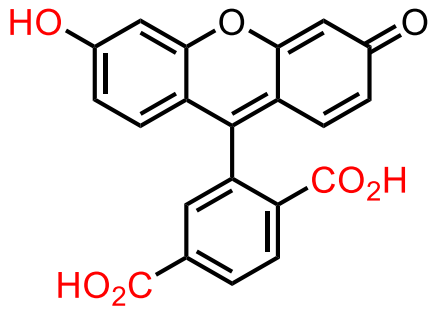

6-carboxyfluorescein
(6C-FLU)

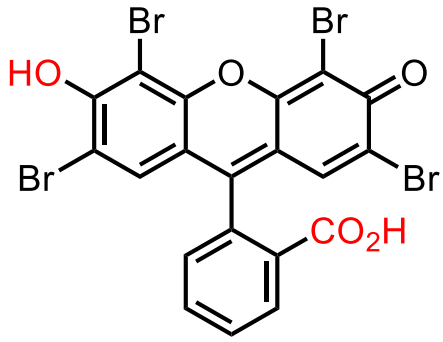

tetrabromofluorescein
(EY)

Figure 3.17 – the structure of the two additional fluorescein derivatives studied in this section.

i. 6-carboxyfluorescein (6C-FLU)

6-Carboxyfluorescein possesses properties very similar to unsubstituted fluorescein, but the additional carboxylate group gives the molecule a higher negative charge at pH 8.5. It was hypothesised that the higher negative charge of **6C-FLU** would result in a stronger electrostatic interaction between fluorophore and cage, as seen for the anions measured using the displacement assay earlier in the chapter. There is also the potential for the higher charge to alter the stoichiometry of association for electrostatic reasons, and this was also investigated.

The first experiment conducted using **6C-FLU** was a standard quenching titration involving addition of the host cage $\mathbf{H^W}$ to a fixed amount (20 µM) of **6C-FLU**. To ensure the data could be fitted to a 1:1 binding curve and compared to that obtained for **FLU**, the concentration of available faces for binding was used in the calculation (this is simply the concentration of cage multiplied by 6).

Figure 3.18 shows the resulting curves for both **FLU** and **6C-FLU** compared. As expected, the quenching of **6C-FLU** is notably stronger at the same concentration of cage added, pointing to a stronger association between the two species. Calculating a 1:1 binding constant using the quenching data for **6C-FLU** gave a value of 3.8×10^5 M^{-1}, higher than that obtained for **FLU**.

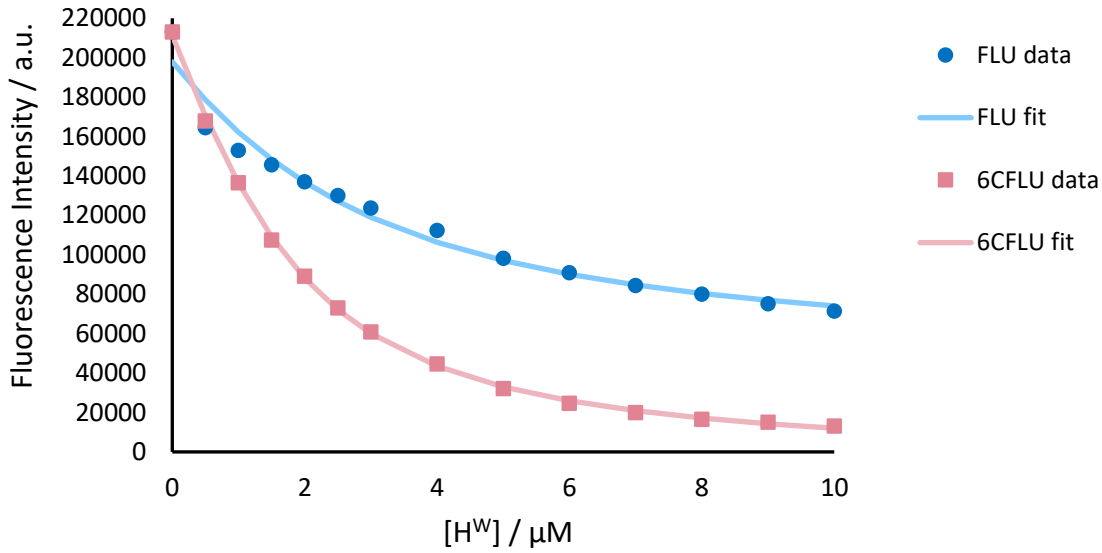

Figure 3.18 – rapid quenching of FLU and its derivative 6C-FLU upon addition of H^W at low concentrations. [FLU/6C-FLU] = 20 µM.

To see whether the binding was reversible as it was for unsubstituted **FLU**, displacement of bound **6C-FLU** was attempted using the anions, F^- and Cl^-. Both anions produced a restoration of fluorescence for **6C-FLU**, shown in Figure 3.19.

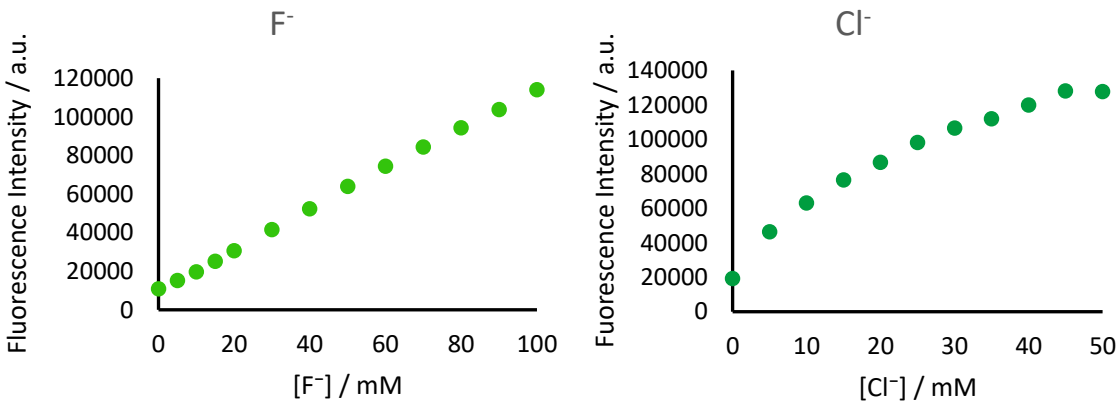

Figure 3.19 – restoration of fluorescence of 6C-FLU upon addition of fluoride and chloride to the assay. Calculated K values are discussed in the main text. [6C-FLU] = 20 µM, [H^W] = 20 µM, 50 mM borate buffer pH 8.5.

The shape of the curves produced for **6C-FLU** displacement showed parallels to those seen using unsubstituted **FLU** earlier in the chapter. Fluoride gave a linear response throughout addition whilst chloride produced a curve similar to that seen previously. Fitting the data obtained here using the same method used for the earlier displacement assay produced binding constant values of 4.5 x 10^0 M^{-1} for fluoride and 2.7 x 10^2 M^{-1} for chloride. The value for chloride is comparable in magnitude to

the value obtained using the **H^W/FLU** combination assay. The value for fluoride, however, cannot be considered accurate, as its linearity will introduce a large error when fitting a binding isotherm to the data; fluoride binds too weakly to displace the stronger-binding **6C-FLU** sufficiently for binding analysis.

With binding strength studies complete, the focus turned to the stoichiometry of binding. As with fluorescein, Job plot experiments were conducted between **6C-FLU** and **H^W**, at three different total concentrations of components: 100 µM, 50 µM and 10 µM. The difference in the form of the graph as the concentration is decreased is noteworthy – both the position and sharpness of the peak of the graph changes for each experiment. The dominating stoichiometry at each concentration decreases with overall concentration.

The maximum for the plot at 100 µM is at 0.8 mole fraction **6C-FLU**, indicative of a 4:1 **6C-FLU**:**H^W** stoichiometry, slightly lower than the 5:1 ratio seen for normal fluorescein. The total charge contributed by four molecules of **6C-FLU** would be 12-, countering the 16+ of the cage and leaving a net positive charge of 4+. As the concentration of both components is reduced to 50 µM, the maximum moves to a lower mole fraction of 0.75, or a 3:1 **6C-FLU**:**H^W** stoichiometry. This trend continues with a 10 µM total concentration of species giving a mole fraction of 0.7, very close to the 0.67 needed for a 2:1 **6C-FLU**:**H^W** stoichiometry. This steady decrease in **6C-FLU**:**H^W** stoichiometry at lower concentrations nicely illustrates concerns about the validity of using the method of continuous variation as reported by Thordarson *et al.* in 2016 to analyse stoichiometries of host-guest complexes.[18] It is clear that conclusions about the possible **6C-FLU**:**H^W** stoichiometry depend strongly on the experimental conditions. We can hypothesise (as with **FLU**) that in the high-concentration limit every face of the cage could have a bound **6C-FLU** anion, but under concentration conditions where the final binding equilibria are unfavourable due to values of K_5 and K_6 being small, those species will not be apparent from the Job plots.

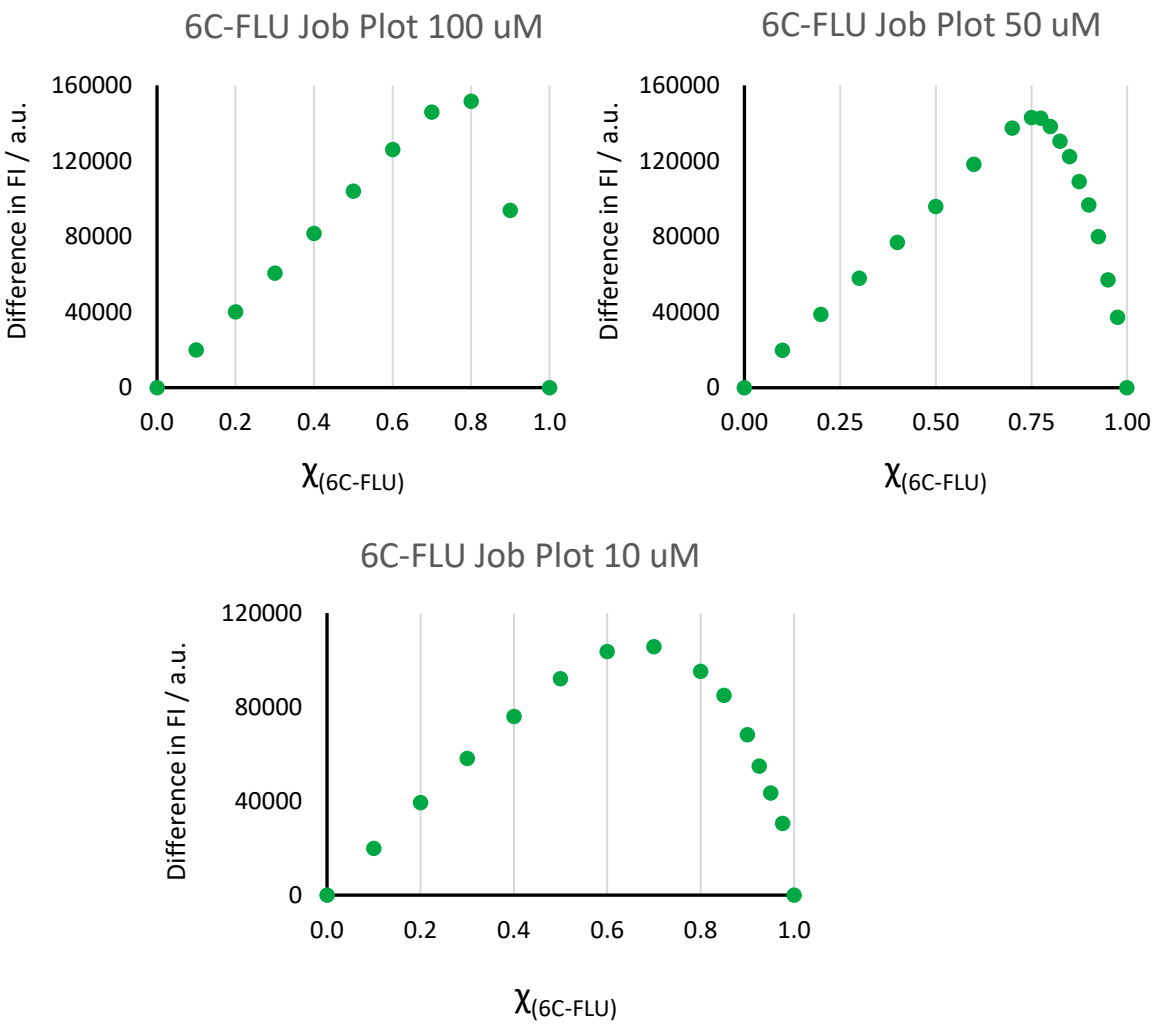

Figure 3.20 – three Job plot experiments conducted at varying concentrations showing a decrease in the maximum speciation with lower component concentration. All were buffered to pH 8.5 as with earlier experiments.

ii) Tetrabromofluorescein (Eosin Y / EY)

Eosin Y (**EY**) is a derivative of fluorescein containing four additional bromine atoms around the xanthene framework at the 2', 4', 5' and 7' positions. The 'Y' in the name stands for 'yellowish' as the emissive wavelength of the molecule is shifted to a lower energy compared to fluorescein, unlike **6C-FLU** which does not have a significantly different emissive wavelength compared to **FLU**.

Quenching of a 20 µM solution of **EY** on addition of portions of $\mathbf{H^W}$ occurred much more quickly than with **FLU**, with a minimum emission (maximum quenching) being reached at only a final concentration of 5 µM of $\mathbf{H^W}$ (a quarter of the concentration of **EY**) with a linear relationship between concentration of cage and fluorescence quenching that reached a minimum at 0.25 equivalents of $\mathbf{H^W}$. The linearity of this result suggests that binding of **EY** to $\mathbf{H^W}$ is at the strong binding limit even at these dilute concentrations, such that each addition of $\mathbf{H^W}$ during the titration was fully forming a 4:1 **EY·**$\mathbf{H^W}$ complex with no $\mathbf{H^W}$ left free in solution. As a quarter of an equivalent of $\mathbf{H^W}$ has fully quenched the fluorescence of **EY**, then a limiting 4:1 **EY**:$\mathbf{H^W}$ stoichiometry must be achieved; it may be higher than this during the earlier points of the titration where **EY** is in large excess.

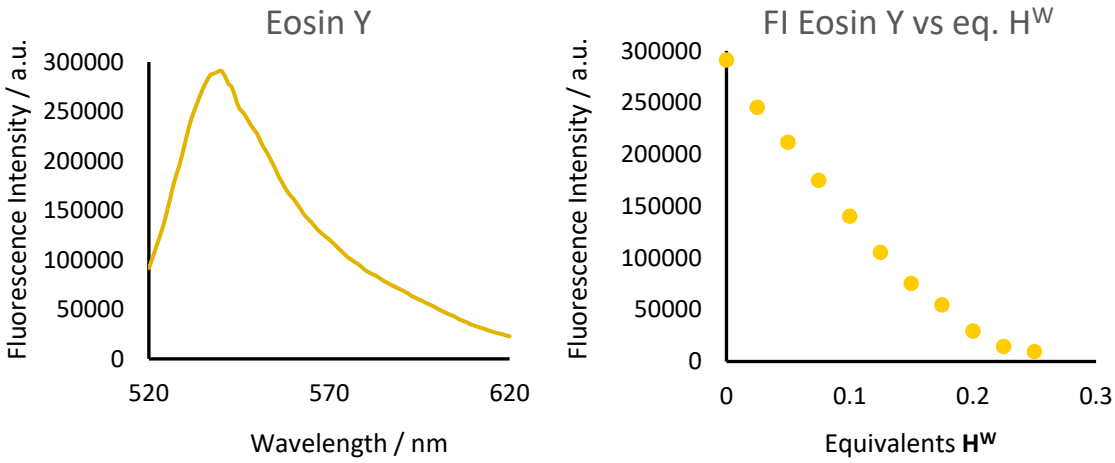

Figure 3.21 – Left: emission spectrum of EY. Right: the linear quenching of EY fluorescence upon addition of H^W. A minimum is reached at 0.25 equivalents at a concentration of 10 µM EY (pH 8.5 buffered).

To confirm the 4:1 **EY**:$\mathbf{H^W}$ stoichiometry that was suggested by the fluorescence quenching titration, a partial Job plot was constructed for **EY** and $\mathbf{H^W}$ at a total concentration of 50 µM. The maximum for this plot is actually seen at a mole fraction for **EY** of 0.86, indicating a 6:1 **EY**:$\mathbf{H^W}$ stoichiometry. With the binding constant of the species being immeasurably high at lower concentrations, observation of a stoichiometry in which an **EY** guest occupies each face of $\mathbf{H^W}$ is conceivable at this higher concentration.

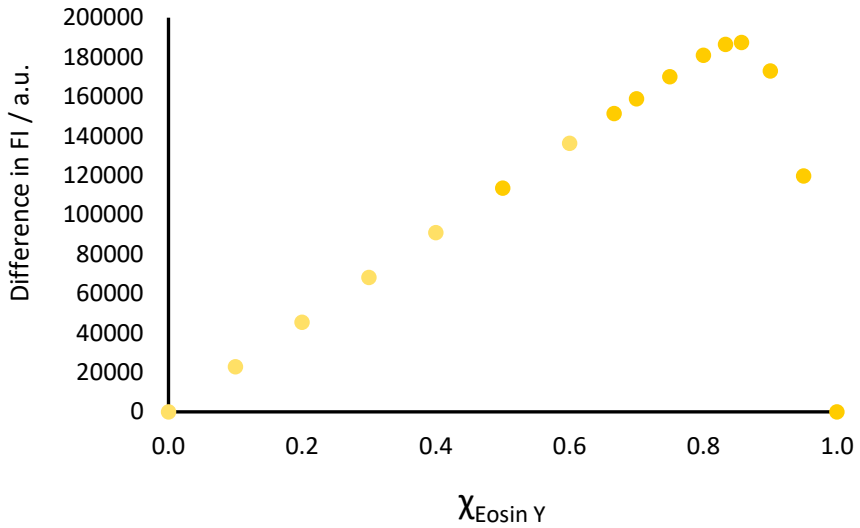

Figure 3.22 – partial Job plot of EY and H^W with a total concentration of 50 µM (pH 8.5 buffered). The fainter data points are simulated as the emission of EY by this point has reached a minimum.

Both **FLU** and **6C-FLU** showed reversibility in binding, with additions of anions into solution displacing the bound fluorophore and restoring the fluorescence emission. This "displacement assay" experiment was trialled using **EY** as the bound fluorophore, but with the anions SO_4^{2-} and Cl^- no displacement of **EY** could be observed – binding of **EY** to $\mathbf{H^W}$ is clearly too strong for this system to be useful as a displacement assay with anions.

3.2.4. Other surface-bound fluorophores

i) 8-hydroxypyrene-1,3,6-trisulfonic acid (HPTS)

Having proven the efficient quenching of anionic fluorophores using a surface-bound interaction with the Co(II) cage $\mathbf{H^W}$, attention was turned to finding other possible fluorescent anions for this system. Many common organic fluorophores can become anionic at moderately basic pH values and so to investigate possibilities that are not fluorescein derivatives, hydroxypyrene tris-sulfonate (**HPTS**) was tested to see if it showed comparable surface-binding behaviour.

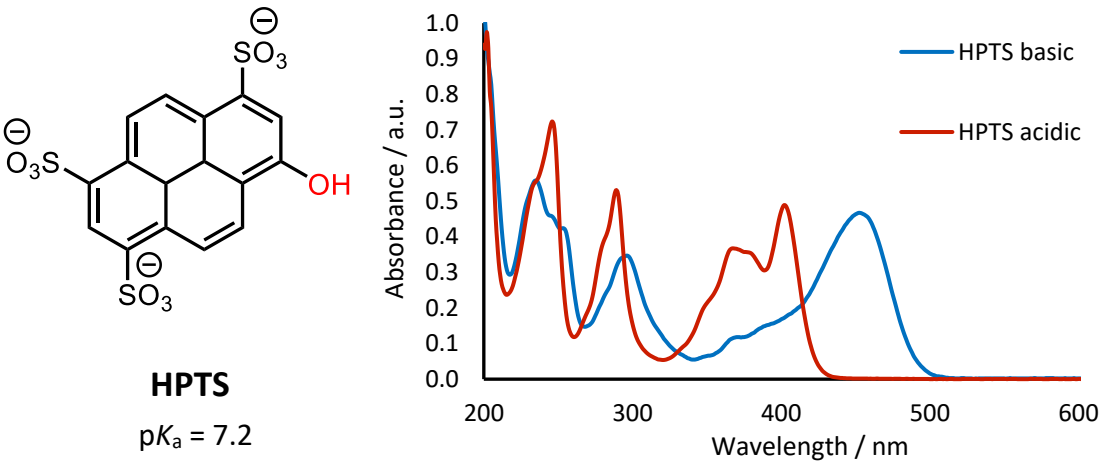

Figure 3.23 – Left: the structure of HPTS with hydroxy group highlighted in red. Right: UV/vis absorption spectra of HPTS in both the protonated and deprotonated states (3-/4-).

HPTS is the hydrophilic equivalent of hydroxypyrene, a polycyclic aromatic molecule. The addition of multiple sulfonate groups results in high water solubility, enhancing its use in fluorescence applications. It is available commercially as a trisodium salt and is responsible for the striking yellow colour of highlighter pens. 1-Hydroxypyrene has been used as a cavity-bound guest for the $\mathbf{H^W}$ in previous work and binds with high affinity. With the additional bulk of the sulfonate groups, as well as its hydrophilicity, it was thought that **HPTS** would not bind within the cavity but might associate to the exterior anion-binding sites of the cage owing to a combination of the negative charge of the molecule and the known affinity of phenolates for the cage's exterior surface.[7] Depending on the pH of the solution, **HPTS** can carry a charge of 3- or 4-. The hydroxyl group has pK_a = 7.2, allowing switching between both charge states. The change in pH affects the UV/vis absorption spectra of the fluorophore along with its colour in solution, shown in Figure 3.28. The absorption peak used for excitation in any fluorescence measurements shifts depending on the pH of the solution; below pH 7.2, the peak used for excitation in fluorescence measurements is at 400 nm, which does not overlap with the absorbance of $\mathbf{H^W}$. Above pH 7.2, this peak shifts to around 450 nm, even further from the cage's absorbance.

For fluorescence quenching experiments, the acidic (3-) and basic (4-) states of **HPTS** were investigated separately: the results are presented below. The first experiment was done under acidic conditions. Initially the **H^W/HPTS** interaction was studied at pH 4 (the pH controlled through addition of 1 M HCl). Incremental additions of **H^W** onto a solution of **HPTS** resulted in a rapid drop in fluorescence emission, with only *ca.* 0.16 equivalents of cage needed to fully quench the **HPTS**. The binding curve obtained was like that seen for **EY**, being a straight line until the emission reached its minimum, indicative of strong **HPTS/H^W** binding with all added **H^W** fully bound to **HPTS** until all **HPTS** was bound.

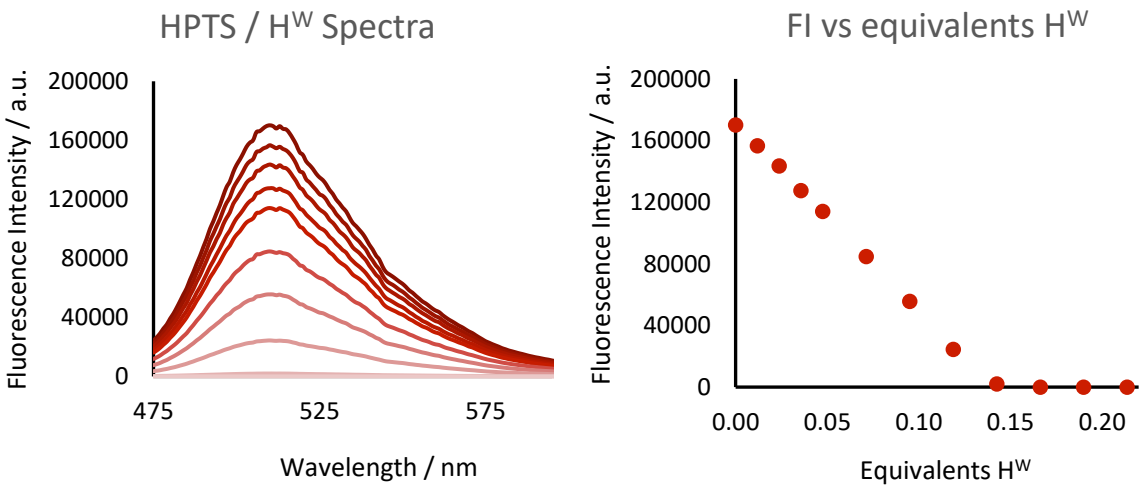

Figure 3.24 – quenching of $(HPTS)^{3-}$ emission upon addition of cage H^W up to 0.2 equivalents. $[(HPTS)^{3-}]$ = 19.65 µM, pH 4.

Given the strong binding and linear decrease in fluorescence intensity during the titration, a binding constant for the **HPTS/H^W** interaction could not be obtained; all we can deduct from this result is that K >> (1/[HPTS]), *i.e.,* >> 10^5 M^{-1}. From the number of equivalents of added **H^W** at which fluorescence is completely quenched, we can see how many **HPTS** molecules surround the cage at this point, as shown previously with **EY**. With the fluorescence reaching maximum quenching around 0.16 equivalents, this points to one cage associating with 6 molecules of **HPTS**, with a guest anion occupying each face of **H^W**. This stoichiometry can be confirmed through a Job plot analysis, which was also carried out.

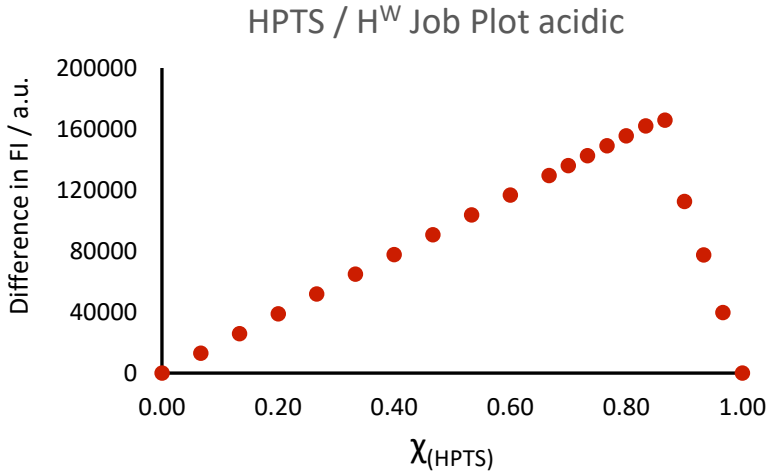

Figure 3.25 – Job plot of $(HPTS)^{3-}$ / H^W with both components at 50 µM at pH 4.

The maximum for this plot comes at a mole fraction for **HPTS** of 0.87, indicative of a 6:1 **HPTS**:**H^W** stoichiometry. This agrees with the observations made for the simple quenching experiment, with full quenching observed at 0.16 equivalents of **H^W**, implying that each **H^W** molecule interacts with (and quenches) 6 **HPTS** anions. The straight lines seen in the Job plot are due to the high binding constant, clearly defining the stoichiometry reached. This stoichiometry suggests that there is a **HPTS** molecule bound to every face of the cage, but the geometry of the binding interaction is unknown. It is possible for the sulfonate groups to be binding in the same manner as seen with the propyl- and butyl- sulfonate anions earlier, or the single phenolate group may be the focus of the interaction, although under acidic conditions this is unlikely as this group would still be protonated.

These experiments were repeated under basic conditions such that **HPTS** now carries a 4- charge. The solution of cage used was brought to pH 8 using NaOH solution and the **HPTS** dissolved in 0.1 M pH 8.5 borate buffer. Addition of the cage to the fluorophore solution again resulted in a rapid linear decrease of fluorescence intensity.

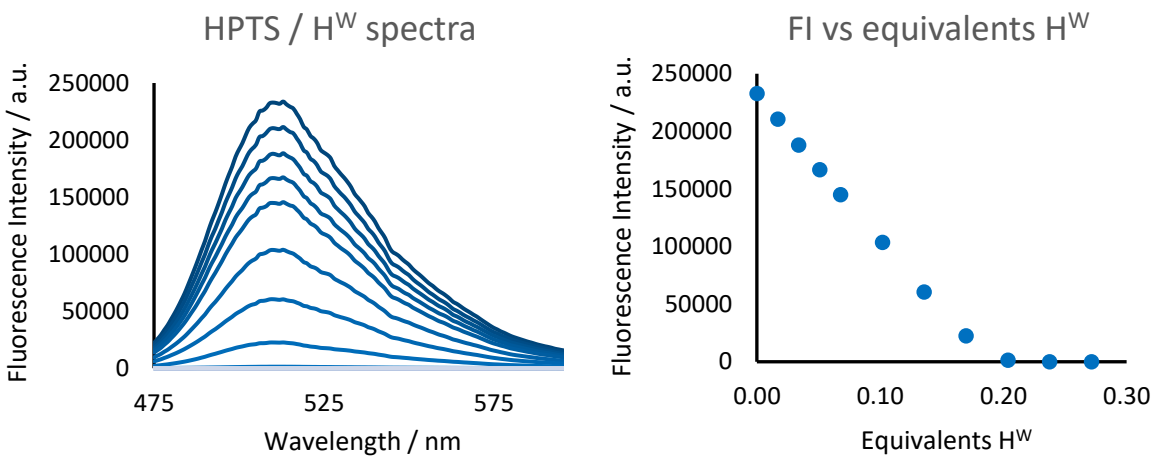

Figure 3.26 – quenching of $(HPTS)^{4-}$ by H^W up to 0.27 equivalents.
$[(HPTS)^{4-}]$ = 20 mM, buffered to pH 8.5.

The fluorescence intensity under basic conditions reaches a minimum after addition of *ca.* 0.25 equivalents of $\mathbf{H^W}$. During this time, the decrease in fluorescence intensity is linear, mirroring the very high association strength seen under acidic conditions. Interestingly, with the **HPTS** molecules having a higher overall charge of 4-, the number binding to one cage has dropped. Under acidic conditions full quenching was observed at around 0.16 equivalents but for this experiment that has increased to 0.25 equivalents of $\mathbf{H^W}$. This implies a 4:1 **HPTS**:$\mathbf{H^W}$ stoichiometry, which was confirmed by a Job plot experiment performed under similar conditions.

As shown in Figure 3.27, the Job plot under basic conditions has a similar shape to the previous data, with two straight lines converging at one point. The peak for this plot is at a mole fraction of 0.8, indicative of a 4:1 stoichiometry for the **HPTS**:$\mathbf{H^W}$ complex. This raises the question as to why the stoichiometry is different when the charge per **HPTS** anion increases: the obvious answer being electrostatic factors with only four 4- anions needed to completely cancel out the 16+ charge on $\mathbf{H^W}$, meaning that the binding constants for binding of the fifth and sixth equivalents of $(\mathbf{HPTS})^{4-}$ will be small and not significant at the concentration used.

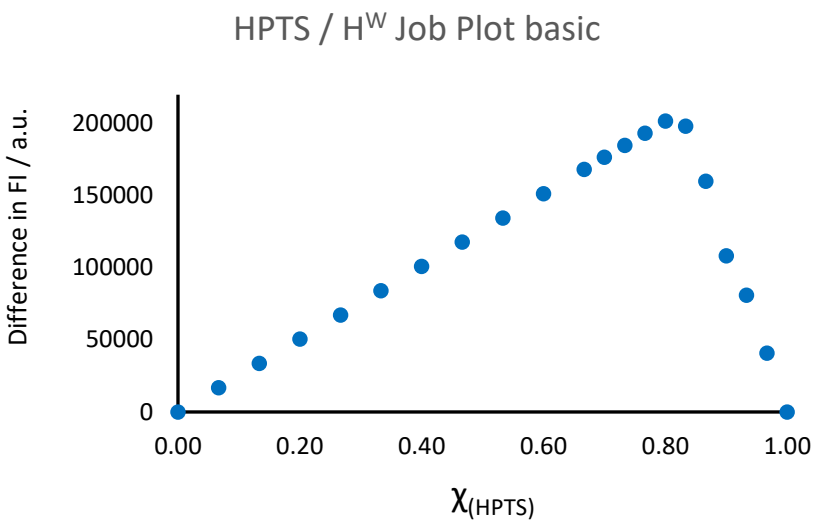

Figure 3.27 – Job plot of $(HPTS)^{4-}$/ H^W with both components at 50 µM buffered to pH 8.5.

To round off the investigation into this fluorophore as a surface binding guest, a displacement experiment was devised. In a similar manner to previous displacements of surface bound fluorophores, a competing anion was added incrementally, and the restoration of emission from displaced (**HPTS**)$^{4-}$ monitored. The anion used for this test was nitrate as it possesses a high binding constant and should be able to displace **HPTS** at reasonable concentrations. The result of this titration is seen below in Figure 3.28.

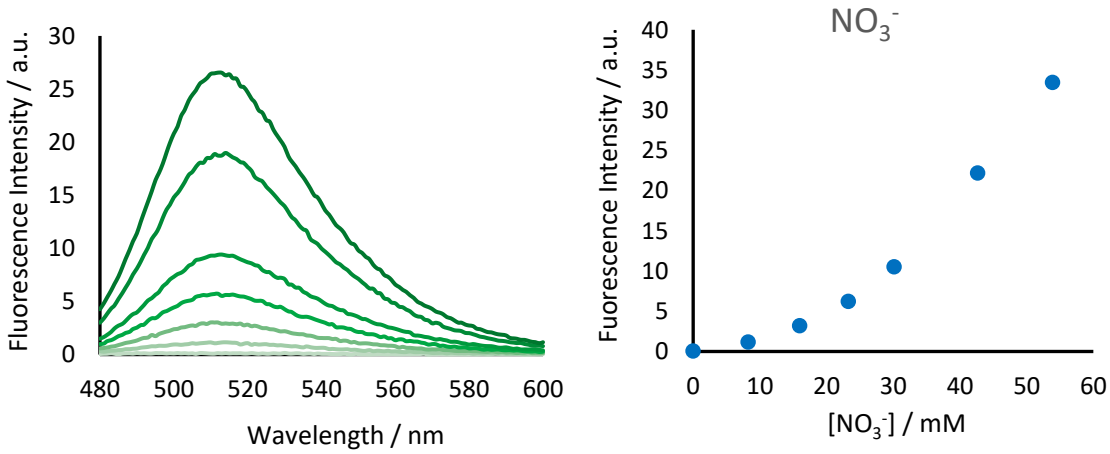

Figure 3.28 – restoration of HPTS fluorescence through addition of NO_3^-.
$[(HPTS)^{4-}]$ = 20 µM, $[H^W]$ = 5 µM, pH 8.5 buffered.

The shape of the curve differs from those seen previously for other surface-bound species. In this instance, there is an upwards trend to the curve – the inverse of that seen for fluorescein. It is not clear what causes the curve to adopt this shape but almost hints at some form of cooperativity; as the concentration of nitrate adhering to the cage increases, it becomes easier for any subsequent nitrate added to bind.

Following this experiment, the anions chloride and sulfate were tested in the same manner. Chloride provided the same upwards trend to the emission whilst sulfate resulted in a linear relationship between concentration and fluorescence intensity. It is not obvious what these results point to regarding the displacement of bound **HPTS**. Binding constants for the anions tested could not be calculated as the data does not fit a simple 1:1 binding isotherm. This concludes the work undertaken using **HPTS** as the surface-bound guest with the cage $\mathbf{H^W}$.

ii) Dansyl acid (DAN)

Following the success of using **HPTS**, other fluorophores appended with sulfonate groups were investigated. Dansyl acid was considered as a suitable candidate. The dansyl group itself is a dimethylamino naphthalimide molecule which is appended with a group such as sulfonyl chloride or sulfonate. Replacing the SO_2Cl group with a SO_3Na group turns dansyl chloride into dansyl acid, a small anionic fluorophore.

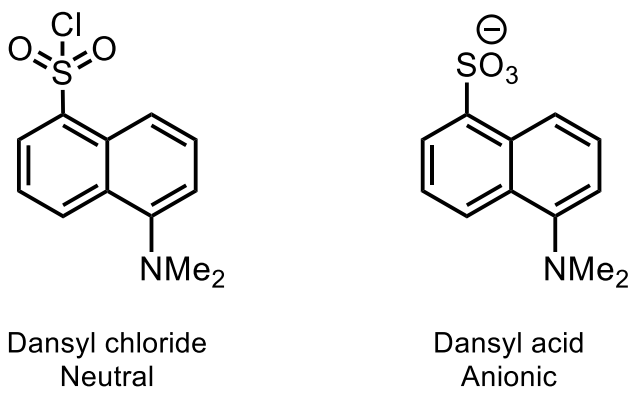

Figure 3.29 – Dansyl chloride, the precursor to Dansyl acid which is the molecule studied. Dansyl acid possesses a sulfonate group which is capable of surface binding.

Dansyl acid is expected to bind to the surface of the cage through the sulfonate group present. As shown during testing of different anionic head groups, sulfonate is expected to bind more strongly than carboxylate or phosphate and so the binding here should be of considerable strength. The data from initial quenching titrations shows that this is the case. Figure 3.30 portrays the steep reduction in emissive intensity upon addition of the cage **H^W**. The dramatic initial decrease suggests multiple molecules of **DAN** are binding simultaneously when in excess relative to the cage. For this reason, the curve does not fit to a 1:1 isotherm and a binding constant could not be obtained for **DAN**.

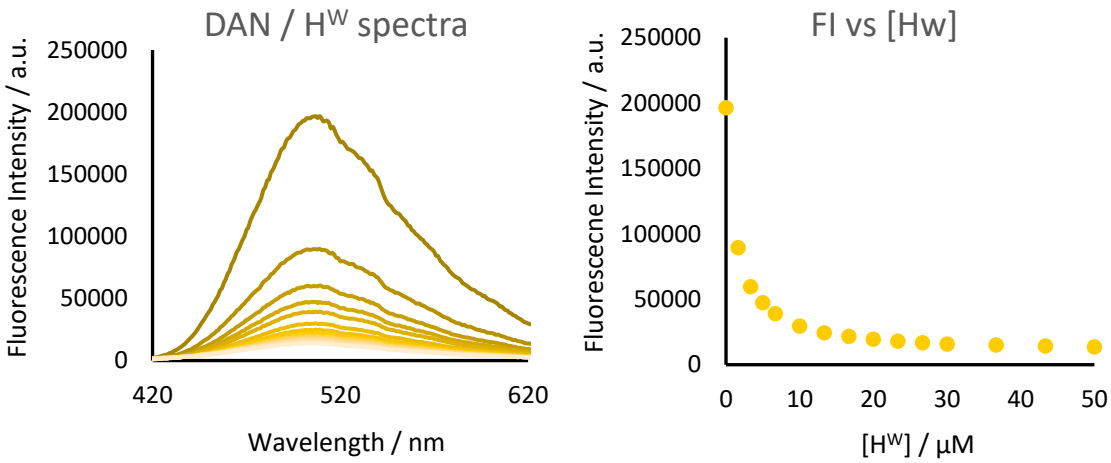

Figure 3.30 – quenching titration of dansyl acid with H^W. [DAN] = 10 µM, [H^W] = 0-50 µM.

Studies of the stoichiometry of binding involved a Job plot between **DAN** and **H^W** as for fluorophores studied previously. The maximum of this plot occurs at 0.87 mole fraction of dansyl acid. As seen with **HPTS** and **FLU**, high stoichiometries for surface bound fluorophores is possible, and **DAN** seems to be no exception to this. A maximum in the Job plot at a mole fraction of 0.87 indicates a 6:1 **DAN**:**H^W** stoichiometry which explains the rapid quenching seen in the previous experiment.

Displacement of **DAN** was attempted using chloride as the competing guest. It was thought that some restoration of fluorescence would be observable, however no change in the emission was seen.

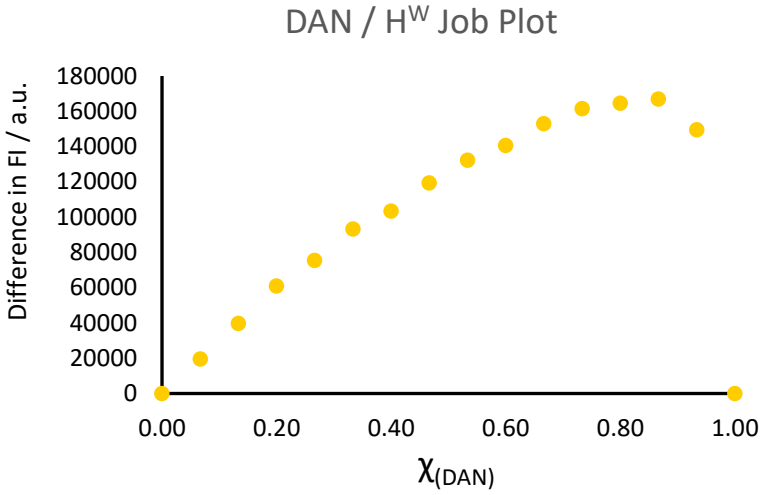

Figure 3.31 – Job plot of DAN/H^W showing a speciation of 6:1 DAN:H^W.
Total concentration of components was 0.1 mM.

3.2.5. Stabilisation of pH-sensitive anionic species

In a publication by the Raymond group, protonated ammonium cations were reported to be stabilised through uptake by the cavity of a negatively charged tetrahedral coordination cage $[Ga_4L_6]^{12-}$, the negative charge of which arises from the presence of dianionic catecholate termini in each ligand. This stabilisation results in a higher pH being required for deprotonation of the cations, allowing catalytic mechanisms involving a protonated transition state to proceed with greater ease.[19,20] Inspired by this mechanism of stabilisation, we set out to investigate whether the cubic coordination cage **H^W** displayed an ability to stabilise anionic pH-sensitive molecules, bound to the cage's surface, in aqueous solution.

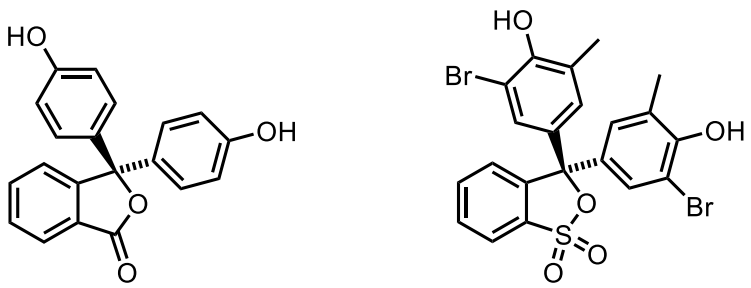

phenolphthalein
phph
pK_a 8.9

bromocresol purple
BCP
pK_a 6.3

Figure 3.32 – pH indicators used to test anionic stabilisation imparted by H^W on surface-bound guests.

To perform these experiments, pH indicator molecules that were detectable by UV/vis measurements were selected as the basis for our investigation. The molecules chosen were the ubiquitous pH indicator phenolphthalein (**phph**), familiar to anyone who has studied A-level or possibly even GSCE chemistry, along with a structurally similar molecule, bromocresol purple (**BCP**).

The titration in this instance is different from previous experiments described within this chapter as the concentration of both the host and guest remain constant, but the pH is varied. These concentrations were phenolphthalein (**phph**) at 80 µM and $\mathbf{H^W}$ at 40 µM. Starting at a pH of 4.22, the pH was increased through sequential additions of 0.1 M NaOH solution. A UV/vis spectrum was recorded after each addition and the absorbance at 560 nm for the anionic for of **phph** plotted against the pH. This was repeated without cage present, and the two resulting curves compared.

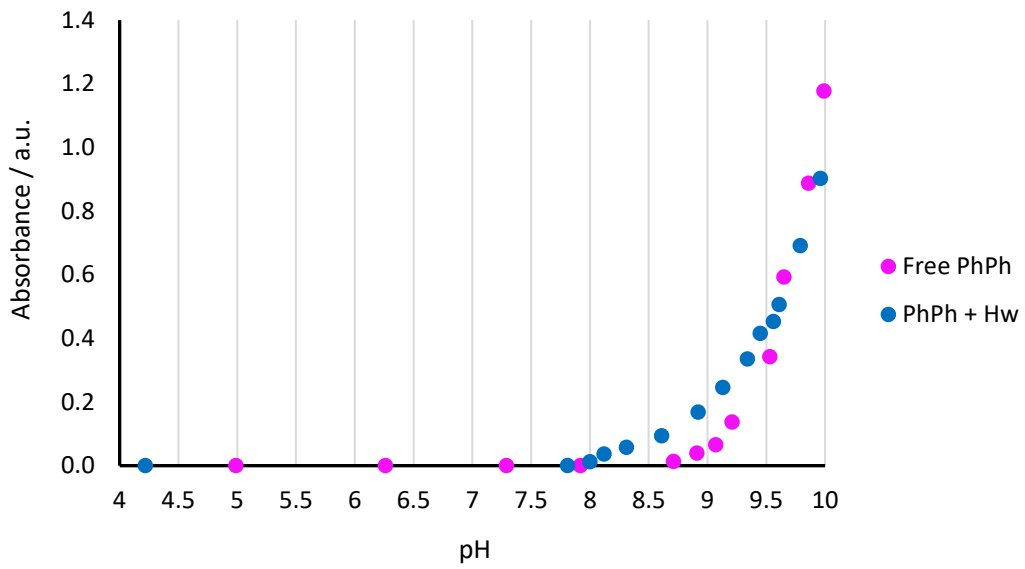

Figure 3.33 – increase in absorbance value of the peak centred around 550/560 nm with increasing pH. The appearance of this peak occurs 0.7 pH units lower for phph + H^W than for free phph. [phph] = 80 µM, [H^W] = 40 µM.

As shown by the curves, the emergence of absorbance by **phph** begins at pH 8 in the presence of $\mathbf{H^W}$; this indicates that the lactone ring is opened, and the species is now di-anionic. For free **phph** this is not seen until pH 8.7 is reached, which suggests that association with $\mathbf{H^W}$ stabilises the anionic form of **phph**. A problem with this experiment arises from solubility limitations of $\mathbf{H^W}$ at high pH. As the pH approaches

10, the cage begins to precipitate out of solution, indicating decomposition. This produces a rising baseline up to the point where measurements become unusable. The second disadvantage is that a complete titration curve cannot be obtained for the same reasons.

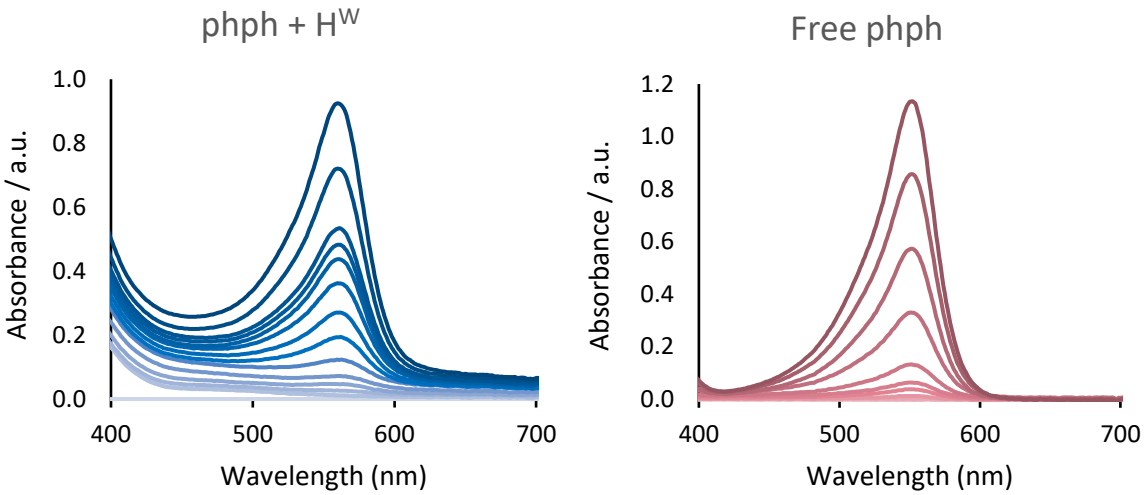

Figure 3.34 – appearance and subsequent increase of the peak caused by the anionic form of phph with increasing pH. The left-hand set of spectra show increase in the baseline beyond 600 nm, which is corrected in the data seen in Figure 3.36.

The data obtained for **phph** in the presence of **H^W** was subject to baseline correction. As the overlaid spectra in Figure 3.34 show, the data for **phph + H^W** shows a slight increase in absorbance across the spectral range, which is absent for free **phph**. To account for this in the curve comparison, the increase at 700 nm was subtracted from the value at 560 nm to give an accurate representation of the peak for **phph** appearing. This is the data seen in Figure 3.33.

To alleviate the issues encountered using **phph**, a second pH titration was performed using bromocresol purple (**BCP**) – another pH indicator, but this time with a pK_a of 6.3 compared to phenolphthalein's 8.9. It was hoped that **BCP** would permit a similar experiment to **phph** using a more moderate pH range. Both **H^W** and **BCP** were at a concentration of 50 µM.

This experiment did produce a full titration curve for the opening of the sulfonate ester group with increasing pH, allowing a more accurate determination of stabilisation to be performed. The difference in absorbance between the start and end of the titration was recorded and then halved to give the midpoint of the

titration. The pH at which this value was reached was recorded for both experiments (with and without **H^W** present) and then compared. For free **BCP**, 50% deprotonation was reached at pH 7.0 whilst for the experiment including **H^W** this was reduced to pH 5.9, just over one unit of pH lower. The stabilisation imparted by the 16+ charge of **H^W** upon binding the dianionic form of **BCP** is clear.

These experiments demonstrate that stabilisation of the anionic form occurs for both phenolic and sulfonic species in the presence of **H^W**. Another indication that association of the coloured dianion form of the indicator molecules has occurred is the red-shift in peak absorption value for both **phph** and **BCP**, which undergo a shift of approximately 10 nm upon addition of **H^W**. The same observation was made for surface-bound fluorophores such as fluorescein earlier in the chapter.

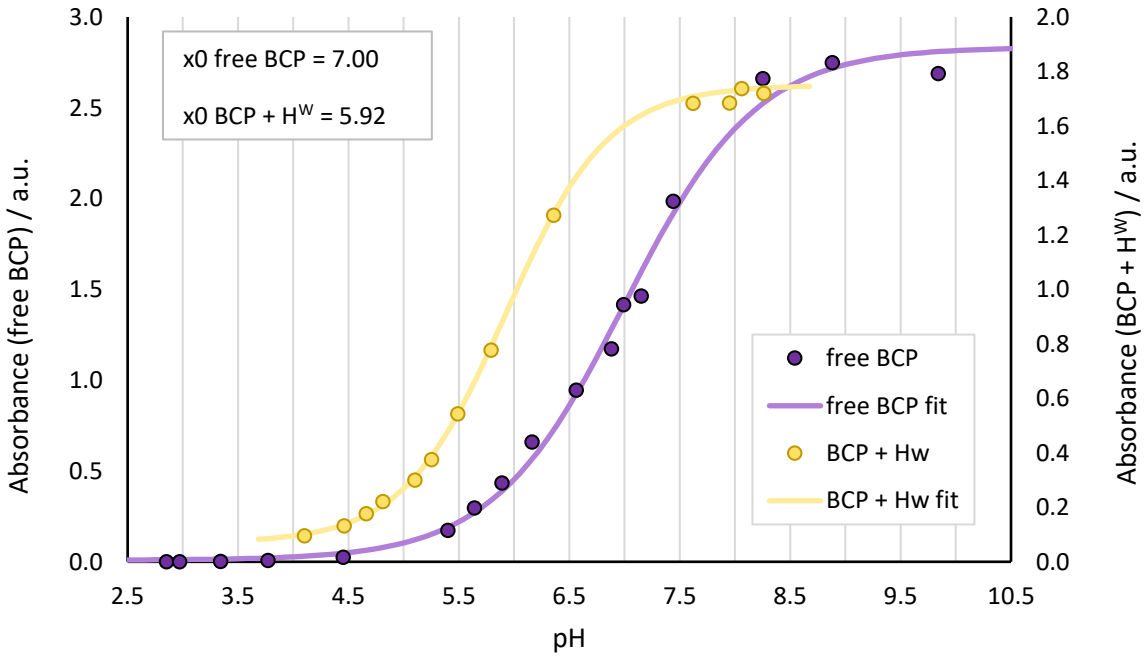

Figure 3.35 – speciation curves for the anionic form of BCP with increasing pH. Addition of H^W stabilises the anionic form by 1.1 units of pH. [BCP] = 50 µM, [H^W] = 50 µM.

3.3. Conclusions

The work undertaken in this chapter set out to determine association constants for species capable of binding to the exterior surface of the coordination cage $\mathbf{H^W}$. This was achieved through development of a fluorescence displacement assay which took inspiration from assays reported in the literature. The ubiquitous fluorophore fluorescein, which has been used abundantly as a fluorescent on/off component in sensors, was studied through a series of binding experiments involving the cage $\mathbf{H^W}$. Fluorescein was found to bind to the cage when in its dianionic form (pH > 6.5) with a binding constant of 1.0×10^5 M^{-1} for a 1:1 interaction with each face of the cube. This served as the basis for the surface-based displacement assay, allowing *K* values for several anionic species to be determined and ranked. Small inorganic anions, both singly and doubly charged, were studied along with larger organic anions such as dicarboxylates. The *K* values for singly charged species broadly followed the Hofmeister series, with strongly solvated anions such as fluoride binding weakly to $\mathbf{H^W}$ whilst the more hydrophobic anions such as nitrate displayed much higher binding constants. The 2- anions such as sulfate and hydrogen phosphate returned higher binding constants than most 1- anions despite being considered more kosmotropic in character. This suggested that electrostatic attraction was also a component of binding strength, which when considering the 16+ overall charge of the cage complex is a logical conclusion to reach. Bulkier poly-carboxylate anions with larger organic frameworks resulted in higher binding constants than were found for any inorganic anion.

To broaden the scope of the host cage's surface-binding capabilities, derivatives of fluorescein were tested for association to $\mathbf{H^W}$. These derivatives were 6-carboxyfluorescein (**6C-FLU**) and tetrabromofluorescein (**EY**), allowing the effect of both increased negative charge and increased hydrophobicity to be examined. Both of these molecules bound to $\mathbf{H^W}$ with higher affinity than unsubstituted **FLU**, with **EY** binding more strongly than **6C-FLU**, suggesting that hydrophobicity provides a larger contribution to exterior binding species than an additional unit of charge. Other anionic fluorophores were also investigated, namely hydroxypyrene tris-sulfonate

and dansyl acid. **HPTS** was found to bind in both its 3- and 4- states at the strong binding limit. **DAN** also bound with high affinity, forming a 6:1 **DAN**:**H^W** complex.

The small concentration of cage (<1 equivalent) needed to fully quench emission from the fluorophores being studied indicated stoichiometries with multiple anionic fluorophores binding to a molecule of **H^W**. To take a closer look at the speciation of these surface-bound guests, Job plots were used to investigate the ratio of guest:cage achievable for each different guest. High stoichiometries were seen for all species with a ratio of up to 6:1 guest to cage observable for (**HPTS**)$^{3-}$ and **DAN**. The dominant stoichiometry could also decrease as the concentration of both components was lowered. This was demonstrated using **6C-FLU** at concentrations of 100 µM, 50 µM and 10 µM.

Stabilisation of anions through association to the cage's exterior has also been demonstrated, using two common pH indicators. The ring opening of phenolphthalein and bromocresol purple occurred at 0.7 and 1.1 units of pH lower in the presence of the cage **H^W**.

3.4. Experimental

3.4.1. Materials and methods

The fluorescent species fluorescein, hydroxypyrene tris-sulfonate (trisodium salt), 6-carboxyfluorescein and Eosin Y were purchased from Acros Organics or Merck Life Sciences and used as received. Inorganic salts used to evaluate anion binding affinities were purchased from Sigma-Aldrich and used as delivered. Fluorescence measurements were carried out using either a BMG ClarioStar plate reader with 96-well plates, or an Agilent Cary Eclipse fluorimeter. UV/vis spectra were obtained using an Implen C40 Nanophotometer. pH adjustments were performed using a Hanna Instruments HI2210 pH meter fitted with a Hamilton SpinTrode probe.

3.4.2. Synthesis of cage H^W

H^W was prepared as described in section 2.4.3.7 of the previous chapter. For the majority of experiments detailed within this chapter, the cage was adjusted to pH 8

before use. This was achieved through incremental addition of NaOH solution (1M) until the desired pH was reached.

3.4.3. Quenching of fluorescent anions by H^W

An example titration: 2 mL of dilute FLU solution was prepared by mixing 20 µL of 1 mM stock FLU solution in 0.1 M NaOH solution with 1480 µL deionised H_2O and 500 µL borate buffer at pH 8.5 (final concentration 10 µM FLU). Separately, 1.5 mL of H·FLU solution was prepared by mixing 15 µL of 1 mM stock FLU solution with 124 µL H^W, 861 µL of H_2O and 500 µL of borate buffer (final concentrations 10 µM FLU, 30 µM H^W). These solutions were then mixed in varying ratios to a volume of 200 µL to increase the concentration of cage from one well to the next. In total, this titration contained 14 wells. The instrument was heated to 308 K for 20 minutes before equilibrating at 298 K before running the samples.

3.4.4. Displacement assay titrations

Fluorescence titrations were performed by preparing a solution of fluorescein FLU (10 µM) and cage H^W (100 µM) in deionised water, which was then used to prepare two solutions at 5/50 µM FLU/H^W through addition of either deionised water or a premade sodium salt solution of the anion under investigation. 50 mM borate buffer at pH 8.5 used for each titration to ensure a constant pH. Titrations were run using between 10 and 14 wells of volume 200 µL comprising of varying ratios of H^W·FLU solution with and without analyte added. The instrument was heated to 308 K for 20 minutes before equilibrating at 298 K for all measurements. Fluorescence spectra between 500 and 600 nm were recorded for each well using an excitation wavelength of 472 nm and the peak emission at 515 nm used to determine binding constants for any analytes studied. Calculation of the binding constants for anions in the displacement assay used software written by Prof. Chris Hunter, as used in previous Ward group publications.[6]

3.4.5. Stabilisation of pH-sensitive species

The pH curves for phenolphthalein and bromocresol purple were constructed by gradually adjusting the pH of solution through addition of 0.1 M NaOH solution and

recording a UV/vis spectrum after each addition. For phenolphthalein, the solutions used were as follows:

Free phph: 1200 µL of stock 0.1 mM phph solution, 300 µL H_2O (1500 µL of phph @ 80 µM). Phph + H^W: 1200 µL of stock 0.1 mM phph solution, 100 µL of 0.4 mM H^W solution and 200 µL H_2O (1500 µL of phph @ 80 µM and H^W @ 40 µM).

The starting pH was brought to pH 4 using 1 M HCl and the titration started from this point.

For bromocresol purple, the solutions used were as follows:

Free BCP: 150 µL of stock 0.5 mM acidic BCP solution and 1350 µL H_2O. (1500 µL BCP @ 50 µM).

BCP + H^W: 150 µL of stock 0.5 mM acidic BCP solution, 120 µL of 0.4 mM H^W solution and 1350 µL H_2O. (1500 µL BCP @ 50 µM and H^W @ 50 µM).

3.4.6. Errors

The *K* values quoted within this chapter in Section 3.2 are presented with an estimated uncertainty of ±10%. The primary source of error associated with the displacement assay lies not with the sample preparation and experimental readings but with the fitting of a binding isotherm to the fluorescence data obtained. This error is typically in the region of 5-10% for the work in this chapter, which outweighs any error in weighing or pipetting during the experimental set up.

3.5. References

1 E. V. Anslyn, *J. Org. Chem.*, 2007, **72**, 687–699.

2 S. L. Wiskur, H. Ait-Haddou, J. J. Lavigne and E. V. Anslyn, *Acc. Chem. Res.*, 2001, **34**, 963–972.

3 B. T. Nguyen and E. V. Anslyn, *Coord. Chem. Rev.*, 2006, **250**, 3118–3127.

4 M. Bonizzoni, L. Fabbrizzi, G. Piovani and A. Taglietti, *Tetrahedron*, 2004, **60**, 11159–11162.

5 K. Ghosh, A. R. Sarkar, A. Samadder and A. R. Khuda-Bukhsh, *Org. Lett.*, 2012, **14**, 4314–4317.

6 S. Turega, W. Cullen, M. Whitehead, C. A. Hunter and M. D. Ward, *J. Am. Chem. Soc.*, 2014, **136**, 8475–8483.

7 W. Cullen, A. J. Metherell, A. B. Wragg, C. G. P. Taylor, N. H. Williams and M. D. Ward, *J. Am. Chem. Soc.*, 2018, **140**, 2821–2828.

8 D. Bastos-González, L. Pérez-Fuentes, C. Drummond and J. Faraudo, *Curr. Opin. Colloid Interface Sci.*, 2016, 23, 19–28.

9 OpenStacks, in *Biology*.

10 M. D. Baer, V. T. Pham, J. L. Fulton, G. K. Schenter, M. Balasubramanian and C. J. Mundy, *J. Phys. Chem. Lett.*, 2011, **2**, 2650–2654.

11 P. Huyskens, L. Sobczyk and I. Majerz, in *Journal of Molecular Structure*, Elsevier, 2002, vol. 615, pp. 61–72.

12 A. S. Özen, F. De Proft, V. Aviyente and P. Geerlings, *J. Phys. Chem. A*, 2006, **110**, 5860–5868.

13 Y. Marcus, *Ion Properties*, Taylor & Francis, 1997.

14 Y. Koga, *Phys. Chem. Chem. Phys.*, 2013, **15**, 14548–14565.

15 S. K. Sanyal and S. K. Mandal, *Electrochim. Acta*, 1983, **28**, 1875–1876.

16 N. Vlachy, B. Jagoda-Cwiklik, R. Vácha, D. Touraud, P. Jungwirth and W. Kunz, *Adv. Colloid Interface Sci.*, 2009, **146**, 42–47.

17 M. D. Ludden and M. D. Ward, *Dalt. Trans.*, 2021, **50**, 2782–2791.

18 D. Brynn Hibbert and P. Thordarson, *Chem. Commun.*, 2016, **52**, 12792–12805.

19 M. D. Pluth, R. G. Bergman and K. H. Raymond, *Science*, 2007, **316**, 85–88.

20 C. J. Hastings, M. D. Pluth, R. G. Bergman and K. N. Raymond, *J. Am. Chem. Soc.*, 2010, **132**, 6938–6940.

3.6. Appendices

3.6.1. Fitting of FLU/H^W in Excel to determine the 1:1 binding constant, *K*.

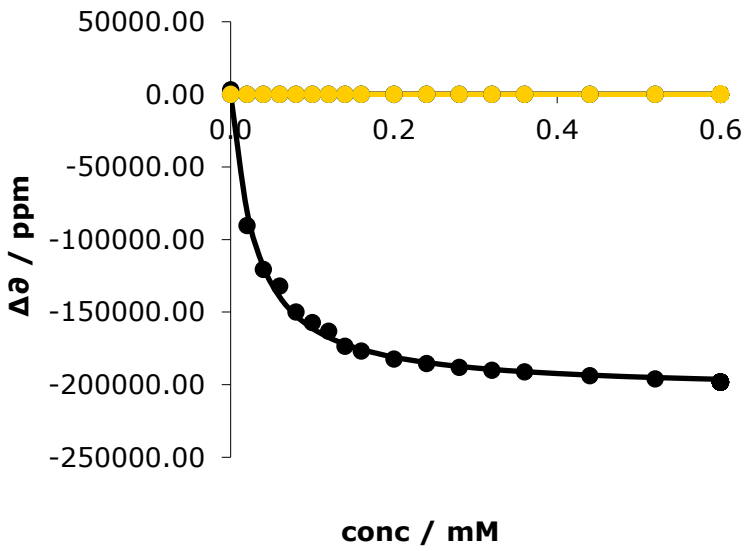

3.6.2. Signal curves for displacement of FLU using various anions.

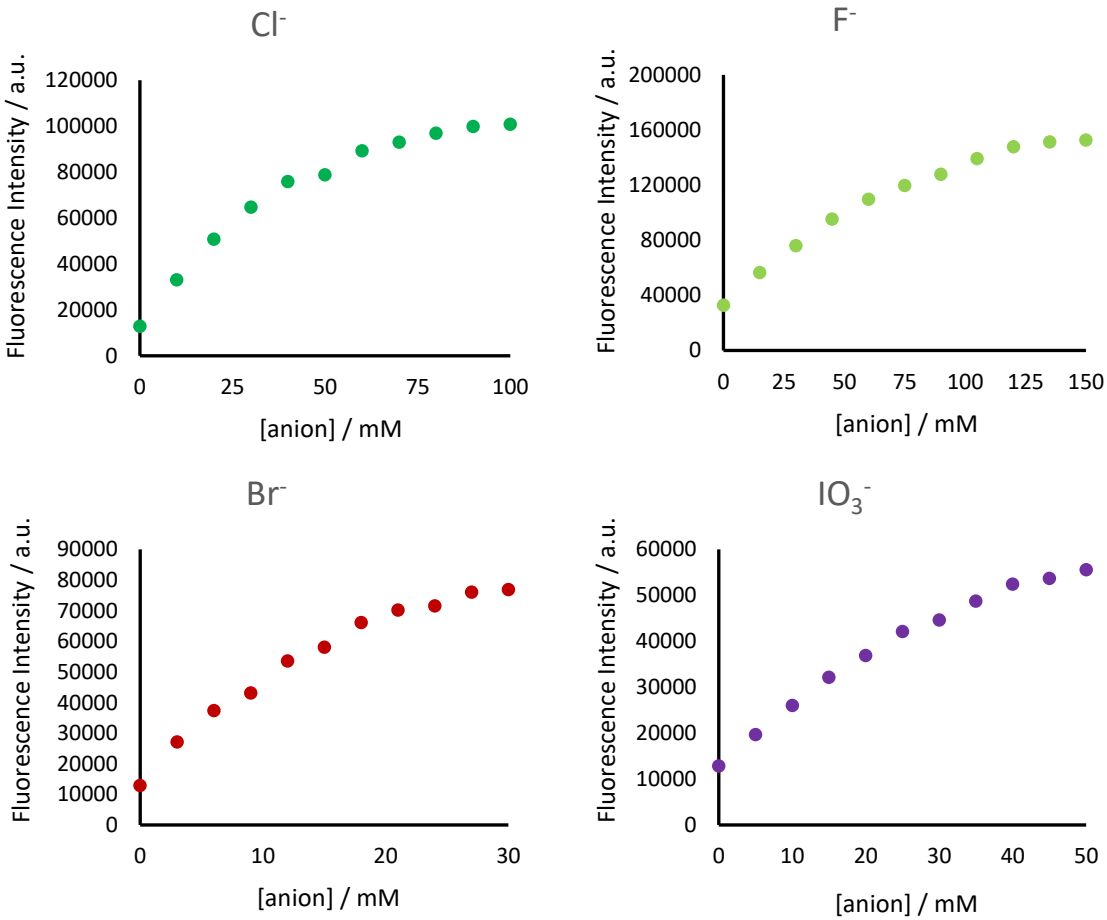

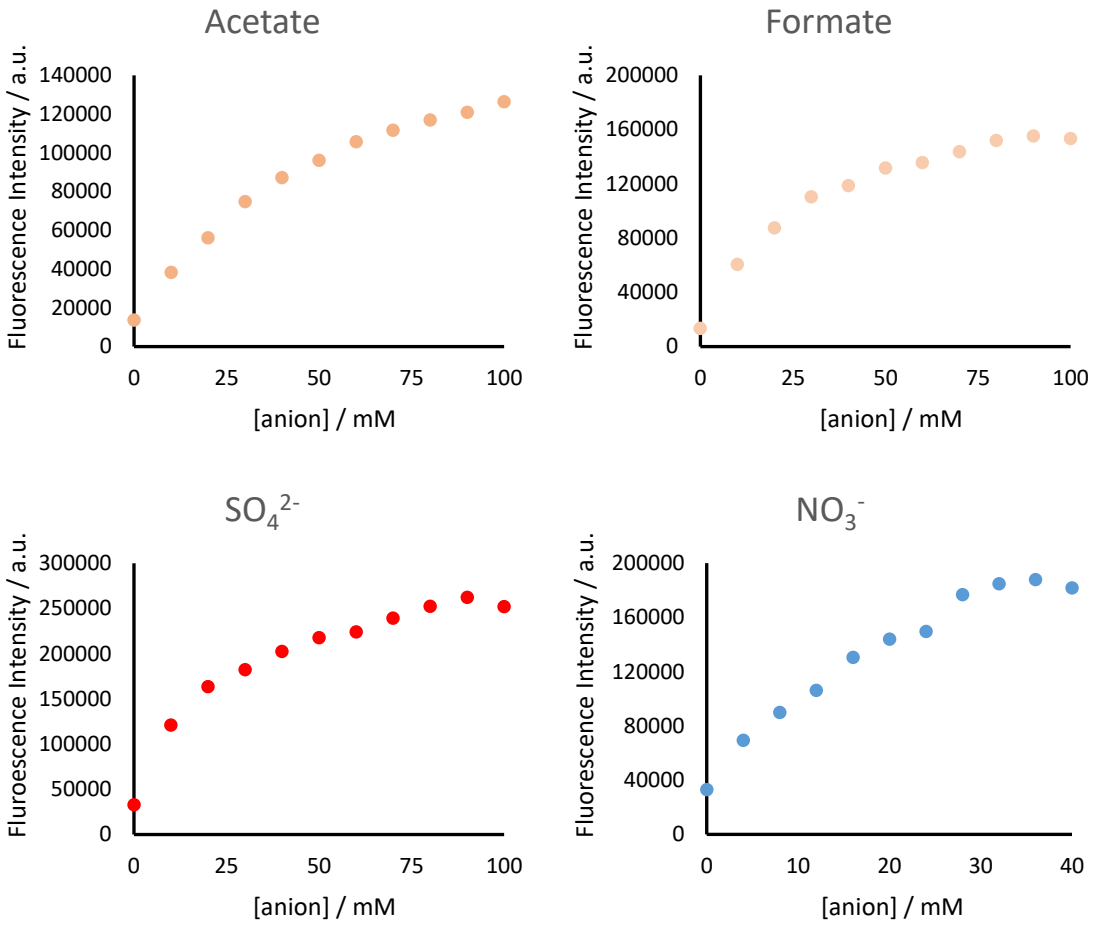

3.6.3. Signal curves of carboxylate and sulfonate molecules displacing FLU from H^W.

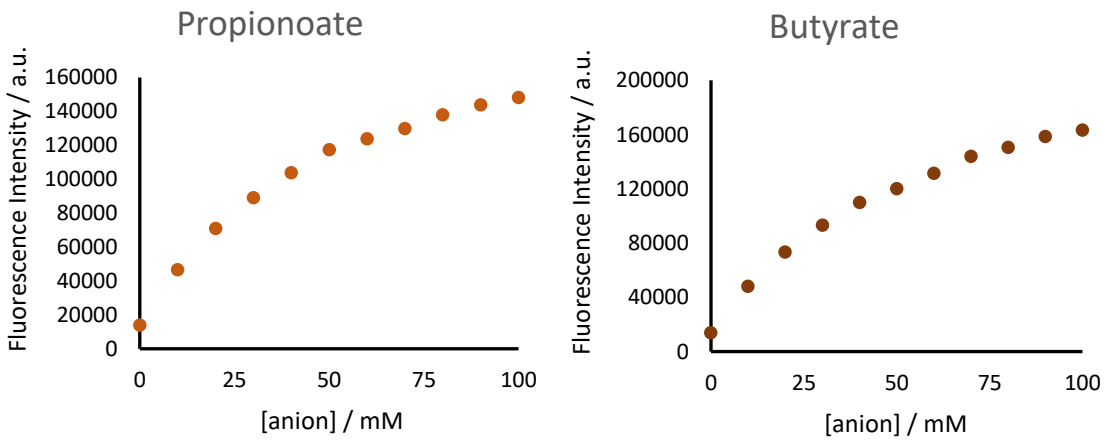

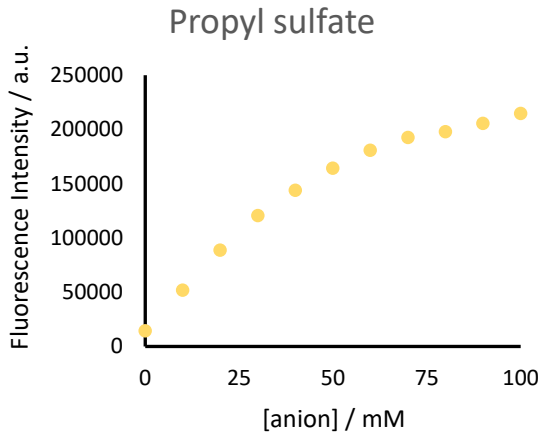

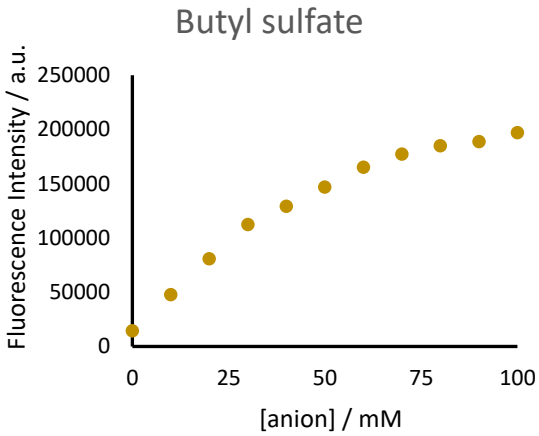

3.6.4. Displacements of $(HPTS)^{3-}$ from H^W.

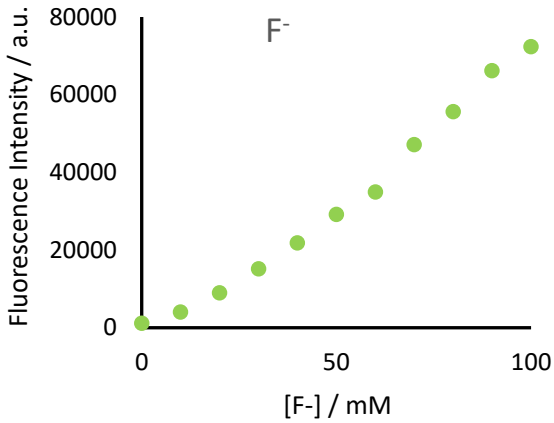

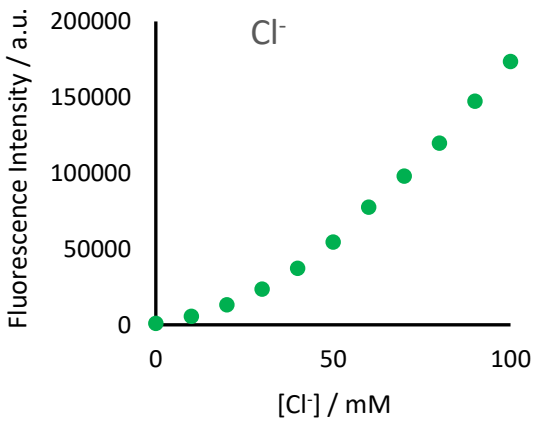

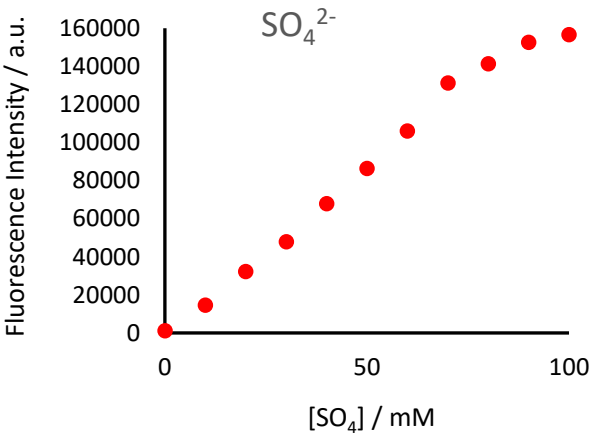

Chapter 4

A colourimetric displacement assay for detection of cavity-bound and surface-bound guests

4.1. Introduction

Colourimetric indicator displacement assays are of interest chemically as they offer considerable advantages over intensity-based assays. The ability to detect chemical binding by eye for an operator is useful for quick, high throughput, qualitative testing. This can be extended to empirical measurements using a spectrometer or fluorimeter depending on the components of the assay. In a colourimetric indicator displacement assay, as with IDAs that were discussed previously, the assay is dependent on an indicator binding to the sensor and undergoing some change in its optical properties; it is then displaced by a competing species, restoring the optical property to its original form. In colourimetric IDAs, the free indicator shows a different colour than when it is bound, which is the basis of the assay.[1]

Traditionally colorimetric assays incorporate an indicator, known as a chromophore, that has strong UV/vis absorption. Common examples of chromophores include molecules such as azo-dye compounds and pH indicators. Many examples cited in the literature combine a positively charged host with a negatively charged indicator such as a fluorescein molecule and are capable of sensing negatively charged guests through displacement of the indicator.[2]

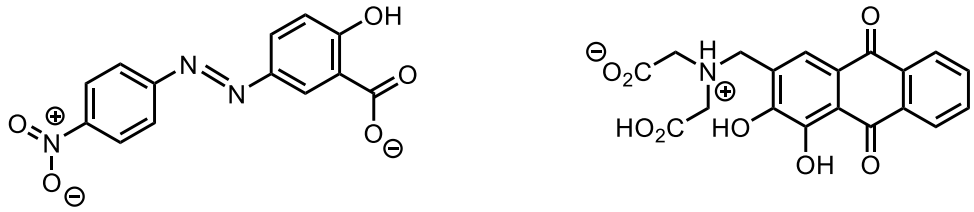

Figure 4.1 – Examples of molecular chromophores. Left: Mordant yellow, an azo dye. Right: alizarin complexone, a quinone-type chromophore.

Fluorescent components may be used in colourimetric sensing assays, as demonstrated by Hossain *et al.*[3] Using a macrocycle-based nickel complex as the host, combined with the fluorophore Eosin Y, the absorption and emission of the fluorophore were blue-shifted upon association with the macrocycle. Oxalate could be selectively bound by this sensor, displacing Eosin Y in the process leading to a red shift in both absorption and emission. This is unlike displacement assays detailed in

previous chapters of this work, which display an increase in emissive intensity at one wavelength rather than constant emission at a moving wavelength, *i.e.,* a change in colour (colourimetric) response.

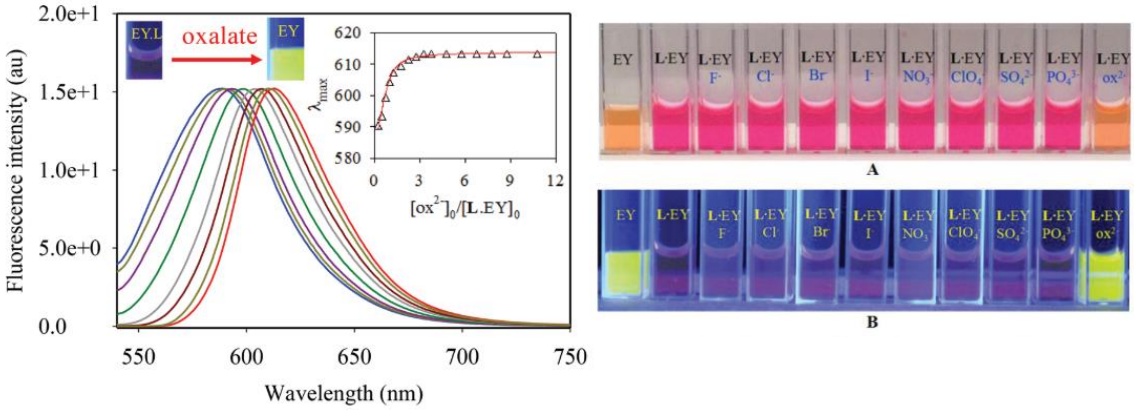

Figure 4.2 – Hossain's oxalate-selective fluorescent sensor incorporating the fluorophore Eosin Y.[3] Studies conducted in H_2O.

Colourimetric assays hold substantial advantages over intensity-based assays that use only one colour. Firstly, small changes in colour are much more easily detectable by the naked eye than small changes in intensity. The human eye is amazingly adaptable to changes in light conditions thanks to the pupil's ability to narrow or widen depending on the brightness of the light source (known as the Pupillary light reflex), meaning that an accurate estimation of luminance by eye is very difficult, if not impossible. In contrast to this, it is predicted that the human eye can detect in excess of one million different shades of colour (the number is only 'predicted' because no-one has sat down and counted them all yet). This disparity in sensitivity of the eye should result in a colourimetric assay being easier to use for an optical-based measurement: a small colour change upon guest binding could be readily visible and confirm that the analyte in question binds without the need for an instrument-based calibration of intensity against a known standard. Secondly, any change in hue arising as the output of a colourimetric assay can be mapped to the CIE colour space. This allows for reproduceable, quantitative measurements, as the conversion to (x,y) coordinates on the CIE chart is simple and does not rely on the arbitrary units of light intensity. Comparison between experiments using one colour of varying intensity becomes difficult without a consistent control sample being used

as a calibrant, as the photomultiplier voltage can be varied from experiment to experiment to provide the greatest dynamic range.

The CIE 1931 colour space (seen in Figure 4.3) is a visual representation of all the chromaticities visible to the human eye. Around the edge of the shape (called the 'gamut') are colours of a single wavelength between the extremes for visible light (400 – 700 nm). Any point within this gamut can be made through a combination of two or more colours. Points on the graph can be denoted using a set of (x,y) coordinates. Fluorescence spectra can be converted from a set of intensities at each wavelength to a pair of coordinates that can be plotted on a CIE chart.

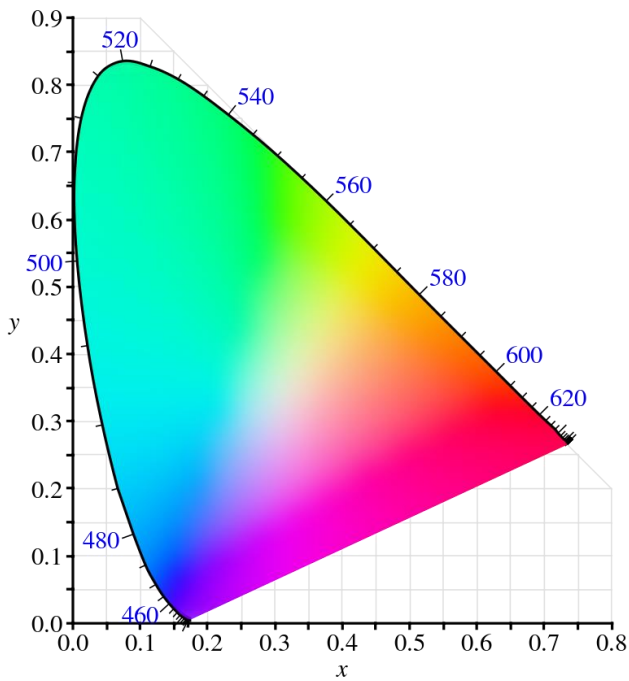

Figure 4.3 – The CIE 1931 colour space

The fluorescence-based displacement assay previously developed by the Ward group involving the host cage $\mathbf{H^W}$ and the fluorophore **MAC** is an example of an assay that could be readily converted from being based on changes in intensity (depending on the amount of **MAC** that is displaced by the incoming analyte) to involving a colour change by having a second component present that emits at a different wavelength. Using this method, different amounts of displaced **MAC** would result in a variable emission intensity at a fixed wavelength, which when combined with the secondary fluorophore of fixed emission intensity would produce a varying ratio of the two

emissive components and hence a range of different colours, easily detectable by eye. This method has been employed successfully by Ward *et al.* previously, using a combination of Ir(III) and Eu(III) metal cations connected by a bis(pyrazolyl-pyridine) bridging ligand, which also chelates to each of the metal termini.[4] Incremental addition of a competing guest species that preferentially bound the Eu(III) produced a decrease in red emission from the Eu(III) complex to the point where no red emission was seen. As the blue Ir(III) emission remains constant throughout guest additions, this colour begins to dominate as the Eu(III) approaches being totally quenched, producing the desired ratiometric response.

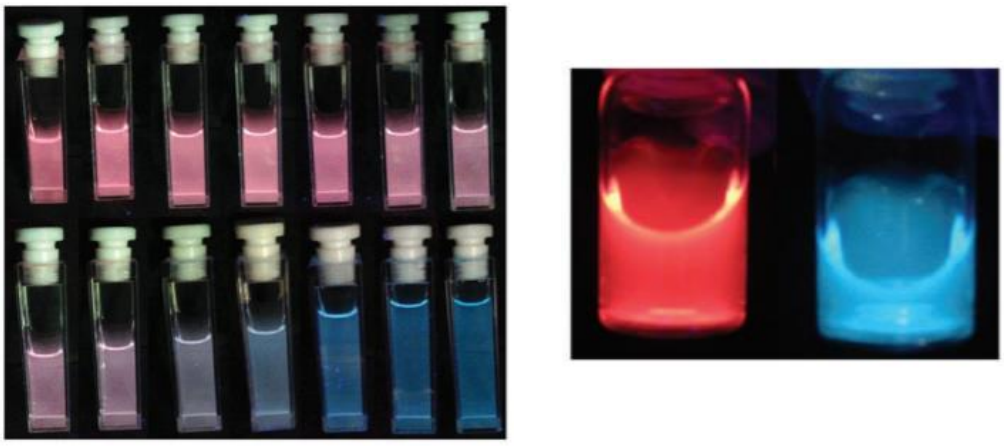

Figure 4.4 – Left: Progressive quenching of Eu(III) emission in an Eu/Ir dyad upon addition of the chemical warfare simulant VO leads to a colour change from red to blue as Eu(III) emission decreases. Right: luminescence response before and after addition of 18 eq. VO in MeCN.[4]

The work detailed in this chapter looks to build on an already functional assay (described in Chapter 3) through means of a second fluorophore to give monitorable changes in colour upon guest binding due to a ratiometric response (a different balance between two independent colour components). The idea when developing this assay involves using a second binding fluorophore that can be displaced in the same manner as **MAC** but with a different emission colour. With a solution of the cage and two differently coloured fluorophores, addition of a guest as an analyte should displace more of one colour of fluorophore than the other, leading to the colour change needed for a colourimetric assay.

4.2. Results and Discussion

4.2.1. Basis of the assay

The proposed design for the assay has many similarities to the displacement assay using **MAC** reported previously by Ward *et al.*[5] but was initially planned to use a mixture of two different cavity-binding chromophores which would be bound to different extents in the presence of $\mathbf{H^W}$. These would possess different binding constants and different emissive wavelengths, such that a competing guest (analyte) will displace more of one bound fluorophore than the other, leading to a different colour response for each analyte. The advantages of the response being different in colour rather than intensity are numerous and have been detailed in the introduction.

4.2.2. Titrations with MAC

The 2014 paper by the Ward group detailing the use of **MAC** in a displacement assay to calculate binding constants for new guests in a cage cavity included values for the quenching of **MAC** by the cobalt cage $\mathbf{H^W}$ and other small organic guests that subsequently displaced it.[5] A logical starting point for developing this assay was to repeat these measurements using the instruments available at this point in time.

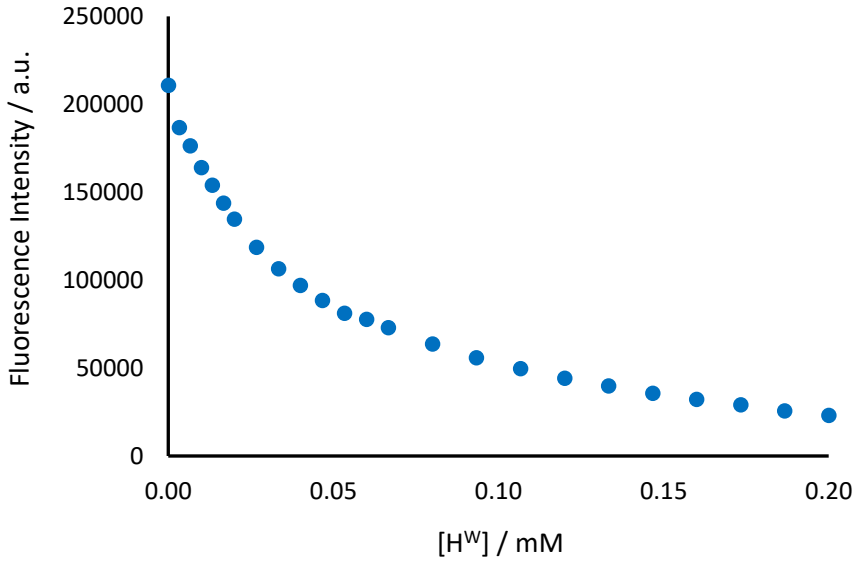

Figure 4.5 – Progressive quenching of MAC upon sequential addition of portions of H^W in H_2O, affording a *K* value of 3.0 x 10^4 M^{-1}. [MAC] = 10 µM.

The first experiment conducted was to re-measure a binding constant for **MAC**, being one of the fluorophores used in the colourimetric assay. The quenching of **MAC** by addition of $\mathbf{H^W}$ during a titration was found to give a curve similar to that reported previously. Extracting a binding constant from this data returned a *K* value of 3.0 x 10^4 M^{-1} for **MAC** binding within the cavity. Comparing this to the published value of 2.0 x 10^4 M^{-1} we see a small difference between the values but good agreement as a whole. To check for displacement of **MAC** occurring to the same extent as for previously reported guests, displacement titrations were run using guests reported in the 2014 paper.[4] The guest cyclooctanone was used to displace **MAC** from within the cage's cavity, producing an increase in fluorescence emission with *K* calculated to be 5.1 x 10^3 M^{-1} (lit. value 2.1 x 10^3 M^{-1}).[5] The resulting graphs from this experiment are shown in Figure 4.6.

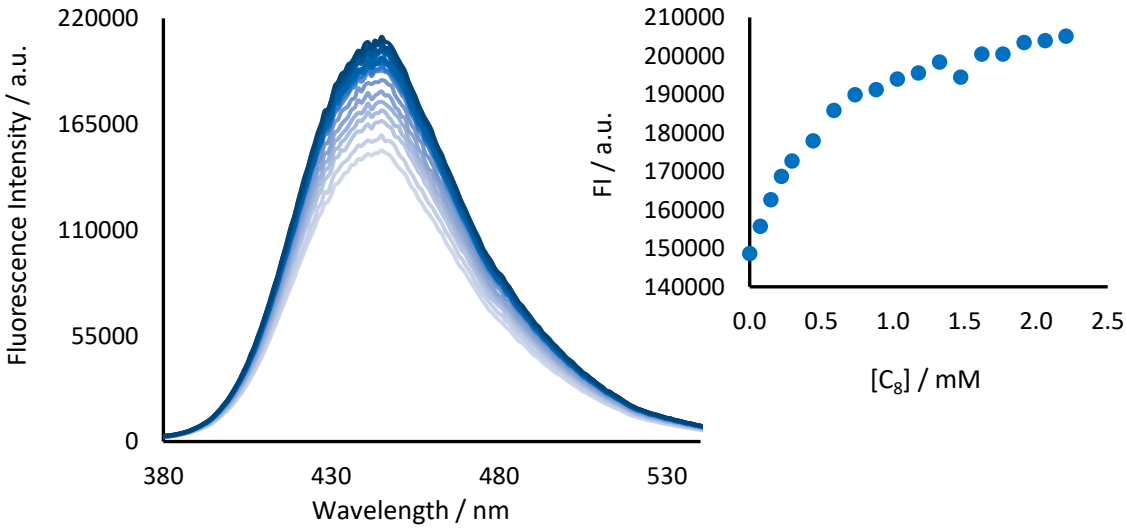

Figure 4.6 – Restoration of MAC fluorescence upon addition of the cyclic ketone C_8. [MAC] = 10 µM, $[H^W]$ = 0.15 mM.

4.2.3. Searching for a secondary fluorophore to use in partnership with MAC

Knowing that small organic fluorophores such as coumarin were able to bind within the cavity, other cavity-binding fluorophores were needed to expand the possible combinations of colours. Coumarin dyes seemed an obvious starting point and so some research into tailoring a molecule to display different photochemical properties was conducted. The fluorescence emission band of coumarin molecules is usually broad and centred around 370 to 500 nm, depending on substituents and polarity of

solvent.[6] Red-shifting the emission of a coumarin can be achieved through specific modifications: for example, adding an electron-donating group such as a diethylamino group in the 7-position, and appending an electron-withdrawing group (*e.g.* a nitrophenyl) in the 3-position, both produce a red-shift in the molecule's emission.[7]

The drawback to adding groups to the coumarin structure to result in emission at a longer wavelength is the additional size contributed by these groups. For cavity-binding guests, there are size restrictions imparted by the cage's interior; addition of a nitrophenyl group would certainly result in the molecule being too large to bind within the cavity. Coumarins tend to bind with the carbonyl group pointing directly into the H-bond donor pocket at a *fac*-tris-chelate vertex of the cage, due to the hydrogen bonding that can occur between the two species. This means that any substituent at the 4-position is very size-constrained as it points towards the internal wall of the cavity, rendering anything larger than a methoxy group undesirable.[8] Rather than continue with searching for a suitable coumarin molecule, it was decided that finding new classes of guest would be more beneficial.

The options for identifying new guests were either to synthesise/buy many potential fluorophores and test them individually with the cage to look for quenching upon binding, or to run initial tests *in silico*. The software package GOLD (Genetic Optimisation of Ligand Docking) was employed as the most time and cost-effective method. The use of GOLD has been documented previously, adapted from being primarily used in biological chemistry to discover ligands for protein binding, to predicting guest binding in the cavity of the coordination cage $\mathbf{H^A}$.[9] By 'training' the program using a set of guests that have experimentally determined binding constants from ^{1}H NMR titrations, the program can predict with reasonable accuracy how strongly a molecule would be bound. There are several contributions required as part of this calculation to give a final value of *K*, seen in the equation below:

$$logK_{calc} = -(203.5 \times f_{ligandclash}) + (0.104 \times f_{ligandtorsion}) + (0.0398 \times f_{partburied}) - (0.118 \times f_{nonpolar}) - (0.326 \times f_{ligandflexibility})$$

Equation 4.1 – The scoring function used for predicting *K* values for potential guests using the software package GOLD.

Having this tool at our disposal meant that the binding behaviour for a series of potential fluorophores could be estimated initially using GOLD. Consultation of the literature provided many groups of fluorescent molecules which were appropriate, based on size and shape, to investigate further. Amongst these were BODIPY dyes, naphthalimides and benzofurazan molecules. BODIPY dyes are popular due to their sharp fluorescence peaks and high quantum yields. They are insensitive to solvent polarity and are stable under physiological conditions, making them excellent in biological applications.[10,11] Naphthalimides are readily synthesised from naphthalic anhydride resulting in a donor-acceptor scaffold, similar to nitrobenzofurazan (NBF). NBF's are known as push-pull dyes due to the presence of opposing electron-donating and electron-withdrawing groups. These groups generate an intramolecular charge transfer (ICT) state after irradiation with light, leading to differing properties depending on the environment. The downside to this is the dye's performance in aqueous media, with ICT-type dyes emitting far more weakly in water than in organic solvents.[12] Perhaps the most surprising result of the virtual screening was the number of molecules that were deemed to not only fit inside the cavity, but to bind with remarkably high affinity. As already demonstrated, the size constraints of the cage are particularly strict, so to find guests with molecular volumes in excess of 250 $Å^3$ that were predicted to fit was a promising result.

4.2.4. Titrations using potential secondary fluorophores

After using GOLD to identify a list of potential fluorescent guests that could be used in combination with the cubic cage $\mathbf{H^W}$, titrations using the guests that scored well had to be performed, to confirm the predicted binding values and observe the magnitude of quenching for individual guests. These experiments were performed through titrating a solution of guest with host added against a solution of guest, keeping the concentration of fluorophore constant throughout.

The first set of data comes from the fluorophore 1-hydroxypyrene. Pyrene is a commonly used polycyclic aromatic fluorophore but being nonpolar has little water solubility. The addition of a hydroxy group aids this sufficiently to use 1-hydroxypyrene for fluorescence measurements in our system.

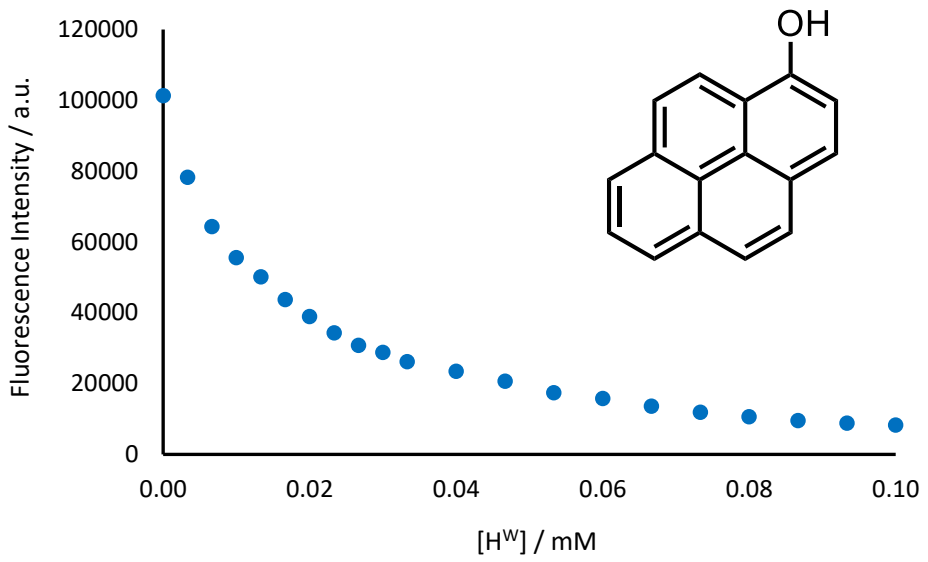

Figure 4.7 – Quenching of 1-hydroxypyrene on addition of the cage H^W in H_2O. [1-OHP] = 10 µM

Addition of increasing amounts of cage $\mathbf{H^W}$ to a solution of 1-hydroxypyrene in water resulted in smooth progressive quenching of fluorescence that fit well to a 1:1 binding isotherm. The value obtained from this fit was 1.1 x 10^5 M^{-1}, towards the upper limit for cavity binding guests observed so far. Another binding constant for this guest is available in the literature for a different system; using the isostructural cage $[Cd_8L^W{}_{12}][NO_3]_{16}$ a binding constant of 1.3 x 10^6 M^{-1} was reported, with the difference in binding constants between $\mathbf{H^W}$ and $[Cd_8L^W{}_{12}][NO_3]_{16}$ for the same guest likely arising from the change in counter-anion.[13] Although this guest binds strongly within these cubic cage assemblies and provides a possible alternative to **MAC** as a fluorescence probe for displacement assays, it cannot be used in conjunction with **MAC** in a two colour system as both components emit in the same region of the visible light spectrum – around the violet/blue end.

Evaluation of binding was repeated for other guests that had been initially screened using the GOLD software. Fluorophore guest molecules were used at a 10 µM concentration, and the host typically at a concentration of 0.2 mM, during titrations. Many potential guests at this point were ruled out due to one or more drawbacks. These included poor solubility for the commercially available BODIPY 493/503, and low emissive intensity for 4-amino-1,8-naphthalimide. Nonetheless, any fluorophore-binding titrations that could be obtained were recorded, the data for which can be found in the appendix (section 4.5.1).

One of the fluorophores that was quenched upon uptake into the cage's cavity was N-methyl-7-nitrobenzofurazan (shortened to **NBF** hereafter). **NBF** emits with a maximum around 560 nm, giving it a yellow colour when fluorescing in solution. The intensity of this emission decreases upon addition of cage as seen in Figure 4.8. Fitting this fluorescence decrease to a 1:1 binding isotherm returns a *K* value of 6.4 x 10^4 M^{-1}.

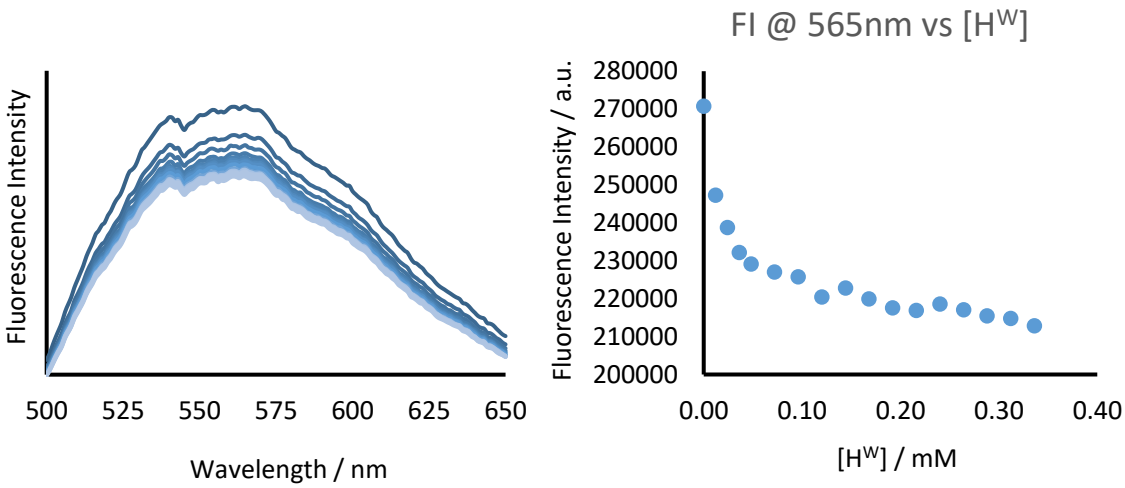

Figure 4.8 – Quenching of NBF by H^W in H_2O. This process does not result in complete quenching of the bound fluorophore. [NBF] = 10 µM.

This data brings to light a potential issue for some fluorophores in this system. Whilst the quenching curve for **NBF** appears to be flattening out as the concentration of $\mathbf{H^W}$ increases beyond 0.1 mM, the residual emissive intensity remains high. Overall, the reduction in emission between the start and end of this particular titration is only around 20%, compared to the 90% reduction seen for **MAC** using similar conditions. This strongly limits the utility of **NBF** as a prove for a displacement assay: the

relatively small extent of quenching seen for **NBF** rendered it unusable in a two-fluorophore system as the colour changes seen upon displacement would be dominated by **MAC**. At this point we concluded that this experiment using displacement of different amounts of two different cavity-bound fluorophores in an attempt to generate a luminescence colour change was not a promising avenue to pursue further, and a different way to achieve the necessary two-colour combination was needed.

4.2.5. MAC/$[Ru(bpy)_3]^{2+}$ system

After the apparent failures of a **H·2G** system containing two competing cavity-binding components with different emission colours, attention was turned to combinations of fluorophores with only one guest occupying the cavity (the variable luminescence component, affected by displacement using the analyte guest) and a second fluorophore free in solution and therefore having a fixed emissive intensity. Displacing the cavity-bound fluorophore should still result in a different balance between the two emission colours and hence give a visible colourimetric response on guest binding. As long as there is an intensity change in the emission of **MAC** upon displacement from the cage cavity by an analyte then a change in colour of the whole system should still be visible.

An obvious candidate for the fixed, non-binding luminescent component for a **H·2G** system that is a different colour from **MAC** is ruthenium tris-bipyridine dichloride. A well-studied metal complex, $[Ru(bpy)_3]^{2+}$ has a broad visible region ^{1}MLCT absorbance centred at ≈450 nm, and exhibits luminescence from the resultant ^{3}MLCT state, generated by inter-system crossing from the initially-populated ^{1}MLCT state. Emission (phosphorescence in this case) is seen as a broad peak with maximum emission between 600-620 nm in H_2O. A quantum yield of 0.042 has been reported in water at 25 °C.[14] Using this in conjunction with **MAC**, which has a quantum yield of 0.5, a ratio of 5:1 $[Ru(bpy)_3]^{2+}$:**MAC** seemed appropriate to balance the two emission intensity components. The UV/vis spectra of the two luminescent species both individually and combined are shown in Figure 4.9.

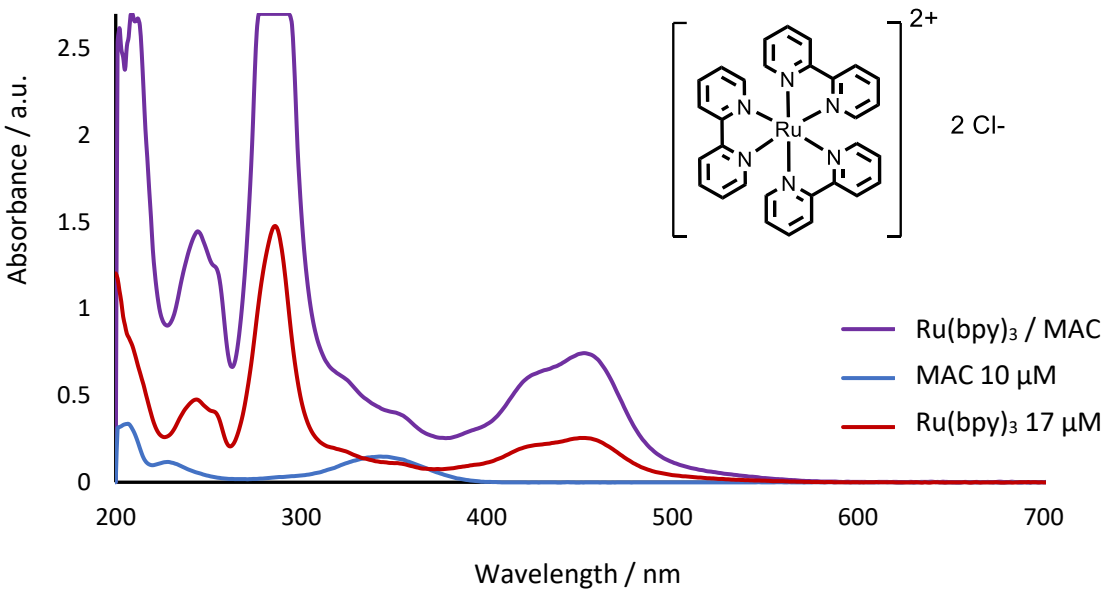

Figure 4.9 – Combined UV/vis absorption spectra for MAC and $Ru(bpy)_3^{2+}$ both individually and combined. An excitation wavelength around 400 nm is usable for this combination and will excite both species. [MAC] = 10 µM, $[Ru(bpy)_3]^{2+}$ = 50 µM for the combined sample.

The absorption peaks for **MAC** and $[Ru(bpy)_3]^{2+}$ can be seen in the spectrum of the combined sample (purple line, Figure 4.9) with the absorption between 380-420 nm resulting in excitation of both species. Using both molecules in conjunction will require an excitation wavelength in this range, although with absorption from the cage $\mathbf{H^W}$ being substantial up to 400 nm, the focus will be towards the longer end of this range to avoid competing absorption by the cage. Figure 4.10 shows the emission spectra for both **MAC** and $[Ru(bpy)_3]^{2+}$ compared. Both spectra were obtained using excitation at the peak absorbance for each species – 343 nm for **MAC** and 457 nm for $[Ru(bpy)_3]^{2+}$. The units of both y-axes differ as the emission of $[Ru(bpy)_3]^{2+}$ is weaker than that of **MAC**, as described earlier.

Mixing $[Ru(bpy)_3]^{2+}$ and **MAC** in a 5:1 ratio for luminescence analysis produced the spectrum seen in Figure 4.11. Use of an excitation wavelength of 390 nm gave two emission peaks of a similar intensity. This provided a starting point for a titration with $\mathbf{H^W}$ to see if the emission of exclusively the blue part of the spectrum was quenched as **MAC** was selectively uptaken into the cavity whilst $[Ru(bpy)_3]^{2+}$ was not.

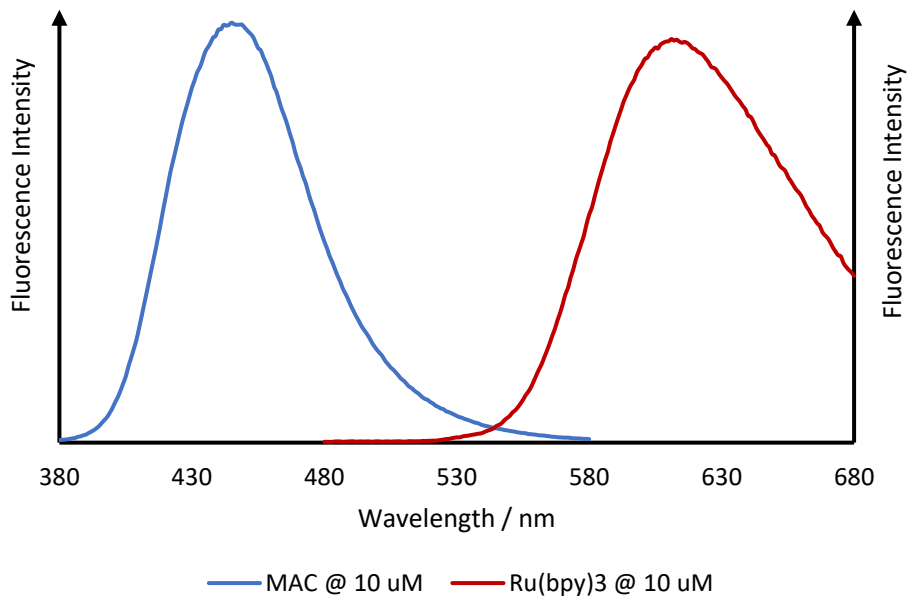

Figure 4.10 – Normalised emission spectra of MAC and $[Ru(bpy)_3]^{2+}$ in H_2O.

Addition of host cage $\mathbf{H^W}$ to a solution containing both $[Ru(bpy)_3]^{2+}$ and **MAC** resulted in a substantial decrease in fluorescence emission for **MAC** as expected; this was also accompanied by a smaller drop in emission for $[Ru(bpy)_3]^{2+}$. This decrease in intensity for the non-binding $[Ru(bpy)_3]^{2+}$ could be attributed to slight background absorption from the cage, which filters out some incident light. However, the much more prominent quenching seen for **MAC** is consistent with it binding within the cavity of $\mathbf{H^W}$. Normalisation against the intensity of the non-binding $[Ru(bpy)_3]^{2+}$ component allows the filtering effect of $\mathbf{H^W}$ to be accounted for, allowing a binding constant for **MAC** to be calculated for this system from the data acquired. The *K* value for **MAC** obtained from this data is calculated to be 3.5×10^4 M^{-1}, which agrees well with the value of 3.0×10^4 M^{-1} calculated for **MAC** alone with $\mathbf{H^W}$ when $[Ru(bpy)_3]^{2+}$ was not also present during the titration.

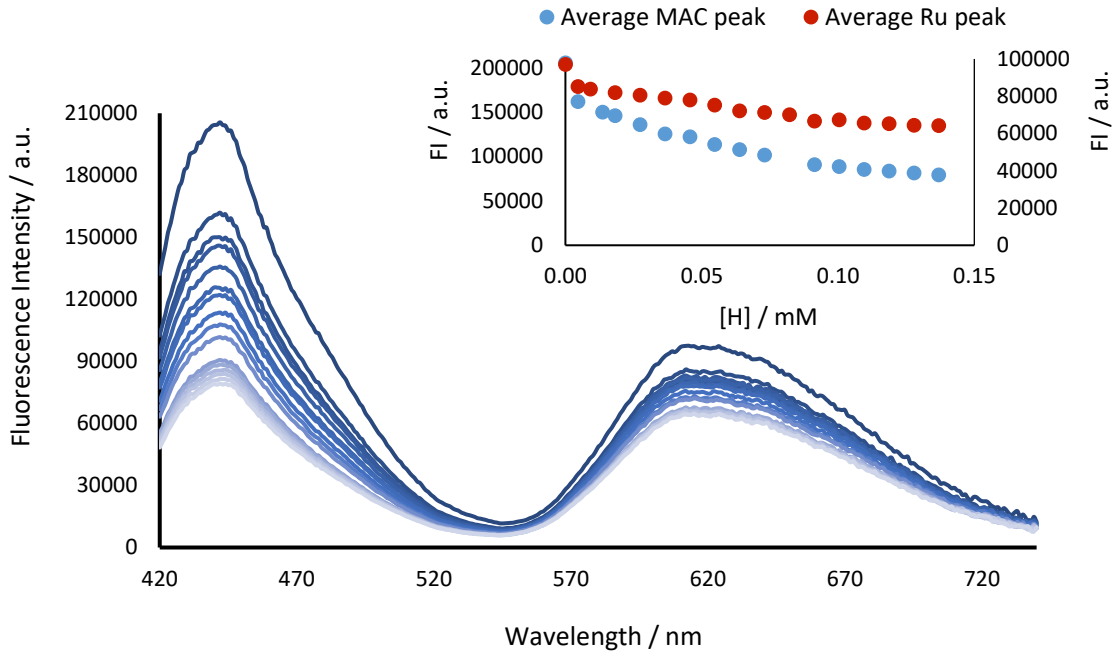

Figure 4.11 – Quenching of a MAC/$[Ru(bpy)_3]^{2+}$ solution by H^W with inset signal curves for 445 and 620 nm. [MAC] = 10 µM, $[Ru(bpy)_3^{2+}]$ = 50 µM. λ_{ex} = 395 nm.

At this point it was seen that the **MAC** / $[Ru(bpy)_3]^{2+}$ combination showed promise as a ratiometric sensor for guest binding. To investigate whether the ratio of the peaks for **MAC** and $[Ru(bpy)_3]^{2+}$ changed upon addition of a competing guest, a titration was performed using the cyclic aliphatic ketones cycloundecanone (C_{11}) and *trans*-1-decalone (T1D), whose binding constants are known from previous work.[5] Cycloundecanone has a high binding constant (10^6 M^{-1}) and will therefore displace **MAC** even at the low concentrations used for these experiments.

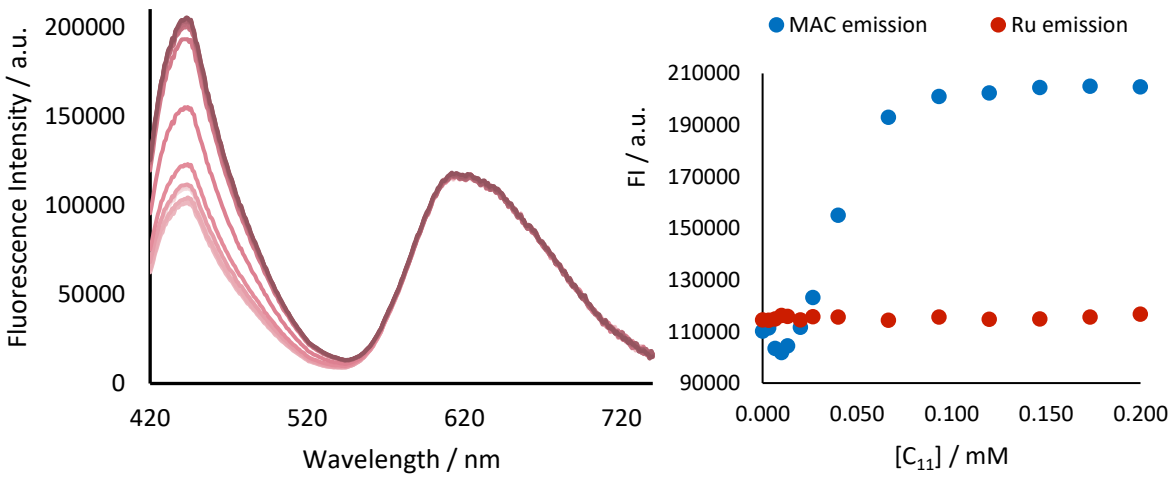

Figure 4.12 – Displacement titration data using cycloundecanone as the competing guest. A binding constant was not retrievable from this data. [MAC] = 10 µM, $[Ru(bpy)_3^{2+}]$ = 50 µM, $[H^W]$ = 0.13 mM.

The data for this experiment involving cycloundecanone is presented in Figure 4.12. As the inset signal curve for the titration clearly shows, the emission for **MAC** is restored upon increasing the concentration of C_{11} in solution whilst the emission of $[Ru(bpy)_3]^{2+}$ remains constant throughout, as expected. The shape of the fluorescence response curve for **MAC** shows a small dip in emission for the first few points before it rises sharply to its maximum emissive intensity. This initial dip is not consistently seen and may be an experimental artefact. A binding constant for C_{11} was not calculated from this data due to the unusual shape of the curve, but the overall result itself was positive – as C_{11} is added it acts as a competing guest and clearly alters the response for the blue part of the spectrum by displacing bound **MAC** whilst not affecting the red emission of the $[Ru(bpy)_3]^{2+}$ component. Overall, a clearly visible change in colour should result from this change in balance between two emission colours.

Trans-1-decalone (T1D) was also used for a displacement titration to confirm that this system displayed a similar response to other cavity-bound guests. The response was similar for T1D, with the emission of **MAC** increasing upon addition of the competing guest whilst the emission from $[Ru(bpy)_3]^{2+}$ remained essentially constant. A *K* value for T1D binding was calculated to be 3.3 x 10^4 M^{-1} from this data (lit. value 9.5 x 10^3 M^{-1}).

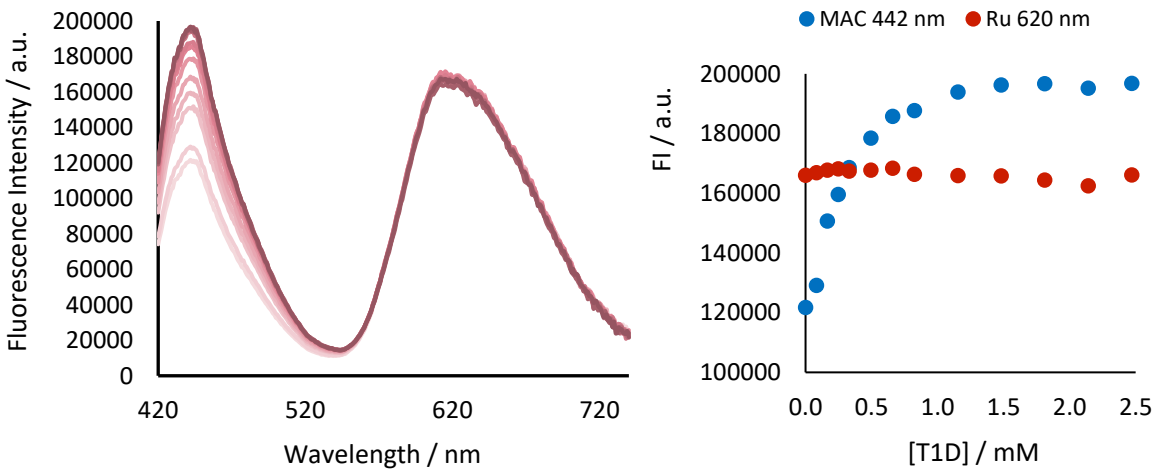

Figure 4.13 – Displacement titration data using trans-1-decalone as the competing guest. *K* was calculated to be 3.45 x10^4 M^{-1}. [MAC] = 10 µM, $[Ru(bpy)_3]^{2+}$ = 50 µM, $[H^W]$ = 0.13 mM.

Perhaps the most important aspect of these titrations is the observable colour change upon addition of the analyte (competing guest). With a focus on the overall colour of the sensor system, the start and end spectra of the titration were converted to (x,y) coordinates to plot on the CIE chart. This provides a useful visual indication of the sensor response and shows the progressive colour change from the red part of the spectrum towards the blue as more **MAC** is displaced by added cycloundecanone. The line drawn between start and end point if extrapolated forwards and backwards to the edges of the gamut reach the coordinates for pure **MAC** and $[Ru(bpy)_3]^{2+}$ emission. Any given mixture of these two components will give a point along that line, shown in Figure 4.14 as a dashed grey line.

The points shown in Figure 4.14 highlight the issue encountered when using the **MAC** / $[Ru(bpy)_3]^{2+}$ combination as the basis for a two-colour ratiometric sensor. Although the two 'pure' colours of the components are very different, the distance between the start and end points of the titration on the CIE chart – which can be termed the 'dynamic range' of the sensor system and depends on the change in balance of the two components – is small, meaning that the change in colour will likewise be small. Fortunately, the human eye is very sensitive to small changes in colour so these two points can be seen as two distinctly different shades of purple. The photograph shown in Figure 4.15 is of the sensor before and after addition of *trans*-1-decalone as described above, with the change in hue towards blue being apparent.

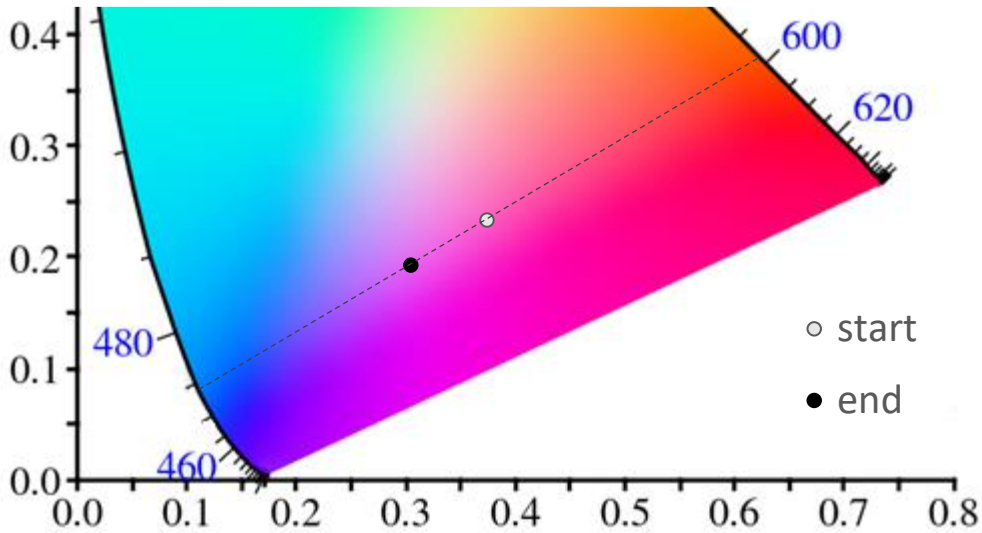

Figure 4.14 – The start and end spectra of the titration using trans-1-decalone converted to CIE coordinates. A clear shift towards the blue region of the colour space can be seen as MAC is displaced by the incoming guest.

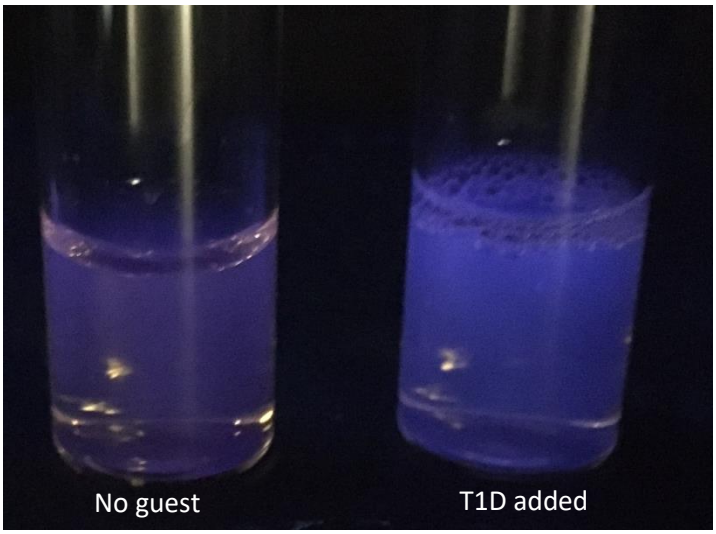

Figure 4.15 – comparison of samples before and after guest addition under a UV lamp. The right-hand sample displays a more noticeable blue colouration compared to the left-hand sample, which is also duller in appearance.

4.2.6. FLU/$[Ru(bpy)_3]^{2+}$ system

Having shown that the combination of **MAC** and $[Ru(bpy)_3]^{2+}$ was able to produce a colourimetric change in response to guest binding, the same process was tested using a combination of fluorescein (**FLU**) and $[Ru(bpy)_3]^{2+}$ as the two reporter components but using anionic guests to displace bound **FLU** from the cage surface to produce the desired colour change. The combination of **FLU** (green emission) and $[Ru(bpy)_3]^{2+}$ (red emission) will generate an orange colour prior to any analyte being added. This colour will steadily change to yellow as the green component of the sensor is increased by displacement of bound **FLU** by an anion such as chloride (see results in Chapter 3).

The quenching of the **FLU** / $[Ru(bpy)_3]^{2+}$ combination upon addition of $\mathbf{H^W}$ is shown in Figure 4.16. With **FLU** possessing a high binding constant to $\mathbf{H^W}$ of 1.0 x 10^5 M^{-1}, the quenching is rapid and does not require much $\mathbf{H^W}$ to bind the **FLU** and reach a low emission intensity. This contrasts with **MAC**, whose weaker binding constant necessitated use of around 15 equivalents of $\mathbf{H^W}$ for the displacement assay under the conditions used. Normalising the data against the $[Ru(bpy)_3]^{2+}$ emission, to account for the slight decrease in emission over the course of the titration arising from a slight filtering effect from the added $\mathbf{H^W}$, allows the steady quenching of **FLU** upon cage binding to be seen clearly.

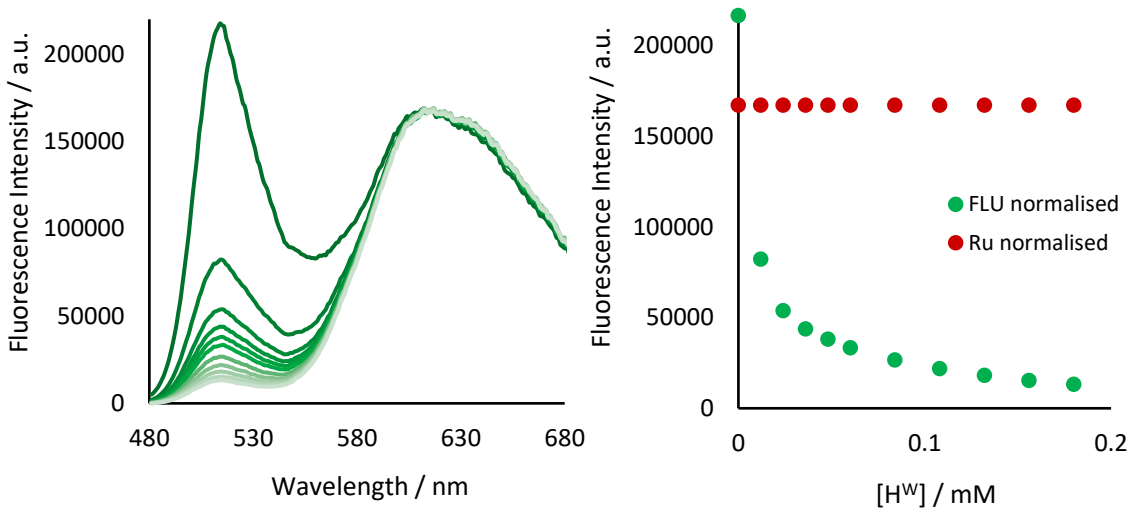

Figure 4.16 – quenching of fluorescein in a FLU/$[Ru(bpy)_3]^{2+}$ system. (Emission spectra are normalised against the relatively invariant Ru-based emission component). [FLU] = 10 µM, $[Ru(bpy)_3]^{2+}$ = 50 µM, 50 mM pH 8.5 borate buffer.

The next step was to attempt displacement of the bound **FLU** with an added anion. The data presented in Figure 4.17 shows the result of a displacement using chloride as the guest competing with **FLU** for the exterior surface of the cage. Instances of cages with chloride as the counter-anion have been reported by the Ward group previously,[15] and chloride binds with reasonable affinity, with a 1:1 anion:face (of $\mathbf{H^W}$) *K* value of 7.5 x 10^2 M^{-1} (see Section 3.2.1).

As the concentration of chloride is increased, the **FLU** emission at 515 nm grows as the **FLU** is displaced by competition from the incoming chloride, whilst the peak for $[Ru(bpy)_3]^{2+}$ remains relatively unchanged. By the end of the titration, the peak due to **FLU** emission has a higher intensity than that of $[Ru(bpy)_3]^{2+}$. This change in the intensity ratio between the two components is the basis of the colour change necessary to detect analyte binding.

As in the previous example, the emissive intensity of $[Ru(bpy)_3]^{2+}$ fluctuates slightly during this experiment, but the spectra have been normalised against the $[Ru(bpy)_3]^{2+}$ emission component so that the relative change of **FLU** emission compared to this is clear. Regarding the colour seen at the start and end of the titration, an obvious shift from orange to yellow is observable, as the green (**FLU**) component of the spectrum is increased as it is displaced by the increasing

concentration of chloride. The more obvious colour change compared to the **MAC** / $[Ru(bpy)_3]^{2+}$ system is due to a greater change of fluorescence intensity by **FLU** when it is displaced (Fig. 4.17 shows an approximately 4-fold increase in **FLU** intensity during the titration, compared to only a 1.7-fold increase for **MAC** emission in Fig. 4.13). This means that the difference in start and end ratio between the two peaks in the emission spectrum is greater which should give a greater dynamic range for this sensor system.

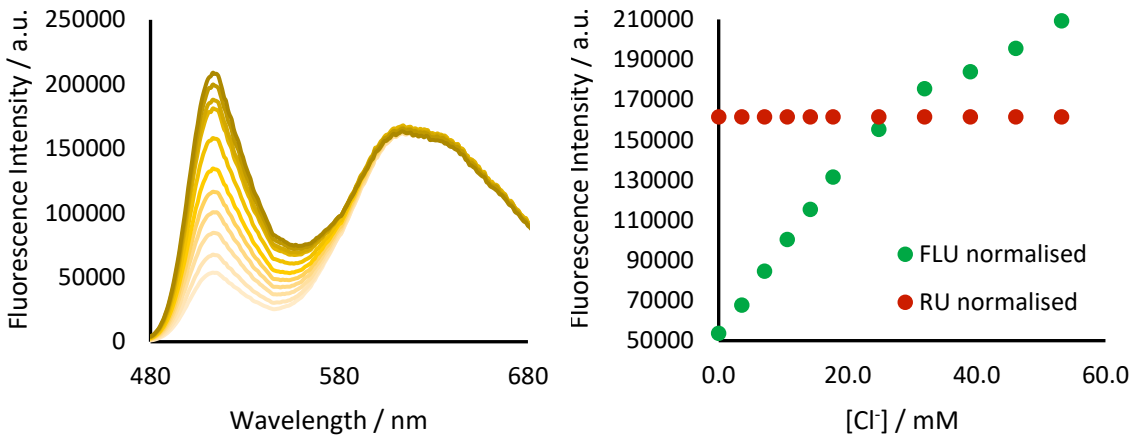

Figure 4.17 – displacement of bound FLU in a FLU/$[Ru(bpy)_3]^{2+}$ system. The emission for FLU increases dramatically with little change to the $[Ru(bpy)_3]^{2+}$ emission. [FLU] = 10 µM, $[Ru(bpy)_3^{2+}]$ = 50 µM, $[H^W]$ = 0.1 mM, 50 mM pH 8.5 borate buffer.

The **FLU** / $[Ru(bpy)_3]^{2+}$ sensor also possesses the ability to distinguish between weakly and strongly binding anions. Using both fluoride and nitrate up to a concentration of 25 mM, the **FLU**-based emission reached through displacement using nitrate was over double that achieved using fluoride. This difference arises naturally from nitrate being a stronger binder (*cf.* Chapter 3) and is significant enough to drastically change the final emission colour, as shown by the final coordinates on the CIE chart.

Figure 4.18 below shows the two emission spectra (converted to (x,y) coordinates on the CIE chart) after 25 mM of anion was added to the $\mathbf{H^W}$/**FLU**/$[Ru(bpy)_3]^{2+}$ sensor system. The final point for NO_3^- is clearly much further along the line between pure $[Ru(bpy)_3]^{2+}$ and pure fluorescein emission, indicative of a higher proportion of **FLU** being displaced by the more strongly binding anion. The difference in binding constants of an order of magnitude (2.5×10^2 *vs.* 3.1×10^3 M^{-1} for F^- and NO_3^-

respectively) gives substantially different end results for the colourimetric changes caused by the anion.

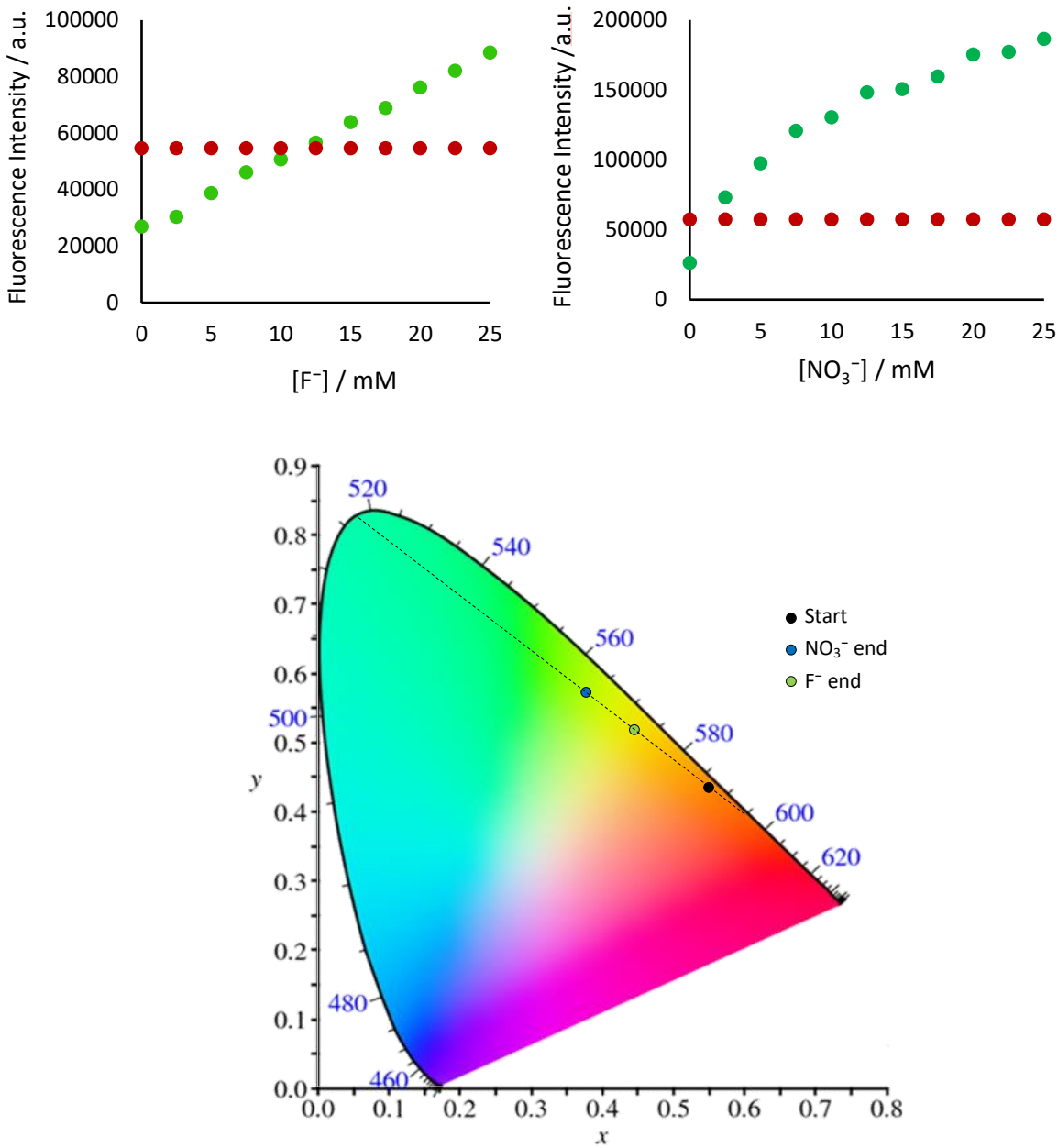

Figure 4.18 – displacement of FLU using two anions of differing affinity for the cage, F^- and NO_3^-. The endpoint of each titration varies as the amount of displaced FLU changes for each anion used. [FLU] = 5 µM, $[Ru(bpy)_3]^{2+}$ = 30 µM, $[H^W]$ = 50 µM, 50 mM pH 8.5 borate buffer.

4.2.7. MAC/FLU system: simultaneous displacement of cavity-bound and surface-bound indicators

Having demonstrated that both **MAC**/$[Ru(bpy)_3]^{2+}$ and **FLU**/$[Ru(bpy)_3]^{2+}$ sensors produce a colourimetric response for the detection of guest binding through different interactions with the host cage, it was hypothesised that use of **MAC** and **FLU** in combination would provide a means of determining whether a guest bound inside or outside of the cage. As these fluorophores are displaced by orthogonal binding mechanisms, a sensor containing both **MAC** and **FLU** should provide a different response depending on which binding mode the analyte uses.

The first step for using two fluorophores bound to the cage was a titration to study the quenching of **MAC** and **FLU** by $\mathbf{H^W}$ when used in combination. For this test a ratio of 5:1 **MAC**:**FLU** was chosen as this gave comparable emission intensity for the two peaks in preliminary tests. $\mathbf{H^W}$ was titrated into a solution of **MAC** and **FLU** in this ratio, producing a decrease in fluorescence of both components.

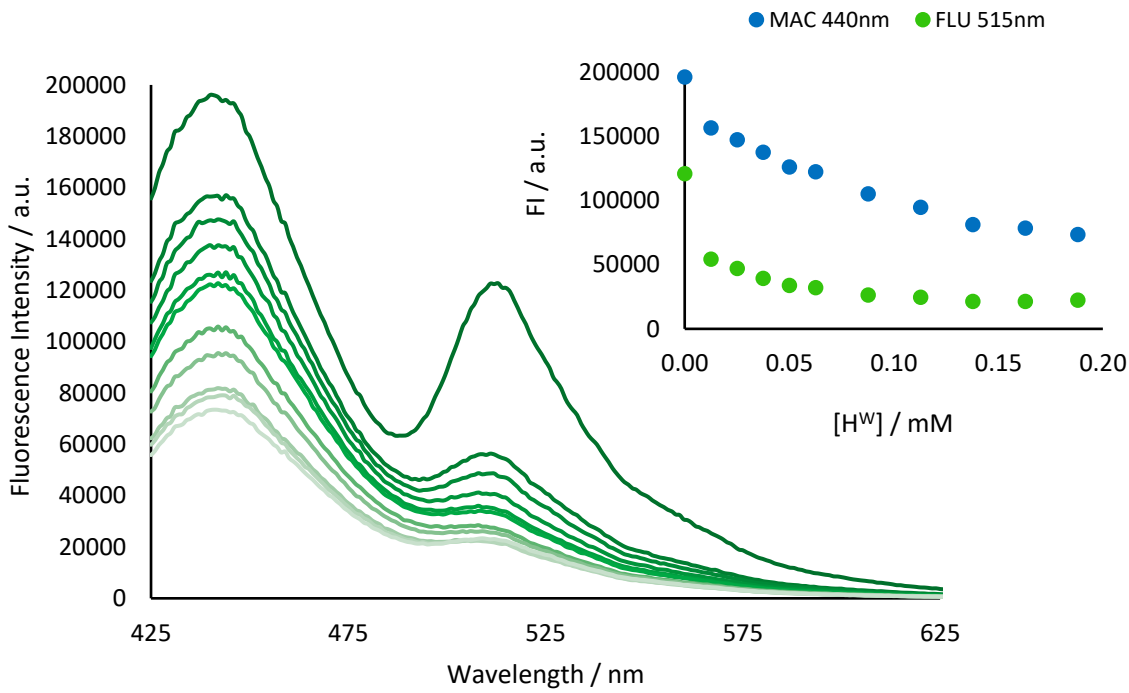

Figure 4.19 – quenching of a combination of MAC/FLU by H^W. A reasonable reduction in fluorescence intensity is seen for both fluorophores. [MAC] = 10 µM, [FLU] = 2 µM, 50 mM pH 8.5 borate buffer.

For displacement tests, the ratio of **MAC**:**FLU** was altered from 5:1 to 1:1 to increase the green component of the fluorescence response. An addition of 0.15 mM of $\mathbf{H^W}$ was sufficient to greatly reduce the emission of both fluorophores by partial uptake of the fluorophores by the cage cavity or surface for **MAC** or **FLU**, respectively.

The first set of displacements tested involved cycloundecanone (C_{11}) and chloride as the neutral and anionic (respectively) analytes being added. The reasoning behind this was that C_{11} has been proven to cavity bind with very high affinity (K = 1.2 x 10^6 M^{-1}) whilst Cl^- has been shown to bind to the cage's exterior in recent studies (Chapters 2 and 3). Using both of these should result in different colour responses being seen: a shift towards blue with C_{11} (which should displace **MAC**) and a shift towards green with Cl^- (which should displace **FLU**).

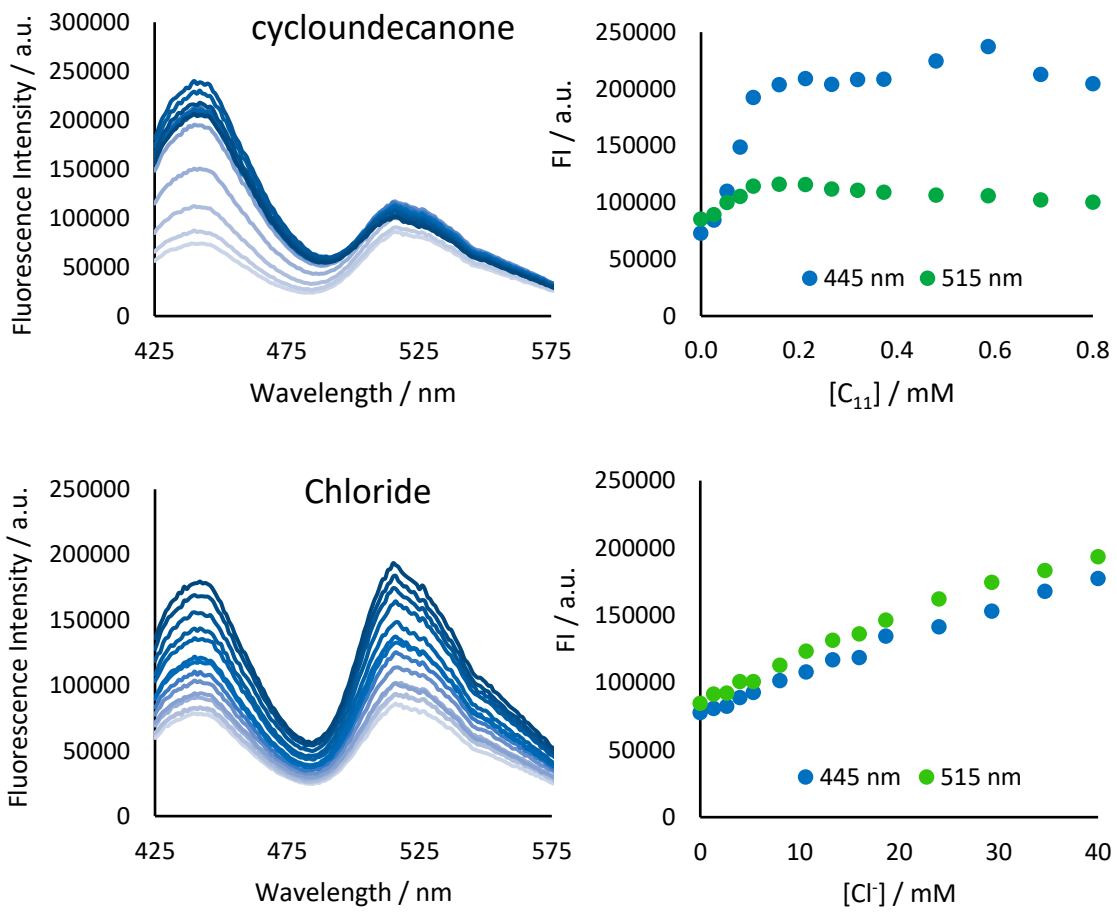

Figure 4.20 – Addition of Cl^- and C_{11} to a H^W/MAC/FLU system. [H^W] = 0.15 mM, [MAC] = 10 µM, [FLU] = 10 µM, 50 mM pH 8.5 borate buffer.

The two analytes caused differing responses from the sensor system, with C_{11} providing a clear increase in the blue emission component of the system, as predicted. Chloride however resulted in an increase in fluorescence for *both* **MAC** and **FLU**, leading to no distinct shift in colour balance towards either blue or green. This was an unexpected result as evidence previously had always pointed towards anions interacting with the cage's exterior, generally (in the solid state) sitting in the 'windows' on each face of the cube. Logically, however, there is no reason why anions would not be able to enter the cage's cavity – chloride ions are small enough to fit through the 4 Å diameter portals and given a large enough excess may end up binding inside the cavity as well as on the cage's surface. Chloride salts of the cage $\mathbf{H^A}$ (described in Chapter 2) have returned lower binding constants than the cage $\mathbf{H^W}$ for the same guests, suggesting that the chloride can cavity-bind and compete with the incoming guest, reducing the other guest's binding constant.

To confirm whether the displacement of **MAC** from the cage cavity by chloride was really occurring, in the absence of any possible complicating factors, an experiment was performed using only **MAC** as the bound fluorophore alongside $\mathbf{H^W}$. Titrating in chloride up to 100 mM resulted in displacement of bound **MAC** with a signal curve like those seen for small cavity-binding organic guests. Fitting this data using a displacement macro to extract a binding constant for chloride gave a value of 2.9 x 10^2 M^{-1}, the same order of magnitude as the value for surface binding determined

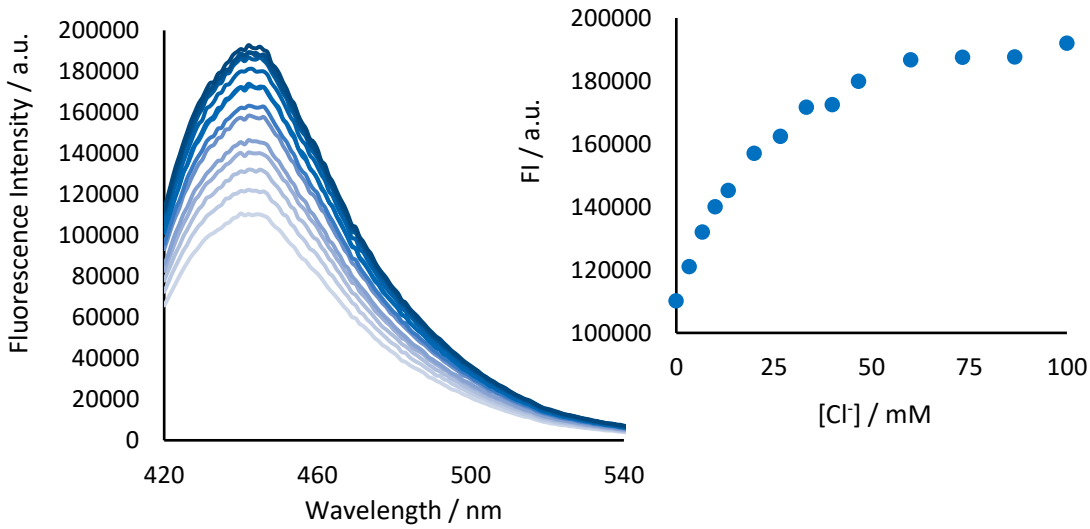

Figure 4.21 – displacement of bound MAC using chloride as the competing guest. This titration focuses solely on cavity-binding and proves that chloride can occupy space within the cage's cavity, displacing MAC in the process. [H^W] = 0.15 mM, [MAC] = 10 mM.

using the fluorescein-based assay. Clearly, chloride ions have the capacity to bind in the cage cavity as well as at the surface sites, albeit fairly weakly.

The **MAC**/**FLU** sensor system had accordingly demonstrated its suitability for determining binding modes of analytes. Chloride had been considered a surface-only guest but testing this with the combination of **MAC** and **FLU** inadvertently proved that both binding mechanisms were in action. Moving forward, bulkier anions were tested using the sensor in an attempt to find a species that would bind to the exterior only (and displace **FLU** only) without also displacing any bound **MAC** from within the cavity.

Having worked with numerous anions using the **FLU**/**H^{W}** system for a separate body of work (Chapter 3), several candidates were identified from this list. To encourage surface binding over cavity binding, bulkier organic anions such as tartrate and ascorbate were favoured. Requirements for these anions were a large size to discourage cavity binding along with hydrophilicity to avoid precipitation of the system upon association. Bulky hydrophobic anions such as tetraphenylborate would result in rapid precipitation of the cage from aqueous solution and so were discounted.

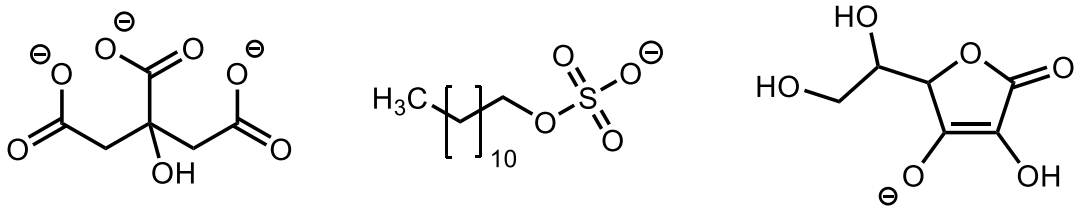

Figure 4.22 – three guests chosen to test for surface-only binding by using the MAC/FLU combination-based sensor.

The first test involved three anions that were larger than all those previously tested. These were trisodium citrate (TSC), sodium dodecyl sulfate (SDS) and sodium ascorbate (Asc). Unfortunately, both TSC and SDS induced precipitation of **H^{W}** upon mixing. Sodium ascorbate, however, produced a notable increase in emission intensity for **FLU** without an increase for **MAC**, indicative of surface-only binding.

Fitting the data for this titration to a 1:1 binding isotherm returns a *K* value for ascorbate of 1.3 x 10^4 M^{-1}.

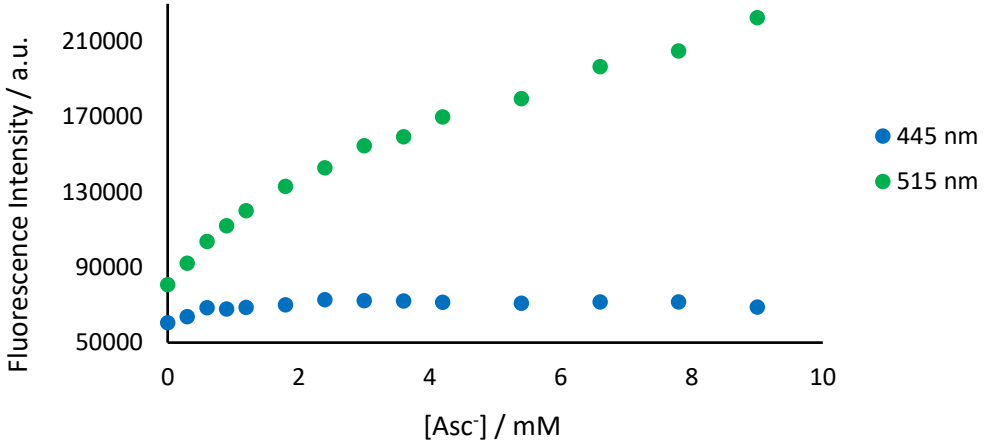

Figure 4.23 – selective displacement of FLU using the guest ascorbate. An increase for the peak at 515 nm is seen whereas the peak at 445 nm remains largely consistent. [MAC] = 10 µM, [FLU] = 20 µM, [H^W] = 0.12 mM, 50 mM pH 8.5 borate buffer.

This increase for the green (**FLU**) emission component only – indicating surface binding but no cavity binding – was the goal for this titration and ascorbate provided this result, with only a very small increase in intensity seen for **MAC**; the predominant colour change observed was for displaced **FLU**, showing that the desired selectivity was achieved. Experiments to follow this result were conceived with the goal being different responses for cavity-bound species and surface-bound species. Comparison of the two guests *trans*-1-decalone and sodium ascorbate demonstrated that differing colour responses for these different methods of binding was possible (Figure 4.24).

To summarise this section, some results obtained using **MAC** and **FLU** in tandem were encouraging. Alongside the displacement of solely **FLU** using sodium ascorbate, displacement of **MAC** selectively was achieved first using C_{11} in the test alongside chloride, and subsequently using *trans*-1-decalone, another cyclic ketone. These results indicate that a parallel analysis of surface-bonding and cavity-binding guests should be possible with this sensor system.

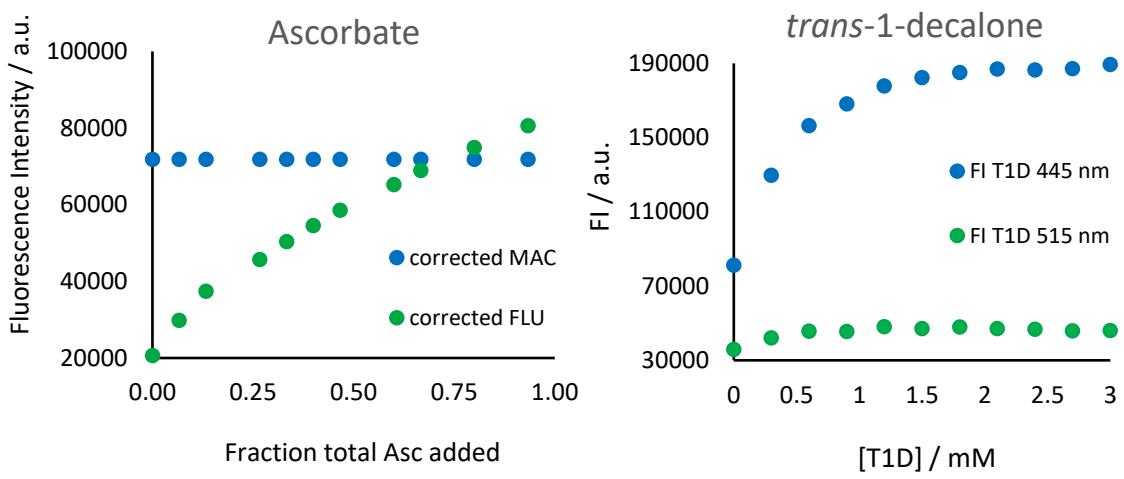

Figure 4.24 – Comparison of the H^W/MAC/FLU sensor output when the analytes sodium ascorbate and *trans*-1-decalone were added. [H^W] = 0.13 mM, [MAC] = 10 µM, [FLU] = 10 µM, 50 mM pH 8.5 borate buffer.

4.2.8. MAC/FLU/$[Ru(bpy)_3]^{2+}$ system (three component RGB sensor)

To extend the scope of the previous sensor system, $[Ru(bpy)_3]^{2+}$ was reintroduced in the same capacity as previous instances, this time alongside the combination of **MAC** and **FLU** to give a three-colour, RGB system. The logic behind adding $[Ru(bpy)_3]^{2+}$ to the already complicated mixture was straightforward; with no analyte present the sensor would appear blue under a hand-held UV lamp. This meant that the analytes that displaced **MAC** were difficult to distinguish as the change in colour was minimal. By changing the starting colour to include a red component courtesy of the $[Ru(bpy)_3]^{2+}$ emission, the starting point on the CIE chart became more central between blue and red. An increase in either the blue or green emission component would shift this point enough to allow the mode of binding to be distinguished visually.

This can be demonstrated in the following set of results. Using three analytes with proven different binding modes – C_8 (cavity binding), Asc^- (surface binding) and Cl^- (combination of both) – three different responses were obtained from the sensor, visible through the direction of movement on the CIE chart between the start and end of the titration.

The cavity-bound cyclooctanone shifts the CIE emission point towards the lower left region of the chart as a result of the displacement of **MAC** only (increase in the blue component). Ascorbate provides a shift directly towards the green region owing to its selective displacement of **FLU**. Chloride displays both effects and as a result shifts largely towards the upper region of the chart but with some lateral movement towards the blue edge of the graph owing to the displaced **MAC**. This dataset provides us with a visual representation of how the three different modes of binding for guest molecules to the cage $\mathbf{H^W}$ can be distinguished using this sensor. A goal of this project was to be able to distinguish analytes using only a UV lamp and the human eye. The samples photographed in Figure 4.25 are those discussed above. The three samples are indeed distinct and can be distinguished based on their appearance.

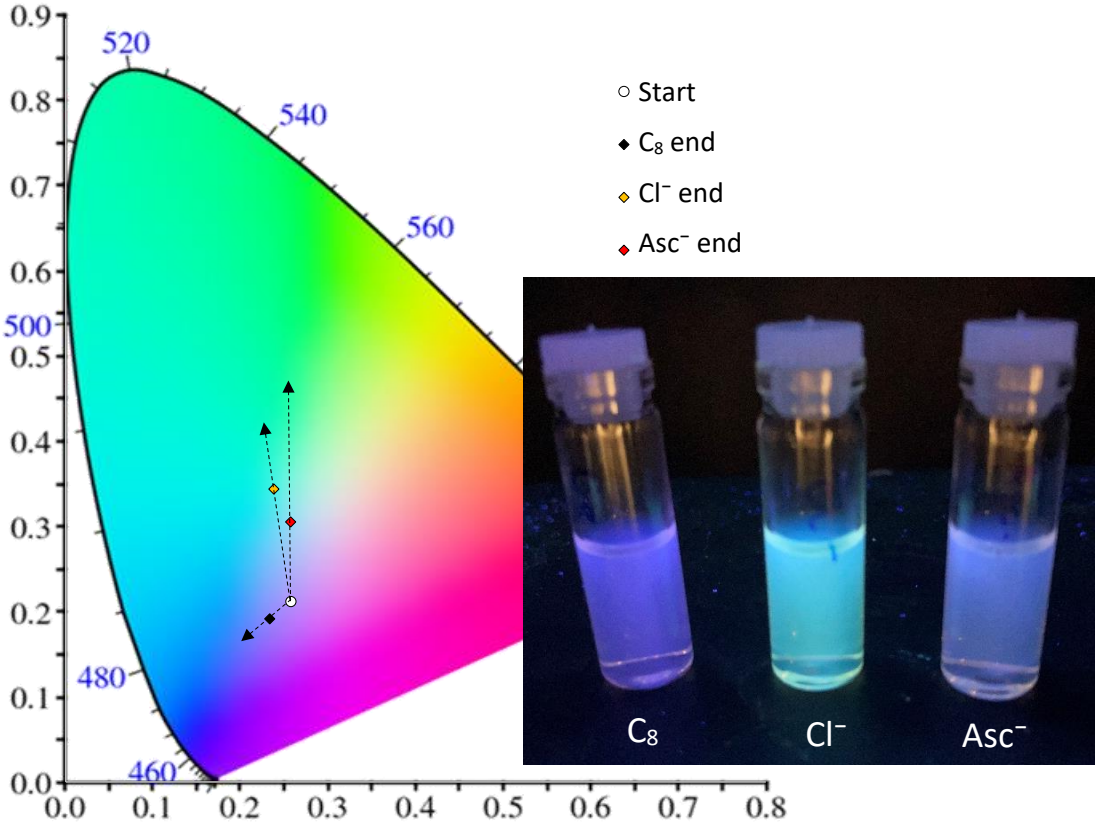

Figure 4.25 – Start and end coordinates for each of the three analytes tested alongside the direction of movement for each point. Inset photo: the three samples after addition of the labelled analyte. [MAC] = 10 µM, [FLU] = 20 µM, $[Ru(bpy)_3^{2+}]$ = 30 µM, $[H^W]$ = 0.15 mM, 50 mM pH 8.5 borate buffer.

Whilst the results presented in Figure 4.25 clearly show the samples are distinct in appearance and can be distinguished by the direction of movement between the start and end of the titration on the CIE chart, there is a discrepancy between the excitation wavelength used on the fluorimeter and the UV lamp used when obtaining images of the samples. The UV lamp when set to long-wave emission emits at 365 nm whilst the sensor was being excited at a wavelength of 395 nm. To counter this discrepancy, the images were obtained with use of a LED-fitted UV torch that emits at 395 nm, purchased online. The introduction of this lamp greatly alters the appearance of the samples when tested. The predominantly blue hue seen for all three samples is no longer apparent, since the excitation wavelength has moved away from the peak for **MAC** towards the peak for both **FLU** and $[Ru(bpy)_3]^{2+}$, resulting in the red and green components increasing at the detriment of the blue component.

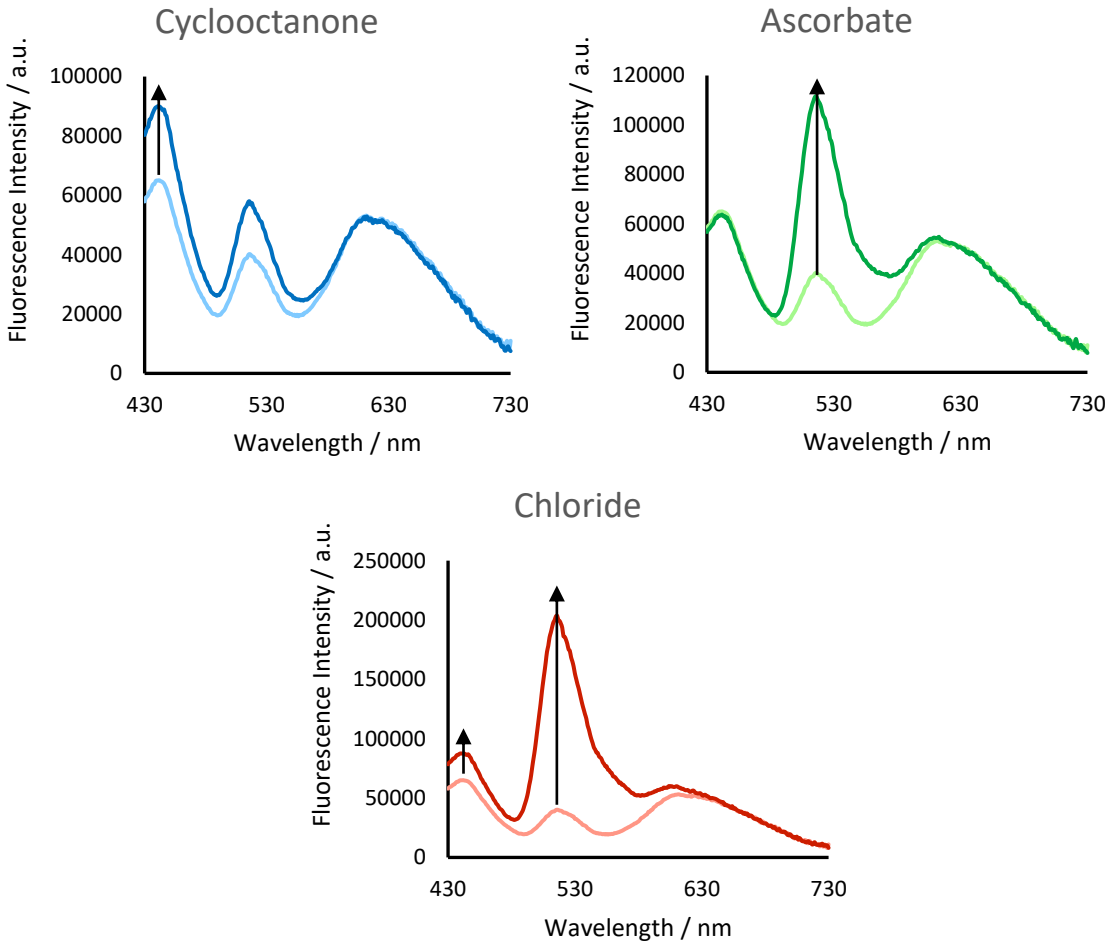

Figure 4.26 – Fluorescence spectra before and after addition of cyclooctanone, ascorbate and chloride to the sensor containing MAC/FLU/$[Ru(bpy)_3]^{2+}$ and H^W. [MAC] = 10 µM, [FLU] = 20 µM, $[Ru(bpy)_3^{2+}]$ = 30 µM, $[H^W]$ = 0.1 mM, 50 mM pH 8.5 borate buffer.

The three samples can again be plotted on the CIE chart showing the movement in coordinates after addition of the analyte. The responses are different for each sample: (predominantly) **MAC** displacement for cyclooctanone, selective **FLU** displacement for ascorbate and both **MAC** and **FLU** displaced by chloride. Figure 4.26 shows the resulting luminescence spectra for each of these experiments.

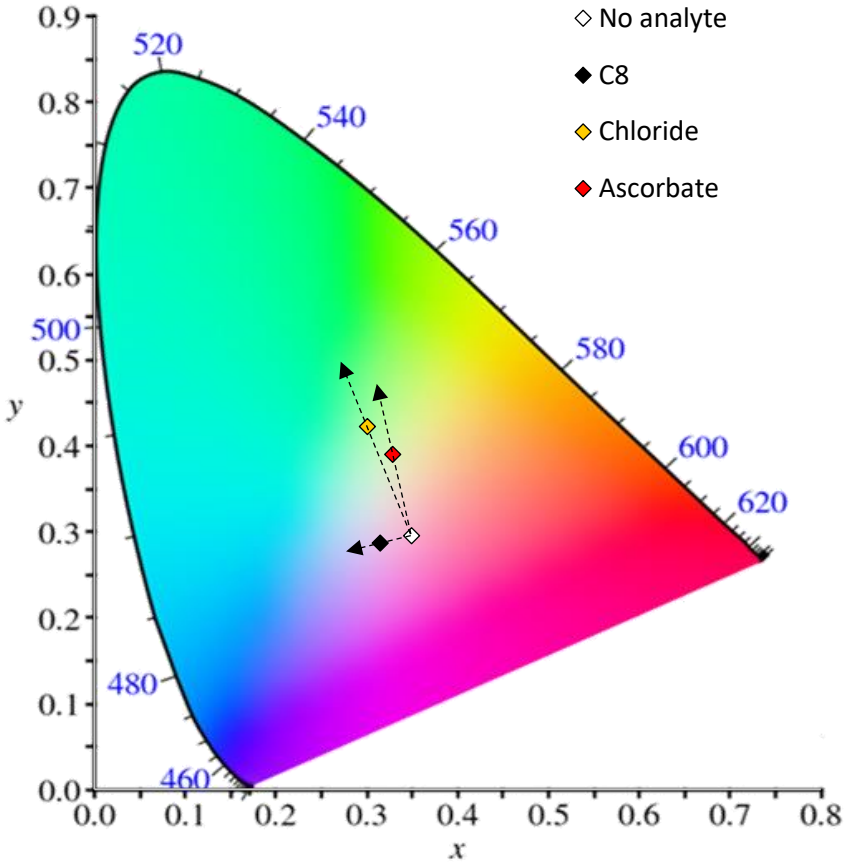

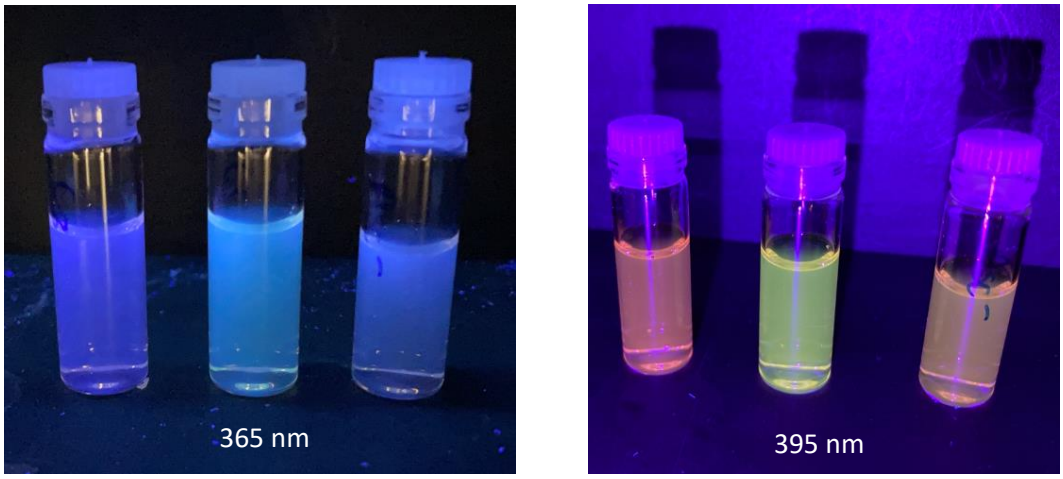

Figure 4.27 – Analyte additions using 395 nm excitation and the samples as seen using a handheld UV lamp emitting at 395 nm. [MAC] = 10 µM, [FLU] = 20 µM, $[Ru(bpy)_3^{2+}]$ = 30 µM, $[H^W]$ = 0.15 mM, 50 mM pH 8.5 borate buffer.

The effect of changing the excitation wavelength to 395 nm can be seen in Figure 4.27, along with the samples seen under UV light. As with the previous experiment using C_8, ascorbate, and chloride as the analytes, the coordinates for before and after addition of the analyte for the three samples move in different directions on the CIE chart, this time from a different starting point. This is because changing the excitation wavelength results in a different starting combination of the RGB emission components.

4.2.9. MAC in conjunction with other surface-bound fluorophores

Having utilised the combination of **MAC** and **FLU** to distinguish between cavity and surface-binding analytes, some of the other surface-binding fluorophores were considered as alternatives to **FLU**. One observation made during titrations involving **MAC** and the cage was that the buffered version of the cage at pH 8.5 seemed to hinder binding of **MAC**, possibly due to the additional hydroxide that would be accumulated around the cage's exterior and possibly in the cavity *cf.* the unexpected behaviour of chloride. In an attempt to alleviate this problem, anionic fluorophores that did not require the solution to be buffered were investigated.

The molecule chosen to be most suitable for testing was sulforhodamine B (abbreviated to **SRB**). **SRB** is similar in structure to **FLU** and its derivatives, and so should behave in the same manner in the presence of the cage. The overall charge on **SRB** (-1) is less than that of **FLU**, due to a quaternary nitrogen atom contributing a positive charge which cancels the negative charge from one of the two sulfonate

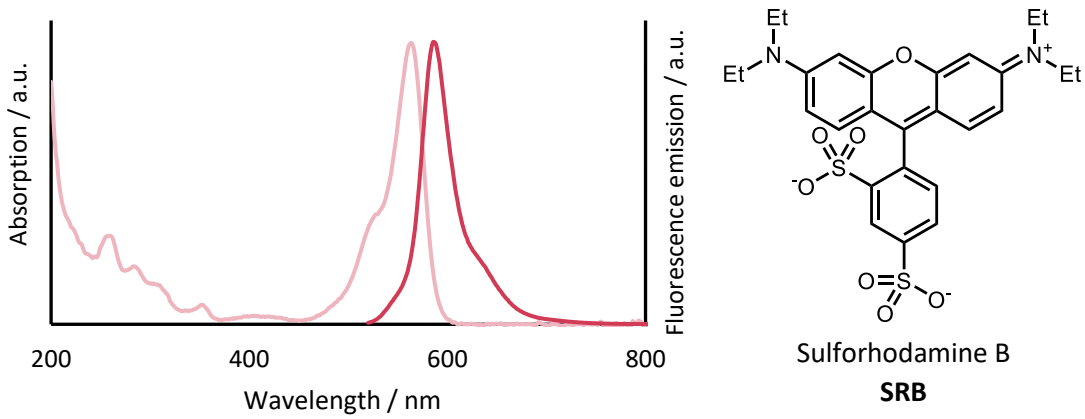

Figure 4.28 – absorption and emission spectra for sulforhodamine B, pictured on the right.

groups. The two sulfonate groups are within close proximity to each other, being located on the separate phenyl ring of the molecule, and **SRB** is expected to bind to the cationic cage surface through this terminus.

Quenching of **SRB** by **H^W** was tested using the same method as for other fluorophores described previously. Sequential additions of **H^W** to a solution of **SRB** resulted in a sharp decrease in fluorescence intensity which was fitted to a binding isotherm using the same Excel-based macro described previously. This returned a *K* value of 1.0 x 10^5 M^{-1}, the same as for **FLU** reported in Chapter 3. The signal curve for the titration was indeed similar in appearance to that of **FLU**, but the minimum emission reached for **SRB** was much higher – quenching of **FLU** by **H^W** results in an 80% reduction in emission compared to only 66% for **SRB**, indicative of less efficient quenching of **SRB** by the cage.

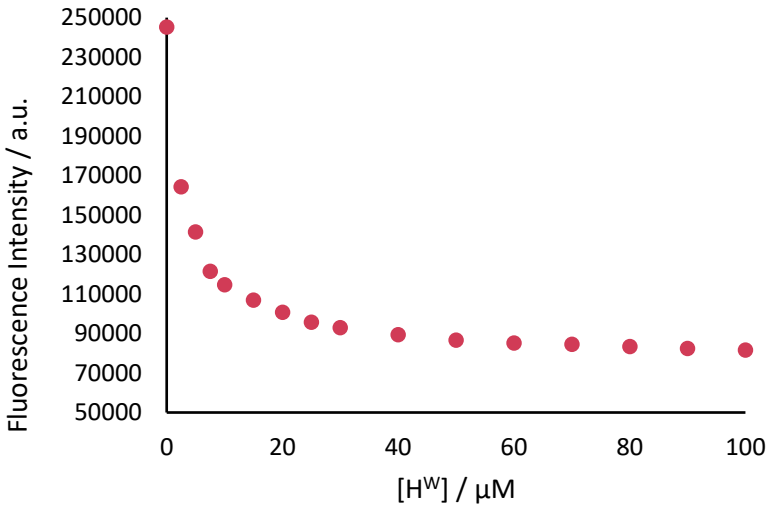

Figure 4.29 – quenching of SRB fluorescence by addition of portions of H^W, points taken from peak emission at 590 nm. [SRB] = 20 µM.

The principal issue affecting the use of **SRB** in an assay is whether displacement of the bound fluorophore is possible using competing analytes such as chloride. To examine this, two displacement experiments were performed using **H^W/SRB** and chloride and sulfate as the competing surface-bound guests. The results of these displacements are shown in Figure 4.30.

Both anions produced reasonable results. An increase in fluorescence was observable for both chloride and sulfate, with a higher final emissive intensity

achieved by sulfate, consistent with results reported in Chapter 3 regarding sulfate's higher binding constant with **FLU** used as the fluorophore being displaced. However, the dynamic range in both experiments is poor relative to **FLU**, with an increase of only 2x the starting emission for chloride and 2.4x for sulfate, which may limit the ability of **SRB** displacement by an analyte to induce a colourimetric response compared to **FLU**.

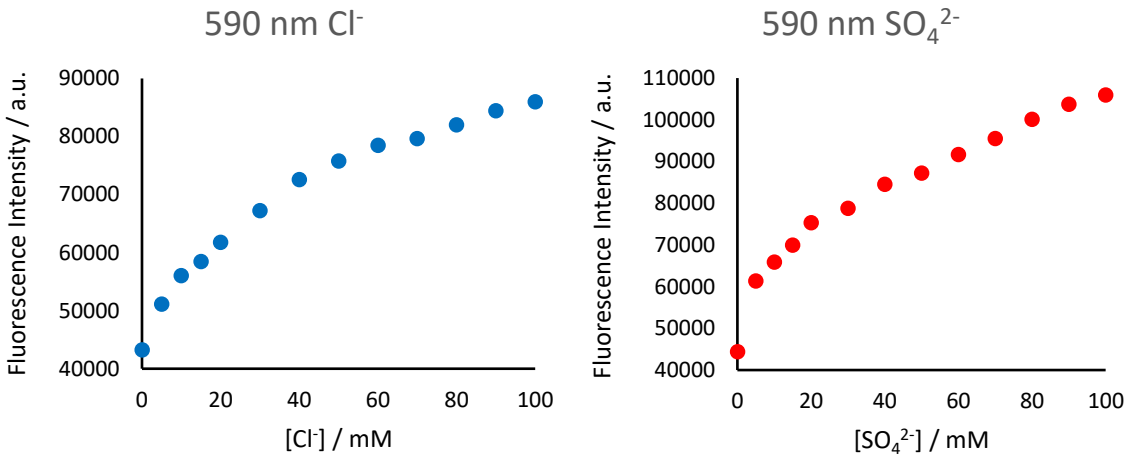

Figure 4.30 – displacement of SRB bound to H^W using chloride and sulfate in a similar manner to the fluorescein displacement assay described in Chapter 3. [SRB] = 10 µM [H^W] = 0.1 mM.

Quenching of **MAC** (blue emission) and **SRB** (red emission) in tandem was tested next. With both molecules at a concentration of 10 µM, addition of $\mathbf{H^W}$ resulted in partial quenching of both fluorophores, with **SRB** quenching reaching a minimum after around 50 µM of $\mathbf{H^W}$ had been added. **MAC**, which binds more weakly, was not fully quenched even after the addition of 0.15 mM of $\mathbf{H^W}$ though the degree of quenching of **MAC** was still significant.

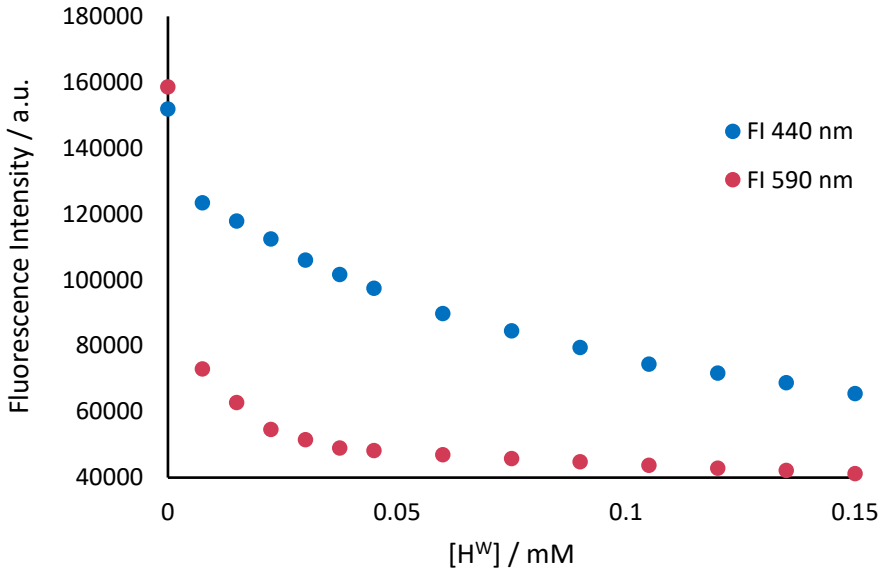

Figure 4.31 – quenching of a MAC/SRB combination by H^W. [MAC] = 10 µM, [SRB] = 10 µM.

Before complicating the system further by adding a third (non-binding) fluorophore to impart some green colour to the solution, displacement experiments using this **MAC/SRB** combination were performed. It was hoped that the selectivity seen for the **MAC/FLU** pair would be replicable, and using the three analytes C_8, Cl^- and Asc^- would produce three different luminescence responses.

Some of the results from the displacements were positive, notably those for C_8 and Cl^-. Using cyclooctanone, an increase for the fluorescence intensity at 440 nm was seen without an increase at 590 nm, suggesting that it was only **MAC** that had been displaced, as expected. With chloride, both the peak at 440 nm and the peak at 590 nm increased in emission, pointing towards both **MAC** and **SRB** being displaced by chloride – this also agreed with previous observations.

Ascorbate, the final analyte tested, sadly did not give such pleasing results. Rather than selectively displacing **SRB** as it did with **FLU** previously, a decrease in emission intensity was seen for *both* **MAC** and **SRB**. The reasons behind this are not clear: we would not expect the surface-binding anion Asc^- to displace bound **MAC** from within the cavity, as the experiments involving **FLU** as the second fluorophore have shown.

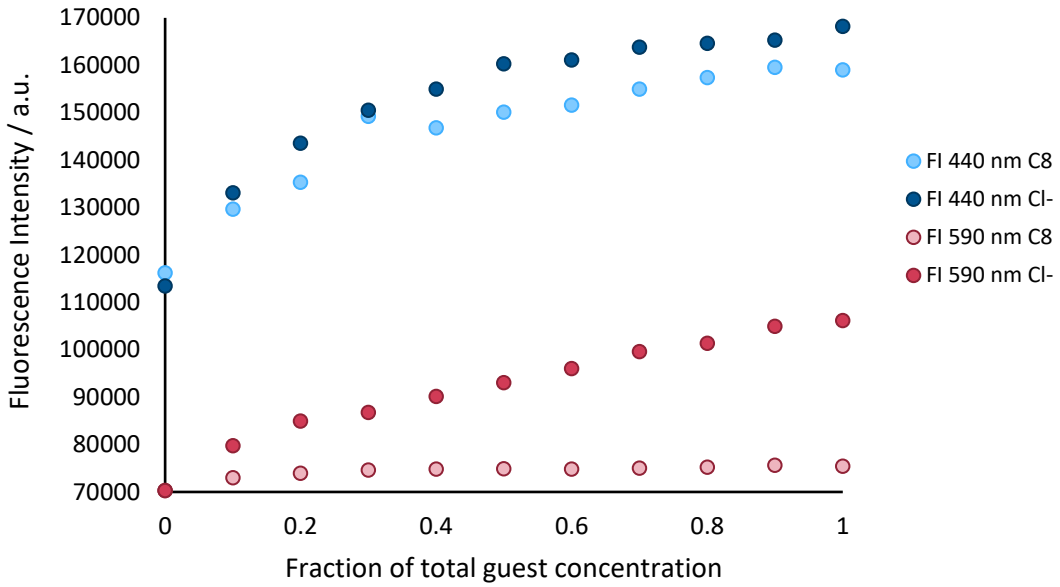

Figure 4.32 – restoration of fluorescence of MAC/SRB using C_8 and Cl^- as the competing guests. The results obtained in this experiment agree with those seen using fluorescein as the surface-bound fluorophore in previous experiments. [MAC] = 10 µM, [SRB] = 10 µM, [H^W] = 0.1 mM.

However, the lack of increase for **SRB** emission suggests this combination of fluorophores does not function the same as **MAC/FLU** did previously. This precluded further testing with this sensor system, as – along with the lack of compatibility with surface-only guests – there was another issue, which is that the colour of the sensor under UV light did not change to the naked eye. When working on this project, one of the goals set was for the sensor to produce a response to different types of guest binding that is detectable to the naked eye under a UV lamp. Using **MAC/SRB** as the displaceable fluorophores did not achieve this target.

4.3. Conclusions

In this chapter, three different variations of a colourimetric sensor based around the coordination cage **H^W** have been discussed. The fluorophores 4-methyl-7-amino coumarin (**MAC**) and fluorescein (**FLU**) interact with **H^W** through uptake into the cage's cavity and adherence to the surface, respectively. This interaction results in quenching of the fluorescence produced by these molecules. Using one or both of these fluorophores in conjunction with a 'bystander' complex – $[Ru(bpy)_3]^{2+}$, which

provided a fixed red emission component – allows for a change in colour to be seen upon displacement of the bound fluorophore. The colour change arises from the varying ratio between either the blue or green emissive peak and the constant red peak provided by the ruthenium complex, which does not interact with the cage system.

The first sensor, using **MAC**/$[Ru(bpy)_3]^{2+}$, allows for distinction between a sample containing a cavity-bound analyte such as the cyclic ketones reported to bind within the cavity of $\mathbf{H^W}$. This is provided by a shift in colour towards the blue region of the CIE chart as **MAC** is displaced.

The second sensor uses a **FLU**/$[Ru(bpy)_3]^{2+}$ pair and can produce a colourimetric response to surface-binding analytes such as common anions (Cl^-, SO_4^{2-} etc). This sensor can also distinguish between anions of differing binding affinity *e.g.*, F^- and NO_3^- at the same concentration.

The third sensor incorporates both **MAC** and **FLU** as the binding components and $[Ru(bpy)_3]^{2+}$ to impart a red component to the colour of the sensor before an analyte is added. This sensor can distinguish between cavity- and surface-bound analytes, giving a different response and therefore a different resulting colour for either mode of binding. Some analytes such as chloride were found to displace both **MAC** and **FLU**, whereas other analytes were found that displaced **MAC** or **FLU** selectively.

Overall, the ability of cages to bind (and have displaced) fluorophores in the cavity and at the surface; and the ability for analyte guests to bind either in the cavity or on the surface; provides two different modes of 'reporting' which can be used independently of one another or in combination – providing a new type of versatile colorimetric sensor suitable for a range of analyte types.

4.4. Experimental

4.4.1. Materials and Methods

The fluorescent species 4-methyl-7-amino coumarin, fluorescein, 1-hydroxypyrene and sulforhodamine B were purchased from Acros Organics or Merck Life Sciences and used as received. Ruthenium tris-2,2'-bipyridyl dichloride salt hexahydrate was purchased from Merck Life Sciences and used as received. Fluorescence measurements were carried out using either a BMG ClarioStar plate reader with 96-well plates, or an Agilent Cary Eclipse fluorimeter. UV/vis spectra were obtained using an Implen C40 Nanophotometer. pH adjustments were performed using a Hanna Instruments HI2210 pH meter fitted with a Hamilton SpinTrode probe.

4.4.2. Synthesis of cage H^W

H^W was prepared as described in section 2.4.3.7. For the majority of experiments detailed within this chapter (any involving fluorescein), the cage was adjusted to pH 8 before use. This was achieved through incremental addition of NaOH solution (1M) until the desired pH was reached.

4.4.3. Synthesis of 4-nitro-7-*N*-methylaminobenzofurazan

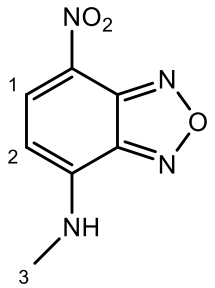

4-nitro-7-chlorobenzofurazan (0.5 g, 2.51 mmol) was dissolved in 100 mL of acetonitrile. To this solution, 1.4 g (15 mmol, 3 eq.) of methylamine (33% by weight, in EtOH) was added and the reaction mixture stirred at room temperature for 1 h. The solution changed colour from yellow to an opaque dark brown. The solvent was removed under reduced pressure, affording a dark red crystalline solid. The product was purified using column chromatography on silica eluted with 40:60 ethyl acetate:hexane, giving a bright orange solid. This powder was dried further *in vacuo*. Afforded 0.196 g, 40% yield.

^{1}H NMR (400 MHz, CD_3OD): δ 8.58 (d, 1H, *J* = 8.4 Hz, H_1), 6.31 (d, 1H, *J* = 8 Hz, H_2), 3.18 (s, 3H, NH-CH_3).

ESI-MS m/z (%): 411.1 (100) $[2M+Na]^+$, 217.1 (10) $[M+Na]^+$

4.4.4. Quenching of fluorophores by H^W

An example titration: 5 mL of a dilute solution (10 µM) of MAC was prepared from a stock solution of MAC of known concentration. Separately, 4 mL of a solution of MAC·H^W was prepared by mixing MAC stock solution with a preprepared sample of H^W and deionised water to make the final concentrations 10 µM and 200 µM for MAC and H^W, respectively. These solutions were then mixed in varying ratios to a volume of 300 µL so as to increase the concentration of cage from one well to the next. These titrations used between 12 and 18 wells per experiment, and a minimum of two repeats was carried out for each titration. The instrument was equilibrated to 298 K for these measurements.

4.4.5. Displacement of bound MAC by competing guests

Displacement titrations were performed using two solutions: one containing MAC and H^W, and the other containing MAC, H^W and the chosen analyte. These were prepared by first making a solution of MAC and H^W at double the desired concentration, which was then split into two vials. One was diluted 1:1 with deionised water whilst the other was diluted with a premade analyte solution such that the concentrations of MAC and H^W were consistent in both solutions (typically 10 µM and 150 µM). This method ensured that the analyte was fully dissolved, and an accurate concentration was known as this was required for calculation of a binding constant, *K*. These solutions were then mixed in varying ratios to a volume of 300 µL so as to increase the concentration of analyte from one well to the next. These titrations used between 12 and 18 wells per experiment, and a minimum of two repeats was carried out for each titration. The instrument was equilibrated to 298 K for these measurements.

4.4.6. Displacement experiments using RGB components

In a similar manner to the experiments detailed in Section 4.4.5, experiments involving $[Ru(bpy)_3]^{2+}$ and FLU alongside MAC were carried out through preparation of a solution containing all four components (MAC, FLU, $[Ru(bpy)_3]^{2+}$ and H^W) at double the desired concentration. Typical component concentrations were 10 µM MAC, 10 µM FLU, 30 µM $[Ru(bpy)_3]^{2+}$ and 150 µM H^W. This sample included borate buffer at pH 8.5, usually at a concentration of 50 mM. This was then split into two samples and diluted 1:1 using deionised water for one sample, and a solution of the analyte under investigation for the other sample. These solutions were then mixed in varying ratios to a volume of 200 µL to increase the concentration of analyte from one well to the next. These titrations used between 11 and 14 wells per experiment, and a minimum of two repeats was carried out for each titration. The instrument was heated to 308 K for 20 minutes before equilibrating at 298 K for all samples.

4.5. References

1 B. T. Nguyen and E. V. Anslyn, *Coord. Chem. Rev.*, 2006, **250**, 3118–3127.

2 S. L. Wiskur, H. Ait-Haddou, J. J. Lavigne and E. V. Anslyn, *Acc. Chem. Res.*, 2001, **34**, 963–972.

3 M. M. Rhaman, F. R. Fronczek, D. R. Powell and M. A. Hossain, *Dalt. Trans.*, 2014, **43**, 4618–4621.

4 A. J. Metherell, C. Curty, A. Zaugg, S. T. Saad, G. H. Dennison and M. D. Ward, *J. Mater. Chem. C*, 2016, **4**, 9664–9668.

5 S. Turega, W. Cullen, M. Whitehead, C. A. Hunter and M. D. Ward, *J. Am. Chem. Soc.*, 2014, **136**, 8475–8483.

6 B. D. Wagner, *Molecules*, 2009, 14, 210–237.

7 N. Ben Azaza, S. Elleuch, S. Khemakhem, Y. Abid and H. Ammar, *Opt. Mater. (Amst).*, 2018, **83**, 138–144.

8 S. Turega, M. Whitehead, B. R. Hall, A. J. H. M. Meijer, C. A. Hunter and M. D.

Ward, *Inorg. Chem.*, 2013, **52**, 1122–1132.

9 W. Cullen, S. Turega, C. A. Hunter and M. D. Ward, *Chem. Sci.*, 2015, **6**, 2790–2794.

10 N. Boens, V. Leen and W. Dehaen, *Chem. Soc. Rev.*, 2012, **41**, 1130–1172.

11 A. Loudet and K. Burgess, *Chem. Rev.*, 2007, **107**, 4891–4932.

12 S. Singha, D. Kim, B. Roy, S. Sambasivan, H. Moon, A. S. Rao, J. Y. Kim, T. Joo, J. W. Park, Y. M. Rhee, T. Wang, K. H. Kim, Y. H. Shin, J. Jung and K. H. Ahn, *Chem. Sci.*, 2015, **6**, 4335–4342.

13 J. R. Piper, L. Cletheroe, C. G. P. Taylor, A. J. Metherell, J. A. Weinstein, I. V. Sazanovich and M. D. Ward, *Chem. Commun.*, 2017, **53**, 408–411.

14 J. Van Houten and R. J. Watts, *J. Am. Chem. Soc.*, 1976, **98**, 4853–4858.

15 W. Cullen, A. J. Metherell, A. B. Wragg, C. G. P. Taylor, N. H. Williams and M. D. Ward, *J. Am. Chem. Soc.*, 2018, **140**, 2821–2828.

4.6. Appendices

4.6.1. Fluorescence quenching of fluorophores by H^W

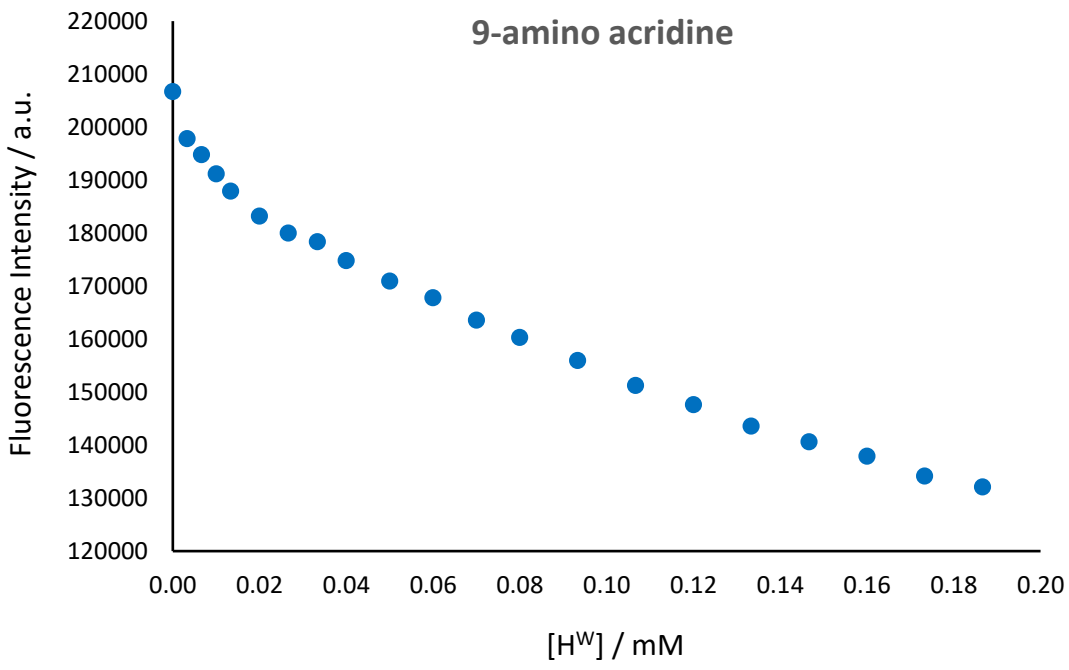

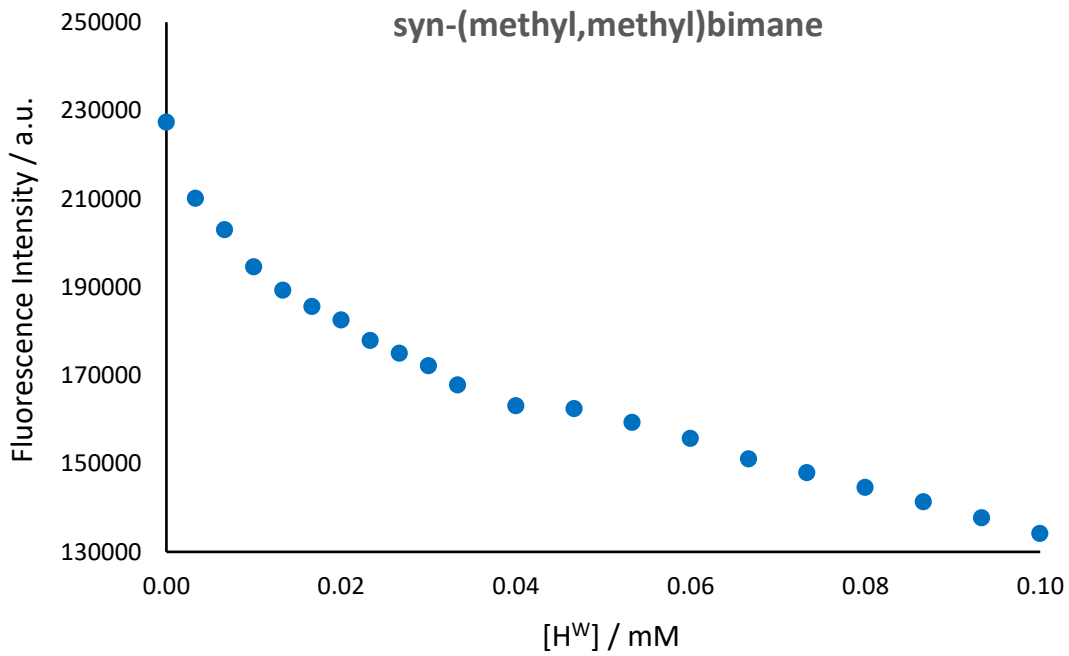

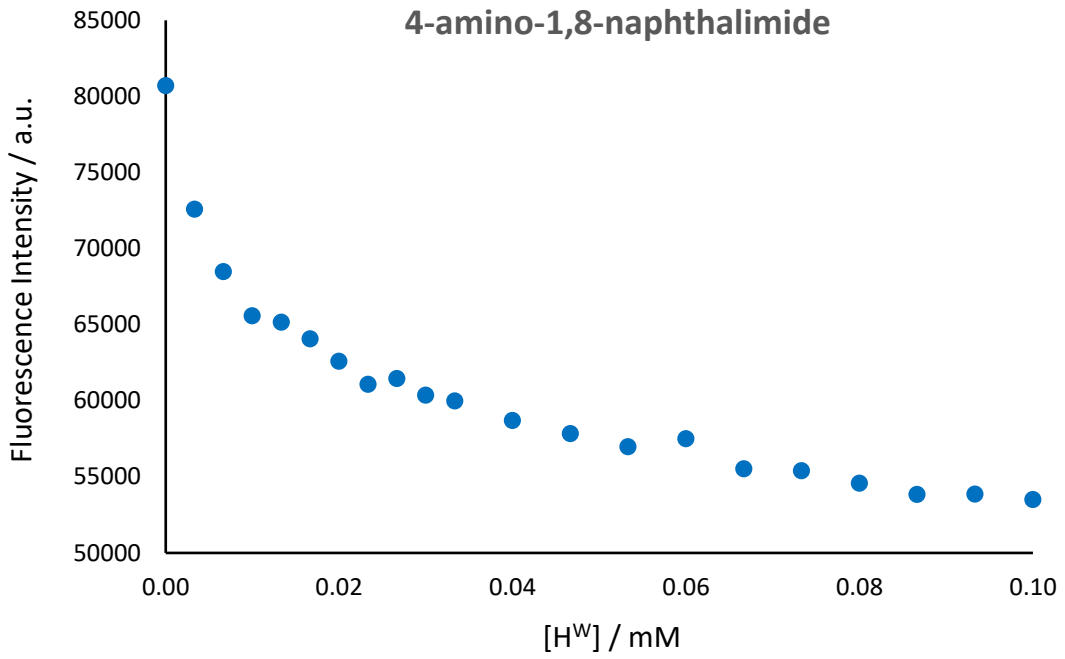
4-amino-1,8-naphthalimide
Fluorescence Intensity / a.u.
85000
80000
75000
70000
65000
60000
55000
50000
0.00
0.02
0.04
0.06
0.08
0.10
[H^W] / mM

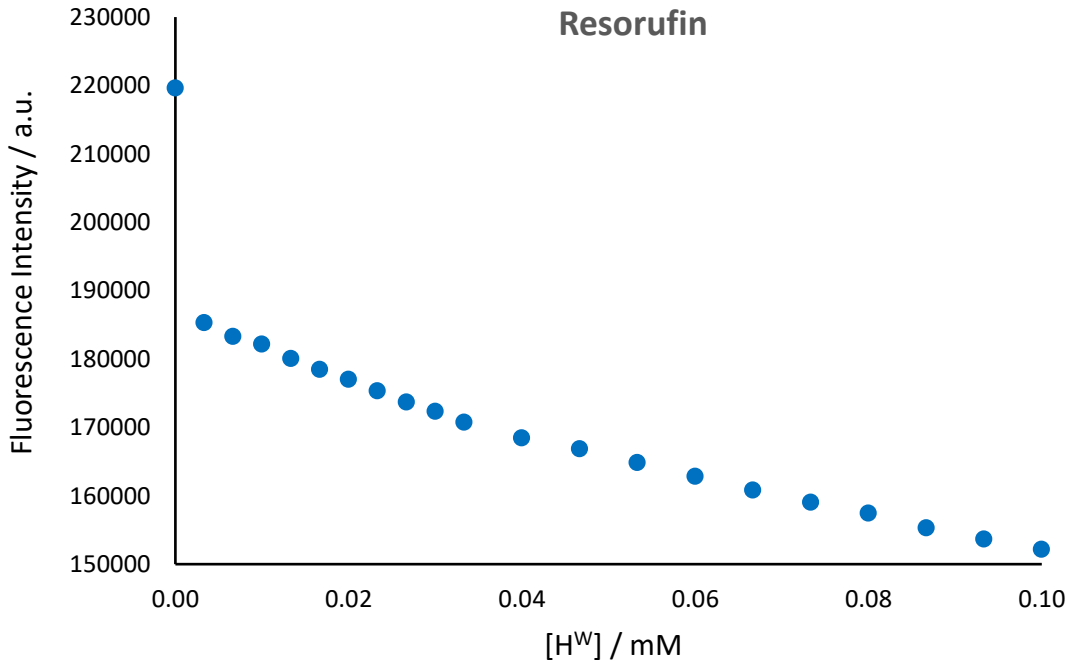
Resorufin
Fluorescence Intensity / a.u.
230000
220000
210000
200000
190000
180000
170000
160000
150000
0.00
0.02
0.04
0.06
0.08
0.10
[H^W] / mM

Chapter 5

Effects of charge: cavity- and surface-based guest binding using a Cr(III)/Co(II) mixed-metal coordination cage

5.1. Introduction

In most cases, coordination cages consist of one type of ligand and one type of metal ion. The metal ion for any homometallic self-assembling structure must be kinetically labile, allowing the metal-ligand coordinative bonds to form and also disassemble until the conformation that provides the thermodynamic minimum is reached. Whilst there are many potential choices of labile metal ion for use in synthesis of a coordination cage, each metal ion in the structure being the same type restricts the potential properties of the complex. Behaviour such as luminescence, magnetism or redox properties can be incorporated into a coordination cage if particular metal ions are used.[1,2] However, the use of some types of metal ion may not be trivial, as many of the metal ions capable of displaying such behaviours are inherently kinetically inert and therefore difficult to use in a self-assembly process. Nonetheless, many examples of complexes that have managed to incorporate 2nd/3rd row d-block metal ions can be found in the literature.

One structural motif that allows inclusion of more inert metals into a supramolecular assembly is a porphyrin ring. Sanders and co-workers demonstrated inclusion of Ru(II) or Rh(III) metal centres situated within porphyrin rings into a coordination cage also featuring two Zn(II) porphyrins connected by a biphenyl or a structurally similar linker, which acts as a template for the formation of the cage.[3]

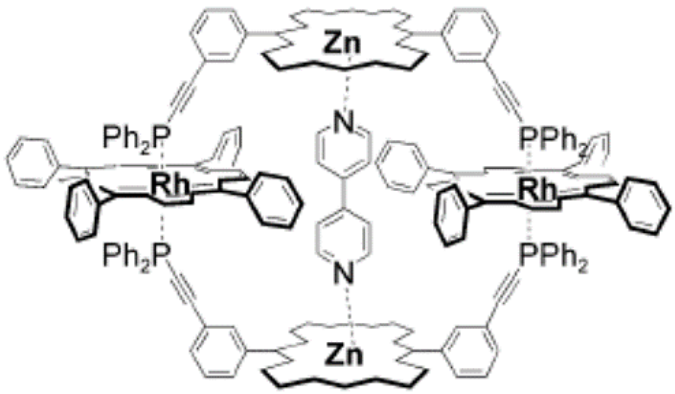

Figure 5.1 – Sanders' porphyrin-based mixed-metal coordination cage.[3]

A more recent example of a coordination cage involving 2nd/3rd row transition metals is the M_6L_4 octahedron reported by Lusby *et al.* in 2012 which consists of $[(Ir(ppy)_2Cl)_2]$ metal vertices and face-capping 1,3,5-tricyanobenzene ligands.[4] The difficulty with using this iridium subunit in a self-assembly pathway is separating the racemic starting material *rac*-$[(Ir(ppy)_2Cl)_2]$ into its enantiomers. If this separation is not done beforehand, the resulting Ir_6L_4 cage is a complex mixture of isomers. Preparatory routes to separating the enantiomers of the racemic starting material have been developed involving chromatography using D- and L-Serine.

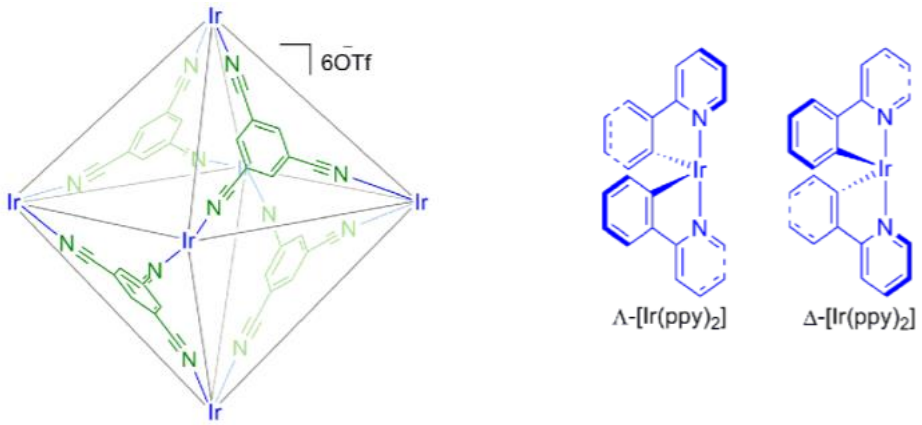

Figure 5.2 – An $[Ir_6L_4]^{6+}$ octahedron reported by Lusby *et al.* containing enantiopure $[Ir(ppy)_2]^+$ vertices.[4]

The Ward group has also previously investigated the design and formation of heterometallic cages. In 2014, a new synthetic route was described, leading to formation of a $[Ru_4Cd_4L_{12}](ClO_4)_{16}$ cubic cage with the same geometry as **H**^{A} (described in Chapter 2).[2] By reacting $RuCl_2(dmso)_4$ with L^A, a solution containing a 3:1 ratio of *mer*:*fac* isomers of $[RuL_3]^{2+}$ was produced, which coincidentally is the required ratio of isomers to form the Ru_4Cd_4 cube if the metal ions occupy alternating positions around the cage's framework. Reacting this solution of $[RuL_3]^{2+}$ with an excess of $Cd(ClO_4)_2$ such that the Cd(II) ions bind to the three pendent pyrazolyl-pyridine units of the $[RuL_3]^{2+}$ unit and crystallising the product afforded the $[Ru_4Cd_4L_{12}](ClO_4)_{16}$ cage. This method has also been used to form the isostructural $[Os_4Zn_4L_{12}](Cl)_{16}$ cage, which has been used for guest binding studies and host-mediated electron transfer.[5]

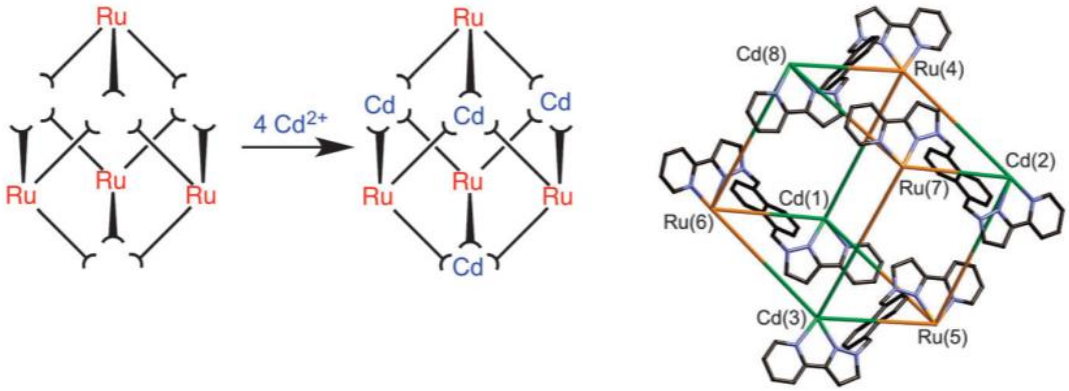

Figure 5.3 – Left: assembly of the mixed-metal $[Ru_4Cd_4L_{12}]^{16+}$ cube with alternating Ru/Cd vertices. Right: the crystal structure of the resulting complex.[2]

More recently, attention has been turned to incorporating metal ions with a higher positive charge into the cage's framework. This aims to increase the overall charge of the complex by using metal ions such as Cr(III) or Ir(III) in place of the Ru(II) vertices as shown in Figure 5.3, giving a complex with a 20+ overall charge compared to the 16+ charge for $\mathbf{H^A}/\mathbf{H^W}$. This method has been attempted by our group in the past using a combination of Os(II) and Zn(II), but with subsequent oxidation of the osmium vertices to Os(III). Difficulties were encountered using this complex, however, as the osmium ions did not retain their Os(III) state for sufficient periods of time. We wanted to investigate the effects of changing an important property of the cage without changing the overall structure and the incorporation of Cr(III) ions at four of the vertices allows this. We hypothesise that the higher charge for this complex will lead to different characteristics, such as increased binding constants for anionic guests. The work reported within this chapter introduces a new mixed-metal cage as a host with guest binding investigated by fluorescence spectroscopy.

5.2. Results and Discussion

5.2.1. Cage synthesis

As touched upon in the introduction to this chapter, the structural design of the Cr/Co cage is the same as for $\mathbf{H^W}$ used throughout the rest of this thesis, with a M_8L_{12} stoichiometry and a cubic structure. Differences of note include the higher overall charge of the complex, and the synthetic route to its formation. Whilst formation of the cage $\mathbf{H^W}$ involves synthesising the ligand in its entirety before a final step of mixing the ligand with a labile Co(II) salt which produces the cage by self-assembly, a different stepwise approach has been used in this instance, more akin to the route used for Ru/Cd and Os/Zn cages previously. The synthesis of the Cr/Co cage described in the following paragraphs was both devised and undertaken by Dr Jerico Piper.

The first step of synthesising a Cr/Co cage involved generating the Cr(III) vertices which would occupy four alternating corners of the cage's structure. These complexes have the formula $[CrL^{1,5\text{-naph}}{}_3](PF_6)_3$ but cannot be formed through simple reaction of $Cr(PF_6)_3$ with the ligand $L^{1,5\text{-naph}}$ due to the inertness of Cr(III). Instead, a precursor complex using PyPzH is produced, forming $[Cr(PyPz)_3]^{3+}$, which can then be modified further by alkylation of the pyrazole NH groups to build a ligand strand from each bound PyPz. To achieve this, an asymmetrical, monosubstituted variant of the ligand $L^{1,5\text{-naph}}$ that possesses only one chelating arm was also designed. Reaction of the $[Cr(PyPz)_3]^{3+}$ complex with the monosubstituted ligand affords the mononuclear complex $[Cr(L^{1,5\text{-naph}})_3]^{3+}$ which has three pendent binding sites. Stirring this complex with $Co(BF_4)_2$ produces the mixed-metal cage $[Cr_4Co_4(L^{1,5\text{-naph}})_{12}][PF_6]_{12}[BF_4]_8$, which will be denoted as $\mathbf{H^{Cr/Co}}$ and is the subject of the studies described hereafter. This synthetic route is pictured in Figure 5.4, overleaf.

Once the $[Cr(L^{1,5\text{-naph}})_3](PF_6)_3$ complex has been formed, this can be mixed with any labile M(II) salt to produce a mixed-metal assembly. The majority of studies within this chapter will use $\mathbf{H^{Cr/Co}}$ to exploit the quenching of fluorescence that Co(II) has demonstrated previously in other work. We have also prepared the isostructural cage $\mathbf{H^{Cr/Zn}}$ using $Zn(BF_4)_2$, which possesses contrasting properties.

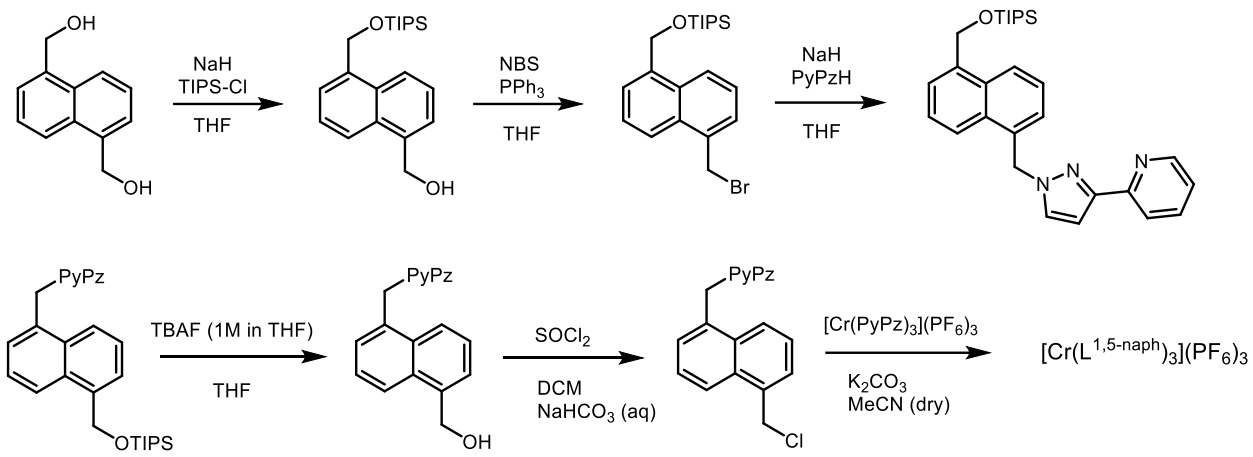

Figure 5.4 – Synthetic route to forming the Cr(III)-based vertices for the mixed-metal cage.

5.2.2. Cage characterisation

a) Mass spectrometry

The cage $\mathbf{H^{Cr/Zn}}$ was studied by mass spectrometry. Using ESI-MS in positive ion mode, we were able to detect fragments at charges of 5+, 6+ and 7+, the peaks of which are presented in the experimental (Section 5.4.2). These all corresponded to a complete $Cr_4Zn_4L_{12}$ assembly with loss of different numbers of counter-anions, confirming the formation of the mixed-metal cage.

b) ^{19}F NMR spectroscopy

A sample of $\mathbf{H^{Cr/Zn}}$ was studied by ^{19}F NMR spectroscopy in an attempt to determine the anionic content of the complex. As expected, peaks for both PF_6^- and BF_4^- anions were present in the spectrum. Integrals of the peaks were taken using deconvolution and a ratio of 3:1 BF_4^-:PF_6^- was calculated. This is not the ratio of anions that was used in the reaction to form the complex and so must correspond to the species that was precipitated out of solution and studied.

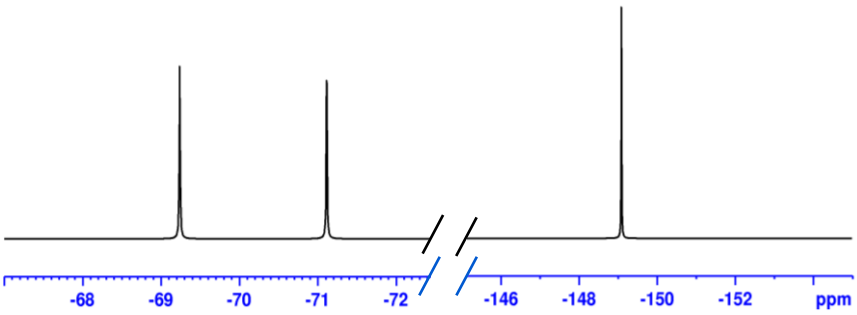

Figure 5.5 – ^{19}F NMR spectrum of $H^{Cr/Zn}$ displaying peaks for both PF_6^- (at -69.2 and -71.1 ppm) and BF_4^- (at -149.2 ppm). Recorded in CD_3CN.

c) UV/vis and fluorescence spectroscopy

The two variants of the cage produced using the procedure described in Section 5.2.1. were studied by UV/vis spectroscopy. Samples of $\mathbf{H^{Cr/Zn}}$ and $\mathbf{H^{Cr/Co}}$ were prepared in acetonitrile to compare their absorption spectra (Figure 5.6).

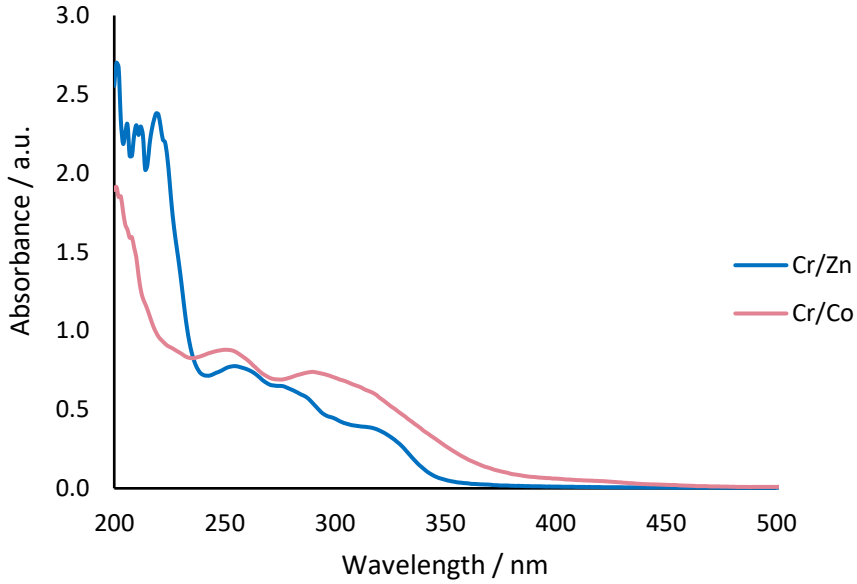

Figure 5.6 – Comparison of UV/vis absorption spectra for the Cr/Zn and Cr/Co cages, recorded in acetonitrile. These samples were diluted 50x before the spectra were obtained.

The two samples have noticeably different absorption spectra, with $\mathbf{H^{Cr/Co}}$ displaying higher absorbance to a much longer wavelength (> 400 nm) than $\mathbf{H^{Cr/Zn}}$. This is a feature of the Co(II) ions present within the assembly: MLCT transitions involving the Co(II) ions produces absorbance bands to a lower energy. The result of this is more intensely coloured solutions of $\mathbf{H^{Cr/Co}}$ compared to $\mathbf{H^{Cr/Zn}}$ when dissolved in either

acetonitrile or water. To make water-soluble analogues of the cages, stirring a suspension of cage powder in water with Dowex (chloride form) produced aqueous solutions of the cage. The UV/vis spectra of the cage $\mathbf{H^{Cr/Co}}$ in both acetonitrile and water were compared to confirm that no significant changes occurred after anion exchange (Figure 5.7).

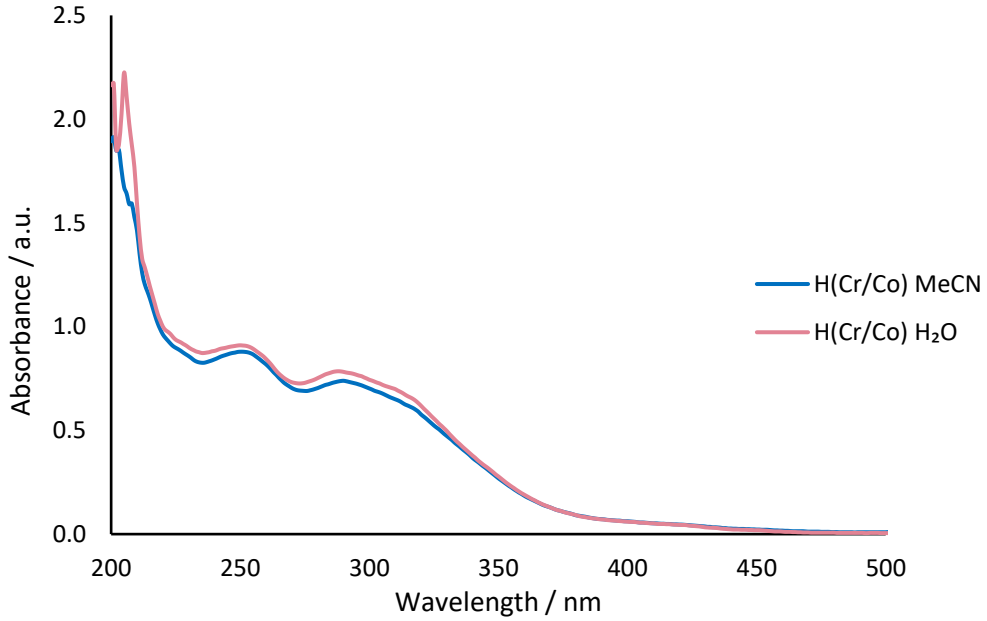

Figure 5.7 – Comparison of UV/vis spectra for $\mathbf{H^{Cr/Co}}$ in water and acetonitrile.

To allow determination of concentration for samples that were anion exchanged, an extinction coefficient measurement was performed using $\mathbf{H^{Cr/Zn}}$ in acetonitrile. The peak seen at 255 nm is common to both the Zn(II) and Co(II) versions of the mixed-metal cage and so can be used to determine a value for ε. A value of 1.89 x 10^5 M^{-1} cm^{-1} was calculated at 255 nm, and this was used to accurately determine concentrations of anion-exchanged cage solutions for experiments performed within the following sections. Full data is presented in the experimental section.

The cage $\mathbf{H^{Cr/Zn}}$ appeared to weakly fluoresce under a UV lamp, and so was tested for emission using a fluorimeter. The absorption and emission spectra for this cage are presented in Figure 5.8. This naphthalene-centred fluorescence is more blue-shifted than fluorescence observed for the homometallic cage $[Cd_8L_{12}](NO_3)_{16}$ which has a peak centred around 400 nm rather than the 340 nm of $\mathbf{H^{Cr/Zn}}$. The shift to 400 nm for the Cd(II)-based cage is attributed to extensive π-stacking arrays between

ligands.[6] This stacking is also present for $\mathbf{H^{Cr/Zn}}$, yet the fluorescence in this case appears to be more dominated by $L^{1,5\text{-naph}}$ fluorescence, with emission of the π-stacked ligands coming from naphthyl (donor) to PyPz (acceptor) charge transfer in the form of a broad excimer peak that appears as a shoulder on the emission spectrum. It is not immediately obvious why the emission appears more blue-shifted for this species compared to the isostructural Cd_8 cage.

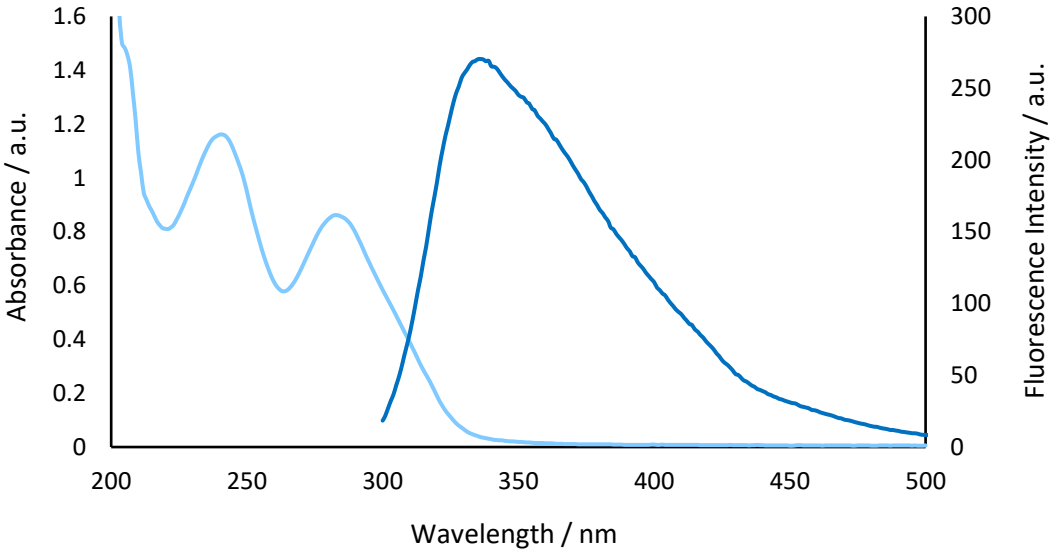

Figure 5.8 – Absorption and emission spectra for the cage $H^{Cr/Zn}$ in water after chloride exchange. λ_{ex} = 280 nm, recorded at 298 K.

5.2.3. Guest binding studies using $H^{Cr/Co}$

a) Quenching of anionic fluorophores

To investigate the host capabilities of the cage $\mathbf{H^{Cr/Co}}$, we opted to use the anionic fluorophores fluorescein (2- in basic solution) and its derivative 6-carboxyfluorescein (3-). We have demonstrated the suitability of anions such as these to act as surface-binding guests for the cage $\mathbf{H^{W}}$, as discussed within Chapter 3 of this thesis, and seek to expand our knowledge of these surface-binding interactions with this work.

To be able to work with anionic fluorophores, the studies must be conducted in aqueous media. To achieve this, Dowex chloride form anion exchange resin was used to exchange the BF_4^- and PF_6^- anions on $\mathbf{H^{Cr/Co}}$ for Cl^- anions, rendering the complex water-soluble. Pleasingly, the exchange was straightforward, with the cage sample dissolving into water after stirring with the resin for *ca.* 20 minutes.

The first experiment carried out involved quenching of fluorescein by $\mathbf{H^{Cr/Co}}$. This experiment was set-up in a similar condition to those reported in Chapter 3, using 10 µM of fluorescein (**FLU**) and in this case addition of up to 0.15 mM of $\mathbf{H^{Cr/Co}}$. The result of this experiment can be seen in Figure 5.9.

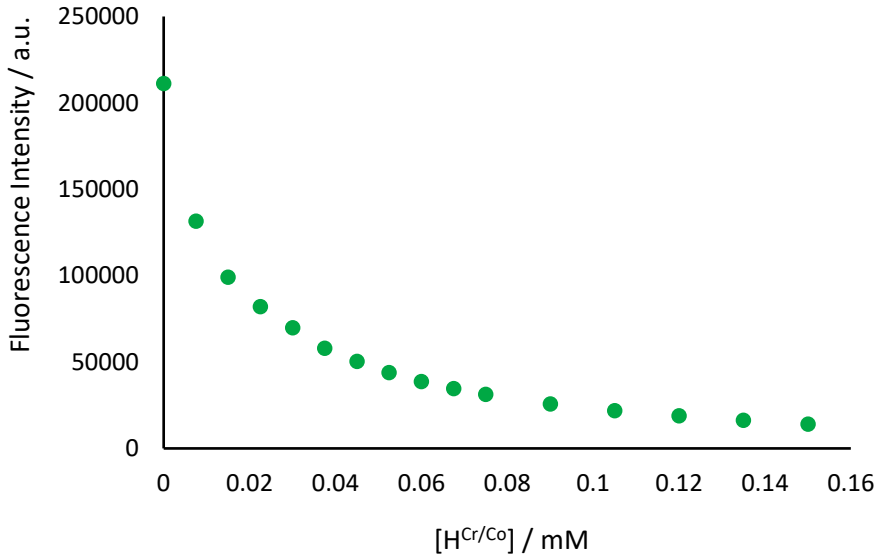

Figure 5.9 – Signal curve for the emission of FLU at 515 nm being quenched by subsequent additions of $H^{Cr/Co}$. [FLU] = 10 µM, [$H^{Cr/Co}$] = 0-150 µM, 50 mM pH 8.5 borate buffer.

As the graph above shows, there is progressive quenching of emission of **FLU** as the concentration of $\mathbf{H^{Cr/Co}}$ is increased throughout the titration. Using the concentration of available binding sites (number of faces present for the incoming guest to bind), a binding constant of 1.2 x 10^4 M^{-1} was calculated for this interaction. This is roughly an order of magnitude lower than that obtained for **FLU** binding to $\mathbf{H^W}$ (1.0 x 10^5 M^{-1}). A reason for this lower binding constant – despite the higher charge of 20+ for $\mathbf{H^{Cr/Co}}$ compared to 16+ for $\mathbf{H^W}$ – could involve the different counter-anion present for this titration compared to when $\mathbf{H^W}$ was used; chloride is present rather than borate which might already be binding strongly to the cage's surface compared to the more hydrophilic borate. In addition, the higher positive charge of $\mathbf{H^{Cr/Co}}$ means that there is a higher concentration of anions present than for $\mathbf{H^W}$, which will compete with **FLU** for the surface-binding sites.

To test whether the counter-anion does play a role in the determination of binding constants for these cages with **FLU**, samples of $\mathbf{H^A}$ and $\mathbf{H^W}$ were stirred with the same Dowex anion-exchange resin to produce $\mathbf{H^A{\cdot}Cl^-}$ and $\mathbf{H^W{\cdot}Cl^-}$. The titration investigating binding of **FLU** was then repeated using each of these cages as their chloride salt, and the results compared with $\mathbf{H^{Cr/Co}{\cdot}Cl^-}$.

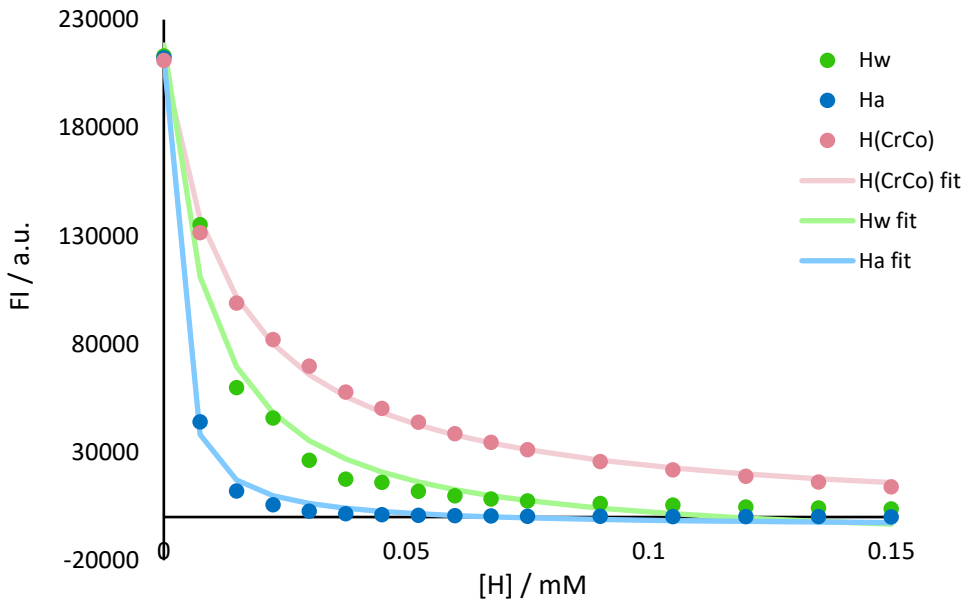

Figure 5.10 – Comparison of signal curves for FLU (515 nm) upon addition of increasing amounts of the three cages H^A, H^W and $H^{Cr/Co}$ (all chloride salts). [FLU] = 10 µM, [H] = 150 µM, 50 mM pH 8.5 borate buffer.

The results of these titrations were surprising. It was expected that with each cage now being its chloride salt, $\mathbf{H^A}$ and $\mathbf{H^W}$ would show similar binding curves for **FLU**, and $\mathbf{H^{Cr/Co}}$ would bind **FLU** with higher affinity due to its higher positive charge. As Figure 5.10 shows, this is not the case in practice: the lowest binding constant calculated was for $\mathbf{H^{Cr/Co}}$, followed by $\mathbf{H^W}$ then $\mathbf{H^A}$ (values given in Table 5.1).

Cage	*K* value / M^{-1}	% bound
$\mathbf{H^{Cr/Co}}$	1.2×10^4	92
$\mathbf{H^W}$	2.1×10^4	95
$\mathbf{H^A}$	1.1×10^5	99

Table 5.1 – Summary of calculated binding constants for fluorescein using three chloride-exchanged cages.

Our reasoning for the mixed-metal cage producing the lowest *K* value is due to the additional chloride ions present around the assembly. We initially considered the increased charge of $\mathbf{H^{Cr/Co}}$ to be a substantial factor in guest binding, specifically with anionic guests such as fluorescein, as the electrostatic factor shown to be involved in binding would be greater. Whilst this remains true, with the increased charge comes additional chloride ions to keep the cage's overall charge neutral. As suggested earlier, we suspect that the reduced binding constant for **FLU** seen using $\mathbf{H^{Cr/Co}}$ may be explained by this larger concentration of (competing) chloride.

$\mathbf{H^{W}}$ when converted to its chloride salt also shows a smaller binding constant than the unconverted BF_4^- analogue. This aligns with experimental data collected for both guest binding and catalysis previously and is an expected result. In contrast to this, the higher *K* value seen when using $\mathbf{H^{A}}$ was unexpected; the reduction of fluorescence intensity for **FLU** was large even at low concentrations of $\mathbf{H^{A}}$. A possible explanation for this observation involves the peripheral hydroxymethyl groups present on the ligand L^{W} and therefore the cage $\mathbf{H^{W}}$. These groups are reasonably acidic when the cage is formed and will likely be deprotonated at pH 8.5, causing the overall charge of the complex to be reduced compared to a cage that does not possess pendent OH's. In addition, the 24 hydroxymethyl groups might simply sterically interfere with **FLU** binding to the surface of $\mathbf{H^{W}}$ in a way that does not occur for $\mathbf{H^{A}}$.

Another point worth making is that $\mathbf{H^{Cr/Co}}$ does not quench the emission of bound **FLU** to the same extent as do the Co_8 cages, with the final residual fluorescence intensity being significantly higher than when $\mathbf{H^{A}}$ or $\mathbf{H^{W}}$ is used. This implies that the Cr(III) ions are unable to quench the excited state of the fluorophore as efficiently as the Co(II) ions do. Evidence that corroborates this suggestion is the fact that the cage $\mathbf{H^{Cr/Zn}}$ is fluorescent from its naphthyl groups – were the Cr(III) ions adept at quenching fluorescence, this would not be the case.

We also evaluated binding of 6-carboxyfluorescein (**6C-FLU**) to $\mathbf{H^{Cr/Co}}$. This molecule is also fluorescent, with very similar properties to fluorescein, but possesses a higher charge of 3- in basic aqueous solution (see Chapter 3). An experiment was performed

to allow comparison **FLU** and **6C-FLU** as surface-bound guests using $\mathbf{H^{Cr/Co}}$ to quench their fluorescence (Figure 5.11).

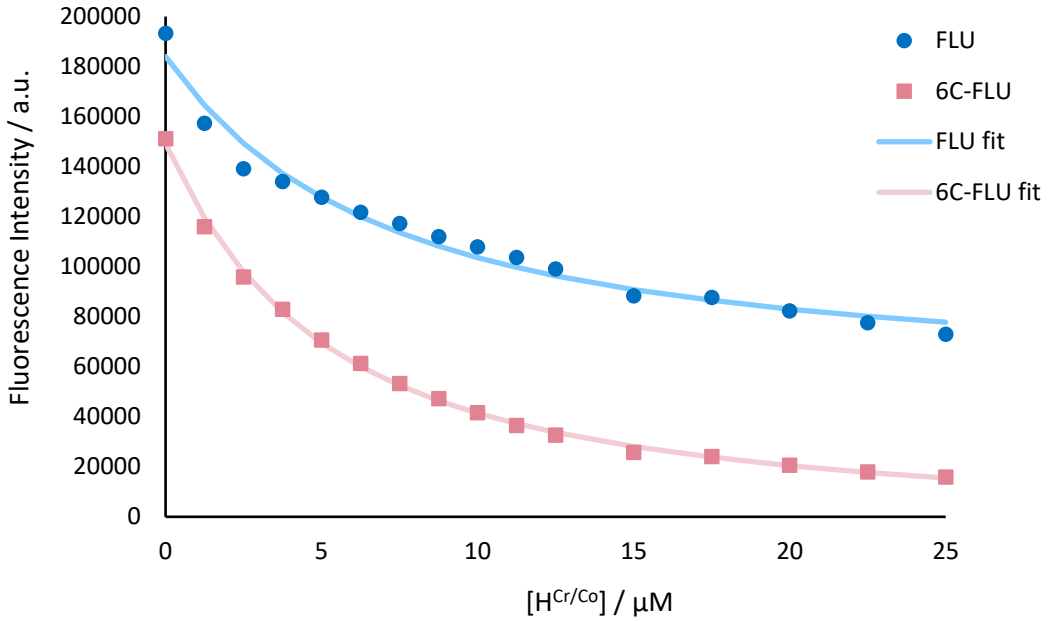

Figure 5.11 – Comparison of quenching of FLU and 6C-FLU by $H^{Cr/Co}$. [FLU/6C-FLU] = 10 µM, 50 mM borate buffer, pH 8.5.

As the above figure shows, the quenching observed for **6C-FLU** is greater than that seen for unsubstituted **FLU**; the emission of **FLU** is reduced by roughly 62% whilst **6C-FLU** displays a reduction of 90% during addition of the same amount of cage $\mathbf{H^{Cr/Co}}$. Fitting the curve for **6C-FLU** to a binding isotherm produced a *K* value of 4.2 x 10^4 M^{-1}, a little under four times that of **FLU**. This comparison of binding constants echoes what we observed with **FLU** and **6C-FLU** when using $\mathbf{H^{W}}$ as reported in Chapter 3 and suggests that the higher charge of $\mathbf{H^{Cr/Co}}$ does not greatly affect the general pattern of binding, with the 3- species **6C-FLU** binding more strongly than the 2- **FLU** for electrostatic reasons.

Cage	FLU *K* value / M^{-1}	6C-FLU *K* value / M^{-1}
$\mathbf{H^{Cr/Co}}$	1.2 x 10^4	4.2 x 10^4
$\mathbf{H^{W}}$	1.0 x 10^5	3.8 x 10^5

Table 5.2 – Comparison of FLU and 6C-FLU quenching by $H^{Cr/Co}$ and H^{W}.

The pyrene-based fluorophore **HPTS** was also tested for binding to the cage $\mathbf{H^{Cr/Co}}$. This molecule was also introduced in Chapter 3 and is of interest due to its ability to exist in 3- and 4- states depending on the pH of the solution. Quenching of **HPTS** by $\mathbf{H^{W}}$ occurred with incalculably high binding constants and a similar result was expected using the mixed-metal cage. The results of quenching experiments using $\mathbf{H^{Cr/Co}}$ and **HPTS** in both acidic and basic solution are shown in Figure 5.12, below.

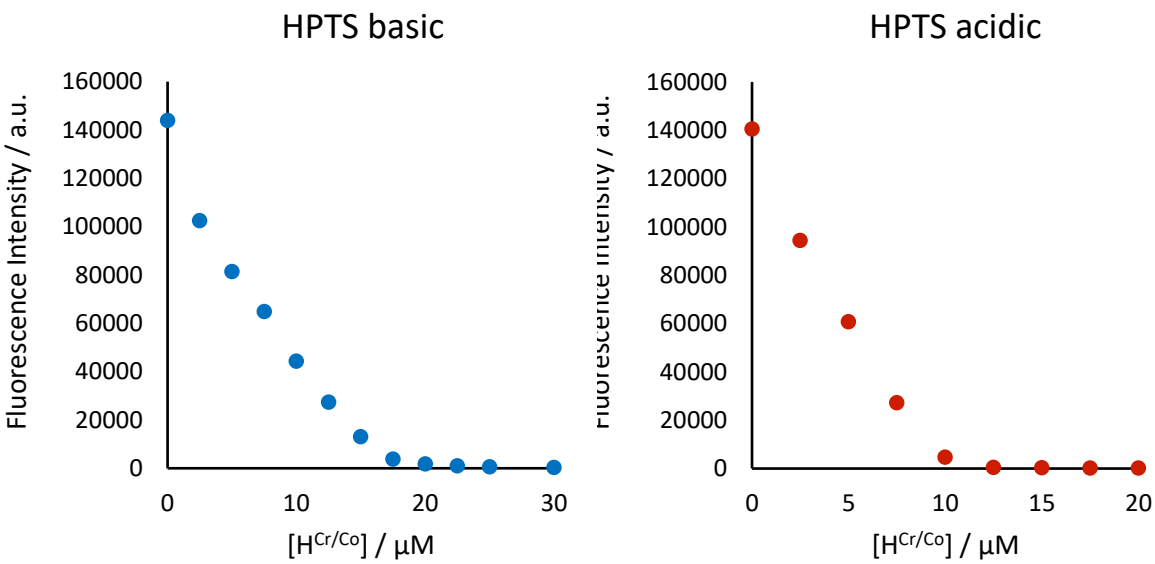

Figure 5.12 – Comparison of quenching titrations for HPTS under both basic and acidic conditions using $H^{Cr/Co}$. [HPTS] = 30 µM, basic conditions used 50 mM pH 8.5 borate buffer, acidic conditions used 1 M HCl to reach a pH of 4.0.

Quenching of **HPTS** under both basic and acidic conditions occurred rapidly upon addition of $\mathbf{H^{Cr/Co}}$ even at very low concentrations. The linearity of the signal curve suggests that binding occurs at the strong-binding limit, explaining why a *K* value could not be calculated from the above data. Interestingly, the minimum emission for **HPTS** is reached at different concentrations of $\mathbf{H^{Cr/Co}}$ depending on solution pH. Basic conditions, with $\mathbf{(HPTS)^{4-}}$ present in solution, resulted in quenching occurring until 20 µM of $\mathbf{H^{Cr/Co}}$, at which point emission has reached a minimum. In contrast, with acidic conditions, $\mathbf{(HPTS)^{3-}}$ produced the same rapid quenching but needing only 12.5 µM of $\mathbf{H^{Cr/Co}}$ to reach the minimum emission. This observation echoes findings when using **HPTS** with the cage $\mathbf{H^{W}}$, where the 3- state of **HPTS** was seen to bind with higher stoichiometry than the 4- state.

To follow these binding experiments, Job plots were constructed using **HPTS** and **H$^{Cr/Co}$** in an effort to see whether the stoichiometry of host/guest complexes is affected by the solution pH.

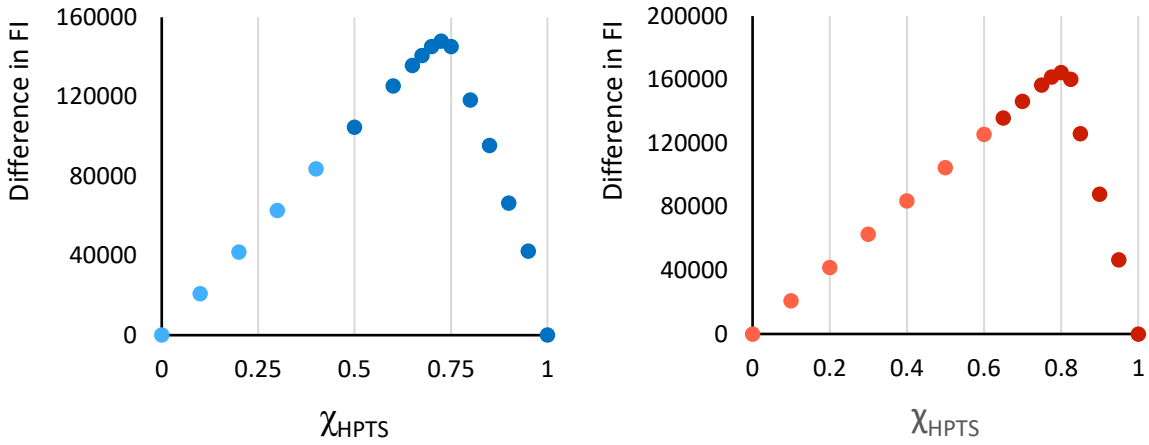

Figure 5.13 – Job plots for HPTS/H$^{Cr/Co}$ recorded in basic (blue) and acidic (red) solution. The lighter coloured data points are simulated.

Both Job plots feature very linear domains, with the x-axis maximum being clear for both experiments. The linearity comes from the strength of binding – weaker binding species such as **FLU** give more curved plots (Chapter 3). The stoichiometry is indicated by the position of the maximum and is different for the basic and acidic experiments. Basic conditions produced a stoichiometry close to 3:1 **HPTS**:**H$^{Cr/Co}$** (maximum seen at χ_{HPTS} = 0.725) whereas acidic conditions displayed a stoichiometry of 4:1 **HPTS**:**H$^{Cr/Co}$** (maximum seen at χ_{HPTS} = 0.8). Again, this result relates to the findings using **H^{W}** in a similar experiment, with acidic conditions providing higher host/guest complex stoichiometries as the smaller negative charge on the guest allows a larger number of them to accumulate around the cage's surface.

b) Displacement of bound FLU by competing anions

The next area of investigation was to see if simple inorganic anions showed comparable binding constants when using **H$^{Cr/Co}$** rather than **H^{W}** in a displacement assay using **FLU** as the indicator. The first anion to be tested was chloride, the anion used first when developing the surface-based displacement assay. The result of this titration is shown in Figure 5.14.

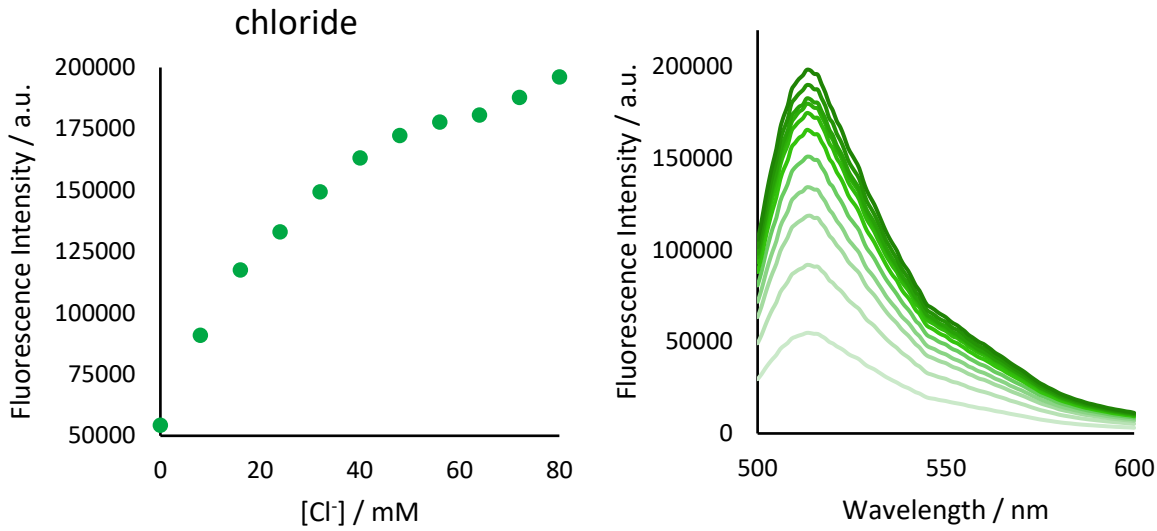

Figure 5.14 – Displacement of bound FLU by chloride using $H^{Cr/Co}$. The signal curve is taken from the peak at 515 nm. [$H^{Cr/Co}$] = 50 µM, [FLU] = 5 µM, 50 mM borate buffer pH 8.5.

You would be forgiven for thinking the graphs shown above are the same two graphs as seen in Figure 3.7 in Chapter 3, as the result when using $\mathbf{H^{Cr/Co}}$ is very similar. As the concentration of chloride is increased, bound fluorescein is displaced from the surface of $\mathbf{H^{Cr/Co}}$, leading to a restoration of fluorescence when **FLU** is free in solution. Taking the fluorescence intensity at 515 nm and plotting this against the concentration of added chloride produces the curve on the left of Figure 5.14. This data can be used to calculate a binding constant for chloride using a $\mathbf{FLU/H^{Cr/Co}}$ assay, which produced a *K* value of 45 M^{-1}. This value is considerably lower than the value for binding to $\mathbf{H^{W}}$, being over an order of magnitude smaller. The anions bromide and sulfate were also tested using the same $\mathbf{FLU/H^{Cr/Co}}$ assay, returning *K* values of 47 and 130 M^{-1} respectively. These values are much smaller than we observed with $\mathbf{H^{W}}$ which is perhaps counter-intuitive, and the values for chloride and bromide are very similar whilst that for sulfate is larger. The fact that sulfate – the only 2- anion – stands out in this group suggests that electrostatic factors dominate binding here, and the similarity of the *K* values for chloride and bromide suggest that hydrophobicity of the anion is less important in this system than it was with $\mathbf{H^{W}}$ as the cage. These observations combined point to a couple of conclusions: firstly, electrostatic factors associated with guest binding appear to be more significant relative to hydrophobicity, which given the higher charge of the cage is understandable.

Secondly, the much lower binding constants in absolute terms seen for all anions could be due to competition from the already-present chlorides (**$H^{Cr/Co}$·Cl^-**) which bind with greater affinity than borate (**H^W**).

Anion	*K* value / M^{-1}
Cl^-	4.5×10^1
Br^-	4.7×10^1
SO_4^{2-}	1.3×10^2

Table 5.3 – Calculated *K* values for three inorganic anions using the FLU/$H^{Cr/Co}$ displacement assay.

c) Quenching of 4-methyl-7-aminocoumarin (MAC)

The focus of studies up to this point has been on anionic guest species, due to the hypothesised differences in binding strength due to the higher charge of **$H^{Cr/Co}$**. This section returns to a well-documented fluorescent guest, **MAC**, to probe the cavity-binding properties of the mixed-metal cage. Whilst the primary difference between **$H^{Cr/Co}$** and **H^W** involves the extra charge provided to the cage assembly by the four Cr(III) ions, the assembly itself remains structurally similar to **H^W**. With this in mind, it could be predicted that a similar *K* value would be obtained for the quenching of **MAC** by **$H^{Cr/Co}$**. An experiment was prepared to investigate the binding strength of **MAC** using this mixed-metal cage.

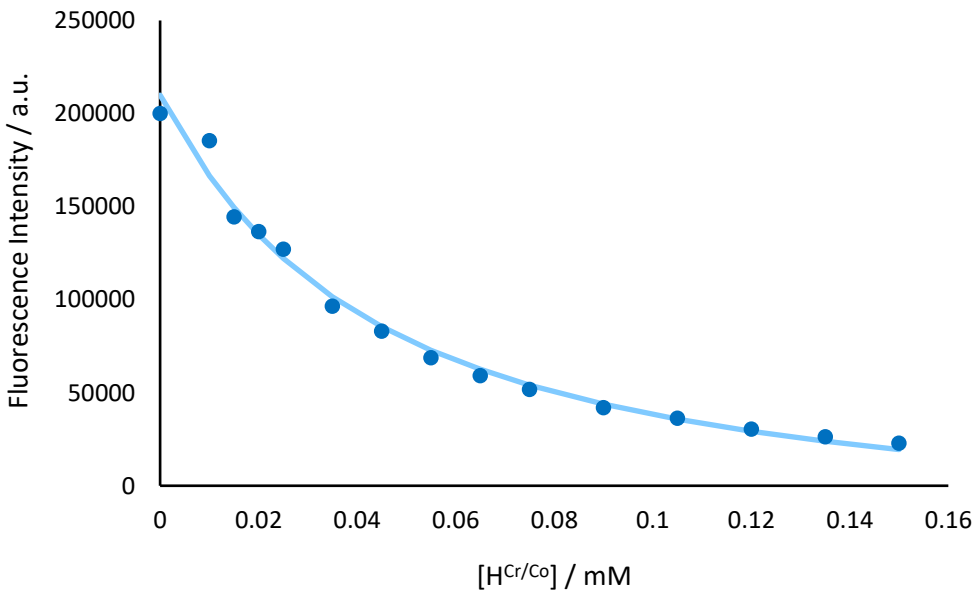

Figure 5.15 – Fluorescence quenching of MAC by $H^{Cr/Co}$ in H_2O. [MAC] = 10 µM, λ_{ex} = 395 nm.

Figure 5.15 shows the decrease in fluorescence intensity of the **MAC** emission seen around 445 nm as the concentration of $\mathbf{H^{Cr/Co}}$ is increased. The error on the fit is 5%, which is larger than can usually be achieved with titrations of this nature.[1] The *K* value calculated from this experiment was 2.7 x 10^4 M^{-1}, which is close to that calculated when using the Co(II)-based $\mathbf{H^{W}}$ (3.0 x 10^4 M^{-1}) in earlier measurements. This is interesting, as this cage is chloride-exchanged and as a result a reduced binding constant for **MAC** was predicted as chloride ions can compete for binding within the cavity of the cage, as demonstrated in Chapter 4.[7] However, other factors associated with guest binding in the cage's cavity, such as the hydrogen-bonding between the incoming guest and the *fac*-site on the interior surface of the cage, could be higher to compensate for this and the end result is little overall difference in cavity-based binding strength between $\mathbf{H^{Cr/Co}}$ and $\mathbf{H^{W}}$.[8]

5.3. Conclusions and Future Work

This chapter set out to investigate the host-guest behaviour of a new mixed-metal cage $\mathbf{H^{Cr/Co}}$ with a 20+ charge and compare the findings to previous work using the cage $\mathbf{H^{W}}$, which carries a 16+ charge. After characterisation of the cage was complete, a number of binding studies were performed in the same manner as for $\mathbf{H^{W}}$ previously. Fluorescein was found to bind to the exterior of $\mathbf{H^{Cr/Co}}$ with a lower affinity, with a *K* value of 1.2 x 10^4 M^{-1} calculated. The lower binding constant was assumed to be due to competition from the chloride counter-anions that were used for this cage to impart water-solubility. The reduction in *K* values extends beyond **FLU** to its counterpart **6C-FLU**, which also returned a binding constant about an order of magnitude lower when using $\mathbf{H^{Cr/Co}}$ compared to $\mathbf{H^{W}}$.

Using **FLU** in combination with $\mathbf{H^{Cr/Co}}$ as a displacement assay for binding of anions provided *K* values for the anions chloride, bromide and sulfate. All three anions returned lower binding constants than were obtained when using $\mathbf{H^{W}}$ in the assay; this is attributed to the presence of chloride anions for $\mathbf{H^{Cr/Co}}$ which are necessary to

[1] Repeats of this study would be beneficial to the data as a whole, but unfortunately no further sample of $\mathbf{H^{Cr/Co}}$ was available beyond this initial measurement.

facilitate water-solubility for the cage. Based on these three results, it appears that electrostatic factors contribute more to anion binding for this cage, which is likely due to the higher charge for the cage complex as a whole.

Binding and stoichiometry studies were conducted using the fluorophore **HPTS**. As with $\mathbf{H^W}$, acidic conditions (with **HPTS** in a 3- state) required fewer equivalents of cage to fully quench the fluorophore's emission and produced a higher stoichiometry when studied *via* a Job plot. Binding for this fluorophore still occurred at the strong binding limit, as seen by the linearity of the quenching.

In contrast to the surface-binding guests, there appears to be no reduction in affinity for the cavity-bound guest **MAC**, which was found to bind with a *K* value of 2.7×10^4 M^{-1}, close in value to that calculated using $\mathbf{H^W}$.

Future work involving the cage $\mathbf{H^{Cr/Co}}$ would begin with a more comprehensive study of the fluorescein-based displacement assay in order to investigate the contributions to guest binding more thoroughly. Using the cage $\mathbf{H^W{\cdot}Cl^-}$ as a point of reference would also allow easier comparison between cages, avoiding the difference in counter-anion. A series of 1- and 2- guests could be used, as was done with the cage $\mathbf{H^W}$, to confirm that the electrostatic component of guest binding influences the binding constant more for the mixed-metal cage. Following this, more studies on binding within the cage's cavity – specifically using **MAC** as the guest – would be beneficial. A comparison of fluorescence quenching using chloride-exchanged cages ($\mathbf{H^A}$, $\mathbf{H^W}$, $\mathbf{H^{Cr/Co}}$) seems a candidate experiment to try. Another different avenue of exploration would be to investigate the effect of higher charge on the catalysis of nitrobenzisoxazole to 2-nitro-4-cyanophenolate.

5.4. Experimental

5.4.1. Cage synthesis

The experimental route and cage synthesis was undertaken by Dr Jerico Piper.

5.4.2. Extinction Coefficient determination using $H^{Cr/Zn}$

2.381 mg of the cage $\mathbf{H^{Cr/Zn}}$ was weighted out and dissolved in 1.45 mL of acetonitrile to make a solution at 0.2 mM (M_W $\mathbf{H^{Cr/Zn}}$ = 8213.88 g mol^{-1}). Using this solution, samples were prepared at 10, 8, 6, 4 and 2 µM in acetonitrile and a UV/vis spectrum recorded for each. The absorbance at 255 nm was plotted against the concentration of cage for each sample and a straight line fitted to the resulting graph. 255 nm was chosen as this is the most clearly defined peak available within the spectrum.

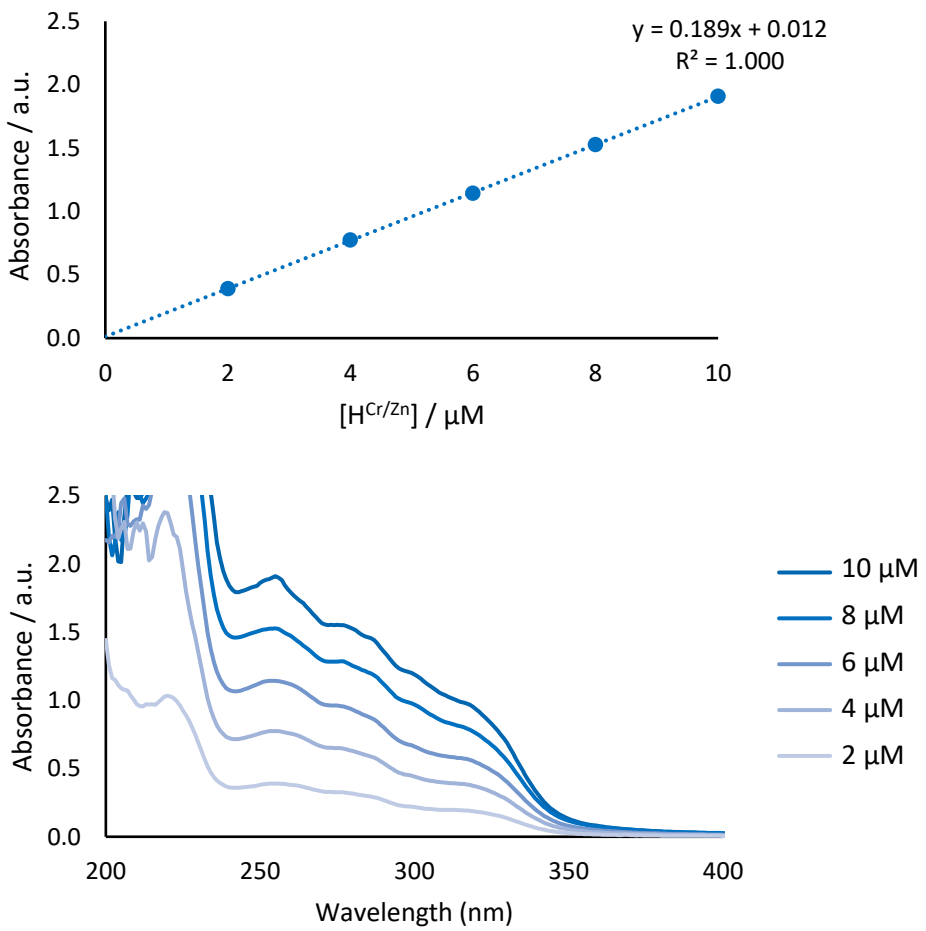

Figure 5.16 – Top: A plot of absorbance at 255 nm vs [$H^{Cr/Zn}$] to obtain the extinction coefficient, ε. Bottom: stacked UV/vis absorption spectra for $H^{Cr/Zn}$ at progressively lower concentrations. Data recorded in MeCN at 298 K.

The value obtained from this experiment, ε = 1.89 x 10^5 M^{-1} cm^{-1} was used for determining sample concentrations when using the cages **H$^{Cr/Zn}$** and **H$^{Cr/Co}$** as the naphthyl groups responsible for these absorption bands are found in both species.

5.4.3. Mass spectrometry

Data for **H$^{Cr/Zn}$**:

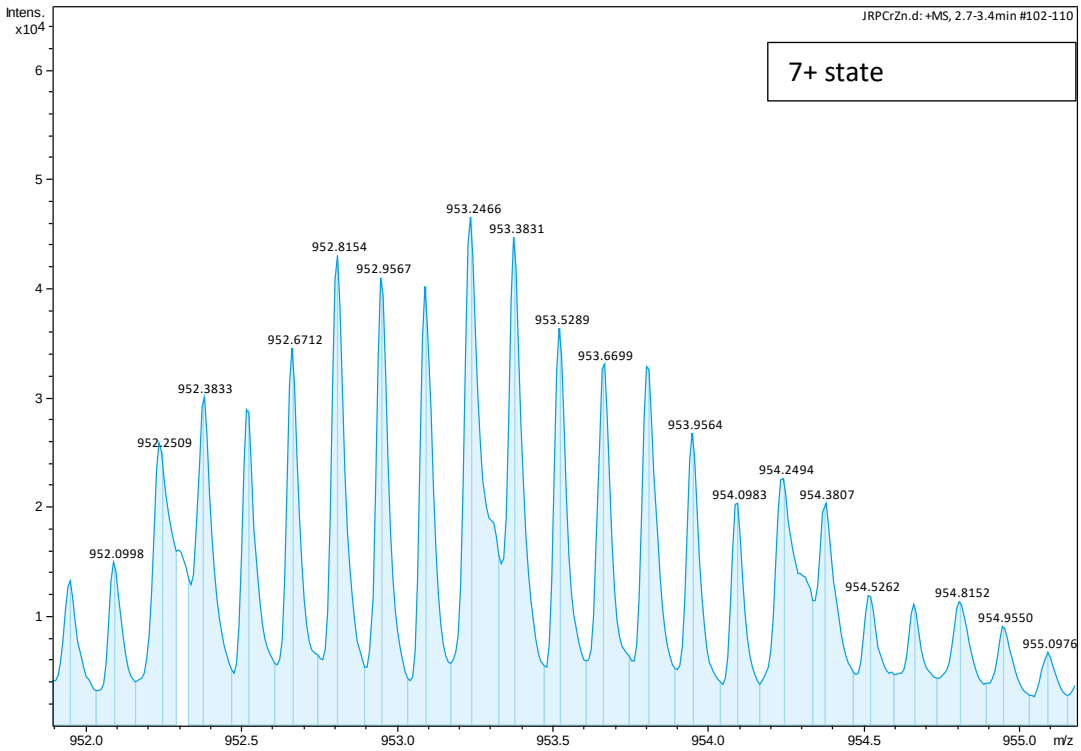

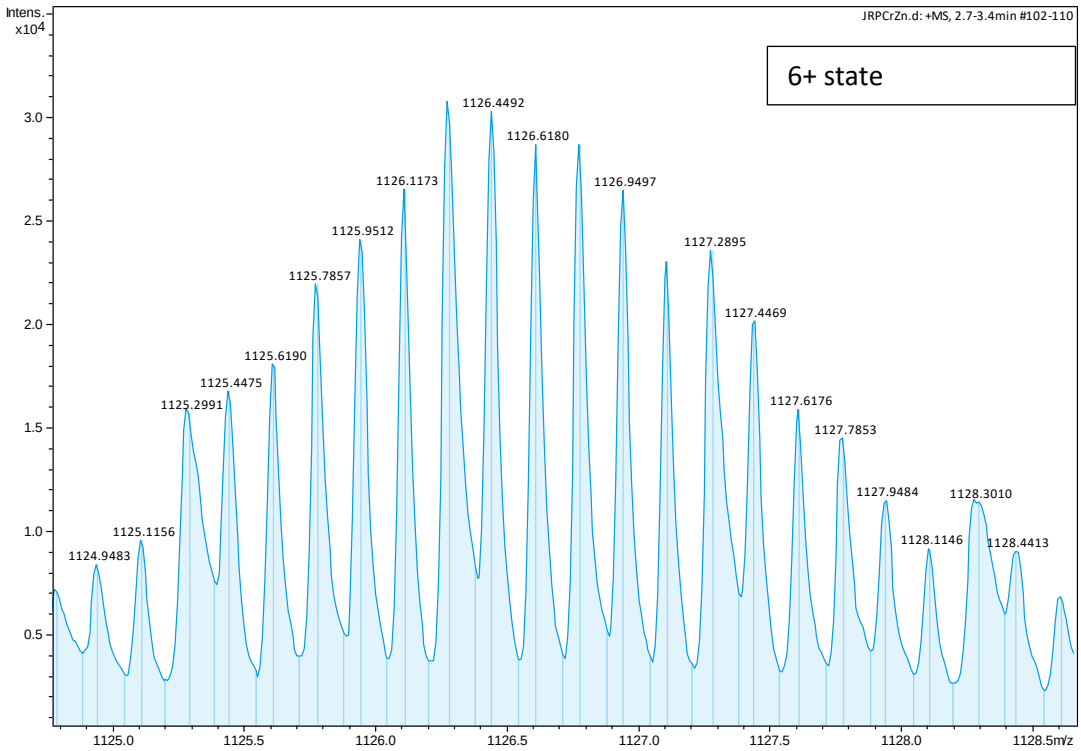

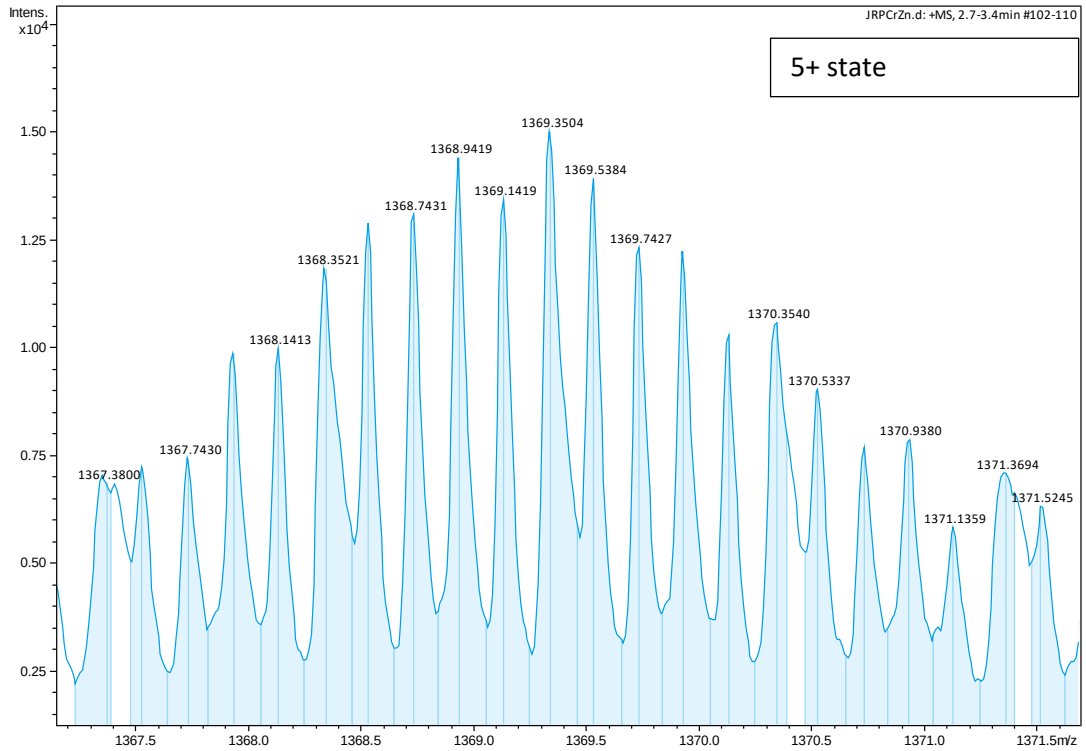

5.4.4. Errors

The *K* values quoted within this chapter in Section 5.2 are presented with an estimated uncertainty of ±10%. The primary source of error associated with the displacement assay lies not with the sample preparation and experimental readings but with the fitting of a binding isotherm to the fluorescence data obtained. This error is typically in the region of 5-10% for the work in this chapter, which outweighs any error in weighing or pipetting during the experimental set up.

5.5. References

1 T. L. Mako, J. M. Racicot and M. Levine, *Chem. Rev.*, 2019, **119**, 322–477.

2 A. J. Metherell and M. D. Ward, *Chem. Commun.*, 2014, **50**, 6330–6332.

3 E. Stulz, S. M. Scott, A. D. Bond, S. J. Teat and J. K. M. Sanders, *Chem. - A Eur. J.*, 2003, **9**, 6039–6048.

4 O. Chepelin, J. Ujma, X. Wu, A. M. Z. Slawin, M. B. Pitak, S. J. Coles, J. Michel, A. C. Jones, P. E. Barran and P. J. Lusby, *J. Am. Chem. Soc*, 2012, **134**, 19334–19337.

5 J. S. Train, A. B. Wragg, A. J. Auty, A. J. Metherell, D. Chekulaev, C. G. P. Taylor, S. P. Argent, J. A. Weinstein and M. D. Ward, *Inorg. Chem.*, 2019, **58**, 2386–2396.

6 J. R. Piper, L. Cletheroe, C. G. P. Taylor, A. J. Metherell, J. A. Weinstein, I. V. Sazanovich and M. D. Ward, *Chem. Commun.*, 2017, **53**, 408–411.

7 W. Cullen, A. J. Metherell, A. B. Wragg, C. G. P. Taylor, N. H. Williams and M. D. Ward, *J. Am. Chem. Soc.*, 2018, **140**, 2821–2828.

8 S. Turega, M. Whitehead, B. R. Hall, A. J. H. M. Meijer, C. A. Hunter and M. D. Ward, *Inorg. Chem.*, 2013, **52**, 1122–1132.

Thesis Summary

The work presented within this thesis set out to explore a field within supramolecular chemistry that had received far less attention than other perhaps more obvious topics of interest: surface interactions between molecular hosts and guests. Searching the literature for articles related to surface interactions within host-guest chemistry still yields relatively few results compared to the closely related area of cavity-based interactions. Using a cubic coordination cage typical of the work conducted by the Ward group in the past, the investigations carried out by myself deviate from those done before and instead utilise the more accessible surface of a molecular host – its exterior surface.

The first realisation of the potential use for the cage's surface to be involved in host-guest chemistry came when looking into water-solubilisation methods through anion exchange. The BF_4^- counter anions that associate with the cage can be exchanged for different anions using a modified Dowex resin with retention of overall cage structure. Water-soluble analogues of the cage can be produced through this method, even without complete removal of the BF_4^- anions, as determined by ^{19}F NMR studies of the converted cages. The relative concentrations of water-soluble cages after anion exchange varied depending on the anion used; a correlation to the Hofmeister series of anions could be seen when looking at the concentration of cage in water and the anion used. With this in mind, we studied the conversion of nitrobenzisoxazole to 2-cyanonitrophenolate *via* the Kemp elimination, which follows previous work using the unsubstituted benzisoxazole. The reaction using nitrobenzisoxazole differs in two respects as the reaction can be tracked by UV/vis, and the reaction occurs on the exterior of the cage as opposed to the cavity. The involvement of the cage's exterior allowed investigation into the effect of addition of other anions on the rate of reaction. The more hydrophobic the anion added, the greater the degree of inhibition seen for the reaction, with a definite correlation between the calculated rate constant k_{cat} and the anion's position on the Hofmeister series. The link between k_{cat} and hydrophobicity was not exact; anions that are the conjugate bases of weak acids such as fluoride or bicarbonate increased the rate of reaction.

Having proven that anions interact with the exterior surface of the cage with varying affinities, a method of quantifying the strength of association was sought after. A fluorescence displacement assay utilising the anionic fluorophore fluorescein was developed, exploiting the fact that fluorescein emission is quenched when associated to the cage's exterior and restored when free in solution. With a binding constant determined for fluorescein, values were also calculated for a range of simple inorganic anions commonly listed in the Hofmeister series, along with larger organic anions such as gluconate and tartrate. The values of *K* calculated for the simple (mostly) inorganic anions again aligned with the anion's position in the Hofmeister series, with hydrophobic anions such as nitrate returning the largest binding constants. This observation can be attributed to the relative solvation of the anions and their preference for the C-H protons available at the binding sites located on the cage's exterior surface. A relationship between the k_{cat} values calculated in Chapter 2 using certain anions and their *K* values calculated in Chapter 3 was noticed, with a very high correlation between the two for the anions iodate, chloride, bromide and nitrate.

The binding and resulting quenching of other anionic fluorophores was investigated using the cage $\mathbf{H^W}$. The fluorescein derivatives 6-carboxyfluorescein and Eosin Y were both found to bind with higher affinity than fluorescein, pointing to contributions to binding from both electrostatics (higher charge of **6C-FLU**) and hydrophobicity (**EY**). Whilst hydrophobicity of guest molecules is a well-known contributory factor to binding from studies of cavity-binding guests, the electrostatic contribution to binding, especially for surface-binding guests, had not been looked at in detail (besides finding that sulfate bound stronger than other anions of similar hydrophilicity when tested using the fluorescein displacement assay). Eosin Y bound at the strong binding limit and so no binding constant was obtained, whilst 6-carboxyfluorescein returned a *K* value roughly four times that of fluorescein. Hydroxypyrene tris-sulfonate, another common anionic fluorophore, was also found to bind at the strong binding limit in both forms $(\mathbf{HPTS})^{4-}$ and $(\mathbf{HPTS})^{3-}$ but the minimum fluorescence intensity was reached at differing concentrations of cage. This led to studies on the stoichiometry of guest binding to the cage's surface using **HPTS**

in both its protonated and deprotonated forms, which revealed that six guest molecules of (**HPTS**)$^{3-}$ can associate with the exterior of the cage at the same time, whereas only four (**HPTS**)$^{4-}$ anions can bind under the same conditions. When performing similar studies using **6C-FLU**, it was shown that increasing dilution of the system results in lower stoichiometries. Fluorescein itself was found to bind with a 5:1 stoichiometry.

For anionic molecules that are not fluorescent but are UV-active, we can still observe a change in optical characteristics upon interaction with the cage's exterior. For the Kemp elimination reaction, the product phenolate **2CNP** absorbs at a longer wavelength in the presence of the cage than it does when free in solution. This shift in the absorption maximum can be linked to a stabilisation effect imparted by the cage and is also seen for bound fluorescein. The pH indicator bromocresol purple was shown to ring-open a whole unit of pH lower when the cage was present, demonstrating the cage's ability to stabilise the anionic form of this indicator.

The binding of anionic guest species to the external recognition sites of the cage $\mathbf{H^{W}}$ does not affect the host-guest chemistry of its cavity. Despite the anions binding in the portals on each face of the cage, this does not affect guest ingress/egress. The cavity-binding fluorophore **MAC** was used in conjunction with **FLU** to investigate whether the quenched fluorophores could be displaced discretely. The guests cyclooctanone, ascorbate and chloride were able to displace **MAC**, **FLU** and both indicators respectively from being bound to $\mathbf{H^{W}}$, producing three individual colourimetric responses. Individual samples containing different guests could be distinguished using this sensor system and a handheld UV lamp with no analytical instrument required. To our knowledge, this is the first reported example of orthogonal displacement of indicators involving a coordination cage.

The effect of the charge of the host complex on guest binding was also studied. Using a mixed-metal cage $\mathbf{H^{Cr/Co}}$ with a higher positive charge than $\mathbf{H^{W}}$, we attempted to investigate guest binding for both anionic and neutral guests. The anionic guests studied returned lower *K* values than when using $\mathbf{H^{W}}$, which was suggested to be due to the presence of chloride counter-anions on $\mathbf{H^{Cr/Co}}$ as opposed to borate. **MAC**, the

only neutral guest studied, was found to have a similar binding constant for both cages.

To summarise, many of the findings reported as part of this work are interwoven and connected between chapters. The themes encompassed within this thesis represent a shift in perspective, with molecular hosts proven to be not only vessels with an ability to contain smaller molecules within but also a collection of surface sites which can themselves be involved in roles such as catalysis or sensing. I fully expect this area to receive further attention in the future and am excited to see how the field moves forward from this point on, for there are many stones that remain unturned.

Publication Reprints

1. Christopher G. P. Taylor, Stephen P. Argent, Michael D. Ludden, Jerico R. Piper, Cristina Mozaceanu, Sarah A. Barnett, and Michael D. Ward, "One Guest or Two? A Crystallographic and Solution Study of Guest Binding in a Cubic Coordination Cage" *Chem. Eur. J.*, 2020, **26**, 3054 –3064.

2. Michael D. Ludden and Michael D. Ward, "Outside the box: quantifying interactions of anions with the exterior surface of a cationic coordination cage" *Dalton Trans.*, 2021, **50**, 2782–2791.

3. Michael D. Ludden, Christopher G. P. Taylor, and Michael D. Ward, "Orthogonal binding and displacement of different guest types using a coordination cage host with cavity-based and surface-based binding sites" *Chem. Sci.*, 2021, **12**, 12640-12650.

4. Michael D. Ludden, Kellie Tuck, Jack C. Dorrat, Nicholas Williams, Jennifer S. Train, Max B. Tipping, Christopher G. P. Taylor, and Michael D. Ward, "Interaction of anions with the surface of a coordination cage in aqueous solution probed by their effect on a cage-catalysed Kemp elimination" *Chem. Sci.,* 2021, **12**, 14781–14791.

Dalton Transactions

ROYAL SOCIETY OF CHEMISTRY

PAPER

View Article Online
View Journal | View Issue

Check for updates

Cite this: *Dalton Trans.*, 2021, **50**, 2782

Outside the box: quantifying interactions of anions with the exterior surface of a cationic coordination cage

Michael D. Ludden and Michael D. Ward *

We describe a study of the binding of anions to the surface of an octanuclear coordination cage $\mathbf{H^W}$, which carries a 16+ charge, in aqueous solution. Anionic aromatic fluorophores such as fluorescein (and derivatives) and hydroxypyrene tris-sulfonate (HPTS) bind strongly to an extent depending on their charge and hydrophobicity. Job plots indicated binding of up to six such fluorescent anions to $\mathbf{H^W}$, implying that one anion can bind to each face of the cubic cage, as previously demonstrated crystallographically with small anions such as halides. The quenching of these fluorophores on association with the cage provides the basis of a fluorescence displacement assay to investigate binding of other anions: addition of analyte (organic or inorganic) anions in titration experiments to an $\mathbf{H^W}$/fluorescein combination results in displacement and restoration of the fluorescence from the bound fluorescein, allowing calculation of 1 : 1 binding constants for the $\mathbf{H^W}$/anion combinations. Relative binding affinities of simple anions for the cage surface can be approximately rationalised on the basis of ease of desolvation (*e.g.* $F^- < Cl^- < Br^-$), electrostatic factors given the 16+ charge on the cage (monoanions < dianions), and extent of hydrophobic surface. The interaction of a di-anionic pH indicator (bromocresol purple) with $\mathbf{H^W}$ results in a pK_a shift, with the surface-bound di-anionic form stabilised by approximately 1 pK_a unit compared to the non-bound neutral form due to the charge on the cage.

Received 10th December 2020,
Accepted 2nd February 2021

DOI: 10.1039/d0dt04211k

rsc.li/dalton

1. Introduction

Much of the interest in the chemistry of coordination cages arises from their host guest chemistry, *i.e.* the ability of hollow cages to act as hosts which can bind guest molecules which occupy the central cavity.[1–4] Such binding of guests inside cage cavities is responsible for multiple applications in supramolecular chemistry including catalysis,[2] sensing,[3] and externally-triggered uptake/release for transport purposes.[4] As a result, the metaphorical spotlight has been largely focussed on guest binding inside the central cavities of the host cages, with all that this implies for design of host cages with suitable cavity properties for specific guests, measurement of and understanding of the various interactions responsible for guest binding, and structural characterisation of cage/guest complexes.

More recently, attention has turned to the interactions between guests and the exterior surfaces of coordination cages as not all interactions of host cages with small molecules need to occur inside the cavity. In our cage family,[5] in particular the M_8L_{12} octanuclear cages which are the basis for this work (Fig. 1),[6] we have found that the windows in the face centres provide sites where counter-ions X^- can bind *via* an array of multiple C–H···X^- hydrogen bonds, aided by the high positive (16+) charge of the cage:[7] this calls to mind the seminal example from Lehn and co-workers in 1996 of a chloride ion binding tightly in the central cavity of a cyclic pentanuclear double helicate,[8] and other related examples of anion binding

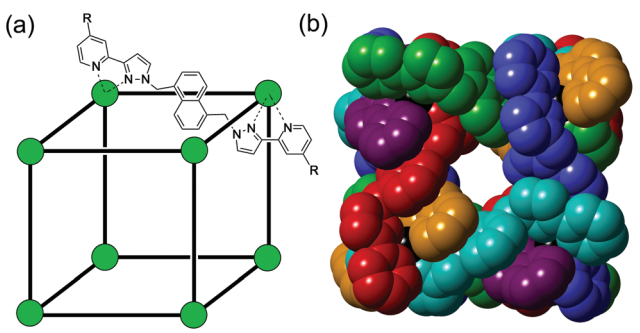

Fig. 1 The host cage $[Co_8L_{12}]^{16+}$, abbreviated as $\mathbf{H^W}$ (R = CH_2OH). (a) A sketch emphasising the cubic array of Co(II) ions and the disposition of one bridging ligand; (b) a space-filling view of the core (without the CH_2OH substituents) showing each ligand coloured separately for clarity.

Department of Chemistry, University of Warwick, Coventry CV4 7AL, UK.
E-mail: m.d.ward@warwick.ac.uk

in cyclic cavities defined by predominantly hydrocarbon-based ligand fragments.[9]

In our M_8L_{12} cages, binding of anions in surface portals in this way means that a cavity-bound guest may be surrounded by an octahedral array of six anions around the cage surface (Fig. 2).[7a] This provides the basis for very effective catalysis of some reactions of cavity-bound guests with surface-bound anions as the two reaction partners are co-located *via* orthogonal interactions: a neutral guest binds inside the cage cavity in water using the hydrophobic effect, but desolvation of anions and binding to the cage surface is driven by electrostatic factors, with the cavity-bound guest and surface-bound anions being independently changeable.[7a,10]

Several other groups have noted the importance of interactions between small molecule guests (particularly counter-ions) and the cage surface. Nitschke and co-workers have shown how tetraphenylborate anions on the exterior of a cage surface – with one phenyl ring pointing into the central cavity – templated formation of an M_6L_4 capsule that more usually required a cavity-based templating agent.[11] In a similar vein the same group reported how surface-binding perchlorate anions template formation of an unusual pentagonal bipyramidal cage that also tightly binds chloride.[12] Nitschke and co-workers have also incorporated specific fluoride-binding sites (Lewis-acidic boron centres) into the exterior surface of an M_4L_4 tetrahedral cage to allow exterior binding of fluoride, which modulates the cage charge and hence its affinity for different solvent phases.[13] Raymond and co-workers have shown how the interaction of tetraphenyborate with a cage exterior surface was driven by quite different thermodynamic effects than binding in the central cavity;[14] and Wu's group have shown how hydrogen-bonded cages, formed using urea/phosphate interactions instead of metal/ligand dative bonds, can be switched between different structural types based on interaction of the cage surfaces with counter-ions of different size and shape.[15] Interaction of solvent molecules and counter-ions with the exterior surfaces of a pair of isostructural tetrahehedral cages bearing different charges has recently been studied in detail by Stelson and co-workers.[16] Overall, the importance of interactions of the exterior surface of cages with species in the surrounding medium is becoming more appreciated as being as important as the more obvious interactions associated with cavity-bound guests – a particular focus of host–guest chemistry that has been with us since the first complexes of crown ethers with alkali metal ions.

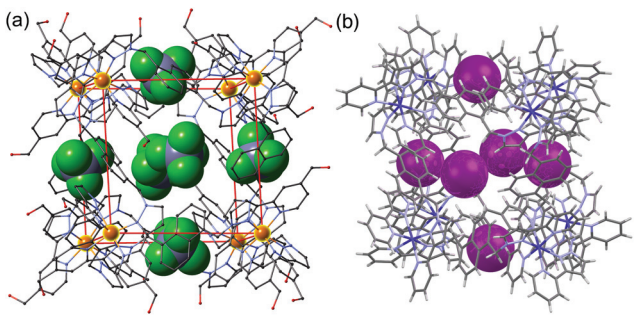

Fig. 2 Crystal structures of different salts of the host system showing the location of anions in the windows in the centre of each face, giving an octahedral array of surface-bound anions surrounding the central cavity: (a) the tetrafluoroborate salt (from ref. 6*b*); (b) the iodide salt (from ref. 7*a*).

In our recent work on cage-based catalysis of the Kemp elimination (reaction of cavity-bound benzisoxazole with the shell of ions surrounding it, either hydroxide or phenolates, due to interactions with the cage surface),[7a,10] it became apparent that the tendency of an anion to bind to the highly cationic M_8L_{12} cage surface in aqueous solution is related to the ease with which it can be desolvated (thus, the binding affinity order with the cage was phenolate > chloride > hydroxide):[7a] in retrospect a fairly unsurprising conclusion, but one which implies that we should be able to control which type of anionic reaction partner binds to the cage surface and surrounds a cavity-bound guest for catalysed reactions. Accordingly, we felt that it would be of interest to undertake a systematic, quantitative study of the affinity of different anions for the M_8L_{12} cage. To do this we have developed a fluorescence displacement assay,[17] utilising our M_8L_{12} cage in combination with an anionic surface-bound fluorophore (fluorescein), which is capable of allowing determination of the association strengths of both organic and inorganic anionic species through a displacement process that leads to an easily-observable change in fluorescence of the fluorophore. In this way we have built up a very clear picture of the interactions of different anions with the surface binding sites of the M_8L_{12} cubic cage.

2. Materials and methods

The studies conducted within this paper use the water-soluble cubic Co_8 cage $\mathbf{H^W}$ which was prepared as previously described.[6b] The fluorescent species fluorescein, hydroxypyrene trissulfonate (trisodium salt), 6-carboxyfluorescein and Eosin Y were purchased from Acros Organics or Merck Life Sciences and used as received. Inorganic salts used to evaluate anion binding affinities were purchased from Sigma-Aldrich and used as delivered. Fluorescence measurements were carried out using either a BMG ClarioStar plate reader with 96-well plates, or an Agilent Cary Eclipse fluorimeter. UV/Vis spectra were obtained using an Implen C40 Nanophotometer.

Fluorescence titrations were performed by preparing a solution of fluorescein (**FLU**; 10 μM) and cage ($\mathbf{H^W}$; 100 μM) in deionised water, which was then used to prepare two solutions at 5/50 μM **FLU**/$\mathbf{H^W}$ through addition of either deionised water or a premade sodium salt solution of the anion under investigation. Samples for titrations were dissolved in 50 mM borate buffer at pH 8.5 to ensure a constant pH. (It follows that there is a high concentration of borate anions always present which may affect binding of other anions under investigation. However, this is fixed for all titration experiments in sections 3.2 and 3.4 and represents part of the standard baseline set of

conditions (like the nature of the solvent) common to all experiments. Although absolute values of binding constants would probably be different with different buffers because different competing anions are present, comparisons within a guest series and – in particular – relative orderings of anion affinities measured under a fixed set of conditions, are legitimate).

Titrations were run using between 10 and 14 wells of a 96-well plate filled to 200 μL each with varying ratios of $\mathbf{H^W}$·**FLU** solution and the analyte under investigation. The instrument was equilibrated to 298 K for all measurements. Fluorescence spectra between 500 and 600 nm were recorded for each well using an excitation wavelength of 472 nm, and the intensity of emission peak of **FLU** at 515 nm was measured to determine binding constants for all analytes studied. Calculation of the binding constants for anions in the displacement assay used software written by Prof. Chris Hunter as described previously.[18a]

3. Results and discussion

3.1. General principles and background

The octanuclear, approximately cubic, coordination cage $\mathbf{H^W}$ (formula $[Co_8L_{12}][BF_4]_{16}$, Fig. 1) possesses a cavity of volume of 409 Å^3 which is slightly elongated with the approximate shape of a rugby ball. The cavity-based host–guest chemistry of this cage has been studied extensively, with small organic guests able to bind within the cavity, entering through small windows on each face of the cube which allow guest ingress/egress.[4f,5,6b,18,19] Binding constants for organic guests within the cavity in aqueous solution have been reported up to 10^6 M^{-1} and correlate closely with hydrophobic surface area.[6b,18a]

The presence of Co(II) ions in the cage result in quenching of fluorescent organic guests when they bind, likely through energy transfer from the fluorophore's excited state to the low energy Co(II) d–d transitions. This quenching of fluorescent guests provided, in previous work, the basis for a fluorescence displacement assay using the organic fluorophore MAC (4-methyl-7-amino coumarin) which is quenched when bound: addition of a guest that could compete for binding within the cavity resulted in partial displacement of MAC and restoration of its fluorescence, to an extent depending on the binding strength of the new guest.[18a] This allowed binding constants for the added guests to be calculated. Based on this, we sought to develop a similar fluorescence displacement assay which would allow us to probe the strength of binding of different anions to the cage exterior surface, which requires a surface-binding, anionic fluorophore that could be displaced by other anions from the binding sites on the cage surfaces.

3.2. Binding of fluorescein and derivatives to $\mathbf{H^w}$

The well-known fluorophore fluorescein (denoted **FLU**, see Chart 1) is a green-emitting xanthene-type dye molecule containing both phenol and carboxyl moieties. When deprotonated, the emission intensity of the molecule increases dramatically. The pK_a of these two groups is 6.3 and 3.4 respectively, meaning that at pH 8 the molecule will be dianionic and should associate with the exterior of $\mathbf{H^W}$ (**FLU** being too large for cavity-binding). Sequential additions of a solution of $\mathbf{H^W}$ to a solution of **FLU** (10 μM) resulted in a rapid decrease in the **FLU** luminescence intensity (Fig. 3) with quenching essentially complete after addition of only two equivalents of $\mathbf{H^W}$.

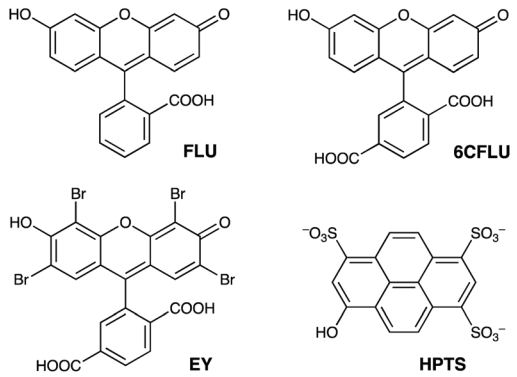

Chart 1 The aromatic, anionic fluorophores used in this work (shown in the forms existing in weakly acidic solution).

The fluorescence data could be fitted to a 1 : 1 binding model, which afforded a binding constant of 1.0×10^5 M^{-1} for interaction of **FLU** with an individual cage face. Although each cage molecule has six equivalent potential anion binding sites, this titration is done under conditions where $\mathbf{H^W}$ is in excess as the titration proceeds which means that a 1 : 1 $\mathbf{H^W}$: **FLU** complex will dominate: species in which multiple **FLU** units bind to one cage would require excess **FLU** (see later).

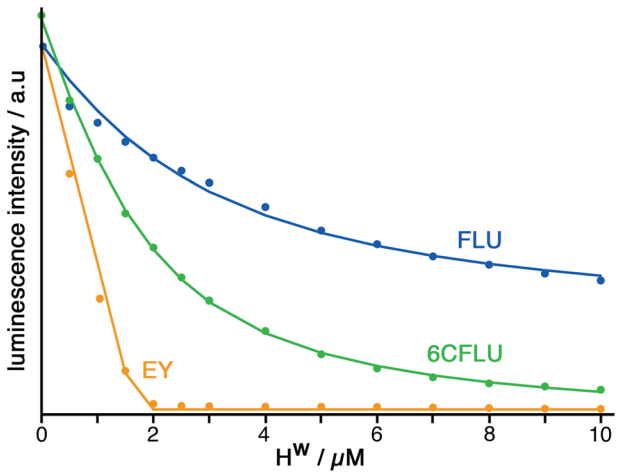

Fig. 3 Results of spectroscopic titrations of H^W with the fluorophores **FLU** (blue), **6CFLU** (green) and **EY** (orange), each at 10 μM in water, showing in each case the progressive quenching of the fluorophore on addition of portions of H^W up to 1 equivalent H^W (6 equivalents of possible binding sites). Circles represent measured data; the blue and green curves for **FLU** and **6CFLU** respectively are the best fits to a 1 : 1 binding isotherm (see main text for binding constants). The relative strength of binding of these fluorophore is clearly **FLU** < **6CFLU** < **EY**.

This means that these fluorescence data fit a simple 1 : 1 binding isotherm which corresponds to formation of the 1 : 1 $\mathbf{H^W}$: **FLU** complex with one **FLU** on one face of the cubic cage. The value of K so obtained was calculated using the concentration of potential binding sites available to account for the statistical effect of each host having six equivalent anion binding sites, and give a K value corresponding to the intrinsic binding constant of **FLU** with one face of $\mathbf{H^W}$.

Given the possibility of each cage being able to quench multiple **FLU** units (potentially, up to six) by surface binding if excess **FLU** is present, and the likelihood that the second and subsequent binding events are still strong, we looked further into the $\mathbf{H^W}$/**FLU** stoichiometry using a Job plot to observe how many faces of the cube could be occupied by guest molecules under what amount to forcing conditions (large excess of **FLU** compared to $\mathbf{H^W}$ at the appropriate point in the Job plot). When $\mathbf{H^W}$ and **FLU** were combined in different mole fractions, the maximum decrease in **FLU**-based fluorescence intensity (compared to unquenched **FLU** at the same concentration) was found at a mole fraction of 0.83 (Fig. 4a), equating to a 5 : 1 stoichiometry of **FLU** : $\mathbf{H^W}$, strongly suggesting that the highly cationic cage $\mathbf{H^W}$ can bind (and quench) several **FLU** units simultaneously, each at a different face. The dominance of five **FLU** units in the speciation rather than six is possibly ascribable to electrostatic factors: each **FLU** has a charge of 2−, so there comes a point where accumulation of several of these will hinder binding of subsequent guests, such that the sixth binding event may not be observed under the dilute conditions used, such that the 1 : 5 species $\mathbf{H^W}\cdot(\mathbf{FLU})_5$ dominates the speciation at this concentration.

We emphasise that there is no contradiction in the observation of a $\mathbf{H^W}\cdot(\mathbf{FLU})_5$ complex in the Job plot under conditions when **FLU** is in excess, and the fitting of fluorescence titration data to a 1 : 1 model under conditions when $\mathbf{H^W}$ is excess (resulting in measurement of a value for K_1 only, with second and subsequent binding constants K_2 up to K_5 not being measurable). We note also that use of Job plots to delineate limiting stoichiometries of supramolecular complexes has serious limitations, as several authors have pointed out recently.[19c,20] However, if we are using conditions under which the quantity being measured is additive (*i.e.* binding of two **FLU** units to a cage causes twice as much loss of luminescence as does binding of one **FLU** unit) then the main pitfall is avoided.

Whilst we do not know the geometry of the $\mathbf{H^W}$/**FLU** interaction – there are two anionic sites on **FLU** under these conditions which could interact with the portals around the cage surface – the carboxylate site will be more hydrophilic than the phenolate site and so more likely to project into the aqueous solvent. We have been unable to obtain X-ray quality single crystals of this $\mathbf{H^W}$/**FLU** ensemble. Our previous work has clearly shown, however, that phenolate anions associate with the cage surface sufficiently strongly to displace chloride and hydroxide,[7a] and we suggest therefore that the $\mathbf{H^W}$/**FLU** interaction primarily involves the phenolate moiety of the **FLU** dianion. We tried to probe this by ^{1}H NMR spectroscopy,

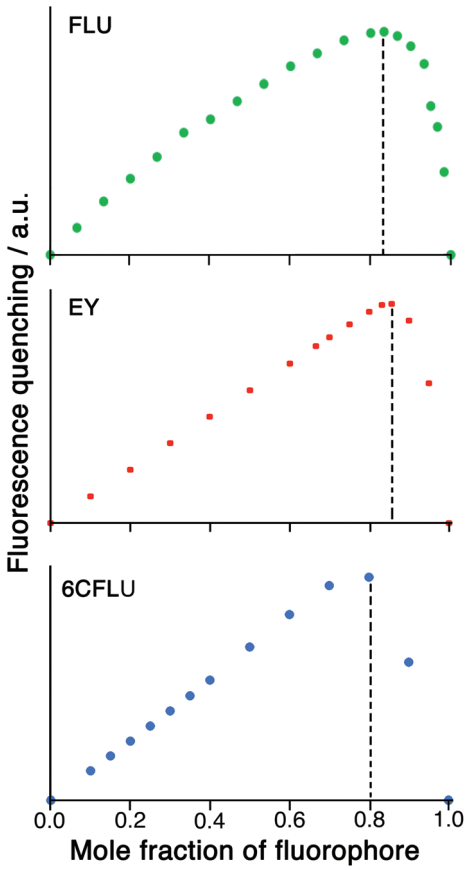

Fig. 4 Job plots illustrating the degree of fluorescence quenching associated with varying mole fractions of $\mathbf{H^W}$/fluorophore combinations for the fluorophores **FLU**, **EY** and **6CFLU**. The y-axis is the fractional decrease in luminescence at each composition compared to what would occur if all of the fluorophore were unbound, that is, it takes account of the varying amount of fluorophore at different mole fractions. The maxima occur at 0.83 (for **FLU**), 0.86 (for **EY**) and 0.80 (for **6CFLU**) consistent with formation 5 : 1, 6 : 1 and 4 : 1 fluorophore : $\mathbf{H^W}$ assemblies, respectively, which dominate the speciation at 100 μM total concentration for **FLU**/**6CFLU** and 50 μM total concentration for **EY**.

looking to see if the protons close to the phenolate unit of **FLU** (and therefore closest to the cage surface) were paramagnetically shifted/broadened to a greater extent than the protons close to the carboxylate site, for example, which might be more remote from the paramagnetic cage surface. Effectively this would use the cage as a paramagnetic shift reagent to probe the geometry of the cage/**FLU** interaction. However the substantial broadening/overlap of **FLU** signals in the presence of cage, and their overlap with cage signals in the same spectra region, meant that this experiment did not yield clear-cut results.

Similar experiments on binding to $\mathbf{H^W}$ were conducted using the related anionic fluorophores 6-carboxyfluorescein and Eosin-Y (abbreviated as **6CFLU** and **EY**, respectively; see Chart 1). These have significant differences from **FLU**, as follows: (i) the additional carboxylate group of **6CFLU** means that it has a charge of 3− compared to 2− for **FLU** under

weakly basic conditions (pK_a 3.4 for the carboxylates); (ii) eosin-Y is tetrabromofluorescein, with the same 2− charge as **FLU** but with higher hydrophobicity due to the additional Br substituents.[21] Thus we can independently change the charge, or the hydrophobicity, of the fluorescein derivative to see how these two parameters affect binding of the fluorophores to the cationic but hydrophobic surface of $\mathbf{H^W}$.

Titration of $\mathbf{H^W}$ into samples of **EY** and **6CFLU** (at 10 μM of fluorophore) in water at pH 8, in the same way as with **FLU**, immediately reveals more rapid quenching of the fluorescence than was obtained with **FLU** (Fig. 3). From the rate at which fluorescence quenching occurs on addition of $\mathbf{H^W}$ the affinity order of these fluorescein derivatives for $\mathbf{H^W}$ is clearly **FLU** < **6CFLU** < **EY**, implying that the additional hydrophobicity of **EY** compared to **FLU** is more significant than the additional negative charge of **6CFLU**. A 1 : 1 binding constant for **6CFLU** can be determined from this data with $K = 3.8 \times 10^5\ \mathrm{M}^{-1}$, however given the near-linearity of the fluorescence decrease of **EY** as $\mathbf{H^W}$ is added we cannot get reliable binding constants with this fluorophore under these conditions: but the binding affinity order (**FLU** < **6CFLU** < **EY**) is clear.

A Job plot for the **EY**/$\mathbf{H^W}$ system using a 50 μM total concentration clearly shows a sharp maximum corresponding to a 6 : 1 ratio of fluorophore to cage for **EY** (Fig. 4b). In contrast, with the **6CFLU**/$\mathbf{H^W}$ system at 100 μM total concentration the maximum in the Job plot at a mole fraction of 0.8/0.2 implies a 4 : 1 stoichiometry under these conditions (Fig. 4c) – fewer equivalents of the anionic fluorophore **6CFLU** are bound to $\mathbf{H^W}$ than was observed with **FLU**, likely due to the higher negative charge.

3.3. Binding of a different anionic fluorophore to $\mathbf{H^W}$: hydroxypyrene tris-sulfonate

Having demonstrated the ability of **FLU** to bind to $\mathbf{H^W}$, we sought to extend this behaviour using other anionic fluorophores. The next choice was hydroxypyrene tris-sulfonate (**HPTS**), also known as pyranine – another well-known fluorophore with a charge of 3− or 4− depending on the pH and whether or not the hydroxy group is deprotonated (pK_a 7.3) in addition to the three sulfonates.

Titration of portions of cage $\mathbf{H^W}$ into a solution of **HPTS** at pH 4, where the anion has a 3− charge, resulted in progressive quenching of the **HPTS** fluorescence, with complete quenching of the fluorophore occurring after addition of only 0.16 equivalents of cage (Fig. 5a). The linearity of the luminescence decrease as $\mathbf{H^W}$ is added indicates that association is at the strong binding limit even under the dilute conditions used (20 μM **HPTS**). The number of equivalents of cage needed for total quenching of **HPTS** (0.16) is also significant and suggests that each cage $\mathbf{H^W}$ is fully quenching six molecules of **HPTS**, with one **HPTS** binding to each face of the cubic host. To confirm this, a Job plot experiment was performed between $\mathbf{H^W}$ and **HPTS** at pH 4 (total concentration of species 50 μM). The maximum for this plot was seen at a mole fraction of **HPTS** of 0.86, confirming the stoichiometry as being 6 fluorophores per cage (Fig. 5b), as also observed with **EY**. It is clear

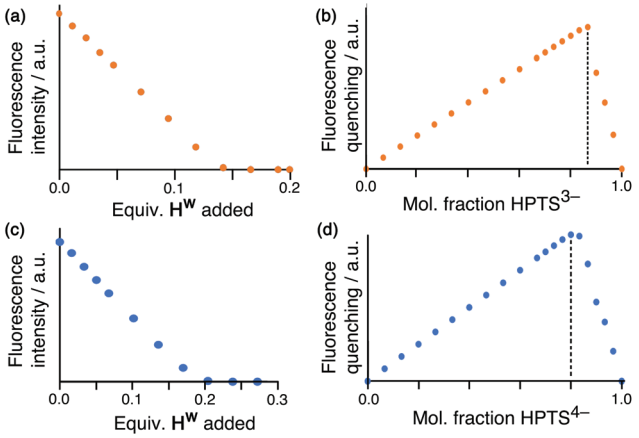

Fig. 5 Results of spectroscopic titrations of $\mathbf{H^W}$ with the fluorophore **HPTS**, using different pH values to give different charge states for **HPTS**. (a) Quenching of $(\mathbf{HPTS})^{3-}$ (at pH 4) on addition of portions of $\mathbf{H^W}$, showing a linear decrease in fluorescence consistent with binding being at the strong limit at this concentration; (b) the associated Job plot showing a maximum at a mole fraction of $(\mathbf{HPTS})^{3-}$ of 0.86, consistent with formation of a 6 : 1 $(\mathbf{HPTS})^{3-}/\mathbf{H^W}$ assembly; (c) quenching of $(\mathbf{HPTS})^{4-}$ (at pH 8) on addition of portions of $\mathbf{H^W}$, showing a linear decrease in fluorescence consistent with binding being at the strong limit at this concentration; (d) the associated Job plot showing a maximum at a mole fraction of $(\mathbf{HPTS})^{4-}$ of 0.80, consistent with formation of a 4 : 1 $(\mathbf{HPTS})^{4-}/\mathbf{H^W}$ assembly.

that **HPTS** binds more strongly to the surface of $\mathbf{H^W}$ than does **FLU**, which may partly be ascribed to its greater charge (3− *vs.* 2−).

As **HPTS** is pH sensitive and can be deprotonated through its phenol group, we conducted the same experiments at pH 8 to observe any differences in binding associated with an even greater negative charge (−4 instead of −3). Again, addition of small portions of $\mathbf{H^W}$ to a solution of **HPTS** at 20 μM under these basic conditions occurs with the same linear decrease in fluorescence intensity with added $\mathbf{H^W}$, indicative of binding at the strong limit at this concentration. However, the stoichiometry has changed with maximum quenching/minimum emission achieved after addition of 0.25 equivalents of cage as opposed to 0.16, implying that each cage $\mathbf{H^W}$ can strongly bind only four **HPTS** units when they are in the 4− state (Fig. 5c). To confirm that this number correlates to the stoichiometry of binding, a Job plot was performed and shows maximum quenching at a mole fraction of **HPTS** of 0.80, indicative of a 1 : 4 cage : $(\mathbf{HPTS})^{4-}$ stoichiometry (Fig. 5d). We ascribe this difference in the binding of $(\mathbf{HPTS})^{3-}$ (six equivalents strongly bound) and $(\mathbf{HPTS})^{4-}$ (four equivalents strongly bound) to electrostatic factors: the cage cation carries a charge of 16+, hence it only needs four $(\mathbf{HPTS})^{4-}$ units to neutralise it. Addition of fifth and then a sixth fluorophore is presumably still possible for steric reasons [*cf.* binding of six $(\mathbf{HPTS})^{3-}$ units] but if these interactions are weaker for electrostatic reasons they will not contribute significantly to the speciation behaviour at the concentration used for these measurements.

3.4. Displacement of fluorescein as the basis of an anion-binding assay

To be able to perform a displacement assay to allow us to quantify binding of anions to the surface of $\mathbf{H^W}$, we chose **FLU** as our indicator, as its binding constant to $\mathbf{H^W}$ is known, which means that the extent of displacement of **FLU** by different anions can be used to evaluate their binding constants (as we have done for our previous displacement assay for cavity-binding guests).[18a] In contrast the stronger binding of the other fluorophores such as **EY** and **HPTS**, and in particular the absence of specific *K* values for binding to $\mathbf{H^W}$, is less desirable for this purpose as the bound fluorophore would be less susceptible to displacement by competing anions. Titration experiments with different anions were performed on a 96 well plate using a plate reader, by monitoring the restoration of **FLU** fluorescence as different anions were added during the titration (see Experimental section). Each titration experiment was repeated at least twice and with a minimum of 10 data points in each repeat experiment; the resulting 1 : 1 binding constants for a range of simple anions are given in Table 1, with representative titration results in Fig. 6.

For initial tests to quantify binding of other anions to $\mathbf{H^W}$, three anions were used: chloride, sulfate and nitrate (as their sodium salts). These were selected as they differ significantly in their position in the Hofmeister series – a ranking of anions based originally on the ability of anions to aggregate proteins in solution, but which is broadly a measure of hydration and hydrophilicity.[22] Addition of salts of these anions to a solution of $\mathbf{H^W}$/**FLU** (typically a combination of 5 μM **FLU** and an excess – 50 μM – of $\mathbf{H^W}$ to ensure essentially complete binding/quenching of **FLU** by the cage) resulted in an increase in the **FLU**-based emission in all three cases as the added anions occupied cage binding sites on the $\mathbf{H^W}$ surface, resulting in displacement of **FLU** from the cage surface. This happened to different extents for a given concentration of different anion types.

The observed increase in fluorescence occurs because as the sites of $\mathbf{H^W}$ are progressively saturated by the added anion, which is in a large excess as small anions are more hydrophilic than FLU and bind to the cage more weakly, the number of free cage surface sites available for FLU to bind steadily decreases and a higher proportion of FLU remains free in solution. Given the likely complexity of the speciation behaviour, with (i) potentially six different stepwise binding constants for analyte anions progressively occupying cage surface sites, and (ii) the effect of different numbers of bound anions on electrostatic repulsion of a FLU unit in the same cage which would modulate its *K* value during a titration, there is no reason to expect that the increase in FLU emission intensity with amount of added analyte anion would show simple behaviour.

However we observed, fortunately, that the steady increase of **FLU** emission intensity as analyte anions were added could be fit to a simple 1 : 1 binding model and we have analysed the

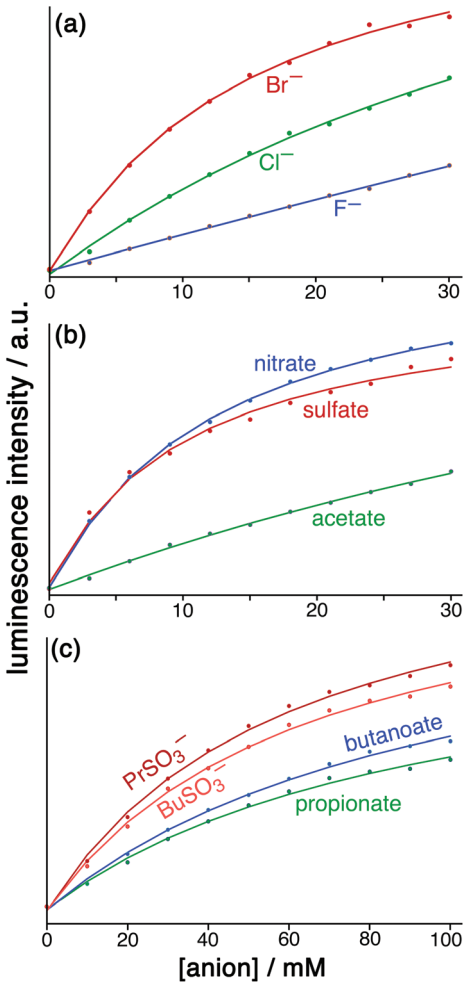

Fig. 6 Results from the displacement assay showing how addition of portions of sodium salts with various anions [(a) halides; (b) nitrate, sulfate and acetate; (c) other organic anions] to a solution containing $\mathbf{H^W}$ (50 μM) and **FLU** (5 μM) in water (pH 8.5) results in a steady increase in the fluorescence from **FLU** as it is displaced from the cage surface by the added anions which compete for the same sites, restoring the **FLU** emission. The measured data (small circles) could in all cases be fit to a 1 : 1 binding isotherm (solid lines) which takes account of the known binding constant of **FLU**, affording the anion binding constants in Table 1.

Table 1 Calculated *K* values for various organic and inorganic ions using the $\mathbf{H^w}$/**FLU** displacement assay described in the main text (water, 298 K, pH 8.5), by addition of sodium salts of the anions to either 5/50 μM **FLU**/$\mathbf{H^W}$ or 10/100 μM **FLU**/$\mathbf{H^W}$. Quoted values are from the best fits of the titration data (see *e.g.* Fig. 6) to 1 : 1 binding isotherms, repeated two or three times and averaged. Estimated uncertainty 20%

Anion	K/M^{-1}	Anion	K/M^{-1}
F^-	350	HCO_2^-	840
Cl^-	750	$CH_3CO_2^-$	470
Br^-	2900	$CH_3CH_2CO_2^-$	440
IO_3^-	470	$CH_3CH_2CH_2CO_2^-$	390
NO_3^-	3100	$CH_3CH_2CH_2SO_3^-$	530
HPO_4^{2-}	2100	$CH_3CH_2CH_2CH_2SO_3^-$	500
SO_4^{2-}	3600	Gluconate (1−)	2900
$S_2O_3^{2-}$	4000	Succinate (2−)	6500
		Malate (2−)	7600
		Tartrate (2−)	7200

data accordingly, and the resulting K values for binding of the simple anions can be compared with each other. This afforded binding constants of 750 M^{-1} for chloride, 3100 M^{-1} for nitrate and 3600 M^{-1} for sulfate (Table 1). Stronger binding of nitrate than chloride is expected based on the basis of its weaker solvation enthalpy, however the even stronger binding of sulfate to the cage goes against this trend. It seems that the high cost of desolvating the very kosmotropic sulfate ion is more than compensated for by the 2− charge which will result in stronger electrostatic interaction with the 16+ cage than occurs with nitrate and chloride, and indeed we saw the effects of increasing anion charge in the comparison of **FLU** with **6CFLU**.

Following the success of these initial experiments, a wider range of additional anions was then tested in a similar manner, again using **FLU** as the indicator species being displaced. The anions studied include (i) common inorganic anions including halides, sulfate, thiosulfate and hydrogen phosphate; (ii) organic alkyl carboxylates and alkyl sulfonates of varying carbon chain length; and (iii) a broader range of organic anions such as tartrate, gluconate, and others. Results are in Table 1.

Amongst the inorganic anions, the singly-charged species largely follow the order of the Hofmeister series: for example fluoride, chloride and bromide show 1 : 1 binding constants of 350, 750 and 2900 M^{-1} respectively, in line with their respective ease of desolvation. In contrast the dianions sulfate, thiosulfate and hydrogen phosphate have significantly higher binding constants (2000–4000 M^{-1}) for the electrostatic reasons described earlier which appear to outweigh the higher cost of desolvation for these anions.

The singly charged alkyl carboxylate and alkyl sulfonate anions all exhibit similar binding constants in the range 390–530 M^{-1}, comparable to the inorganic mono-anions. Comparison between different alkyl carboxylate anions is interesting as there is essentially no difference between the binding constants with alkyl chain length: the hydrophobicity of the anion as a whole does not make a significant difference. The implication is that the desolvation of the carboxylate unit and its interaction with the cage surface is the same in each case, with the alkyl chain projecting outwards into the solvent and therefore not undergoing a change in environment when the polar carboxylate terminus binds to the cage surface. This contrasts markedly with what happens on binding of guests inside the cage cavity, when increasing the hydrophobic content of the guest increases its binding strength in the cavity as the whole guest is removed from the aqueous phase when it binds.[6b,18a,19d] Formate is an exception here (840 M^{-1}) with a significantly higher binding constant than the alkyl carboxylates, which is consistent with a previous report that the formate ion is less well hydrated than alkyl carboxylates.[23]

We note a similar lack of sensitivity to the nature of the alkyl chain with propyl and butyl sulfonate anions whose binding constants to the cage are the same within experimental error despite the different hydrophobicities of the alkyl chains. The carboxylates however bind to $\mathbf{H^W}$ slightly less well than the sulfonates, *cf* the pair $C_3H_7SO_3^-$ and $C_3H_7CO_2^-$ which have 1 : 1 binding constants of 530 and 440 M^{-1} respectively. This implies stronger hydration of the carboxylates that the sulfonates and is also consistent with the known relative behaviour of carboxylates and alkyl sulfates.[24]

More hydrophilic organic anions such as gluconate, malate, succinate, and tartrate were also tested (as their sodium salts) with the results in Table 1. The concentrations used for these needed to be typically an order of magnitude lower than in the previous experiments as higher concentrations showed a tendency to precipitate the cage out of solution. The sequence succinate, malate and tartrate are all linear C_4 dicarboxylates but with 0, 1 and 2 additional OH groups on the carbon skeleton. All have higher binding constants (*ca.* 6500–7500 M^{-1}) than we saw for any of the mono- or di-anions discussed above which suggests that, in addition to high electrostatic interaction between the 2− anion and the 16+ cage surface, the hydrophobicity associated with the central alkyl unit facilitates binding (*cf.* the stronger binding of **EY** compared to **FLU** based on its extra hydrophobicity). The presence or absence of the OH groups appears to make little difference, however. Compared to these the mono-anion gluconate has a slightly smaller binding constant of 2900 M^{-1}, as expected, though it is substantially larger than for the simpler inorganic anions and alkyl mono-carboxylates reported in Table 1.

Given the complexity of the combination of factors underpinning the anion/cage interaction (not just electrostatics and hydrophobicity but possibly also changes of conformation associated with rigidification of flexible species;[19d] direct hydrogen-bonding interactions involving CH donors around the cage portals and different electron-rich H-bond acceptor atoms on the anions; and changes in bulk solvation associated with complex formation) we prefer not to speculate or over-analyse further. The key points from this section are that (i) this displacement assay provides a convenient and effective way to evaluate cage/anion interactions, which are of direct relevance to potential use of the cage as a vehicle for catalysis;[5,7a,10] and (ii) within the range of inorganic anions of the same charge (−1) there is a clear relation of binding constant of anion with its position in the Hofmeister series, such that less well solvated anions (such as bromide) bind more strongly to $\mathbf{H^W}$ than more highly solvated anions (such as fluoride).

3.5. Stabilisation of anionic species through association with the cage $\mathbf{H^W}$

Having investigated the interaction between a range of anionic species and the exterior surface of $\mathbf{H^W}$, we turned our attention to investigating any possible stabilisation of these anions imparted through the association with the cationic cage surface. Raymond *et al.* reported a stabilisation of ammonium cations by *ca.* 4 pH units inside a highly anionic cage: this ability of the anionic cage to stabilise protonated species could be used to facilitate acid-based catalysis of bound guests even under basic conditions.[25] To see whether a similar pK_a shift was observable between the cage $\mathbf{H^W}$ and anionic species, we

monitored the behaviour of the pH indicators phenolphthalein (**PP**) and bromocresol purple (**BCP**) as surface-bound guests during a pH titration.

In the first experiment (in contrast to others reported in this paper) the concentration of both the host cage (40 μM) and **PP** (80 μM) remain constant; the ratio of cage : **PP** and the concentration are sufficient to ensure near-complete binding of **PP** to the surface sites of $\mathbf{H^W}$. Starting at a pH of 4.22 (unbuffered), the pH was increased by sequential additions of 0.1 M NaOH solution. A UV/Vis spectrum was recorded after each addition and the absorbance at 560 nm plotted against the pH. This was repeated without cage present and the two resulting curves compared. For free **PP** the onset of the characteristic pink colour occurred at pH 8.7; in the presence of $\mathbf{H^W}$ the same optical density was achieved by pH 8.0 indicating that the dianionic form of **PP** (containing a carboxylate and a phenolate, resulting from opening of the lactone ring) is being stabilised by its interaction with $\mathbf{H^W}$. However we could not get a complete pH titration curve for this experiment because as the pH was raised further precipitation occurred, probably because of formation of an insoluble $\mathbf{H^W}$/(phenolphthalein anion) complex or decomposition of $\mathbf{H^W}$ under more strongly basic conditions.

To avoid the problems associated with using high pH, a similar experiment was performed but using **BCP** which has a pK_a of 6.3 compared to 9.4 for **PP**: in its dianionic form it contains both sulfonate and phenolate anionic centres. With both $\mathbf{H^W}$ and **BCP** at a concentration of 50 μM, monitoring the absorbance during a steady increase in pH by addition of aqueous NaOH provided a full sigmoidal curve characteristic of an acid–base titration (Fig. 7) with the mid-points giving pK_a values in our hands of 7.0 for **BCP** on its own but 5.9 in the presence of $\mathbf{H^W}$. Thus, the surface-bound dianion is stabilised by ≈1 pK_a unit by its interaction with the 16+ exterior surface of $\mathbf{H^W}$. This is smaller than the effect than seen by Raymond and co-workers,[25] but in their case the guest was fully encapsulated inside the cavity of a 12− cage and therefore was positioned much closer to a larger number of stabilising opposite charges. The effect of stabilisation of the surface-bound anion in this case however is clear.

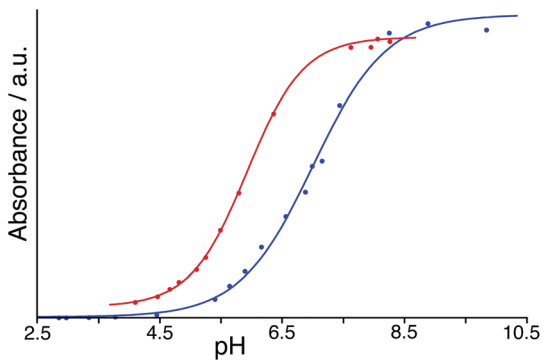

Fig. 7 pH titrations showing the change in absorbance arising from deprotonation of **BCP** in the absence (blue), and presence (red), of excess $\mathbf{H^W}$ in water. Derived pK_a values are in the main text; the stabilisation of the deprotonated form of **BCP** by *ca.* 1 pK_a unit in the presence of $\mathbf{H^W}$ is clear. In both cases small circles represent measured data and the solid lines represent the best calculated fit to a pH curve.

4. Conclusions

In this work we have examined systematically the interaction of our cationic, cubic coordination cage $\mathbf{H^W}$ with anions at the surface binding sites. This is a much less well trodden path (both for us with this particular cage host, and more broadly for the field of coordination cages in general) than the study of binding of small-molecule guests in the central cavity: although less obvious, it is however just as important for understanding the catalysed reactions of cavity-bound guests with surface-bound anions.[7a]

Aromatic organic fluorophores which are anionic (**FLU** and some derivatives; **HPTS** in its two different charge states) bind strongly to the surface of $\mathbf{H^W}$ with quenching of fluorescence, with binding driven by a combination of electrostatic factors and hydrophobicity. These fluorophores are all too large to bind inside the cavity, but are proposed to interact with the cage exterior surface in the windows at the centre of each face where small inorganic anions have been shown to bind from X-ray crystallography experiments. Surface binding of these aromatic anions was further supported by Job plot experiments which showed fluorophore : $\mathbf{H^W}$ ratios of 4 : 1, 5 : 1 or 6 : 1 (depending on charge and hydrophobicity of the fluorophore) with the maximum observed ratio of 6 : 1, shown by both **EY** and $(\mathbf{HPTS})^{3-}$, indicating that one anion interacts with every surface of the cubic cage $\mathbf{H^W}$. These interactions are strong with the weakest binder (**FLU**) having $K \approx 1 \times 10^5$ M^{-1}, **6CFLU** having $K \approx 4 \times 10^5$ M^{-1} (for binding of the fluorophore to one face of the cage), and **EY** being at the strong binding limit even at the dilute concentrations used.

Using **FLU** as the indicator, a fluorescence displacement assay has been developed which allows us to determine the affinity of a range of other anions to the surface of $\mathbf{H^W}$ according to how well increasing concentrations of the analyte anions displace **FLU** and restore its fluorescence. The affinity of a range of simple inorganic anions for $\mathbf{H^W}$ broadly follows the Hofmeister series for 1− species with the most strongly solvated anions such as fluoride binding the most weakly. However the inorganic dianions SO_4^{2-}, $S_2O_3^{2-}$ and HPO_4^{2-} do not follow the Hofmeister series, with the higher cost of desolvating them being more than compensated for by electrostatic factors given the 16+ charge on the cage, such that they bind more strongly to $\mathbf{H^W}$ than do mono-anions such as halides. Organic dicarboxylates bind considerably more strongly, possibly due to the hydrophobicity of their alkyl skeleton, though these are still much weaker binders than the aromatic fluorophores such as $(\mathbf{FLU})^{2-}$ which have a much more substantial hydrophobic surface area.

Finally, a pH titration shows that the anionic form of bromocresol purple is stabilised by ≈1 pK_a unit in the presence of $\mathbf{H^W}$ due to its interaction with the cationic surface. This is

similar in principle to, but smaller in magnitude than, the pK_a shifts seen by Raymond and co-workers for guests that were fully encapsulated inside the cavity of a highly charged cage host.

In conclusion, the ability to measure the interaction of $\mathbf{H^W}$ with anions at its exterior surface complements the well-understood host guest chemistry associated with the central cavity: and since both recognition components are required for the catalytic processes that we have seen, we will be able to build on this to develop more effective catalytic processes in which cavity-bound neutral molecules react with surface-bound anions.

Author contributions

MDL performed all experimental work and analysed the data. MDW conceived and supervised the project. MDL and MDW contributed equally to writing the manuscript.

Conflicts of interest

There are no conflicts to declare.

Acknowledgements

We thank EPSRC for a PhD studentship to MDL (grant number EP/N509796/1); the University of Warwick for additional financial support; and Prof. Chris Hunter (University of Cambridge) for valuable discussions and provision of the software used to determine binding constants (ref. 18*a*).

Notes and references

1 (*a*) T. R. Cook and P. J. Stang, *Chem. Rev.*, 2015, **115**, 7001; (*b*) T. R. Cook, Y.-R. Zheng and P. J. Stang, *Chem. Rev.*, 2013, **113**, 734; (*c*) R. Chakrabarty, P. S. Mukherjee and P. J. Stang, *Chem. Rev.*, 2011, **111**, 6810; (*d*) M. M. J. Smulders, I. A. Riddell, C. Browne and J. R. Nitschke, *Chem. Soc. Rev.*, 2013, **42**, 1728; (*e*) D. Zhang, T. K. Ronson and J. R. Nitschke, *Acc. Chem. Res.*, 2018, **51**, 2423; (*f*) H. Vardhan, M. Yusubov and F. Verpoort, *Coord. Chem. Rev.*, 2016, **306**, 171.

2 (*a*) Y. Fang, J. A. Powell, E. Li, Q. Wang, Z. Perry, A. Kirchon, X. Yang, Z. Xiao, C. Zhu, L. Zhang, F. Huang and H.-C. Zhou, *Chem. Soc. Rev.*, 2019, **48**, 4707; (*b*) C. J. Brown, F. D. Toste, R. G. Bergman and K. N. Raymond, *Chem. Rev.*, 2015, **115**, 3012; (*c*) M. Yoshizawa, J. K. Klosterman and M. Fujita, *Angew. Chem., Int. Ed.*, 2009, **48**, 3418; (*d*) M. Otte, *ACS Catal.*, 2016, **6**, 6491; (*e*) C. M. Hong, R. G. Bergman, K. N. Raymond and F. D. Toste, *Acc. Chem. Res.*, 2018, **51**, 2447; (*f*) W.-X. Gao, H.-N. Zhang and G.-X. Jin, *Coord. Chem. Rev.*, 2019, **386**, 69.

3 (*a*) Y. Sun, C. Chen, J. Liu and P. J. Stang, *Chem. Soc. Rev.*, 2020, **49**, 3889; (*b*) M. Zhang, M. L. Saha, M. Wang, Z. Zhou, B. Song, C. Lu, X. Yan, X. Li, F. Huang, S. Yin and P. J. Stang, *J. Am. Chem. Soc.*, 2017, **139**, 5067; (*c*) C.-L. Liu, R.-L. Zhang, C.-S. Lin, L.-P. Zhou, L.-X. Cai, J.-T. Kong, S.-Q. Yang, K.-L. Han and Q.-F. Sun, *J. Am. Chem. Soc.*, 2017, **139**, 12474; (*d*) J. Wang, C. He, P. Wu, J. Wang and C. Duan, *J. Am. Chem. Soc.*, 2011, **133**, 12402; (*e*) Y. Jiao, J. Wang, P. Wu, L. Zhao, C. He, J. Zhang and C. Duan, *Chem. – Eur. J.*, 2014, **20**, 2224; (*f*) X.-Z. Li, L.-P. Zhou, L.-L. Yan, D.-Q. Yuan, C.-S. Lin and Q.-F. Sun, *J. Am. Chem. Soc.*, 2017, **139**, 8237.

4 (*a*) A. B. Grommett and J. R. Nitschke, *J. Am. Chem. Soc.*, 2017, **139**, 2176; (*b*) A. Garci, J.-P. Mbakidi, V. Chaleix, V. Sol, E. Orhan and B. Therrien, *Organometallics*, 2015, **34**, 4138; (*c*) T. Grancha, A. Carné-Sánchez, L. Hernández-López, J. Albalad, I. Imaz, J. Juanhuix and D. Maspoch, *J. Am. Chem. Soc.*, 2019, **141**, 18349; (*d*) A. M. Castilla, T. K. Ronson and J. R. Nitschke, *J. Am. Chem. Soc.*, 2016, **138**, 2342; (*e*) S. Löffler, J. Lübben, L. Krause, D. Stalke, B. Dittrich and G. H. Clever, *J. Am. Chem. Soc.*, 2015, **137**, 1060; (*f*) W. Cullen, S. Turega, C. A. Hunter and M. D. Ward, *Chem. Sci.*, 2015, **6**, 625.

5 M. D. Ward, C. A. Hunter and N. H. Williams, *Acc. Chem. Res.*, 2018, **51**, 2073.

6 (*a*) I. S. Tidmarsh, T. B. Faust, H. Adams, L. P. Harding, L. Russo, W. Clegg and M. D. Ward, *J. Am. Chem. Soc.*, 2008, **130**, 15167; (*b*) M. Whitehead, S. Turega, A. Stephenson, C. A. Hunter and M. D. Ward, *Chem. Sci.*, 2013, **4**, 2744; (*c*) M. D. Ward, C. A. Hunter and N. H. Williams, *Chem. Lett.*, 2017, **46**, 2.

7 (*a*) W. Cullen, A. J. Metherell, A. B. Wragg, C. G. P. Taylor, N. H. Williams and M. D. Ward, *J. Am. Chem. Soc.*, 2018, **140**, 2821; (*b*) J. R. Piper, L. Cletheroe, C. G. P. Taylor, A. J. Metherell, J. A. Weinstein, I. V. Sazanovich and M. D. Ward, *Chem. Commun.*, 2017, **53**, 408.

8 B. Hasenknopf, J.-M. Lehn, B. O. Kneisel, G. Baum and D. Fenske, *Angew. Chem., Int. Ed. Engl.*, 1996, **35**, 1838.

9 (*a*) B. L. Schottel, H. T. Chifotides and K. R. Dunbar, *Chem. Soc. Rev.*, 2008, **37**, 68; (*b*) J.-F. Ayme, J. E. Beves, D. A. Leigh, R. T. McBurney, K. Rissanen and D. Schultz, *J. Am. Chem. Soc.*, 2012, **134**, 9488; (*c*) S. P. Argent, H. Adams, T. Riis-Johannessen, J. C. Jeffery, L. P. Harding, O. Mamula and M. D. Ward, *Inorg. Chem.*, 2006, **45**, 3905.

10 W. Cullen, M. C. Misuraca, C. A. Hunter, N. H. Williams and M. D. Ward, *Nat. Chem.*, 2016, **8**, 231.

11 F. J. Rizzuto, W. Y. Wu, T. K. Ronson and J. R. Nitschke, *Angew. Chem., Int. Ed.*, 2016, **55**, 7958.

12 I. A. Riddell, M. M. J. Smulders, J. K. Clegg, Y. R. Hristove, B. Breiner, J. D. Thoburn and J. R. Nitschke, *Nat. Chem.*, 2012, **4**, 751.

13 N. Mihara, T. K. Ronson and J. R. Nitschke, *Angew. Chem.*, 2019, **58**, 12497.

14 C. Sgarlata, J. S. Mugridge, M. D. Pluth, B. E. F. Tiedemann, V. Zito, G. Arena and K. N. Raymond, *J. Am. Chem. Soc.*, 2010, **132**, 1005.

15 B. Li, B. Zheng, W. Zhang, D. Zhang, X.-J. Yang and B. Wu, *J. Am. Chem. Soc.*, 2020, **142**, 6304.
16 A. C. Stelson, C. M. Hong, M. C. Groenenboom, C. A. E. Little, J. C. Booth, N. D. Orloff, R. G. Bergman, K. N. Raymond, K. A. Schwarz, F. D. Toste and C. J. Long, *Commun. Chem.*, 2019, **2**, 54.
17 (*a*) B. T. Nguyen and E. V. Anslyn, *Coord. Chem. Rev.*, 2006, **250**, 3118; (*b*) L. You, D. Zha and E. V. Anslyn, *Chem. Rev.*, 2015, **115**, 7840.
18 (*a*) S. Turega, W. Cullen, M. Whitehead, C. A. Hunter and M. D. Ward, *J. Am. Chem. Soc.*, 2014, **136**, 8475; (*b*) J. S. Train, A. B. Wragg, A. Auty, A. J. Metherell, D. Chekulaev, C. G. P. Taylor, S. P. Argent, J. A. Weinstein and M. D. Ward, *Inorg. Chem.*, 2019, **58**, 2386.
19 (*a*) W. Cullen, S. Turega, C. A. Hunter and M. D. Ward, *Chem. Sci.*, 2015, **6**, 2790; (*b*) W. Cullen, K. A. Thomas, C. A. Hunter and M. D. Ward, *Chem. Sci.*, 2015, **6**, 4025; (*c*) C. G. P. Taylor, S. P. Argent, M. D. Ludden, J. R. Piper, C. Mozaceanu, S. A. Barnett and M. D. Ward, *Chem. – Eur. J.*, 2020, **26**, 3054; (*d*) C. G. P. Taylor, W. Cullen, O. M. Collier and M. D. Ward, *Chem. – Eur. J.*, 2017, **23**, 206; (*e*) A. J. Metherell, W. Cullen, N. H. Williams and M. D. Ward, *Chem. – Eur. J.*, 2018, **24**, 1554.
20 (*a*) P. Thordarson, *Chem. Soc. Rev.*, 2011, **40**, 1305; (*b*) F. Ulatowski, K. Dabrowa, T. Balakier and J. Jurkzac, *J. Org. Chem.*, 2016, **81**, 1746; (*c*) D. B. Hibbert and P. Thordarson, *Chem. Commun.*, 2016, **52**, 12792.
21 A. Priimagi, G. Cavallo, P. Metrangelo and G. Resnati, *Acc. Chem. Res.*, 2013, **46**, 2686.
22 (*a*) K. D. Collins and M. W. Washabaugh, *Q. Rev. Biophys.*, 1985, **18**, 323; (*b*) M. G. Cacace, E. M. Landau and J. J. Ramsden, *Q. Rev. Biophys.*, 1997, **30**, 241; (*c*) R. J. Clarke and C. Lupfert, *Biophys. J.*, 1999, **76**, 2614.
23 Y. Koga, *Phys. Chem. Chem. Phys.*, 2013, **15**, 14548.
24 N. Vlachy, B. Jagoda-Cwiklik, R. Vácha, D. Touraud, P. Jungwirth and W. Kunz, *Adv. Colloid Interface Sci.*, 2009, **146**, 42.
25 (*a*) M. D. Pluth, R. G. Bergman and K. H. Raymond, *Science*, 2007, **316**, 85; (*b*) M. D. Pluth, R. G. Bergman and K. N. Raymond, *Acc. Chem. Res.*, 2009, **42**, 1650.

Chemical Science

ROYAL SOCIETY OF CHEMISTRY

EDGE ARTICLE

View Article Online
View Journal | View Issue

Check for updates

Cite this: *Chem. Sci.*, 2021, **12**, 12640

All publication charges for this article have been paid for by the Royal Society of Chemistry

Orthogonal binding and displacement of different guest types using a coordination cage host with cavity-based and surface-based binding sites†

Michael D. Ludden, Christopher G. P. Taylor and Michael D. Ward *

The octanuclear Co(II) cubic coordination cage system **H** (or $\mathbf{H^W}$ if it bears external water-solubilising substituents) has two types of binding site for guests. These are (i) the partially-enclosed central cavity where neutral hydrophobic organic species can bind, and (ii) the six 'portals' in the centres of each of the faces of the cubic cage where anions bind *via* formation of a network of CH···X hydrogen bonds between the anion and CH units on the positively-charged cage surface, as demonstrated by a set of crystal structures. The near-orthogonality of these guest binding modes provides the basis for an unusual dual-probe fluorescence displacement assay in which either a cavity-bound fluorophore (4-methyl-7-amino-coumarin, **MAC**; λ_{em} = 440 nm), or a surface-bound anionic fluorophore (fluorescein, **FLU**; λ_{em} = 515 nm), is displaced and has its emission 'switched on' according to whether the analyte under investigation is cavity-binding, surface binding, or a combination of both. A completely orthogonal system is demonstrated based using a $\mathbf{H^W}$/**MAC**/**FLU** combination: addition of the anionic analyte ascorbate displaced solely **FLU** from the cage surface, increasing the 515 nm (green) emission component, whereas addition of a neutral hydrophobic guest such as cyclooctanone displaced solely **MAC** from the cage central cavity, increasing the 440 nm (blue) emission component. Addition of chloride results in some release of both components, and an intermediate colour change, as chloride is a rare example of a guest that shows both surface-binding and cavity-binding behaviour. Thus we have a colourimetric response based on differing contributions from blue and green emission components in which the specific colour change signals the binding mode of the analyte. Addition of a fixed red emission component from the complex $[Ru(bipy)_3]^{2+}$ (**Ru**) provides a baseline colour shift of the overall colour of the luminescence closer to neutral, meaning that different types of guest binding result in different colour changes which are easily distinguishable by eye.

Received 4th August 2021
Accepted 24th August 2021

DOI: 10.1039/d1sc04272f

rsc.li/chemical-science

1 Introduction

Coordination cages – hollow, pseudo-spherical metal/ligand assemblies – are well known to be able to bind small molecular guests in their central cavities,[1] with a range of consequences for, and potential applications in, areas such as catalysis,[2] sensing[3] and transport.[4] The focus on guest binding has mostly been occupancy of these central cavities, as they present an obvious binding site with well-defined size, shape and (sometimes) functional group characteristics which obviously relate to their molecular recognition properties.

More recently, we[5,6] and others[7,8] have noticed that the exterior surfaces of cages also provide recognition sites for, principally, ionic guests. The same characteristics of the interior surface of a cage (hydrophobicity arising from organic ligand components; charge density arising from metal ion vertices; possibly the presence of functional groups) that facilitate guest binding can also exist at the exterior surfaces. Although – by definition – the exterior surfaces are not enclosed and do not provide the clearly defined three-dimensional cavities that the interior surfaces provide, they still offer opportunities for cages to interact with small molecules or ions. In particular, in our octanuclear M_8L_{12} cubic cage family $\mathbf{H}/\mathbf{H^W}$ (Fig. 1), the portals in the cage faces provide a preorganised cyclic array of multiple weak CH hydrogen-bond donors from the ligand array, and – according to crystallographic evidence obtained with many different anions – these converge on an anion that is located in the portal.[5a]

Thus the $\mathbf{H}/\mathbf{H^W}$ cages combine both a central cavity for binding of hydrophobic organic guests, whose binding strength correlates with hydrophobic surface area;[9] and surface-binding sites for anions, with the binding strength of the anion correlating with the ease of desolvation of the anion.[6] A recent

Department of Chemistry, University of Warwick, Coventry CV4 7AL, UK. E-mail: m.d.ward@warwick.ac.uk

† Electronic supplementary information (ESI) available: Summary of crystallographic data and brief discussion; experimental protocols associated with the assays. CCDC 2101190–2101194. For ESI and crystallographic data in CIF or other electronic format see DOI: 10.1039/d1sc04272f

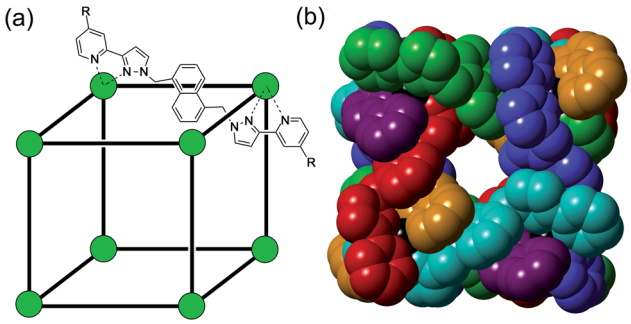

Fig. 1 The host cage $[Co_8L_{12}]^{16+}$, abbreviated as H^W (R = CH_2OH) or **H** (R = H). (a) A sketch emphasising the cubic array of Co(II) ions and the disposition of one bridging ligand; (b) a space-filling view of the core (without the CH_2OH substituents) showing each ligand coloured separately for clarity.

example of the importance of this combination is the efficient cage-based catalysis of the Kemp elimination reaction of benzisoxazole with hydroxide to give 2-cyanophenolate, using the cage $\mathbf{H^W}$ as the catalyst.[10] The cage-based catalysis (>10^5 fold rate enhancement, depending on pH) relies on a shell of surface-bound and hence partially desolvated hydroxide ions, attracted to the portals around the cage surface by the high positive charge of the cage, being brought into close proximity to the neutral benzisoxazole guest which is bound in the central cavity. Thus, cavity-binding of a neutral hydrophobic guest, and electrostatically-driven surface-binding of hydroxide ions, cooperate very effectively to promote catalysis by co-locating the two reaction partners using different interactions: even under weakly basic conditions (pH 8 in bulk solution) the accumulation of hydroxide ions at the cage surface, surrounding the cavity-bound guest, is such that the *local* pH in the cavity is effectively 13–14.[5a]

We have used fluorescence-based methods to investigate both types of guest binding associated with $\mathbf{H^W}$, as the cage quenches fluorescent guests which bind either in the cavity or at the surface-based sites. Thus 4-methyl-7-amino-coumarin (**MAC**) binds in the central cavity in water, principally due to its hydrophobicity, and its fluorescence is quenched by the nearby Co(II) ions.[9a] Similarly the di-anionic fluorophore fluorescein (**FLU**) is an exterior surface binder, anchored to the portals in the six face centres, and is likewise quenched on binding by proximity to the Co(II) ions.[6] These effects have been used independently as the basis of two different types of fluorescence displacement assay (FDA) – a measurement of a binding constant in which the analyte under evaluation competitively displaces a fluorescent (but quenched) indicator, whose binding constant is known. The binding of the analyte can then be evaluated from how much of the fluorescence from the indicator is restored when it is displaced by the analyte which competes for the same binding site.[11] In the first case binding of neutral organic guests in the cavity of $\mathbf{H^W}$ displaces (and restores fluorescence from) a cavity-bound **MAC** molecule, which allows binding of a wide range of non-chromophoric guests to be evaluated.[9a] In the second case displacement of **FLU** from the cage surface by a range of simple organic and inorganic anions restored its florescence, likewise allowing binding constants of the various anions for the surface binding sites to be evaluated.[6] Such analyses have allowed us to probe independently the affinities of different guests for either cavity- or surface-based binding sites on the same cage host using quite distinct interactions.

Accordingly in this paper we report further studies, both crystallographic and solution-based, into the ability of the **H**/$\mathbf{H^W}$ cage system to participate in cavity-based and surface-based binding of different types of guest independently of one another. In the first part of the paper we report crystallographic studies showing how 'crystalline sponge' experiments can be performed with a combination of cavity-based and surface-based guests, to introduce a guest into the cavity of a host cage **H** and also to change the anion shell surrounding it, in single-crystal to single-crystal transformations.[12] In the second part of the paper we describe how the two different types of FDA can be combined in a single analytical process, allowing evaluation of the ability of specific guests to occupy the cavity or surface sites of $\mathbf{H^W}$ in solution a single experiment, giving a unique colorimetric response according to how much of the distinct cavity-bound and surface-bound fluorescent indicators are displaced by a particular type of analyte. Whilst there have been some examples of displacement assays that use different spectroscopic measurements on the same displaced dye to report on different aspects of guest binding (*e.g.* both concentration and enantiomeric excess of a chiral amine binding),[13] we believe this to be the first example of such an assay based on independent displacements of two different fluorescent indicators that are bound in different ways to the same host.

These demonstrations of the independence of the two types of cage/guest interaction, both in crystalline sponge experiments and in solution, will in addition extend our ability to develop new supramolecular catalysts. Given that the potential generality of this type of cage-based catalysis is driven by the ability to surround any cavity-binding organic guest with a high local concentration of any surface-binding ion,[5a] being able to control binding of both components independently of one another will be the basis of further progress in identifying catalytic process that can be mediated by the cage.

2 Results and discussion

2.1. Crystalline sponge experiments showing combined guest uptake and anion exchange

We have reported many examples of cage/guest complexes that were prepared using the crystalline sponge method, whereby X-ray quality single crystals of the cage **H** were soaked in a pure organic guest (if the guest is an oil), or a concentrated solution of the guest in MeOH, for several hours. This can result in uptake of guest into the cage cavity without loss of crystallinity.[5a,14] As-prepared crystals of **H** contain a network of methanol molecules in the cage cavity, and BF_4^- counter-anions, some of which occupy the portals around the cage surface.[15] Interestingly, although the counter-ions occupy the portals and apparently block access to the cage interior, guests

are still taken up into the cavity during these crystalline sponge experiments which implies that a considerable degree of dynamic behaviour in the crystals is possible at room temperature without loss of crystallinity. Crystals of **H** can also undergo anion-exchange in the same way, with immersion of **H** crystals in concentrated methanolic Bu_4NI resulting in the fluoroborate anions surrounding the cage being replaced by iodide anions in the cage portals.[5b] Thus we have demonstrated how crystalline sponge experiments with **H** can be used to introduce either cavity-bound guests or to replace surface-bound anions. Here, we show that both can be accomplished in a single experiment.

Single crystals of **H** (tetrafluoroborate salt) prepared by the usual solvothermal method[15] were soaked for several hours in concentrated methanolic solutions containing both a known cavity-binding guest (**MAC**) and the tetrabutylammonium salt of the desired replacement anion (iodide, nitrate, hexafluorophosphate, triflate, sulfate). Subsequent X-ray diffraction experiments confirmed that in some cases *both* types of guest had been taken up, with **MAC** occupying the cage cavity and the new anion type displacing tetrafluoroborate from the binding sites around the cage surface.

In **H·MAC·I** (Fig. 2) the cage cavity contains one **MAC** guest and a pair of MeOH molecules (25% fractional site occupancy each in the asymmetric unit which consists of one half of the cage: hence one MeOH total), mutually disordered over the inversion centre at the centre of the cage cavity; additionally, iodide anions have replaced the fluoroborate anions in the portals around the cage surface (Fig. 2a). As usual the cavity-binding neutral guest molecule displays H-bonding interactions with the H-bond donor pockets of the cage interior: these pockets are formed at the two *fac* tris-chelate vertices at opposite ends of the cavity, by a convergent collection of CH protons which lie close to a Co(II) ion and are therefore in a region of high positive electrostatic potential.[16] Given the disorder of the **MAC** guest with the MeOH molecules a detailed analysis of the H-bonding interactions is inappropriate but the presence of multiple CH···O interactions, with H···O distances in the range 2.5–2.8 Å between cage interior surface and electron rich regions of the **MAC** guest, is clear and these are emphasised in Fig. 2c. Some of the iodide ions around the cage surface likewise display disorder over two closely-spaced positions, but atom I(2) has 100% occupancy, and the space-filling view in Fig. 2b shows how nicely this iodide ion sits in the portal on the 16+ cage surface, surrounded by CH protons from the ligands. Iodide is of course a weak hydrogen-bond acceptor.[17] Many of the H···I distances in this cyclic array are longer than the sum of the van der Walls radii and therefore constitute very weak interactions, but the I(2)···H(13A) distance is 3.03 Å and some others are in the range 3.1–3.2 Å. Overall we could explicitly locate 13.6 iodide anions per 16+ complex cation. It is worth pointing out that with tetrafluoroborate rather than iodide as the counter-anion, the crystalline sponge experiment to absorb **MAC** results in uptake of a stacked pair of guests into the cage cavity.[14] In this new structure of **H·MAC·I** however, one of the surface-bound iodide ions forms an OH···I hydrogen-bonding interaction with one of the MeOH molecules in the cavity (O···I separation 3.34 Å); hence the nature of the surface bound ion is having an effect on what is bound into the central cavity in the crystalline state.

H·MAC·(NO_3) (Fig. 3) behaves similarly to the iodide salt, in that there is one **MAC** guest with 0.55 site occupancy, disordered with a MeOH molecule having a site occupancy of 0.35 on the other side of the cavity. This means a total average occupancy of 1.1 **MAC** guests and 0.7 MeOH guests, requiring that some cage molecules in this crystalline sample contain a stacked pair of **MAC** guests: *e.g.* we could have 55% of the

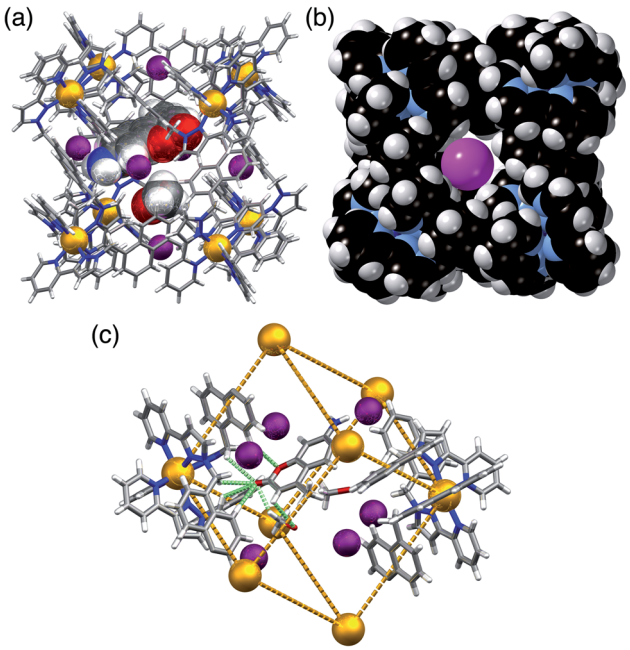

Fig. 2 Views of the crystal structure of H·MAC·I. (a) A view of the complete cage showing the array of six surface-bound iodide anions (purple) as well as the cavity-bound guests (one MAC and one MeOH) shown space-filling. (b) A space-filling view of the cage looking onto one of the faces, emphasising the binding of the iodide anion I(2) (which has 100% occupancy) in the surface portals. (c) Partial view of the cage host, showing the six iodide guests, and showing the H-bonding interactions between MAC and the cage interior surface (green dashed lines indicate CH···O contacts with H···O separations of <3 Å).

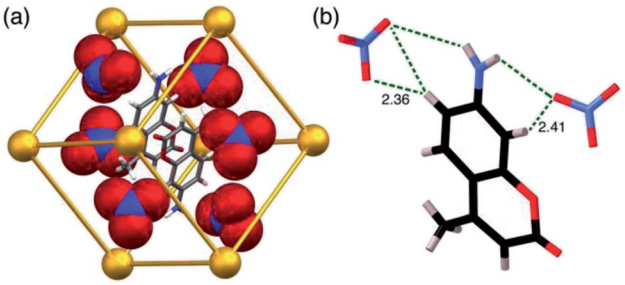

Fig. 3 Views of the crystal structure of H·MAC·(NO_3). (a) A view showing the metal ions that define the cubic cage, the MAC guests, and the array of six nitrate anions around the surface (shown space-filling); (b) a view showing CH···O and NH···O interactions between a MAC guest and two of the surrounding nitrate anions.

molecules in the crystal containing a stacked pair of **MAC** guests and the remaining 45% of the molecules containing only MeOH. The anion exchange from BF_4^- to nitrate is incomplete, with the lattice containing 13 nitrate ions and three BF_4^- anions per cage complex cation; however the positions in the cage portals are all occupied by the nitrate anions (Fig. 3a). Again we see hydrogen-bonding interactions between cavity-bound and surface bound guests: Fig. 3b highlights the CH···O and NH···O interactions between the **MAC** guest and the surface-bound nitrate anions. The nitrate anions also form a network of CH···O contacts (≥2.5 Å for the O···H distances) with CH units from the ligand array around the portals in the same way as seen for the other anions.

A similar experiment using **MAC** as the cavity-bound component coupled with Bu_4NPF_6 to provide anion-exchange affords **H·MAC·(PF$_6$)**. Again we see a set of six surface-bound anions surround in the central cavity, but the cavity now contains a stacked pair of **MAC** guests (Fig. 4) which have site occupancies of 1 each, *i.e.* two per cage cavity, so the occupancy in the crystal is complete. The arrangement of this stacked guest pair is very similar to what we have reported before,[14] although in this case the two guests are crystallographically inequivalent rather than being related by inversion. The H-bonding of each **MAC** carbonyl group with the H-bond donor pockets on the cage interior is clear with multiple CH···O contacts having H···O separations as low as 2.44 Å, with all such contacts of <3 Å highlighted in Fig. 4a. The hexafluorophosphate anions again occupy the cage portals, making multiple CH···F contacts with the surrounding ligand array of which the shortest is 2.43 Å (Fig. 4b). The view in Fig. 4c emphasises how the octahedral array of anions surrounds and interacts with the stacked pair of cavity-bound guests. Specifically each **MAC** guest has outwardly-directed CH (two aromatic, plus one from the methyl group) and NH protons which project towards the portals and form H···F contacts with F atoms of nearby hexafluorophosphate anions, with H···F contacts as short as 2.33 (for an NH···F contact) and 2.48 Å (for a CH···F contact). Given the positional disorder of some of the F atoms in the hexafluorophosphate anions these distances should not be over-analysed: but the general picture of multiple H-bonding contacts between cavity-bound guests and the surface-bound anions, as shown in Fig. 4c, is clear: and we note that this accessibility of cavity-bound guests to surface-bound anions underpins the catalytic activity that we observed in previous studies.[5,10]

H·MAC·(SO$_4$) (Fig. 5) has guest occupancies similar to those of the iodide salt, with site occupancies of 0.5 per **MAC** and 0.5 per MeOH in each half of the cage, summing to one of each per cage. This is the first instance of a structurally-characterised cage of this family containing a dianion. The sulfates behave similarly to the mono-anions described above in that some of them occupy portals on the cage surface surrounding the cavity-bound guest, participating in CH···O contacts with the ligands that define the portals (Fig. 5). However only four of the six portals contain an embedded sulfate anion (Fig. 5a), which are involved in multiple CH···O interactions with H···O distances down to 2.5 Å with the surrounding ligand array. In addition, there are some hydrogen-bonding contacts between a surface-bound sulfate and cavity-bound **MAC** guest with a CH···O interaction involving an aromatic CH of the guest having an H···O separation of just 2.33 Å, and an NH···O interaction with the coumarin amine group having an H···O separation of 2.67 Å. The **MAC** guest shows the usual H-bonding interactions with the cage interior surface that have been described before.

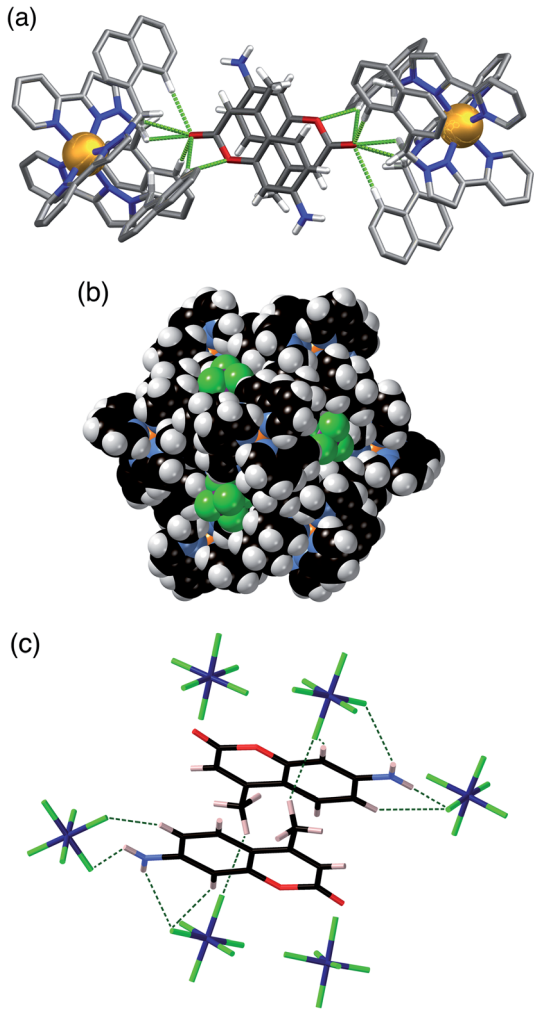

Fig. 4 Views of the crystal structure of **H·MAC·(PF$_6$)**. (a) A view showing the stacked pair of **MAC** guests with part of the surrounding cage, emphasising the H-bonding interactions between inwardly-directed CH protons on the cage surface and the **MAC** guests: CH···O interactions with H···O distances of <3 Å are shown by green dotted lines. (b) A space-filling view of the cage looking onto one of the metal vertices, emphasising the binding of the hexafluorophosphate anions (green) in the surface portals. (c) The array of six hexafluorophosphate anions surrounding the two cavity-bound **MAC** molecules, with short (<3 Å) H···F contacts between **MAC** and $[PF_6]^-$ anions arising from CH···F or NH···F interactions shown by green dotted lines.

H·(CF$_3$SO$_3$) is unusual, and particularly significant for the purposes of this work, in that it contains both cavity-bound as well as exterior anions; the presence of the cavity-bound triflate anion precludes binding of **MAC** which is not present in this structure although it was available in the crystal soaking experiment. Fig. 6a shows a view of the cage containing a triflate anion, disordered over two equivalent positions astride the

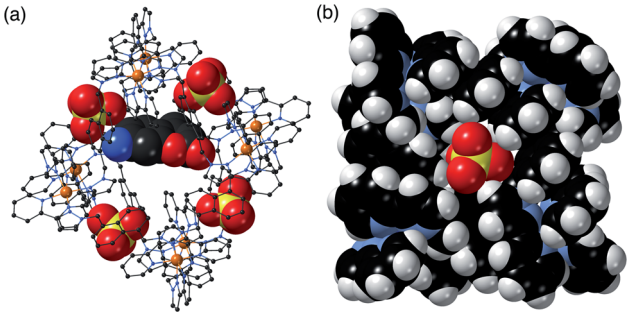

Fig. 5 Views of the crystal structure of **H·MAC·(SO$_4$)**. (a) A view of the complete cage in wireframe showing the four surface-bound sulfates in space-filling mode, with a space-filling **MAC** guest included; (b) a space-filling view onto one face showing how the sulfate anion occupies the portal in the centre of the face *via* multiple CH···O contacts.

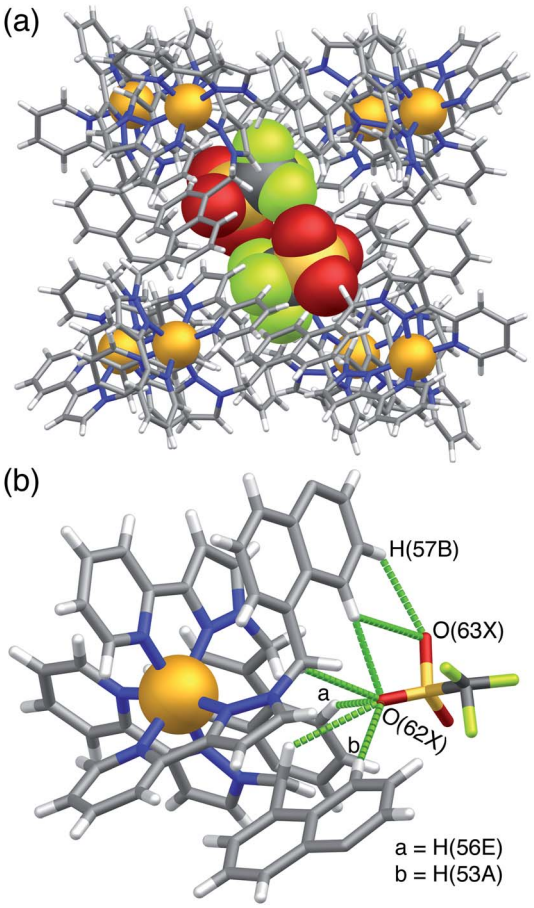

Fig. 6 Views of the crystal structure of **H·(CF$_3$SO$_3$)** (F, green; O, red; S, yellow). (a) A view of the complete cage in wireframe showing the two half-occupancy triflate anions in space filling mode; (b) a view showing the hydrogen-bonding interactions of the triflate anion with the interior surface of the cage around one of the *fac* tris-chelate vertices, with H···O contacts of <3 Å shown by purple dashed lines.

inversion centre with 0.5 site occupancy in each position. Two of the O atoms [O(62X) and O(63X)] project into the H-bond donor pocket at the *fac* tris-chelate site around Co(2) that is defined by the convergent set of naphthyl CH and methylene CH$_2$ protons, such that there are – in the usual way – multiple CH···O hydrogen bonds between encapsulated anion as H-bond acceptor and the cage surface which acts as the H-bond donor, with H···O contacts down to 2.50 Å [O(62X)···H(53A)], 2.61 Å [O(62X)···H(56E)] and 2.72 Å [O(63X)···H(57B) (Fig. 6b). The 0.5 site occupancy of each triflate could mean that half of the cage cavities have taken up a pair of anions in the crystalline sponge process, but this would result in unfeasibly short inter-anion contacts (a 2.39 Å O···F contact which is significantly less than the sum of the van der Waals radii). This strongly implies that each cage contains one cavity-bound triflate anion that is randomly located in one of the two equivalent off-centre positions. The lattice contains an additional crystallographically distinct cage complex unit (lying on a threefold symmetry axis rather than astride an inversion centre) and this also contains a triflate ion but the disorder there is far more severe so the geometry cannot be discussed in detail. Triflate anions outside the cavity form a range of O···HC contacts with the cage exterior surface: but the important point to emphasise is that this is the first observation of a cavity-bound anion in any of the crystal structures we have obtained with this cage system.

The overall messages from this set of related structures are that (i) simultaneous exchange of both cavity-based (neutral) and surface-bound (anionic) guests is possible in a single crystalline sponge experiment, in addition to the possibilities, reported earlier,[5,9,10,14] of introducing each guest type on its own; and (ii) we can see in several cases close contacts between the cavity-bound guests and the surrounding anion array in the form of short CH···X contacts. It follows from this that binding of the two guest types may not be genuinely orthogonal events, *i.e.* wholly independent of one another, although the results of the displacement assays reported in the next section show that this is approximately true in some cases and forms the basis of the two-indicator displacement assay.

2.2. Independent displacement of cavity-bound and surface-bound fluorophores by different guests

2.2.1 Testing the two types of fluorescence displacement assay individually. Given the ability of the cage to accommodate cavity-bound and surface-bound guests independently of one another, we wished to investigate the possibility of each guest type being independently addressable in a FDA, with each guest type being displaced independently according to the nature of the analyte. The obvious choice for the cavity-binding fluorophore, based on our previous work, is **MAC** (Chart 1; λ_{em} 445 nm, blue), given its strong binding inside **H^w** in water,[9a] the structural characterisation of examples of cage/**MAC** complexes,[14] and the fact that it has already been used in a FDA to evaluate binding strengths of other cavity-binding guests.[9a] Likewise, the obvious choice for a fluorescent surface-bound anion is fluorescein, **FLU** (Chart 1; λ_{em} 515 nm, green) whose strong binding to the surface of **H^w** and its consequent use in a displacement assay for evaluating relative binding strengths of other anions has also recently been described.[6] Importantly, the cavity-binding fluorophore (**MAC**)[9a] and the surface-binding

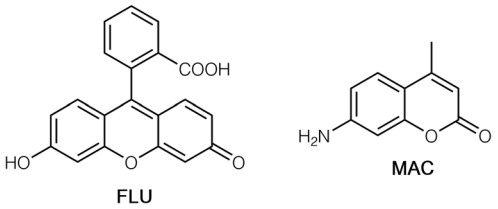

Chart 1 Structural formulae of FLU and MAC.

fluorophore (**FLU**)[6] have different fluorescence colours such that displacement of different amounts of each according to where the guest binds to $\mathbf{H^W}$ should provide a diagnostic colorimetric response. Note that although we used unsubstituted cage **H** for the crystalline sponge X-ray diffraction experiments reported above because of the ease of growth and robustness of its single crystals,[14] for solution studies in water we used $\mathbf{H^w}$ whose twenty-four hydroxymethyl substituents render it water-soluble: apart from these exterior groups the two are isostructural with essentially identical cavities.[9b]

We started by using **MAC** or **FLU** as fluorescent reporters of guest binding, as we have done before, but added one variation to the process.[6,9a] Although we can calculate binding constants from titrations which displace these guests and result in a growth in fluorescence intensity, a simple change in fluorescence intensity alone is of limited value as an analytical tool without careful calibration: and this is particularly true where a naked-eye test for substrate binding is sought as the human eye is poor at estimating absolute light intensity values. We could however convert this change in fluorescence intensity of one component to a ratiometric response by adding to the system a fixed amount of the red-luminescent species $[Ru(bipy)_3]Cl_2$ (denoted **Ru**). The dication of **Ru** will not associate with the 16+ cation of $\mathbf{H^W}$ in solution: but the presence of a fixed red luminescence component as a baseline means that during the titrations with cavity-binding or surface-binding guests which liberate **MAC** or **FLU** respectively, the steady increase in the blue or green luminescence component combines with the fixed red luminescence component of **Ru** to give an obvious change in the overall hue – *i.e.* the intensity-only change in one emission component is converted to a ratiometric response as the balance between the fixed (red) and variable (blue or green) emission changes. This is a technique that has been used elsewhere to convert an intensity-based luminescence change into a ratiometric change for sensing applications.[18]

Initially we used the host cage $\mathbf{H^W}$ (150 μM), **MAC** (10 μM) and **Ru** (50 μM) as the sensor system. With these proportions the steady-state luminescence spectrum shows the characteristic blue emission maximum of residual free **MAC** (the fraction that is not quenched by binding to inside $\mathbf{H^W}$) and the red phosphorescence of **Ru** at *ca.* 620 nm. On addition of portions of the hydrophobic, cavity-binding guest *trans*-1-decalone, we observed (Fig. 7a) a progressive increase in the **MAC** fluorescence component as this is displaced, whereas the **Ru**-based emission component was essentially invariant. Fitting the rise

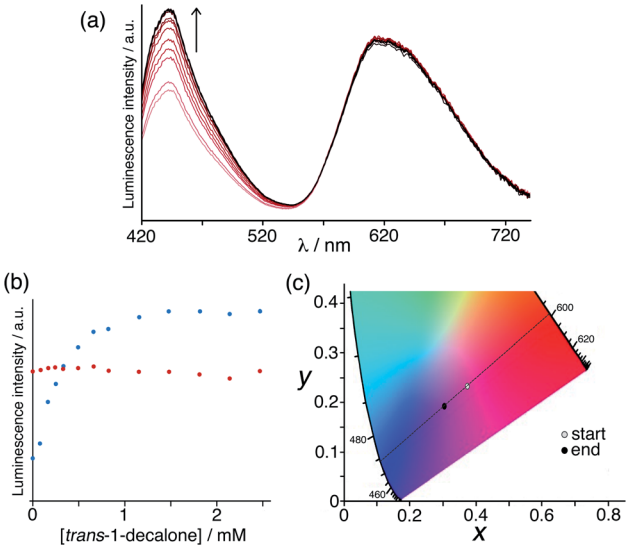

Fig. 7 Results of titration of the cavity-binding guest *trans*-1-decalone into a combination of $\mathbf{H^W}$ (150 μM), **MAC** (10 μM) and **Ru** (50 μM) in water. (a) Fluorescence changes associated with MAC being displaced from the cage cavity (λ_{exc} = 395 nm); (b) plot of the peak intensity data from part (a) during the titration; (c) shift in overall emission colour on a CIE colour-space chart during the titration.

in **MAC** fluorescence (Fig. 7b) to a 1 : 1 binding isotherm using the same software as reported previously,[9a] that takes account of competition between **MAC** and the *trans*-1-decalone, we obtained a *K* value of guest binding of 3×10^4 M^{-1}: this is slightly higher than the value of 1×10^4 M^{-1} reported earlier which may be ascribed to the different experimental conditions.[9a] Significantly however there is now an overall colour change associated with adding increased blue fluorescence to a fixed red phosphorescence background, which is shown on a CIE colour space diagram in Fig. 7c as an overall colour shift towards purple.

A similar experiment to probe surface anion binding, and convert it to a visible colorimetric response, was conducted using $\mathbf{H^W}$ (130 μM), **FLU** (10 μM) and **Ru** (50 μM). The steady-state emission spectrum showed the expected broad, red **Ru**-based emission centred at 620 nm and a green emission component at 515 nm associated with the small proportion of un-quenched **FLU**. Titration of portions of NaCl, NaF or $NaNO_3$ into this solution (Fig. 8a illustrates the effect of added chloride) resulted in displacement of **FLU** from the cage surface by the added ions and an increase in the green emission component only (Fig. 8b), with the most hydrophilic anion (fluoride) showing the smallest effect.[6] When combined with the fixed red emission from **Ru**, the increased green emission from displaced **FLU** results in an overall colour change from orange to yellow as illustrated on the CIE diagram in Fig. 8c. As we might expect – but it is still nonetheless pleasing – the magnitude of the luminescence colour shift on the CIE diagram that is induced by the three different anions correlates with how well these anions bind to the cage surface (Fig. 8c),[6] with nitrate having the largest effect and fluoride the smallest.

2.2.2 Combining the two types of fluorescence displacement assay in a single system. Having confirmed the previously-

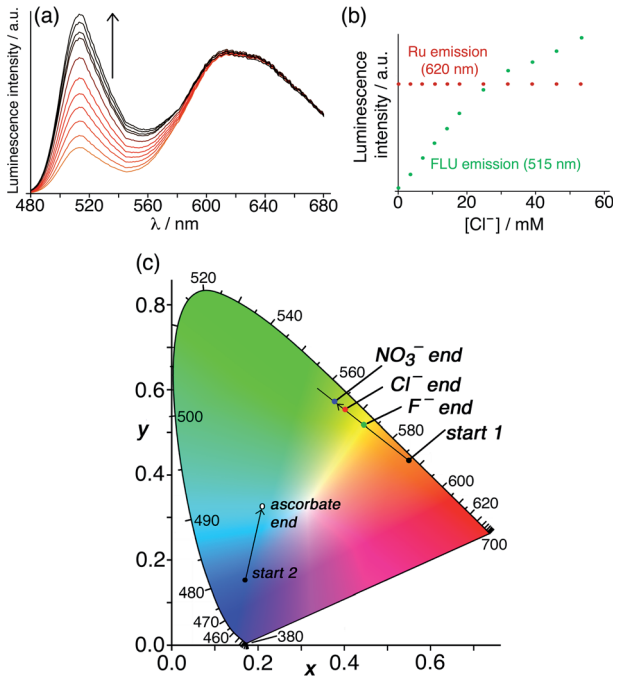

Fig. 8 Results of titrations of the surface-binding anionic guests chloride, fluoride and nitrate into a combination of H^W (130 μM), **FLU** (10 μM) and **Ru** (50 μM) in water. (a) Fluorescence changes associated with **FLU** being displaced from the cage surface during titration with chloride (λ_{exc} = 450 nm); (b) plot of the peak intensity data of both emission components from part (a) during the titration; (c) shift in overall emission colour (beginning from '*start 1*') on a CIE colour-space chart during similar titrations with nitrate, chloride and fluoride, confirming that nitrate binds most strongly of these three anions to the cage surface due its hydrophobicity. (Note that the data relating to addition of ascorbate [beginning from '*start 2*'] relate to the titrations in Fig. 10, *q.v.*)

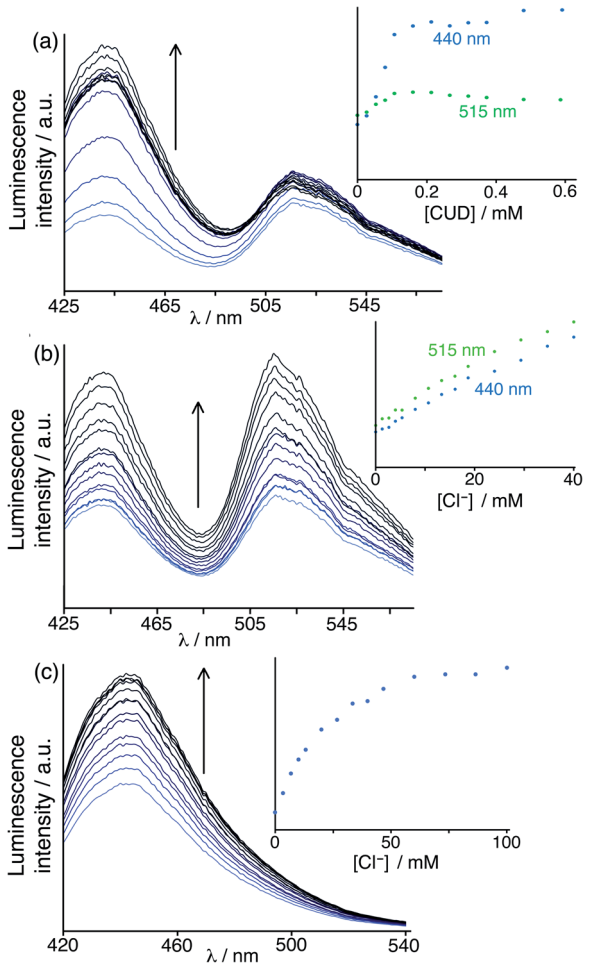

Fig. 9 (a) Results of titration of the guest cycloundecanone into a combination of H^W (150 μM), **FLU** (10 μM) and **MAC** (10 μM) at pH 8 in water (λ_{exc} = 395 nm), showing predominantly displacement of cavity-bound **MAC**; (b) results of a similar experiment using chloride as the analyte, unexpectedly showing displacement of *both* cavity-bound **MAC** and surface-bound **FLU**; and (c) a displacement assay experiment using H^W (150 μM)/**MAC** (10 μM) with added chloride to confirm that chloride can in fact show cavity-binding as well as surface-binding, with the increase in fluorescence from displaced **MAC** fitting to a 1 : 1 binding isotherm (see main text). In each case the intensity changes at the emission maxima during the titration are shown as insets.

established behaviour of the two sensing modalities using cavity-binding and surface-binding guests, but converting the outputs to a ratiometric change between two differently-coloured emission components, the next step was to see if we could combine these in one system. The goal is to have a single sensor system that responds to both cavity-binding and surface-binding analytes, giving a different colour response for each.

The initial assay system was based on the host cage $\mathbf{H^W}$ (150 μM), using the cavity-binding guest **MAC** (10 μM) and the surface-binding fluorophore **FLU** (10 μM), at pH 8 in water. In this case the presence of two fluorophores, which will be affected to different extents by binding of different guest types, will provide the desired ratiometric response: so to start with an additional fixed red-emissive **Ru** component was not used. The un-bound fractions of **MAC** and **FLU** in this mixture gives a combination of blue and green emission components. Fig. 9a shows how addition of portions of the hydrophobic cavity-binding guest cycloundecanone ($K \approx 10^6$ M^{-1} for cavity binding in water)[9a] to the above mixture resulted in a rapid increase in the blue component as the **MAC** is progressively displaced from the cage cavity; in contrast the green emission component from surface-bound **FLU** is very little affected. When evaluating the effects of chloride ions, however – expecting chloride to selectively displace **FLU** from the cage surface and boost only the green emission component – we were surprised to observe a clear increase in *both* emission components (Fig. 9b).

This implies that, in solution, chloride not only binds to the cage surface and displaces **FLU** (as previously reported),[6] but is also capable of binding inside the cage cavity and displacing **MAC**. Whilst the majority of the crystal structures we have obtained of salts of **H** or $\mathbf{H^W}$ have the anions occupying only surface portals around the cage and not occupying the central cavity, the crystal structure of triflate salt (reported above, Fig. 6) showed for the first time that cavity-binding of small anions is also possible in the solid state, and therefore it should also be possible in solution. In addition, the fact that binding constants

of neutral organic guests tend to be smaller in aqueous solution when chloride is used as the counter-ion[5b] does imply that chloride has the ability to bind both in the cavity and at the cage surface in solution.

To check this we did a FDA analysis using the $\mathbf{H^W}$/**MAC** pair and adding small portions of chloride in a standard titration (Fig. 9c), and indeed found that chloride could indeed displace **MAC** from the cavity restoring its fluorescence, giving a 1 : 1 cavity-based binding constant of 290 M^{-1} (*cf.* the 1 : 1 binding constant to an individual surface binding site of 750 M^{-1}).[6] This rather unexpected result perfectly confirms the potential value of the dual-mode displacement assay based on two different fluorescence reporters in that it identifies a hitherto unknown mode of binding of chloride in the cage cavity.

In search of an anionic guest that would show surface binding *only* and would have no effect on cavity-bound **MAC**, we considered organic anions which should be too large to bind inside the cavity. Many such anions as their sodium salts (*e.g.* citrate, dodecyl sulfate) immediately resulted in formation of insoluble precipitates with the 16+ $\mathbf{H^W}$ cation. However, titration of portions of sodium ascorbate into the $\mathbf{H^W}$ (150 μM)/**MAC** (10 μM)/**FLU** (10 μM) mixture resulted in a steady increase in the green **FLU** emission component with no significant change in the **MAC** component, indicative of surface-binding only. Fitting this luminescence data to a 1 : 1 binding isotherm, taking account of the presence of two competing surface-binding species, gave a K value for 1 : 1 binding at a surface site for ascorbate of 1.3×10^4 M^{-1}: significantly weaker than for **FLU** (which is a dianion) but significantly stronger than smaller ions such as halides or nitrate due to the hydrophobic organic backbone.[6] The fluorescence intensity changes following titration with (surface-binding) ascorbate are shown in Fig. 10a, alongside the essentially orthogonal changes following titration with (cavity-binding) *trans*-1-decalone (Fig. 10b). *This pair of titration results nicely illustrates a key goal of this work: the ability to interrogate binding of different types of guest using two orthogonal recognition processes in a single sensor system.* An illustration on a CIE diagram of the colour change between start and end of the titration with ascorbate (data from Fig. 10a) is included in Fig. 8c, beginning at point 'start 2', with an increase in the green emission component as **FLU** is displaced being very clear.

The final optimisation of this dual-mode FDA sensor involved addition of the red-emissive **Ru** component to the cocktail. When we did this initially in the $\mathbf{H^W}$/**MAC**/**Ru** or $\mathbf{H^W}$/**FLU**/**Ru** systems, the additional presence of the fixed **Ru**-based red emission allowed the intensity changes from displacement of either **MAC** or **FLU** on their own to be converted to a ratiometric luminescence change with a visible colour shift. In this case however the purpose is different. With both **FLU** and **MAC** present as components of the sensor that respond to orthogonal stimuli there is already a ratiometric response according to analyte type. However, the change in blue/green balance results in small changes of hue against a strongly coloured background: if the same colour change can be shifted towards the

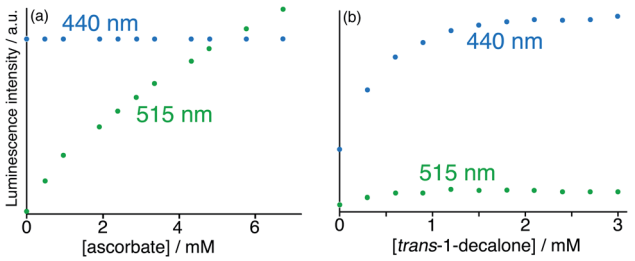

Fig. 10 Results of titration of the guests (a) ascorbate and (b) *trans*-1-decalone into a combination of H^W (150 μM), FLU (10 μM) and MAC (10 μM) at pH 8 in water (λ_{exc} = 395 nm), showing the essentially orthogonal nature of the binding of these two guests and the differing fluorescence responses. Evolution of spectra followed the general appearance shown in Fig. 9; shown here are the peak intensity changes for fluorescence from the FLU and MAC components during the titrations, from which it is clear that ascorbate selectively displaces FLU from the surface of H^W whereas *trans*-1-decalone selectively displaces MAC from the cavity. The colour shift towards green associated with addition of ascorbate and displacement of FLU is included in the CIE diagram in Fig. 8c, beginning from *'start 2'*.

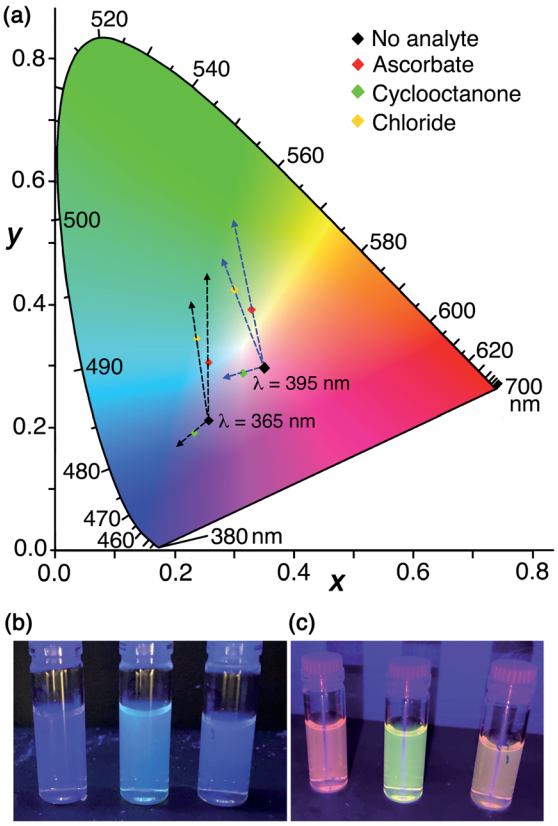

Fig. 11 (a) A CIE diagram showing the fluorescence colour changes associated with addition of ascorbate, cyclooctanone, or chloride to a mixture of H^W (150 μM), MAC (10 μM), FLU (20 μM) and Ru (30 μM). The two sets of dashed arrows starting at different starting points indicate the directions of colour shifts generated by different analytes using 365 nm (black arrows) or 395 nm excitation (blue arrows), respectively. These arrows are just to aid the eye: the end-points of each titration are illustrated by the coloured points. (b and c) Photos of end-points of the titrations with (from left to right) cyclooctanone, chloride and ascorbate taken under (b) 365 nm excitation and (c) 395 nm excitation respectively.

centre of the CIE diagram – closer to a white starting point – by addition of a fixed red component, small changes in hue will be more visually obvious.

For this final set of experiments, accordingly, we used as the sensor system $\mathbf{H^W}$ (150 μM), **MAC** (10 μM), **FLU** (20 μM) and **Ru** (30 μM): this system again shows nicely the orthogonality of the two independent indicator displacement assays but with the overall colour shifted towards the centre of the CIE colour chart (Fig. 11). The increase in blue emission arising from addition of portions of cyclooctanone (displacing **MAC** from the cavity), and the increase in green emission arising from addition of portions of sodium ascorbate (displacing **FLU** from the surface) are both clear. The resulting colour shifts associated with addition of each analyte are shown on the CIE diagram in Fig. 11a which indicates changes in overall emission colour when using 365 nm excitation. The effect of added chloride, which displaces some of each type of fluorophore given that chloride can participate in both cavity-based and surface-based binding, is a colour shift in an intermediate direction between the responses triggered by ascorbate and cyclooctanone: thus we have a system where we can see immediately the nature of the binding interactions of a guest according to the 'direction of travel' of the overall colour change on the CIE diagram. Bromide shows the same mixed response as chloride with a direction of travel of the colour change indicating displacement of mostly surface-bound **FLU** but also a small amount of cavity-bound **MAC**: thus both of these halide anions are capable of some cavity binding which ascorbate clearly is not. Fluoride in contrast showed no cavity binding but displaced only the surface-bound **FLU** fluorophore. We also investigated use of triflate in a similar experiment to see if mixed-mode binding occurs, given the evidence from the crystalline sponge for its ability to bind inside the cavity, but it resulted in precipitation of an insoluble $\mathbf{H^W}$/triflate salt.

The visual response can be altered further by using a different excitation wavelength which results in a different balance between the starting R/G/B emission components. The outcome of the same experiment visualised using 395 nm instead of 365 nm excitation is also shown in Fig. 11a using the labelled starting point on the CIE diagram. The difference between using 365 nm and 395 nm excitation in a hand-held lamp to visualise the colour changes is clear: the directions of colour shift on the CIE diagram caused by each added analyte are similar in both cases, but when using 395 nm excitation the difference is more apparent to the eye as the changes start from a point closer to neutral white. This is shown in Fig. 11b and c; in the latter case (395 nm excitation) the visual difference in emission colours associated with addition of cavity-binding or surface-binding guests, or a guest that does both, is more obvious than it is when using 365 nm excitation.

3 Conclusions

The ability of the octanuclear cubic host cage to accommodate two different types of guest in different ways (neutral hydrophobic organic guests inside the cavity; anionic guests at the six portals on the cage surface) has been studied both crystallographically (using **H**) and *via* displacement assays in aqueous solution (using $\mathbf{H^w}$, bearing water-solubilising substituents). Crystalline sponge experiments have shown that, starting with the 'empty' cage **H** (*i.e.* containing solvent molecules in the cavity in the crystalline state) as its fluoroborate salt, it is possible to include both a cavity-binding guest (**MAC**) and any of several different surface-binding anions (iodide, nitrate, sulfate and others) in a single experiment. Taken together with previous work on incorporating cavity-binding guests or surface-binding guests separately into crystals using crystalline sponge experiments, it is clear that the uptake of the two different types of guest into their distinct binding sites in $\mathbf{H^W}$ can be managed independently of one another.

Solution experiments using $\mathbf{H^W}$ with cavity-bound (**MAC**) and surface-bound (**FLU**) fluorescent guests, either individually or in combination, confirmed that these different guest types can be separately displaced by appropriate competing guests, with hydrophobic cavity-binders (*e.g.* cyclic aliphatic ketones) displacing **MAC** and anionic surface-binders (*e.g.* ascorbate, nitrate) displacing **FLU**. This provides the basis of a sensor system which provides two different fluorescence-based responses to two different analyte types in a single scaffold, *i.e.* a ratiometric sensor system that changes the balance between blue and green fluorescence according to where the guest binds. Unexpectedly one anionic guest (chloride) shows the ability to bind in the cage cavity as well as to the surface, and it therefore displaces both fluorophores, providing a fluorescence-based response that is a combination of the responses obtained from 'pure' cavity-binders or surface binders. Adding a red emission component in the form of $[Ru(bipy)_3]^{2+}$ to the system shifts the overall balance of emission colour towards white, with separate R/G/B luminescence components, of which the red component is fixed and the green and blue components are variable. The result is that changes in the blue or green emission components from the ensemble arising from the presence of cavity-binding or surface-binding analytes generates clearly visible and distinct colour changes according to their mode of binding to $\mathbf{H^W}$; the visibility of the colour changes can also be improved by choice of excitation wavelength with 395 nm excitation showing the difference particularly clearly (Fig. 11c).

We note that there is an interesting conceptual parallel to be drawn between the 'dual-input, dual-output' nature of this cage-based analytical system, and molecular logic gates[19] in which different combinations of chemical stimuli provide the inputs which control the luminescence output (*e.g.* *p*H and solvent;[20] pO_2 and metal ion concentration;[21] *p*H and pO_2).[22]

4 Materials and methods

4.1. X-ray crystallography

The crystalline sponge experiments were performed as described in a previous paper,[14] by immersing pre-grown crystals of **H** (as the tetrafluoroborate salt) into a concentrated MeOH solution containing a mixture of **MAC** and the tetrabutylammonium salt of the relevant anion. Information on the

crystal properties, data collections and refinements associated with the structure determinations of the supramolecular complexes of **H** are collected in Table S1† of ESI. The data collections were performed in Experiment Hutch 1 of beamline I-19 at the UK Diamond Light Source synchrotron facility,[23] using methodology, data processing and software described previously.[14]

4.2. Synthesis and spectroscopy

The water-soluble Co_8 cage $\mathbf{H^W}$ bearing hydroxymethyl substituents that was used for all aqueous solution studies,[9b] and the analogous unsubstituted cage **H** that was used for the crystalline sponge experiments,[15] were prepared as previously reported. The fluorescent reporters 4-methyl-7-amino-coumarin (**MAC**) and fluorescein (**FLU**) were obtained from Sigma-Aldrich and used as received. Fluorescence measurements were carried out using either a BMG ClarioStar plate reader with 96-well plates, or an Agilent Cary Eclipse fluorimeter. UV/Vis spectra were obtained using an Implen C40 Nanophotometer. The detailed methodology for the fluorescence displacement assay experiments reported in this paper using either surface-binding **FLU**,[6] or cavity-binding **MAC**,[9a] is described in detail in Section 2 of the ESI.†

Data availability

Experimental data are in the figures or the ESI.† Raw data in the form of fluorescence spectra during titrations are available in XL format from MDW.

Author contributions

MDL: synthesis of cages, and all solution spectroscopic measurements of the displacement assays. CGPT: crystalline sponge experiments and X-ray crystallography. MDW: project conception, supervision, and manuscript preparation.

Conflicts of interest

There are no conflicts to declare.

Acknowledgements

We thank EPSRC for a PhD studentship to MDL (grant number EP/N509796/1); the University of Warwick for additional financial support; the Diamond Light Source for the X-ray beamtime (proposal CY25064); and Dr Sarah Barnett and the staff of beamline I-19 for their assistance.

Notes and references

1 (*a*) T. R. Cook and P. J. Stang, *Chem. Rev.*, 2015, **115**, 7001; (*b*) T. R. Cook, Y.-R. Zheng and P. J. Stang, *Chem. Rev.*, 2013, **113**, 734; (*c*) R. Chakrabarty, P. S. Mukherjee and P. J. Stang, *Chem. Rev.*, 2011, **111**, 6810; (*d*) M. M. J. Smulders, I. A. Riddell, C. Browne and J. R. Nitschke, *Chem. Soc. Rev.*, 2013, **42**, 1728; (*e*) D. Zhang, T. K. Ronson and J. R. Nitschke, *Acc. Chem. Res.*, 2018, **51**, 2423; (*f*) H. Vardhan, M. Yusubov and F. Verpoort, *Coord. Chem. Rev.*, 2016, **306**, 171; (*g*) S. Pullen, J. Tessarolo and G. H. Clever, *Chem. Sci.*, 2021, **12**, 7269; (*h*) S. Goeb and M. Sallé, *Acc. Chem. Res.*, 2021, **54**, 1043; (*i*) E. G. Percastegui, T. K. Ronson and J. R Nitschke, *Chem. Rev.*, 2020, **120**, 13480.

2 (*a*) Y. Fang, J. A. Powell, E. Li, Q. Wang, Z. Perry, A. Kirchon, X. Yang, Z. Xiao, C. Zhu, L. Zhang, F. Huang and H.-C. Zhou, *Chem. Soc. Rev.*, 2019, **48**, 4707; (*b*) C. J. Brown, F. D. Toste, R. G. Bergman and K. N. Raymond, *Chem. Rev.*, 2015, **115**, 3012; (*c*) M. Yoshizawa, J. K. Klosterman and M. Fujita, *Angew. Chem., Int. Ed.*, 2009, **48**, 3418; (*d*) M. Otte, *ACS Catal.*, 2016, **6**, 6491; (*e*) C. M. Hong, R. G. Bergman, K. N. Raymond and F. D. Toste, *Acc. Chem. Res.*, 2018, **51**, 2447; (*f*) W.-X. Gao, H.-N. Zhang and G.-X. Jin, *Coord. Chem. Rev.*, 2019, **386**, 69; (*g*) Y. Xue, X. Hang, J. Ding, B. Li, R. Zhu, H. Pang and Q. Xu, *Coord. Chem. Rev.*, 2021, **430**, 213656; (*h*) M. Morimoto, S. M. Bierschenk, K. T. Xia, R. G. Bergman, K. N. Raymond and F. D. Toste, *Nat. Catal.*, 2020, **3**, 969; (*i*) A. B. Grommet, M. Feller and R. Klajn, *Nat. Nanotechnol.*, 2020, **15**, 256.

3 (*a*) Y. Sun, C. Chen, J. Liu and P. J. Stang, *Chem. Soc. Rev.*, 2020, **49**, 3889; (*b*) M. Zhang, M. L. Saha, M. Wang, Z. Zhou, B. Song, C. Lu, X. Yan, X. Li, F. Huang, S. Yin and P. J. Stang, *J. Am. Chem. Soc.*, 2017, **139**, 5067; (*c*) C.-L. Liu, R.-L. Zhang, C.-S. Lin, L.-P. Zhou, L.-X. Cai, J.-T. Kong, S.-Q. Yang, K.-L. Han and Q.-F. Sun, *J. Am. Chem. Soc.*, 2017, **139**, 12474; (*d*) J. Wang, C. He, P. Wu, J. Wang and C. Duan, *J. Am. Chem. Soc.*, 2011, **133**, 12402; (*e*) Y. Jiao, J. Wang, P. Wu, L. Zhao, C. He, J. Zhang and C. Duan, *Chem.–Eur. J.*, 2014, **20**, 2224; (*f*) X.-Z. Li, L.-P. Zhou, L.-L. Yan, D.-Q. Yuan, C.-S. Lin and Q.-F. Sun, *J. Am. Chem. Soc.*, 2017, **139**, 8237; (*g*) N. Dey and C. J. E. Haynes, *ChemPlusChem*, 2021, **86**, 418; (*h*) S. Borsley, J. A. Cooper, P. J. Lusby and S. L. Cockroft, *Chem.–Eur. J.*, 2018, **24**, 4542.

4 (*a*) A. B. Grommet and J. R. Nitschke, *J. Am. Chem. Soc.*, 2017, **139**, 2176; (*b*) A. Garci, J.-P. Mbakidi, V. Chaleix, V. Sol, E. Orhan and B. Therrien, *Organometallics*, 2015, **34**, 4138; (*c*) T. Grancha, A. Carné-Sánchez, L. Hernández-López, J. Albalad, I. Imaz, J. Juanhuix and D. Maspoch, *J. Am. Chem. Soc.*, 2019, **141**, 18349; (*d*) A. M. Castilla, T. K. Ronson and J. R. Nitschke, *J. Am. Chem. Soc.*, 2016, **138**, 2342; (*e*) S. Löffler, J. Lübben, L. Krause, D. Stalke, B. Dittrich and G. H. Clever, *J. Am. Chem. Soc.*, 2015, **137**, 1060; (*f*) W. Cullen, S. Turega, C. A. Hunter and M. D. Ward, *Chem. Sci.*, 2015, **6**, 625; (*g*) B.-N. T. Hguyen, A. B. Grommet, A. Tron, M. C. A. Georges and J. R. Nitschke, *Adv. Mater.*, 2020, **32**, 1907241; (*h*) A. J. McConnell, C. J. E. Haynes, A. B. Grommet, C. M. Aitchison, J. Guilleme, S. Mikutis and J. R. Nitschke, *J. Am. Chem. Soc.*, 2018, **140**, 16952.

5 (*a*) M. D. Ward, C. A. Hunter and N. H. Williams, *Acc. Chem. Res.*, 2018, **51**, 2073; (*b*) W. Cullen, A. J. Metherell, A. B. Wragg, C. G. P. Taylor, N. H. Williams and M. D. Ward, *J. Am. Chem. Soc.*, 2018, **140**, 2821; (*c*)

C. Mozaceanu, C. G. P. Taylor, J. R. Piper, S. P. Argent and M. D. Ward, *Chemistry*, 2020, **2**, 22.

6 M. D. Ludden and M. D. Ward, *Dalton Trans.*, 2021, **50**, 2782.

7 (*a*) F. J. Rizzuto, W. Y. Wu, T. K. Ronson and J. R. Nitschke, *Angew. Chem., Int. Ed. Engl.*, 2016, **55**, 7958; (*b*) I. A. Riddell, M. M. J. Smulders, J. K. Clegg, Y. R. Hristova, B. Breiner, J. D. Thoburn and J. R. Nitschke, *Nat. Chem.*, 2012, **4**, 751.

8 (*a*) C. Sgarlata, J. S. Mugridge, M. D. Pluth, B. E. F. Tiedemann, V. Zito, G. Arena and K. N. Raymond, *J. Am. Chem. Soc.*, 2010, **132**, 1005; (*b*) C. Sgarlata and K. N. Raymond, *Anal. Chem.*, 2016, **88**, 6923; (*c*) C. Sgarlata, J. S. Mugridge, M. D. Pluth, V. Zito, G. Arena and K. N. Raymond, *Chem.–Eur. J.*, 2017, **23**, 16813.

9 (*a*) S. Turega, W. Cullen, M. Whitehead, C. A. Hunter and M. D. Ward, *J. Am. Chem. Soc.*, 2014, **136**, 8475; (*b*) M. Whitehead, S. Turega, A. Stephenson, C. A. Hunter and M. D. Ward, *Chem. Sci.*, 2013, **4**, 2744; (*c*) A. J. Metherell, W. Cullen, N. H. Williams and M. D. Ward, *Chem.–Eur. J.*, 2018, **24**, 1554.

10 W. Cullen, M. C. Misuraca, C. A. Hunter, N. H. Williams and M. D. Ward, *Nat. Chem.*, 2016, **8**, 231.

11 (*a*) A. C. Sedgwick, J. T. Brewster II, T. Wu, X. Feng, S. D. Bull, X. Qian, J. L. Sessler, T. D. James, E. V. Anslyn and X. Sun, *Chem. Soc. Rev.*, 2021, **50**, 9; (*b*) B. T. Nguyen and E. V. Anslyn, *Coord. Chem. Rev.*, 2006, **250**, 3118.

12 (*a*) M. Hoshino, A. Khutia, H. Xing, Y. Inokuma and M. Fujita, *IUCrJ*, 2016, **3**, 139; (*b*) K. Rissanen, *Chem. Soc. Rev.*, 2017, **46**, 2638.

13 (*a*) K. L. Wen, S. S. Yu, Z. Huang, L. M. Chen, M. Xiao, X. Q. Yu and L. Pu, *J. Am. Chem. Soc.*, 2015, **137**, 4517; (*b*) S. L. Pilicer, P. R. Bakhshi, K. W. Bentley and C. Wolf, *J. Am. Chem. Soc.*, 2017, **139**, 1758.

14 C. G. P. Taylor, S. P. Argent, M. D. Ludden, J. R. Piper, C. Mozaceanu, S. A. Barnett and M. D. Ward, *Chem.–Eur. J.*, 2020, **26**, 3054.

15 I. S. Tidmarsh, T. B. Faust, H. Adams, L. P. Harding, L. Russo, W. Clegg and M. D. Ward, *J. Am. Chem. Soc.*, 2008, **130**, 15167.

16 (*a*) A. J. Metherell and M. D. Ward, *Dalton Trans.*, 2016, **45**, 16096; (*b*) S. Turega, M. Whitehead, B. R. Hall, A. J. H. M. Meijer, C. A. Hunter and M. D. Ward, *Inorg. Chem.*, 2013, **52**, 1122.

17 S. J. Pike, J. J. Hutchinson and C. A. Hunter, *J. Am. Chem. Soc.*, 2017, **139**, 6700.

18 (*a*) A. J. Metherell, C. Curty, A. Zaugg, S. T. Saad, G. H. Dennison and M. D. Ward, *J. Mater. Chem. C*, 2016, **4**, 9664; (*b*) Y. Dong, J. Cai, Q. Fang, X. You and Y. Chi, *Anal. Chem.*, 2016, **88**, 1748; (*c*) Y. Zhou and B. Yan, *J. Mater. Chem. C*, 2015, **3**, 9353; (*d*) T. J. Sorensen, A. M. Kenwright and S. Faulkner, *Chem. Sci.*, 2015, **6**, 2054; (*e*) C. Song, Z. Ye, G. L. Wang, J. Yuan and Y. Guan, *Chem.–Eur. J.*, 2010, **16**, 6464; (*f*) S. E. Plush and T. Gunnlaugsson, *Dalton Trans.*, 2008, 3801.

19 D. C. Magri, *Coord. Chem. Rev.*, 2021, **426**, 213598.

20 L. A. Trifoi, G. K. Hodgson, N. P. Dogantzis and S. Impellizzeri, *Front. Chem.*, 2020, **8**, 470.

21 M. de Sousa, M. Kluciar, S. Abad, M. A. Miranda, B. de Castro and U. Pischel, *Photochem. Photobiol. Sci.*, 2004, **3**, 639.

22 T. Gunnlaugsson, D. A. MacDónail and D. Parker, *Chem. Commun.*, 2000, 93.

23 D. R. Allan, H. Nowell, S. A. Barnett, M. R. Warren, A. Wilcox, J. Christensen, L. K. Saunders, A. Peach, M. T. Hooper, L. Zaja, S. Patel, L. Cahill, R. Marshall, S. Trimnell, A. J. Foster, T. Bates, S. Lay, M. A. Williams, P. V. Hathaway, G. Winter, M. Gerstel and R. W. Wooley, *Crystals*, 2017, **7**, 336.

Chemical Science

ROYAL SOCIETY OF CHEMISTRY

EDGE ARTICLE

View Article Online
View Journal | View Issue

Check for updates

Cite this: *Chem. Sci.*, 2021, **12**, 14781

All publication charges for this article have been paid for by the Royal Society of Chemistry

Interaction of anions with the surface of a coordination cage in aqueous solution probed by their effect on a cage-catalysed Kemp elimination†

Michael D. Ludden,[a] Christopher G. P. Taylor,[a] Max B. Tipping,[a] Jennifer S. Train,[b] Nicholas H. Williams,[b] Jack C. Dorrat,[c] Kellie L. Tuck[c] and Michael D. Ward*[a]

An octanuclear M_8L_{12} coordination cage catalyses the Kemp elimination reaction of 5-nitro-1,2-benzisoxazole (NBI) with hydroxide to give 2-cyano-4-nitrophenolate (CNP) as the product. In contrast to the previously-reported very efficient catalysis of the Kemp elimination reaction of unsubstituted benzisoxazole, which involves the substrate binding inside the cage cavity, the catalysed reaction of NBI with hydroxide is slower and occurs at the external surface of the cage, even though NBI can bind inside the cage cavity. The rate of the catalysed reaction is sensitive to the presence of added anions, which bind to the 16+ cage surface, displacing the hydroxide ions from around the cage which are essential reaction partners in the Kemp elimination. Thus we can observe different binding affinities of anions to the surface of the cationic cage in aqueous solution by the extent to which they displace hydroxide and thereby inhibit the catalysed Kemp elimination and slow down the appearance of CNP. For anions with a −1 charge the observed affinity order for binding to the cage surface is consistent with their ease of desolvation and their ordering in the Hofmeister series. With anions that are significantly basic (fluoride, hydrogen carbonate, carboxylates) the accumulation of the anion around the cage surface accelerates the Kemp elimination compared to the background reaction with hydroxide, which we ascribe to the ability of these anions to participate directly in the Kemp elimination. This work provides valuable mechanistic insights into the role of the cage in co-locating the substrate and the anionic reaction partners in a cage-catalysed reaction.

Received 3rd September 2021
Accepted 25th October 2021

DOI: 10.1039/d1sc04887b

rsc.li/chemical-science

Introduction

The ability of coordination cages to act as molecular containers, binding small-molecule guests inside their central cavity,[1–4] is now very well established and has led to a wide range of functional behaviours including catalysis,[2] sensing,[3] and transport.[4] As part of our work in this area using an octanuclear cubic M_8L_{12} cage (Fig. 1),[5] we have demonstrated that the accumulation of counter-ions around the exterior surface of a cationic cage is just as important a phenomenon as the binding of neutral guest molecules inside the cavity.[6–10] This is a conclusion that has also been reached by others who have demonstrated how interactions of metal/ligand cage assemblies with counter-ions at the exterior surface can play fundamentally important roles in controlling structure and speciation behaviour of cage assemblies, as well as their ability to bind guests in the central cavity.[11–13] Notably, Lusby and co-workers recently demonstrated how the positive charge associated with the surface of a cage host based on poorly-coordinating anions plays a crucial role in cage-catalysed reactions by stabilising anions, enhancing the acidity of reacting partners by several pK_a units;[12] and a while ago Raymond and co-workers demonstrated the same effect in the opposite sense, with a highly negatively charged cage strongly stabilising (by 4 pK_a units) protonation of a bound guest, leading to the possibility of acid-based catalysis even under weakly basic conditions.[13] Such charge-based effects are, clearly, equally as important as the more obvious host/guest effects based on cavity size and shape when considering the properties of cage-based systems.

The two types of guest binding that we have observed with our cage system in water – cavity-based binding of neutral hydrophobic organic molecules, and the binding of anions in the surface portals on the faces of the cage – have different origins with the former being substantially driven by the hydrophobic effect, and the latter by an electrostatic ion-pairing effect.[5] The result is that the host cage co-locates the two guest types, bringing neutral organic species and anions into close

[a]Department of Chemistry, University of Warwick, Coventry CV4 7AL, UK. E-mail: m.d.ward@warwick.ac.uk

[b]Department of Chemistry, University of Sheffield, Sheffield S3 7HF, UK

[c]School of Chemistry, Monash University, Melbourne, VIC3800, Australia

† Electronic supplementary information (ESI) available: Detailed breakdown of rate constant calculations from plate reader experiments, and some additional figures. CCDC 2107397. For ESI and crystallographic data in CIF or other electronic format see DOI: 10.1039/d1sc04887b

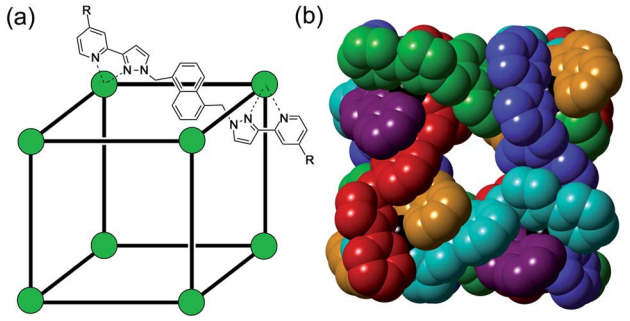

Fig. 1 The host cage $[Co_8L_{12}]^{16+}$, abbreviated as **H** (R = H) or $\mathbf{H^W}$ (R = CH_2OH). (a) A sketch emphasising the cubic array of Co(II) ions and the disposition of one bridging ligand; (b) a space-filling view of the core (without the CH_2OH substituents) showing each ligand coloured separately for clarity.

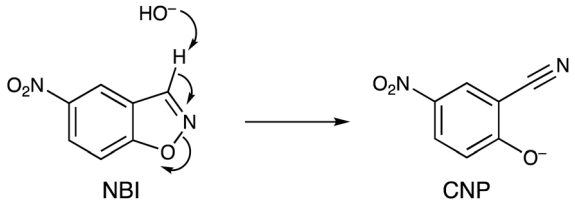

Scheme 1 Kemp elimination reaction of 5-nitro-1,2-benzisoxazole (NBI) to generate 2-cyano-4-nitrophenolate (CNP).

proximity, which is the basis of catalysis of a range of reactions.[5–9] The best example of cage-based catalysis we have demonstrated is the Kemp elimination: reaction of cavity-bound benzisoxazole with the shell of closely-adjacent hydroxide ions that accumulated around the cage surface, effectively giving a high local pH even when the bulk pH was modest. This effect resulted in a rate acceleration of up to 2×10^5 fold compared to the uncatalysed reaction under the same conditions. The high catalytic turnover (>100 cycles with no loss of activity) arises because the reaction product, the 2-cyanophenolate anion, is sufficiently hydrophilic to exit the cavity and preferentially reside in the external aqueous phase, thereby ensuring no loss of activity due to the product blocking the cage cavity.[6]

We subsequently showed that the 2-cyanophenolate anion could itself accumulate around the cage surface and act as the base to deprotonate a cavity-bound benzisoxazole molecule in an autocatalytic cycle.[7] It was apparent from this work and other control experiments that the tendency of anions to accumulate around the M_8L_{12} cage surface (which has a 16+ charge) is not just driven by electrostatic factors but has a strong hydrophobicity component, with anions that are relatively hydrophobic and weakly hydrated having a higher affinity for the cage surface compared to more hydrophilic and strongly hydrated anions.[6,7] We were able to exploit this recently in development of a fluorescence-based displacement assay to evaluate the ability of different anions to bind to the cage surface.[10] Fluorescein dianions at pH ≈ 8 are relatively hydrophobic because of their large aromatic surface area and bind strongly to the M_8L_{12} cage surface in aqueous solution, completely quenching the fluorescein's fluorescence. Titrations with different analyte ions displaced the fluorescein units from the cage surface, restoring their fluorescence, to varying extents according to the binding affinity of the analyte anion: using this method we could generate an affinity order of different anions for the M_8L_{12} cage surface.[10]

In this paper we show how the differing binding abilities of different anions to the M_8L_{12} cage surface can be used to modulate the catalysis of a Kemp elimination reaction using the substrate 5-nitro-1,2-benzisoxazole (NBI) (Scheme 1).[14] This is a more tractable substrate to use for this cage-catalysed reaction than the original example (unsubstituted 1,2-benzisoxazole) as the reaction product 2-cyano-4-nitrophenolate (hereafter abbreviated CNP) has a strong absorbance at around 400 nm which can be conveniently monitored using UV/Vis spectroscopy rather than requiring ^{1}H NMR spectroscopy, allowing large numbers of experiments to be run quickly and cheaply in parallel in a plate reader. The reaction itself, it should be emphasised, is not of major significance in terms of the importance of the product generated. However it provides a convenient way to monitor the effects of anion accumulation around the cage surface on cage-catalysed reactivity,[2] and is equally relevant to control of catalysis in other 'nanoreactors' such as micelles and vesicles where catalysis can occur on the same basis – *viz.* by co-locating hydrophobic (in the cavity) and anionic (at the surface) reaction partners.[14a,15]

We found – somewhat to our surprise – that the cage-catalysed Kemp elimination of NBI occurs around the exterior surface of the cage rather than inside the cavity, as we have observed with some other substrates,[8,9] despite the fact that NBI can occupy the cavity (as a crystal structure demonstrates). However, this does not hinder our ability to demonstrate how different anions affect the cage-based catalysis by displacing hydroxide ions (one of the reaction partners) from around the cage surface. This nicely illustrates the control that can be achieved in co-locating both neutral hydrophobic species and anions around the cage surface, a key component in developing further examples of cage-based catalysis.

Results and discussion

Guest binding and the structure of the cage/NBI assembly

The Co_8L_{12} octanuclear cubic cage system used in this work (denoted **H** or $\mathbf{H^W}$, according to the absence or presence of water-solubilising hydroxymethyl groups on the exterior surface, and usually prepared as the tetrafluoroborate salt), which has formed the basis of several studies on cage-based catalysis,[5–9] is shown in Fig. 1. The use of NBI for further studies of the cage-catalysed Kemp elimination reaction, as mentioned above, is pragmatically driven by the ease with which multiple datasets can be measured using a UV/Vis plate reader given the strong visible absorbance of the CNP product anion. Our first priority was to investigate its binding in the cavity of the Co_8L_{12} cage both in solution and the solid state. A ^{1}H NMR titration in which aliquots of NBI were added to a solution of $[Co_8L_{12}]Cl_{16}$ ($\mathbf{H}\cdot Cl_{16}$) in water[7] showed a small but

steady shift of several of the (paramagnetically-shifted) NMR signals, indicative of guest binding being in fast exchange on the NMR timescale; fitting the data to a 1 : 1 binding isotherm afforded a K value of 2×10^4 M^{-1} (Fig. 2). This is higher than we observed with unsubstituted benzisoxazole (4×10^3 M^{-1}),[6] though the counter-ion of the cage used in that experiment was different for solubility reasons which can have an effect on K values, so the two numbers are not directly comparable. In water the dominant contribution to guest binding is the hydrophobic effect,[16] and it has been shown recently that nitro substituents – despite their locally dipolar nature – are not effectively hydrated and best described as 'hydroneutral'.[17] The increase in surface area of NBI compared to unsubstituted benzisoxazole will therefore increase the contact area with the hydrophobic interior cage surface and displace more water molecules from the cage cavity when it binds, so a higher binding constant for NBI binding compared to benzisoxazole can be rationalised.[16c] It is clear that NBI binds in fast exchange inside the cubic cage cavity in water, and that under the dilute solution conditions 1 : 1 host : guest binding occurs, as we have commonly seen with many other guests.[5]

A crystal structure of the host cage complex with NBI bound in the cavity was determined (Fig. 3), with the sample prepared by the 'crystalline sponge' method[18] that we have used before:[19] a single crystal of $[Co_8L_{12}](BF_4)_{16}$ was immersed in a concentrated solution of NBI in MeOH for 24 hours, resulting in uptake of NBI guests into the cage cavity without loss of crystallinity. Structural analysis revealed that the cavity is occupied a stacked pair of symmetry-equivalent NBI guests (site occupancy 0.57 each) which lie across the crystallographic inversion centre at the centre of the cage molecule – an arrangement which we have seen with several other planar aromatic guests of comparable size.[19] Based on a molecular volume for NBI of 144 Å^3 and a cage cavity volume of 409 Å^3 this leads to a cavity occupancy of 70% for the cage containing two NBI guests. This is higher than the value of *ca.* 55 ± 9% that is considered the optimal cavity occupancy in solution,[20] but such high cavity occupancies are known in the solid state when a guest array is tightly packed because of *e.g.* π-stacking or hydrogen-bonding to the walls of the host,[19,21] both of which occur here. We emphasise that this is not a reflection of what happens in dilute solution where – as the NMR titration showed – 1 : 1 binding dominates the speciation, because the crystalline sponge experiment is carried out

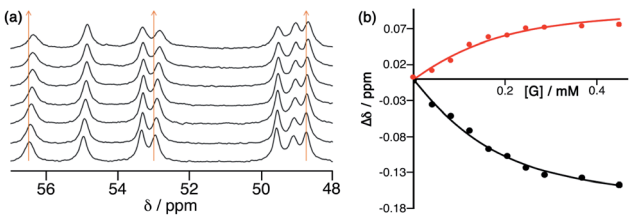

Fig. 2 ^{1}H NMR titration of NBI into an aqueous solution of H·Cl_{16}, showing (a) the small shifts in some signals as guest binding occurs in the cage cavity, and (b) fitting of some of these gradual shifts with added NBI to a 1 : 1 binding isotherm, giving $K = 2 \times 10^4$ M^{-1} (see main text).

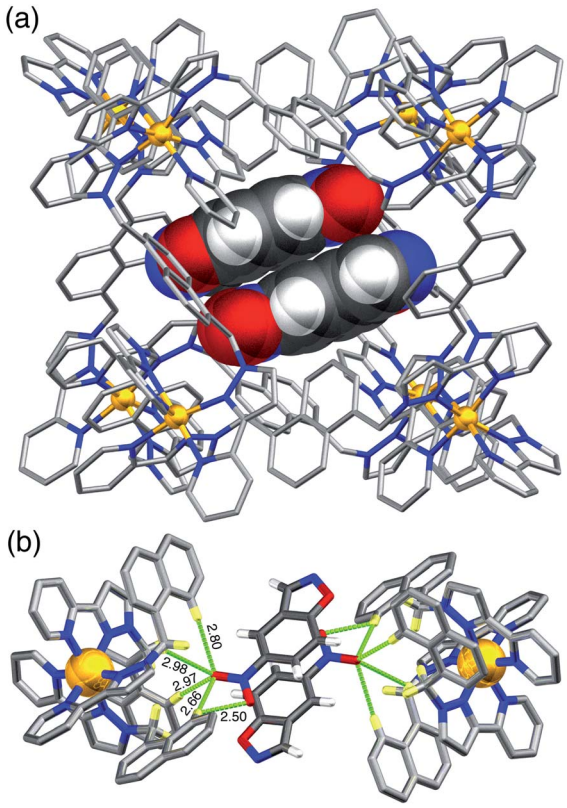

Fig. 3 Crystal structure of the complex of host cage H containing a stacked pair of NBI guest molecules (lying either side of an inversion centre). (a) View of the whole complex with the host cage shown in wireframe and the two NBI guests, shown space-filling; (b) the network of CH···O hydrogen-bonding interactions (distances shown in Å) between the convergent set of inwardly-directed CH protons from the ligands which provide the H-bond donor site, and the O atoms of the nitro group on the guests which are the H-bond acceptors.

under forcing, non-equilibrium conditions using a large excess of guest.[19] In solution, even though a second guest could in principle bind, this will not be significant because – at the low concentrations used for spectroscopic measurements – $K_2 \ll K_1$.

Each NBI molecule is oriented such that the nitro group is directed towards one of the two *fac* tris-chelate vertices, which lie at either end of the long diagonal of the cubic cage array, where there is an inwardly-directed set of CH protons from the ligand set which converge to make an H-bond donor site comparable in strength to a phenol.[22] There are several CH···O interactions between these ligand protons and the electron-rich oxygen atoms of the nitro groups (distances in Å included in Fig. 3b). This type of H-bonding interaction between the electron-rich regions of guests and the H-bond donor site on the cage interior surface is a recurrent feature of these cage/guest structures,[5,19,22] and contributes substantially to the strengths of guest binding in organic solvents.[23] The stacked guests are exactly parallel to one another (because of the inversion centre) with their mean planes separated by a typical π-stacking distance of 3.32 Å. We note that this orientation of the guest in the cavity is different from what we observed with unsubstituted

benzisoxazole, when it was the N and O atoms of the isoxazole ring that acted as the H-bond acceptors and are docked into the *fac* tris-chelate H-bond donor site,[6] rather than (as here, with NBI) the nitro group: neutral organic nitro groups are known to be able to act as H-bond acceptors, albeit weakly, given the negative charge density on the O atoms.[24] This difference of orientation of NBI compared to benzisoxazole in the cavity turns out to be significant (see later). As usual, the anions [tetrafluoroborate, arising from use of $Co(BF_4)_2$ in the cage synthesis] occupy the windows in the centre of each face, anchored by multiple CH···F hydrogen-bonds to the surrounding ligand array, such that six anions surround the cavity-bound guests.[5,7]

Catalysis of the Kemp elimination reaction with NBI

Given that NBI does bind inside the cage cavity in aqueous solution, we expected that the cage-catalysed Kemp elimination would occur by the same mechanism that we observed with unsubstituted nitrobenzisoxazole, with the cavity-bound substrate surrounded by a high local concentration of surface-bound hydroxide ions.[6] This turned out not to be the case. Initial experiments did show clearly that the cage has a catalytic effect on the reaction (Fig. 4), with the background reaction of NBI with hydroxide ions in buffered solution at pH 7 being accelerated by addition of cage $\mathbf{H^w}$ to an extent that is linear with concentration of cage added (*i.e.* the catalysed reaction is first order in catalyst; see Fig. 4c).

Under the conditions used, the rate of the background reaction – conversion of NBI to CNP – had an observed first-order rate constant of 1.8×10^{-5} s^{-1}; in the presence of 0.125 mM $\mathbf{H^w}$, this increased to a total rate (background + catalysed) of 1.53×10^{-4} s^{-1} and the catalysed reaction was confirmed to be first-order in NBI based on analysis of initial rates during the first hour. Subtracting the background rate from the observed rate in the presence of $\mathbf{H^w}$ and dividing by catalyst concentration gives a second-order rate constant of $k_2 = 1.08$ M^{-1} s^{-1} (Table 1, entry a) for the $\mathbf{H^w}$-catalysed reaction at 298 K and pH 7. For comparison purposes this is *ca.* two orders of magnitude smaller than the equivalent figure for the catalysed reaction with benzisoxazole which occurs much more efficiently.[6]

A key observation indicates that, in this case, the catalysed reaction is not occurring in the cage cavity: blocking the cavity with an unreactive but strongly binding guest (cyclo-undecanone, CUD; $K > 10^6$ M^{-1})[15] does not significantly slow down the reaction. In our earlier work, with benzisoxazole as substrate, the very fast reaction was slowed in the presence of CUD to the background rate: *i.e.* the catalysis was completely inhibited when the cage cavity was blocked and the substrate could not bind.[6] In contrast, with NBI as substrate, the reaction continues unchanged in the presence of CUD (see ESI†). We have observed before that some other substrates undergo cage-

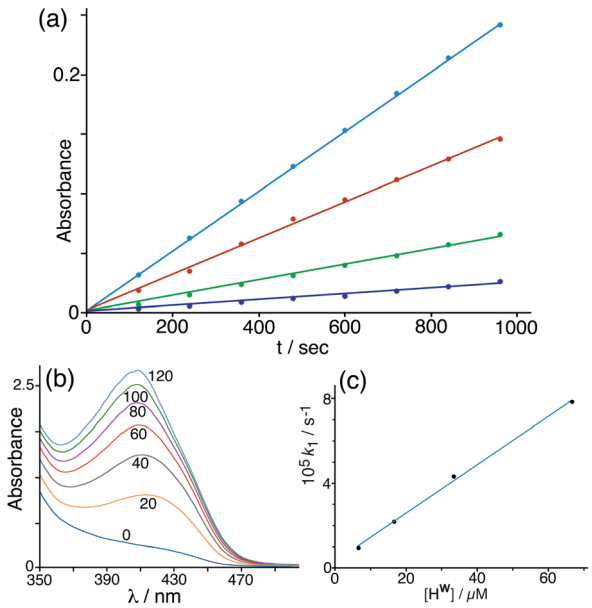

Fig. 4 (a) Progress of the Kemp elimination reaction (background-corrected) using NBI as substrate at various catalyst concentrations (from bottom up: 6.7 μM; 16.7 μM; 33 μM; 67 μM): these show first order behaviour in NBI in the form of linear ln[NBI] *vs. t* plots. Reaction progress was monitored by absorbance at 408 nm. (b) Progress of a typical catalysed experiment (0.125 mM $\mathbf{H^w}$) showing increasing absorbance from the CNP product with time (shown in minutes for each trace). (c) Observed reaction (initial) rate *vs.* catalyst concentration, confirming first order behaviour in catalyst $\mathbf{H^w}$. Conditions: 298 K, pH 7; 0.25 mM NBI; varying concentrations of $\mathbf{H^w}$ as indicated. The slope of this line gives a value for the second-order reaction rate constant k_2 of 1.18 M^{-1} s^{-1} which may be compared with the values given in Table 1 (entries a and p).

Table 1 Second-order rate constants for $\mathbf{H^w}$-catalysed Kemp-elimination reaction with NBI in the presence of different concentrations of added sodium salts[a]

Entry	Added anion (as Na^+ salt)	Conc./mM	k_2/M^{-1} s^{-1}
a	None	—	1.08
b	F^-	1.67	1.14
c	Cl^-	1.67	0.81
d	Br^-	1.67	0.29
e	NO_3^-	1.67	0.23
f	IO_3^-	1.67	0.89
g	HCO_3^-	1.67	1.51
h	SO_4^{2-}	1.67	0.85
i	F^-	16.7	1.60
j	Cl^-	16.7	0.34
k	Br^-	16.7	0.12
l	NO_3^-	16.7	0.12
m	IO_3^-	16.7	0.84
n	HCO_3^-	16.7	Decomposes
o	SO_4^{2-}	16.7	0.73
p	None	—	1.24
q	F^-	1.0	1.28
r	Formate	1.0	1.38
s	Acetate	1.0	1.54
t	HCO_3^-	1.0	2.15

[a] All experiments performed at 298 K and pH 7. Experiments a–o: 0.125 mM $\mathbf{H^w}$; 0.2 mM NBI. Experiments p–t: 0.05 mM $\mathbf{H^w}$; 0.1 mM NBI. All rate constants derived from initial-rate data during the first 2000 seconds. Estimated errors in k_2, ±5%; all plate-reader measurements from which these rate constants are derived were performed in quadruplicate and averaged (see ESI).

catalysed reactions with hydroxide ions at the exterior surface of the cage: the observations described above with NBI are consistent with this type catalysis occurring.[8,9] The exterior surface is just as hydrophobic as the interior surface and so will allow some aggregation with hydrophobic species such as NBI. This association will be weaker than cavity-binding as the guest is not surrounded by the host so there will be less overlap of hydrophobic host and guest surfaces compared to cavity binding. Nonetheless, this brings the substrate into contact with the high local concentration of hydroxide ions that accumulate around the cage surface for electrostatic reasons. In addition, the reaction is occurring in a more favourable solvation environment for the product, in the exterior aqueous phase rather than the interior hydrophobic cavity (though this also solvates the hydroxide ions, reducing their activity). Catalysis of this type of elimination reaction is therefore not limited to the interior cavity of the cage, although our previous work with benzisoxazole showed that catalysis on the interior was far more efficient.[5,6]

Given that NBI clearly does bind inside the cage cavity in solution, it is curious that cavity-bound catalysis does not work in the way that it does with unsubstituted benzisoxazole.[6] Molecular modelling provides some insight to this. Molecular models of host cage **H** containing one molecule of either benzisoxazole or NBI as guest were calculated using the molecular docking program 'GOLD', by posing one molecule of the guest inside the cavity of a (rigid) host cage whose structure comes from crystallographic data (Fig. 5).[25] With a single molecule of benzisoxazole as guest, in the energy-minimised structure the C–H proton that is removed during the Kemp elimination is directed towards a portal and is therefore accessible to a surface-bound anion (Fig. 5a). In contrast, with NBI as guest, its different orientation in the cavity – which was obtained as the minimum-energy structure from multiple different initial cage/NBI geometries, see ESI† – is associated with H-bonding of the nitro group to the cage interior surface (seen also in the crystal structure reported above, but with a stacked pair of guests). This means that the C–H proton is no longer directed towards a portal and – in this conformation of the adduct – is less accessible to a surface-bound anion (Fig. 5b). Thus, the different steric properties of the cage/guest complex could be significant here.

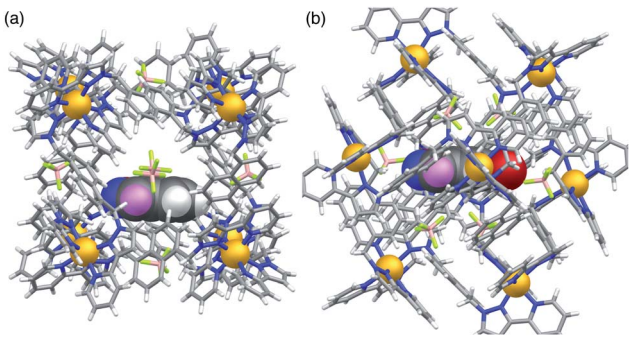

Fig. 5 Molecular models of the host cage H containing (a) one molecule of benzisoxazole and (b) one molecule of NBI. The views are arranged to show the same edge-on orientation of the guest, looking down on to the C–H proton (coloured purple) that is the one extracted as the first step in the Kemp elimination. In (a) the C–H proton is clearly directed towards a portal and accessible to a surface-bound anion; in (b) the different orientation of the NBI guest in the cavity makes the C–H proton less accessible.

An additional possibility could be that, even if a cavity-bound NBI is accessible to a surface-bound hydroxide ion, the pathway to formation of the expanded, ring-opened product is inhibited in the cavity by the additional bulk of the nitro group. Similar loss of reactivity has been demonstrated for cage-bound P_4, for example, arising from the fact that reaction of P_4 with O_2 results in initial formation of bulky intermediate species that cannot be accommodated in the confined space.[26] The overall effect in our case is that catalysis does happen, but outside the cavity, and much more slowly than for the cavity-based reaction of unsubstituted benzisoxazole.[6]

Interaction of the product phenolate anion with the cage surface

We need to highlight at this point an issue which complicates monitoring of the reaction progress using the absorbance of the CNP anion. During the catalysis studies described in this paper we noticed that the absorption maximum of the product anion CNP was red-shifted by the presence of $\mathbf{H^w}$. In aqueous solution without cage present, λ_{max} for the lowest-energy charge-transfer absorption of CNP is 379 nm: but in the presence of $\mathbf{H^w}$ this is red-shifted to 405 nm, which we ascribe to interaction of the anion with the cage surface at the anion-binding sites in the windows.[6,7,10] This red-shift happens in exactly the same way with both $\mathbf{H^w}$ and the unsubstituted but otherwise isostructural cage **H** (Fig. 6a) indicating that the hydroxymethyl pendant groups attached to $\mathbf{H^w}$ are not involved in this interaction: this is consistent with the windows at the face centres being involved, as we have seen crystallographically for many small inorganic anions.[5,27] Significantly, this red-shift in λ_{max} for CNP is complete after addition of about 0.3 equivalents of either **H** or $\mathbf{H^w}$, indicating that multiple (≈ 3) CNP anions can interact with a single cage molecule, consistent with surface rather than cavity binding. This is exactly consistent with the behaviour that we have seen with other large/soft aromatic anions such as fluorescein, where multiple anions can interact with the surface of a single $\mathbf{H^w}$ molecule depending on the concentrations of components.[10]

We can use this red-shift to put the binding affinity of the CNP anion for the cage surface into an affinity series with other anions. Fig. 6b shows the results of adding an excess of a range of different inorganic monoanions (halides, iodate, nitrate) to a solution of 0.05 mM $\mathbf{H^w}$ and 0.1 mM CNP at pH 7. Initially λ_{max} for CNP is at 405 nm, as the two equivalents of CNP are fully bound to $\mathbf{H^w}$. Addition of 0.5 mM of fluoride or iodate (hydrophilic anions which bind weakly to the cage surface)[10] did not change the λ_{max} value, indicating that these anions could not displace CNP even when present in excess. Addition of 0.5 mM of bromide or nitrate – more weakly hydrophilic anions which bind more strongly to the cage surface as they are easier to desolvate[10] – in contrast results in λ_{max} for CNP shifting to

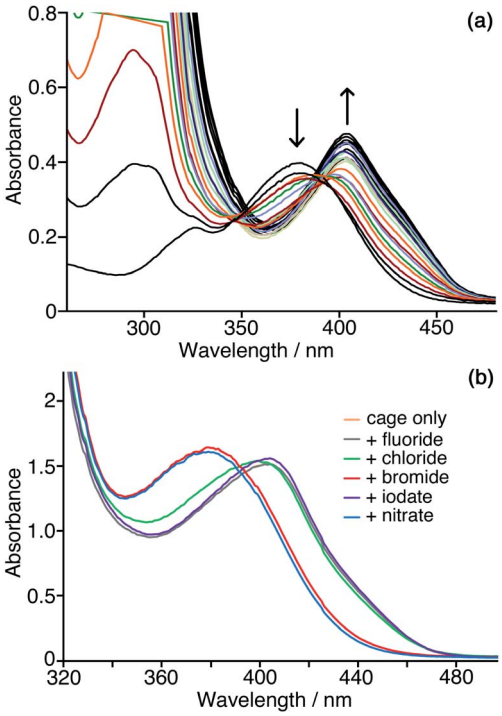

Fig. 6 Interaction of the CNP anion with the cage surface. (a) Addition of small samples (2 μM concentration increments) of H to a solution of CNP (0.05 mM) in water, showing the red-shift in the CNP absorbance maximum as it binds to the cage surface; the red-shift of the maximum is complete after addition of *ca.* 0.3 equiv. of cage, thereafter only small changes in intensity occur. (b) Effects of addition different inorganic mono-anions (10 equiv.) to displace CNP from the surface of H^w in water. Conditions: 0.05 mM H^w and 0.1 mM CNP at pH 7. Note that the spectrum for 'cage only' (orange trace) is completely concealed under the spectrum recorded with added fluoride (purple trace), indicating the lack of ability of highly-solvated fluoride to displace CNP from the cage surface.

379 nm, which is the value for the free anion, indicating complete displacement. With addition of 10 equivalents of chloride (green line in Fig. 6b), an intermediate result is obtained, with a slight blue shift of λ_{max} to 399 nm and a change in curve shape with the emergence of increased absorbance between 340–380 nm associated with some free CNP: so we can see a slight amount of displacement of CNP from the surface of $\mathbf{H^w}$ but it is far from complete even in the presence of a large excess of chloride, indicating that the affinity order of these two is CNP > chloride. We know from our previous work that the affinity order of inorganic monoanions for the surface of $\mathbf{H^w}$ is nitrate > bromide > chloride > iodate > fluoride (following the Hofmeister series).[10] We can now insert CNP into that sequence to give an affinity order of anions for the cage surface of nitrate > bromide > CNP > chloride > iodate > fluoride, with the hydrophobicity and ease of desolvation of CNP positioning it between chloride and bromide in the affinity order of anions.

This shift of λ_{max} for the CNP anion according to whether it is bound to the cage surface or free in aqueous solution – which depends on any competing anions present (Fig. 6) – affects the reaction monitoring because the proportion of bound *vs.* free CNP will change as the reaction proceeds, meaning that the absorbance at one fixed monitoring wavelength may not follow the Beer–Lambert law. We can partly compensate for this in two ways. Firstly, the absorbance for the catalysis reactions was monitored by recording UV/Vis spectra over the whole relevant range rather than just observing the absorbance at one wavelength, and the most appropriate monitoring wavelength was selected for each experiment calculation according to where λ_{max} was located. Secondly, rate constants discussed in this paper are based on measurements of initial rates during the early stages of the reaction when the curves fit well to simple first-order behaviour at a given catalyst concentration, and the absorption maximum had not significantly drifted because of a change in balance between free and cage-bound CNP.

Effect of added anions on the cage-based catalysis

In Fig. 7a is shown the effect of adding a fixed concentration (1.67 mM, as the sodium salt) of a range of different anions to a catalysis reaction using 0.125 mM $\mathbf{H^w}$ and 0.2 mM NBI (buffered at pH 7). In the as-synthesised cage, 0.125 mM $\mathbf{H^w}$ (with its 16+ charge) is accompanied by 2 mM tetrafluoroborate, but hydrolysis of tetrafluoroborate following dissolution generates borate and fluoride[28] which accordingly are also present as part of the baseline conditions, as is the ionic background from the 16.7 mM phosphate buffer: so the discussion of anion effects in this section is relative to the effects of this fixed background. The initial rates for the catalysed reactions in the presence of the different additional anions (with rates for the background reaction in the absence of catalysts subtracted) have been used to calculate the second-order rate constants in Table 1.

We can immediately see two contrasting effects, according to how basic the added anions are. Compared to the experiment with 0.125 mM $\mathbf{H^w}$ on its own, addition of non-basic anions reduces the reaction rate, with – for example – addition of 1.67 mM or 16.7 mM bromide causing a decrease in k_2 by factors of *ca.* 3 or 9 respectively (Table 1, entries d and k). This is in line with what we have observed before:[7,10] bromide has a higher affinity than does hydroxide for the cationic but hydrophobic cage surface, due to its smaller desolvation enthalpy.[29] Bromide therefore preferentially accumulates around the cage, reducing the local concentration of hydroxide and slowing down the reaction. The order in which the added monoanions inhibit the Kemp elimination reaction is $IO_3^- < Cl^- < Br^- < NO_3^-$, which is the same as the affinity order of these anions for the cage surface that we established recently using our recent fluorescence-displacement assay.[10] In fact the correlation of the k_2 value in the presence of these anions (measured in this work, Table 1) with K (the 1 : 1 binding constant with an anion-binding site in a cage face)[10] is strikingly linear ($R^2 > 0.999$; Fig. 7b): the extent of inhibition of the surface-catalysed Kemp elimination is directly related to the affinity of the anion for the cage surface. For chloride, bromide and nitrate this is the expected order based on the Hofmeister series.[30] Iodate does not figure in some lists of the Hofmeister series,[30a] but recently the iodate anion has been shown to be more strongly hydrated than

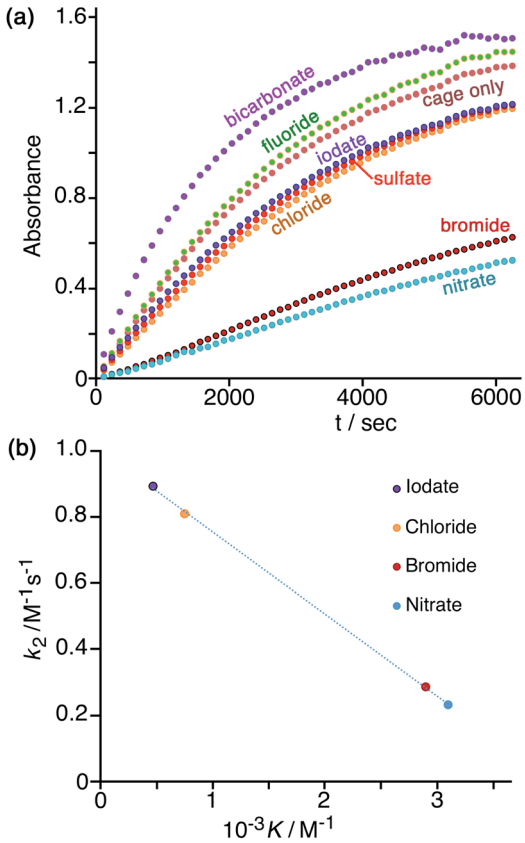

Fig. 7 (a) Progress of cage-catalysed Kemp eliminations (background-subtracted) using NBI as substrate, monitoring formation of CNP by its absorbance in the 380–410 nm region (conditions: aqueous solution at pH 7 using 16.7 mM phosphate buffer; 0.125 mM $\mathbf{H^w}$; 0.2 mM NBI; various different added anions as sodium salts, 1.67 mM. Shown are results from individual plate-reader experiments; four such repeats are averaged to give the k_2 values in Table 1). (b) Correlation between reduction in second-order rate constant for catalysis (k_2) in the presence of various anions (this work), based on analysis of initial rates, and the binding constant of that anion for a cage surface binding site (K, from ref. 10).

many other oxyanions due to a highly polarised I(δ+)/O(δ−) charge distribution and therefore acts as a more powerful kosmotrope than chloride[31] – exactly in agreement with what we observe.

The effect of sulfate, the only 2− anion of this series, on inhibiting the cage-catalysed Kemp elimination of NBI is however out of step with the high affinity of sulfate for the cage surface that we measured earlier.[10] Although sulfate is expensive to desolvate,[29] it nonetheless has a high affinity for the cage surface, possibly because its high desolvation enthalpy is offset by strong electrostatic attraction between 16+ cage and 2− anion: its 1 : 1 binding constant to a cage surface binding site is higher than that of bromide and nitrate.[10] Its ability to inhibit the Kemp elimination of NBI by accumulating around the cage surface is therefore smaller than we expected (Table 1, entries h and o) on the basis of the 1 : 1 anion/cage binding constants. However there will be an additional electrostatic effect in play here: whilst one sulfate dianion binds strongly to $\mathbf{H^w}$, its 2− charge limits the number of *additional* sulfates that will approach the cage. Indeed we observed before that such effects are significant, with the trianion of hydroxypyrene-tris(sulfonate) $[HPTS]^{3-}$ forming a 6 : 1 HPTS : $\mathbf{H^w}$ complex under forcing conditions, but the tetra-anion $[HPTS]^{4-}$ forming a neutral 4 : 1 HPTS : $\mathbf{H^w}$ complex at the same concentration.[10] Thus, a small number of sulfate anions may indeed bind strongly to $\mathbf{H^w}$, as the 1 : 1 K value suggests, but its ability to saturate the cage surface and exclude all hydroxide ions will be electrostatically inhibited, such that some hydroxide will still have access to the cage surface and facilitate the catalysed reaction with NBI, as we observe. It is notable that increasing the concentration of sulfate tenfold from 1.67 mM (Table 1, entry h) to 16.7 mM (Table 1, entry o) has very little additional effect on the inhibition.

Finally, these experiments are carried out in phosphate buffer, which is a mixture of mono- and dianionic inorganic phosphate, and so these specific electrostatic effects of more highly charged anions are already present in the background baseline activity. Hence, the specific electrostatic impact of dianionic sulfate (relative to the other anions) may already be present, and so the additional impact is much reduced under these conditions as sulfate substitutes for dianionic phosphate. In contrast to the effects of the above anions which all have an inhibitory effect, addition of a basic anion such as HCO_3^- *increases* the catalysed reaction rate, with k_2 increasing slightly by a factor of *ca.* 1.5 (Table 1, entry g) by addition of 1.67 mM $NaHCO_3$. Given that the solution is buffered at pH 7 this cannot be ascribed to a pH change on addition of $NaHCO_3$, but it can plausibly be ascribed to the fact that the HCO_3^- ions that will accumulate around the cage surface can act as bases in the Kemp elimination in a way that bromide, nitrate *etc.* do not. This result suggests that HCO_3^- ions deprotonate NBI and initiate the Kemp elimination more rapidly than do hydroxide ions. This of course is inconsistent with the relative pK_a values of these anions: but it is consistent with the lower hydration enthalpy of HCO_3^- resulting in a higher local concentration of it around the cage surface than the more strongly solvated HO^- ions can achieve.[29] An experiment in the absence of cage (Fig. 8a) showed that this effect does not arise from the anions alone but requires the additional presence of $\mathbf{H^w}$ to bring the anions into close proximity with the NBI substrate, co-locating the two reaction partners. A 50% increase in reaction rate is small, likely because of (i) the high background concentration of other anions from the buffer and cage counter-ions, and (ii) the fact that the reaction is happening at the cage exterior surface where hydroxide ions can also access the substrate. However the fundamental difference between (i) the weakly accelerating behaviour of HCO_3^-, and (ii) the inhibitory nature of other non-basic anions, on the catalysis by $\mathbf{H^w}$ is very clear.

Similarly, addition of fluoride causes a small increase in reaction rate (Fig. 7a and 8b) which we ascribe to its weak basicity, as discussed above for HCO_3^-, though the effect is smaller (addition of 1.67 mM and then 16.7 mM fluoride results in increases in k_2 by *ca.* 5% and then 50% respectively; Table 1, entries b and i). We investigated this effect of the basicity of the added anion further using the simple carboxylates acetate and

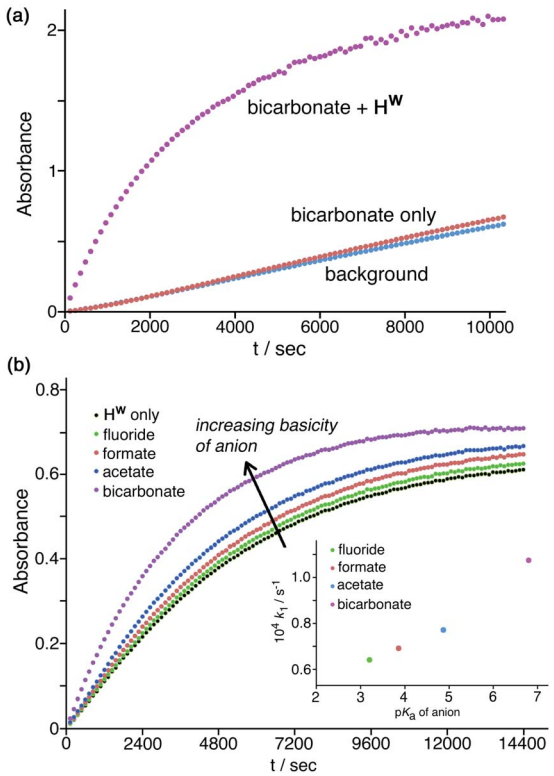

Fig. 8 Effects of anion basicity on catalysis reaction rates. Shown are results from individual plate-reader experiments; four such repeats are averaged to give the k_2 values in Table 1. (a) Experiment showing how added HCO_3^- has no effect on the background reaction rate when H^W is not present; both H^W and HCO_3^- need to be present to see the additional rate-accelerating effect. Conditions: 0.2 mM NBI; 0.125 mM H^W; pH 7 using 16.7 mM phosphate buffer. (b) Reaction progress curves (pH 7; 298 K; 0.05 mM H^W; 0.1 mM NBI) for the cage-catalysed Kemp elimination with NBI in the absence of any added anion, and then with added fluoride, formate, acetate or hydrogen carbonate as their sodium salts (1.0 mM) [inset: correlation of catalysed pseudo first-order reaction rates with pK_a of added anion].

formate in addition to fluoride and HCO_3^-, giving a pK_a range for the added anions ranging from 3.2 (fluoride), 3.8 (formate), 4.8 (acetate), and 6.4 (HCO_3^-) (Table 1, entries p–t). With the same concentration of added anion, all resulted in an increase in the catalysed reaction rate compared to the reaction rate in the presence of $\mathbf{H^W}$ alone, with a clear correlation between anion basicity and increase in reaction rate (Fig. 8b). The particularly substantial effect of HCO_3^- may be because of the presence of traces of the more powerful base carbonate (pK_a 10.3). Although at pH 7 there should be very little of this present in bulk solution, the stabilising effect of the 16+ charge of the cage moves this pK_a value for surface-bound carbonate downwards,[10] meaning that the rate-enhancing effect of added $NaHCO_3$ may include a contribution from carbonate as well as from hydrogen carbonate. As mentioned above the absolute effects are small – a difference of >3 pK_a units between different anions results in just a factor of 2 difference in initial catalysed rates, as shown in Fig. 8b, and reasons for this have been suggested. However the trend is again clear and confirms the role of $\mathbf{H^W}$ in solution in co-locating the NBI substrate and the anion which acts as base to initiate the Kemp elimination reaction.

The differing effects of the halides (chloride and bromide retarding the catalysis by displacing hydroxide from around the cage surface, but fluoride accelerating the catalysis because of its weakly basic nature) are clearly illustrated in Fig. 9 which shows the effects of adding up to 200 equivalents of these anions in small portions. On incremental additions of fluoride the reaction rate steadily increases until it has approximately

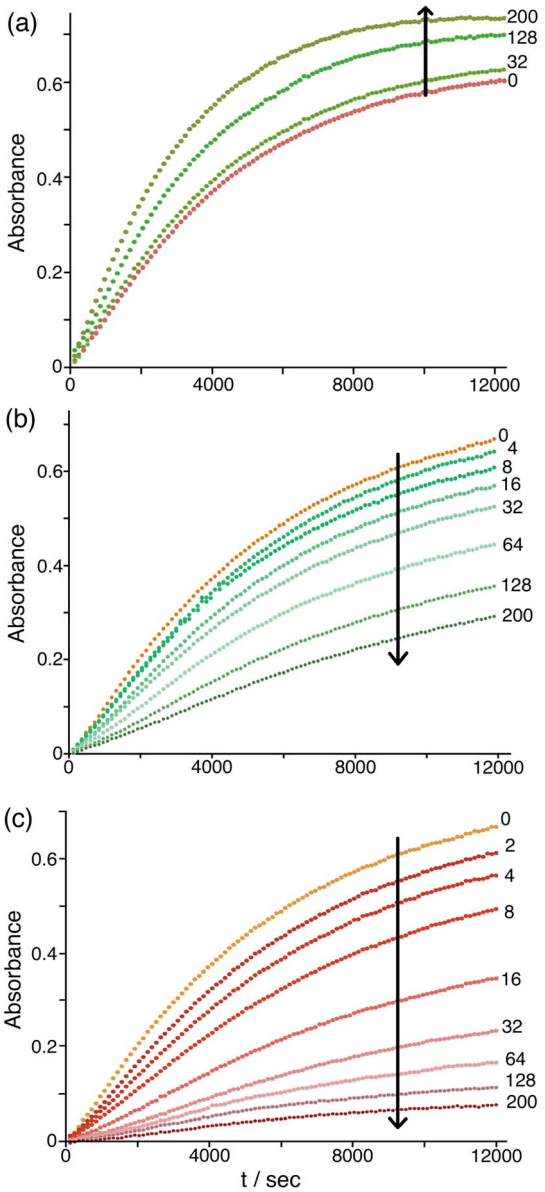

Fig. 9 Effect of increasing concentrations of halide ions [(a) fluoride; (b) chloride; (c) bromide] on the progress of the H^W-catalysed Kemp elimination reaction of NBI (background subtracted), monitoring formation of CNP by its absorbance in the 380–410 nm region. Conditions: 16.7 mM pH 7 aqueous phosphate buffer; 0.05 mM H^W; 0.1 mM NBI; concentration of added halide, 0.05–10 mM. The numbers on the curves are numbers of equivalents of added halide ion per cage. Shown are results from individual plate-reader experiments; four such repeats are averaged to give the k_2 values in Table 1.

Table 2 Crystal parameters, data collection and refinement details for the structure of the H/NBI complex

Complex	$\mathbf{H \cdot NBI_{1.14}}$
Formula	$C_{374.84}H_{392.48}B_{14.2}Cl_{1.8}Co_8F_{56.8}N_{74.24}O_{34.36}$
Molecular weight	8255.24
T/K	100(1)
Radiation wavelength/Å	Synchrotron (0.6889)
Crystal system	Monoclinic
Space group	$C2/c$
a/Å	33.12481(19)
b/Å	30.0412(2)
c/Å	40.1650(3)
β/°	95.9731(6)
V/Å^3	39 751.6(3)
Z	4
ρ/g cm^{-3}	1.379
Crystal size/mm^3	0.13 × 0.10 × 0.08
μ/mm^{-1}	0.409
Data, restraints, parameters	63 327, 6797, 2523
Final R_1, wR_2[a]	0.0886, 0.3254
Largest diff. peak/hole/e Å^{-3}	1.33/−0.74

[a] The value of R_1 is based on 'observed' data with $I > 2\sigma(I)$; the value of wR_2 is based on all data.

doubled after 200 equivalents of fluoride are added. In contrast there are obvious reductions in reaction rate as more and more chloride or bromide are added, with bromide having a greater effect for the reasons discussed earlier. Overall these observations confirm the presence of two distinct effects on the catalysis associated with accumulation of anions around the surface of $\mathbf{H^w}$: (i) the generally inhibiting effect on the Kemp elimination associated with displacement of hydroxide, to an extent depending on the binding affinity of the anions for the cage surface; but (ii) an accelerating effect in those cases where the new anion can itself act as base, as shown by the relationship between the magnitude of this effect and the anion basicity (Fig. 8b and 9a).

One final point to note in this section is that we can clearly see, in those cases when the reaction is most inhibited (notably in the presence of chloride, nitrate or bromide; *e.g.* in Fig. 7a and 9b, c), a slightly sigmoidal component to the reaction progress curve. This could be indicative of an autocatalytic[7,32] mechanism becoming significant in which the product of the reaction – which here would be the CNP anion, itself a 'soft' (hence, weakly solvated) but weakly basic[33] anion – acting as the base to deprotonate another equivalent of starting material and propagate the reaction, as we saw before with our cavity-bound Kemp elimination catalysis.[7] In such situations the reaction accelerates as the product (the catalyst) accumulates, until substrate runs out, resulting in the characteristic sigmoidal shape for the reaction progress profile.[32] However we can conclusively rule this out here. A simple test for autocatalysis is that adding a small amount of product to the start of the reaction should accelerate the reaction, but that does not happen: instead, addition of increasing amounts of CNP at the start of the reaction progressively inhibits it, on the same basis as the other anions which displace hydroxide from around the cage surface. So autocatalysis is not happening here, presumably because of the poor basicity of the CNP anion.[33] Instead we ascribe the small sigmoidal contribution in the reaction profiles when the reaction is particularly strongly inhibited to the change in λ_{max} of the CNP absorption maximum that we discussed earlier. A change in balance between cage-bound and free CNP as the reaction proceeds could lead to the extinction coefficient at the monitoring wavelength increasing slightly as the reaction proceeds which would give this effect. This vindicates our decision to use initial rates as the basis for comparison between the effects of different anions, which are the values used in Table 1: general trends associated with the effects of different added anions are quite clear.

Conclusion

In contrast to our previously reported cavity-catalysed Kemp elimination using the cage $\mathbf{H^w}$ as catalyst and benzisoxazole as substrate,[6,7] use of NBI as substrate resulted in much lower catalytic rate enhancement with the reaction occurring outside the cage cavity, at the exterior surface which is nonetheless both hydrophobic and cationic and therefore provides a locus for co-location of the hydrophobic NBI substrate and the anionic reaction partner (normally hydroxide). We could therefore use the reaction rate as a way to monitor the affinity of the cage surface for different types of added anion, as accumulation of other anions around the cage surface displaces hydroxide and slows down the surface-catalysed reactions. We observed that for a range of simple mono-anions the affinity for the cage surface followed the Hofmeister series, with more weakly solvated anions (*e.g.* bromide, nitrate) having a higher affinity for binding to the cage surface[10] and therefore causing a greater degree of inhibition of the Kemp elimination. In opposition to this effect, if the added anions are themselves basic, their accumulation around the cage surface can accelerate the reaction to an extent related to their basicity. Although these added anions (fluoride, acetate, hydrogen carbonate *etc.*) are weaker bases than hydroxide they are present in the reaction medium at much higher concentrations than hydroxide at pH 7, resulting in a high local concentration close to the NBI substrate around the cage surface, accounting for this observation. The CNP anion itself can bind to the cage surface, more strongly than chloride but less strongly than bromide, as demonstrated by UV/Vis spectroscopy; the absence of autocatalysis suggests that it is too weakly basic to complete significantly with hydroxide.

Overall the role of the cage in bringing hydrophobic organic species and anions into proximity, which is the basis of the catalytic effects that we have previously observed,[6–9] is very clear, which is useful to know considering the possibilities for catalysis that arise from accumulation of phenolate anions at the cage surface. The nucleophilicity of phenolate anions, for example, may provide the basis for reactions with a cavity-bound electrophile if multiple phenolates can surround a cavity-bound guest giving a high local concentration.[7] More generally we can imagine that any of a vast range of reactions between a neutral/hydrophobic organic substrate in the cavity, and an anionic nucleophile with a high local concentration due

to accumulation at the cage surface, are ripe targets to investigate for catalysis in this way.

Experimental

Samples of **H** (used for the crystalline sponge experiment)[34] and $\mathbf{H^W}$ (used for solution catalysis studies)[16b] were prepared as previously described. Inorganic salts used to evaluate anion binding affinities were purchased from Sigma-Aldrich and used as delivered. Catalysis studies were carried out at 298 K using a BMG ClarioStar plate reader with 96-well plates by measuring UV/Vis spectra of the emerging 2-cyano-4-nitrophenolate anion (350–500 nm) and then monitoring the reaction by taking the absorbance at the maximum which shifts slightly between experiments according to the nature of other anions present (see main text). The extinction coefficient of the CNP absorption maximum was taken as 15 800 M^{-1} cm^{-1} irrespective of whether CNP is free or cage-bound; the small error introduced by this (see Fig. 6b) is subsumed in the ±5% estimated uncertainty for the rate constant values in Table 1. Samples for catalysis studies were prepared as described in the relevant figure captions and buffered at pH 7 using 16.7 mM phosphate buffer. Each dataset reported is based on the average of four individual measurements with different samples. The starting material NBI was prepared according to the literature procedure.[14c] The ESI contains the data used for the rate constant calculations in Table 1.

Information on the crystal properties, data collection and refinement parameters associated with the structure determination of the **H**/**NBI** host–guest complex is collected in Table 2. The data collection was performed in Experiment Hutch 1 of beamline I-19 at the UK Diamond Light Source synchrotron facility,[35] using methodology, data processing and software outlined previously.[19] CCDC deposition number: 2107397.†

Data availability

Data that is not in the ESI is available from the corresponding author (MDW) on request.

Author contributions

Synthesis: MDL, JST. Binding constant measurement: JST. X-Ray crystallography: CGPT. Plate reader and UV/Vis spectroscopic measurements: MDL, MBT, JD, KLT. Data analysis: MDL, NHW, KLT. Manuscript preparation: MDW, NHW, MDL. Project conception and supervision: MDW.

Conflicts of interest

There are no conflicts to declare.

Acknowledgements

We thank EPSRC for a PhD studentship to MDL (grant number EP/N509796/1); the Universities of Warwick and Monash University for a 'Monash/Warwick Alliance' Accelerator grant to MDW and KLT; and the Royal Society for an International Exchange grant IES/R3/170177 to MDW.

Notes and references

1 (*a*) T. R. Cook and P. J. Stang, *Chem. Rev.*, 2015, **115**, 7001; (*b*) T. R. Cook, Y.-R. Zheng and P. J. Stang, *Chem. Rev.*, 2013, **113**, 734; (*c*) R. Chakrabarty, P. S. Mukherjee and P. J. Stang, *Chem. Rev.*, 2011, **111**, 6810; (*d*) M. M. J. Smulders, I. A. Riddell, C. Browne and J. R. Nitschke, *Chem. Soc. Rev.*, 2013, **42**, 1728; (*e*) D. Zhang, T. K. Ronson and J. R. Nitschke, *Acc. Chem. Res.*, 2018, **51**, 2423; (*f*) H. Vardhan, M. Yusubov and F. Verpoort, *Coord. Chem. Rev.*, 2016, **306**, 171.

2 (*a*) Y. Fang, J. A. Powell, E. Li, Q. Wang, Z. Perry, A. Kirchon, X. Yang, Z. Xiao, C. Zhu, L. Zhang, F. Huang and H.-C. Zhou, *Chem. Soc. Rev.*, 2019, **48**, 4707; (*b*) C. J. Brown, F. D. Toste, R. G. Bergman and K. N. Raymond, *Chem. Rev.*, 2015, **115**, 3012; (*c*) M. Yoshizawa, J. K. Klosterman and M. Fujita, *Angew. Chem., Int. Ed.*, 2009, **48**, 3418; (*d*) M. Otte, *ACS Catal.*, 2016, **6**, 6491; (*e*) C. M. Hong, R. G. Bergman, K. N. Raymond and F. D. Toste, *Acc. Chem. Res.*, 2018, **51**, 2447; (*f*) W.-X. Gao, H.-N. Zhang and G.-X. Jin, *Coord. Chem. Rev.*, 2019, **386**, 69.

3 (*a*) Y. Sun, C. Chen, J. Liu and P. J. Stang, *Chem. Soc. Rev.*, 2020, **49**, 3889; (*b*) M. Zhang, M. L. Saha, M. Wang, Z. Zhou, B. Song, C. Lu, X. Yan, X. Li, F. Huang, S. Yin and P. J. Stang, *J. Am. Chem. Soc.*, 2017, **139**, 5067; (*c*) C.-L. Liu, R.-L. Zhang, C.-S. Lin, L.-P. Zhou, L.-X. Cai, J.-T. Kong, S.-Q. Yang, K.-L. Han and Q.-F. Sun, *J. Am. Chem. Soc.*, 2017, **139**, 12474; (*d*) J. Wang, C. He, P. Wu, J. Wang and C. Duan, *J. Am. Chem. Soc.*, 2011, **133**, 12402; (*e*) Y. Jiao, J. Wang, P. Wu, L. Zhao, C. He, J. Zhang and C. Duan, *Chem.–Eur. J.*, 2014, **20**, 2224; (*f*) X.-Z. Li, L.-P. Zhou, L.-L. Yan, D.-Q. Yuan, C.-S. Lin and Q.-F. Sun, *J. Am. Chem. Soc.*, 2017, **139**, 8237.

4 (*a*) A. B. Grommett and J. R. Nitschke, *J. Am. Chem. Soc.*, 2017, **139**, 2176; (*b*) A. Garci, J.-P. Mbakidi, V. Chaleix, V. Sol, E. Orhan and B. Therrien, *Organometallics*, 2015, **34**, 4138; (*c*) T. Grancha, A. Carné-Sánchez, L. Hernández-López, J. Albalad, I. Imaz, J. Juanhuix and D. Maspoch, *J. Am. Chem. Soc.*, 2019, **141**, 18349; (*d*) A. M. Castilla, T. K. Ronson and J. R. Nitschke, *J. Am. Chem. Soc.*, 2016, **138**, 2342; (*e*) S. Löffler, J. Lübben, L. Krause, D. Stalke, B. Dittrich and G. H. Clever, *J. Am. Chem. Soc.*, 2015, **137**, 1060; (*f*) B.-N. T. Nguyen, A. B. Grommett, A. Tron, M. C. A. Georges and J. R. Nitschke, *Adv. Mater.*, 2020, **32**, 1907241.

5 (*a*) M. D. Ward, C. A. Hunter and N. H. Williams, *Acc. Chem. Res.*, 2018, **51**, 2073; (*b*) M. D. Ward, C. A. Hunter and N. H. Williams, *Chem. Lett.*, 2017, **46**, 2.

6 W. Cullen, M. C. Misuraca, C. A. Hunter, N. H. Williams and M. D. Ward, *Nat. Chem.*, 2016, **8**, 231.

7 W. Cullen, A. J. Metherell, A. B. Wragg, C. G. P. Taylor, N. H. Williams and M. D. Ward, *J. Am. Chem. Soc.*, 2018, **140**, 2821.

8 C. G. P. Taylor, A. J. Metherell, S. P. Argent, F. M. Ashour, N. H. Williams and M. D. Ward, *Chem.–Eur. J.*, 2020, **26**, 3065.
9 C. Mozaceanu, C. G. P. Taylor, J. R. Piper, S. P. Argent and M. D. Ward, *Chemistry*, 2020, **2**, 22.
10 M. D. Ludden and M. D. Ward, *Dalton Trans.*, 2021, **50**, 2782.
11 (*a*) F. J. Rizzuto, W. Y. Wu, T. K. Ronson and J. R. Nitschke, *Angew. Chem., Int. Ed.*, 2016, **55**, 7958; (*b*) I. A. Riddell, M. M. J. Smulders, J. K. Clegg, Y. R. Hristove, B. Breiner, J. D. Thoburn and J. R. Nitschke, *Nat. Chem.*, 2012, **4**, 751; (*c*) N. Mihara, T. K. Ronson and J. R. Nitschke, *Angew. Chem., Int. Ed.*, 2019, **58**, 12497; (*d*) C. Sgarlata, J. S. Mugridge, M. D. Pluth, B. E. F. Tiedemann, V. Zito, G. Arena and K. N. Raymond, *J. Am. Chem. Soc.*, 2010, **132**, 1005; (*e*) B. Li, B. Zheng, W. Zhang, D. Zhang, X.-J. Yang and B. Wu, *J. Am. Chem. Soc.*, 2020, **142**, 6304; (*f*) A. C. Stelson, C. M. Hong, M. C. Groenenboom, C. A. E. Little, J. C. Booth, N. D. Orloff, R. G. Bergman, K. N. Raymond, K. A. Schwarz, F. D. Toste and C. J. Long, *Commun. Chem.*, 2019, **2**, 54.
12 J. Wang, T. A. Young, F. Duarte and P. J. Lusby, *J. Am. Chem. Soc.*, 2020, **142**, 17743.
13 (*a*) M. D. Pluth, R. G. Bergman and K. H. Raymond, *Science*, 2007, **316**, 85; (*b*) M. D. Pluth, R. G. Bergman and K. N. Raymond, *Acc. Chem. Res.*, 2009, **42**, 1650.
14 (*a*) J. E. Klijn and J. B. F. N. Engberts, *J. Am. Chem. Soc.*, 2003, **125**, 1825; (*b*) J. E. Klijn and J. B. F. N. Engberts, *Org. Biomol. Chem.*, 2004, **2**, 1789; (*c*) F. Hollfelder, A. J. Kirby, D. S. Tawfik, K. Kikuchi and D. Hilvert, *J. Am. Chem. Soc.*, 2000, **122**, 1022.
15 C. A. Bunton, F. Nome, F. H. Quina and L. S. Romsted, *Acc. Chem. Res.*, 1991, **24**, 357.
16 (*a*) S. Turega, W. Cullen, M. Whitehead, C. A. Hunter and M. D. Ward, *J. Am. Chem. Soc.*, 2014, **136**, 8475; (*b*) M. Whitehead, S. Turega, A. Stephenson, C. A. Hunter and M. D. Ward, *Chem. Sci.*, 2013, **4**, 2744; (*c*) A. J. Metherell, W. Cullen, N. H. Williams and M. D. Ward, *Chem.–Eur. J.*, 2018, **24**, 1554.
17 N. Sagawa and T. Shikata, *Phys. Chem. Chem. Phys.*, 2014, **16**, 13262.
18 (*a*) M. Hoshino, A. Khutia, H. Xing, Y. Inokuma and M. Fujita, *IUCrJ*, 2016, **3**, 139; (*b*) K. Rissanen, *Chem. Soc. Rev.*, 2017, **46**, 2638.
19 C. G. P. Taylor, S. P. Argent, M. D. Ludden, J. R. Piper, C. Mozaceanu, S. A. Barnett and M. D. Ward, *Chem.–Eur. J.*, 2020, **26**, 3054.
20 (*a*) M. R. Ams, D. Ajami, S. L. Craig, J. S. Yang and J. Rebek, *J. Am. Chem. Soc.*, 2009, **131**, 13190; (*b*) S. Mecozzi and J. Rebek, *Chem.–Eur. J.*, 1998, **4**, 1016; (*c*) J. Rebek, *Acc. Chem. Res.*, 2009, **42**, 1660.
21 (*a*) R. Puttreddy, N. K. Beyeh, E. Kalenius, R. H. A. Ras and K. Rissanen, *Chem. Commun.*, 2016, **52**, 8115; (*b*) W. Zhang, D. Yang, J. Zhao, L. Hou, J. L. Sessler, X.-J. Yang and B. Wu, *J. Am. Chem. Soc.*, 2018, **140**, 5248; (*c*) R. Djemili, L. Kocher, S. Durot, A. Peuronen, K. Rissanen and V. Heitz, *Chem.–Eur. J.*, 2019, **25**, 1481.
22 A. J. Metherell and M. D. Ward, *Dalton Trans.*, 2016, **45**, 16096.
23 S. Turega, M. Whitehead, B. R. Hall, A. J. H. M. Meijer, C. A. Hunter and M. D. Ward, *Inorg. Chem.*, 2013, **52**, 1122.
24 (*a*) C. R. Shugrue, J. R. DeFrancisco, A. J. Metrano, B. D. Brink, R. S. Nomoto and B. R. Linton, *Org. Biomol. Chem.*, 2016, **14**, 2223; (*b*) T. R. Kelly and M. H. Kim, *J. Am. Chem. Soc.*, 1994, **116**, 7072; (*c*) C. V. K. Sharma and G. R. Desiraju, *J. Chem. Soc., Perkin Trans. 2*, 1994, 2345.
25 (*a*) W. Cullen, S. Turega, C. A. Hunter and M. D. Ward, *Chem. Sci.*, 2015, **6**, 2790; (*b*) https://www.ccdc.cam.ac.uk/solutions/csd-discovery/components/gold/, last accessed 11/5/2021.
26 P. Mal, B. Breiner, K. Rissanen and J. R. Nitschke, *Science*, 2009, **324**, 1697.
27 M. D. Ludden, C. G. P. Taylor and M. D. Ward, *Chem. Sci.*, 2021, **12**, 12640.
28 (*a*) R. E. Mesmer, K. M. Palen and C. F. Baes Jr, *Inorg. Chem.*, 1973, **12**, 89; (*b*) S. Radosavljević, V. Ŝćepanović, S. Stević and D. Milojković, *J. Fluorine Chem.*, 1979, **13**, 465.
29 D. W. Smith, *J. Chem. Educ.*, 1977, **54**, 540.
30 (*a*) B. Kang, H. Tang, Z. Zhao and S. Song, *ACS Omega*, 2020, **5**, 6229; (*b*) W. Kunz, P. Lo Nostro and B. W. Ninham, *Curr. Top. Colloid Interface Sci.*, 2004, **9**, 1.
31 (*a*) A. P. dos Santos, A. Diehl and Y. Levin, *Langmuir*, 2010, **26**, 10778; (*b*) M. Baer, V.-T. Pham, J. L. Fulton, G. K. Schenter, M. Balasubramanian and C. J. Mundy, *J. Phys. Chem. Lett.*, 2011, **2**, 2650.
32 (*a*) A. J. Bissette and A. J. Fletcher, *Angew. Chem., Int. Ed.*, 2013, **52**, 12800; (*b*) A. Vidonne and D. Philp, *Eur. J. Org. Chem.*, 2009, 593; (*c*) P. Schuster, *Monatsh. Chem.*, 2019, **150**, 763; (*d*) E. A. Wintner and J. Rebek Jr, *Acta Chem. Scand.*, 1996, **50**, 469.
33 M. D. Liptak, K. C. Gross, P. G. Seybold, S. Feldgus and G. C. Shields, *J. Am. Chem. Soc.*, 2002, **124**, 6421.
34 I. S. Tidmarsh, T. B. Faust, H. Adams, L. P. Harding, L. Russo, W. Clegg and M. D. Ward, *J. Am. Chem. Soc.*, 2008, **130**, 15167.
35 D. R. Allan, H. Nowell, S. A. Barnett, M. R. Warren, A. Wilcox, J. Christensen, L. K. Saunders, A. Peach, M. T. Hooper, L. Zaja, S. Patel, L. Cahill, R. Marshall, S. Trimnell, A. J. Foster, T. Bates, S. Lay, M. A. Williams, P. V. Hathaway, G. Winter, M. Gerstel and R. W. Wooley, *Crystals*, 2017, **7**, 336.